

Gertz I. Likhtenshtein

Nitroxides

Brief History, Fundamentals, and Recent Developments



Springer

Springer Series in Materials Science

Volume 292

Series Editors

Robert Hull, Center for Materials, Devices, and Integrated Systems,
Rensselaer Polytechnic Institute, Troy, NY, USA

Chennupati Jagadish, Research School of Physical, Australian National University,
Canberra, ACT, Australia

Yoshiyuki Kawazoe, Center for Computational Materials, Tohoku University,
Sendai, Japan

Jamie Kruzic, School of Mechanical & Manufacturing Engineering,
UNSW Sydney, Sydney, NSW, Australia

Richard M. Osgood, Department of Electrical Engineering, Columbia University,
New York, USA

Jürgen Parisi, Universität Oldenburg, Oldenburg, Germany

Udo W. Pohl, Institute of Solid State Physics, Technical University of Berlin,
Berlin, Germany

Tae-Yeon Seong, Department of Materials Science & Engineering,
Korea University, Seoul, Korea (Republic of)

Shin-ichi Uchida, Electronics and Manufacturing, National Institute of Advanced
Industrial Science and Technology, Tsukuba, Ibaraki, Japan

Zhiming M. Wang, Institute of Fundamental and Frontier Sciences - Electronic,
University of Electronic Science and Technology of China, Chengdu, China

The Springer Series in Materials Science covers the complete spectrum of materials research and technology, including fundamental principles, physical properties, materials theory and design. Recognizing the increasing importance of materials science in future device technologies, the book titles in this series reflect the state-of-the-art in understanding and controlling the structure and properties of all important classes of materials.

More information about this series at <http://www.springer.com/series/856>

Gertz I. Likhtenshtein

Nitroxides

Brief History, Fundamentals, and Recent
Developments



Springer

Gertz I. Likhtenshtein
Department of Chemistry
Ben-Gurion University of the Negev
Beersheba, Israel

Institute of Problems of Chemical Physics
Russian Academy of Science
Chernogolovka, Moscow Region, Russia

ISSN 0933-033X ISSN 2196-2812 (electronic)
Springer Series in Materials Science
ISBN 978-3-030-34821-2 ISBN 978-3-030-34822-9 (eBook)
<https://doi.org/10.1007/978-3-030-34822-9>

© Springer Nature Switzerland AG 2020

This work is subject to copyright. All rights are reserved by the Publisher, whether the whole or part of the material is concerned, specifically the rights of translation, reprinting, reuse of illustrations, recitation, broadcasting, reproduction on microfilms or in any other physical way, and transmission or information storage and retrieval, electronic adaptation, computer software, or by similar or dissimilar methodology now known or hereafter developed.

The use of general descriptive names, registered names, trademarks, service marks, etc. in this publication does not imply, even in the absence of a specific statement, that such names are exempt from the relevant protective laws and regulations and therefore free for general use.

The publisher, the authors and the editors are safe to assume that the advice and information in this book are believed to be true and accurate at the date of publication. Neither the publisher nor the authors or the editors give a warranty, expressed or implied, with respect to the material contained herein or for any errors or omissions that may have been made. The publisher remains neutral with regard to jurisdictional claims in published maps and institutional affiliations.

This Springer imprint is published by the registered company Springer Nature Switzerland AG
The registered company address is: Gewerbestrasse 11, 6330 Cham, Switzerland

Preface

It is known that there are delicate links and fine parallels between an art and science. Both these spheres of human endeavor involve a unique combination of professional skill and creative search. Sometimes, an intuitive line of a great poet or philosopher may be likened to the opening of a new horizon in science. Thus, the composer Maurice Ravel in his famous “Bolero” allegorically depicts the process of birth and development of an epochal discovery that gives rise to many advantages. Like that opening musical movement, the first publication on synthesis a nitroxide by Fremy in 1825 initiated, after a long lag period, the birth and rapid development of a novel class of stable nitroxide radicals which happened to be extremely important in both aspects, basic and applied.

At present, the science of nitroxides widely extended her “hands” to chemistry, physics, and biology. The application of nitroxides ranges from use as spin labels and antioxidants in biological studies, charge carriers for energy storage, basis for magnetic materials' mediators in polymerization reactions, functional spin probes for pH, oxygen, and thiol levels to catalysts in chemical and electrochemical oxidation reactions.

Classical and modern physical chemistry and chemical physics, chemical kinetics, organic, inorganic, and quantum chemistry provide an arsenal of physical methods and establish a basis for the investigation of structure and action mechanism of processes involving nitroxides.

This book embraces all principal aspects of structure and physicochemical action mechanisms of nitroxides. It is a view of nitroxides by a physicochemist with long-term experience in the area. The book is not intended to provide an exhaustive survey of each topic but rather a discussion of their theoretical and experimental background and recent developments. The literature of nitroxides is so vast, and many scientists have made important contribution in the area that it is impossible in the space allowed for this book to give a representative set of references. In fact, for each section in this area one can write several books. The author apologizes to those he has not been able to include.

Research on nitroxide which combines their fundamental importance for human welfare and intellectual fascination for investigation will promote solving exciting and complicated problems in chemistry, biology, and physics.

Chapter 1 of the monograph is a brief outline of 175 years history of nitroxides. Chapters 2 and 3 form the theoretical and experimental chemical background for nitroxide numerous application. Chapter 4 is a general survey of fundamentals of electron spin resonance and nuclear magnetic resonance, and main physical methods directly related to nitroxide. Advantages in design and use of nitroxide biradicals are reviewed in Chap. 5. Chapter 6 presents a review on the use of tethered nitroxide–fluorophore molecules as probes of redox status, antioxidant activity, oxidative stress, and free radical reaction. Nitroxide-mediated polymerization (NMP) is the subject of Chap. 7. Chapter 8 describes role nitroxides as the base for magnetic materials. Involving nitroxide radicals and their derivatives in biological processes is in focus of Chap. 9. Applications of nitroxides as spin labels and probes constitute the contents of Chap. 10. Chapter 11 is devoted to the use of nitroxyls to solve some of the physicochemical problems.

The monograph is intended for scientists and engineers working in the fields of chemistry, physics, and biology in which nitroxyls currently find or would find their application. Book, as a whole, and separate chapters can be used as a subsidiary manual for instructors, graduate and undergraduate students of university chemistry, physics, and biophysics departments.

Department of Chemistry, Ben-Gurion University of the Negev and Institute of Problem of Chemical Physics, Russian Academy of Science provided excellent conditions for writing this book for which the author is extremely grateful.

Moscow Region, Russia/Beersheba, Israel

Gertz I. Likhtenshtein

Contents

1	Nitroxides: 170 Years of History	1
1.1	Long Preamble of a Tale (1845–1960)	1
1.2	“Golden” Decade (1962–1972)	3
1.3	New Era	8
1.4	Concluding Remarks	12
	References	14
2	Nitroxide Basic Physical Properties	21
2.1	Introduction	21
2.2	Spin Electron–Spin Nuclear Interactions in Nitroxides	23
2.3	Relationships Between the Structure and Properties of Nitroxide	25
	References	33
3	Nitroxide Chemical Reactions	35
3.1	Introduction	35
3.2	Nitroxide Redox Potential	36
3.3	Oxoammonium Cation Reactions	42
3.4	Nitroxide Cross-Coupling Reactions	47
3.5	Nitroxides in Electrocatalysis	50
3.6	Nitroxides as Radical Scavenger	54
3.7	Nitroxide Reaction with Typical Antioxidants	58
3.8	Nitroxide Redox Behavior in Biological Systems	63
	References	65
4	ESR and NMR as Tools for Nitroxides Studies	71
4.1	Introduction	71
4.2	Spin Electron–Spin Electron Interactions. Distance Determination	73
4.2.1	Spin Electron–Spin Nuclear Interactions	82
	References	88

5	Nitroxide Biradicals	93
	Alexander I. Kokorin	
5.1	Introduction—Historical Notes	93
5.2	Electron Spin Exchange in Nitroxide Biradicals	96
5.3	X-Ray Structures and DFT Calculations	100
5.4	Intramolecular Dynamics in Biradicals	107
5.5	Applications of Biradicals	112
	References	113
6	Fluorophore–Nitroxide (Profluorescent Nitroxide) Probes	119
6.1	Introduction	119
6.2	Structure and Synthesis of Dual Fluorophore–Nitroxide Compounds	120
6.2.1	Profluorescent Nitroxides as Redox Probes	128
6.3	Fluorescence Detection of Free Radicals	142
6.4	Photophysical and Photochemical Properties of Fluorescence–Nitroxide	143
6.4.1	Dual Compounds for Photoswitching Magnetic Materials	143
6.4.2	Photophysical Effects in Paramagnetic Complexes Bearing Nitroxides	146
6.4.3	Factors Affected on Intramolecular Fluorescence Quenching, Electron Transfer, and Photoreduction in Dual Compounds	149
	References	156
7	Nitroxide-Mediated Polymerization	161
7.1	Introduction	161
7.2	Mechanism of the Nitroxide-Mediated Polymerization	162
7.3	Nitroxide-Mediated Polymerization Kinetics	165
7.4	Surface and Dispersed Systems	168
7.5	NMP in Creation of Complex Macromolecular Architectures	172
7.6	NMP and Polymer Materials	174
7.7	Nitroxide on Inorganic Templates	176
7.8	NMP for Organic Electronics and Other Devices	177
7.9	NMP and Materials for Biomedical Applications	179
7.10	NMP Miscellaneous Applications	181
	References	181
8	Nitroxides as Materials	187
8.1	Introduction	187
8.2	Nitroxide Bearing Liquid Crystals	188
8.3	Nitroxide Crystal Structure Materials	197

8.4	Nitroxides in Electric Batteries	200
8.5	Nitroxide Single-Crystal Molecular Magnet	206
	References	212
9	Nitroxides in Disease	217
9.1	Introduction	217
9.2	Nitroxides in Cancer	217
9.2.1	Cells	217
9.2.2	Animals	225
9.3	Miscellaneous	226
	References	230
10	Spin Labeling	235
10.1	Introduction	235
10.2	Nitroxide Labeling	236
10.2.1	Proteins and Peptides	236
10.2.2	Lipid Membranes	249
10.2.3	Nucleic Acids	251
10.3	Spin Tools	255
10.3.1	Background	255
10.3.2	Spin Oximetry	257
10.3.3	Spin pH Meter	258
10.3.4	Spin Redox Probe	258
10.3.5	SH Moiety Assay	260
10.3.6	Spin Imaging	261
10.3.7	Molecular Dynamics. Spin Viscose Meter	264
10.3.8	Spin Polarity Meter	267
10.4	Alternative Spin Labeling	267
	References	275
11	Nitroxides Miscellaneous Application	283
11.1	Multispin Nitroxides	283
11.1.1	Spin Trapping	285
11.2	Spin Label-Spin Probe Method	289
11.2.1	Fundamentals	289
11.2.2	Nitroxide in Investigation of Electrostatic Effects	291
11.3	Immersion Depth of Nitroxide Fragment	295
11.4	Nitroxides in Cotton and Cellulose Physicochemistry and Technology	297
11.5	Spin Cascade	302
11.6	Nitroxides in Matrices	304
	References	306
	Index	311

About the Author



Prof. Gertz I. Likhtenshtein received his Ph.D. and his Doctor of Science from the Semenov Institute of Chemical Physics at the Russian Academy of Science in Moscow, where he was appointed to the position of Head of Laboratory of Chemical Physics of Enzyme Catalysis in 1966, becoming a full professor in 1976. In 1992, he moved to the Department of Chemistry at the Ben-Gurion University of Negev, Israel, as a full professor in charge of the Laboratory of Chemical Biophysics and has been an Emeritus since 2003. He has authored eleven scientific books and around 390 papers, and his awards include the Medal of the Exhibition of Economic Achievement, the USSR Diploma of Discovery, the USSR State Prize, the V. V. Voevodsky International Price for Electron Spin Resonance, the N. M. Emanuel Price for Biophysical Chemistry, and the Diploma of the Israel Chemical Society. Professor Likhtenshtein is a Foreign Member of the Academy of Science of Republic Tadjikistan and was a member of the International ESR Society, the American Biophysical Society, the Israel Chemical Society, and the Israel ESR Society. His recent main scientific interests focus on the analysis of biologically important molecules.

Chapter 1

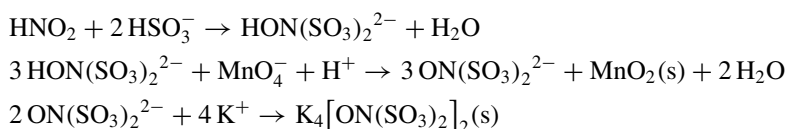
Nitroxides: 170 Years of History



1.1 Long Preamble of a Tale (1845–1960)

As an each way, a long road of the 174 years history of stable radicals bearing a >N-O group has started with the first step. This step has been made in 1845 by Edmond Frémy (1814–1894), a director the Muséum national d'histoire naturelle, who was one of understanding chemists of nineteenth century [1]. Edmond Frémy published numerous articles in the *Annales de Chimie et de Physique*, seven volumes of *Traité de chimie générale*, and ten volumes *Encyclopédie Chimique*, in collaboration with several other scientists. But his main advantage, which left memories in the chemical history, was a synthesis and characterization of disodium nitrosodisulfonate (potassium nitrosodisulfonate, Frémy's salt (Fig. 1.1a).

A synthesis of potassium nitrosodisulfonate, occurring by the following scheme:



now can be readily performed in a high school student chemical laboratory. Frémy's salt is long-lived radical in water and other solvents in unaerobic conditions. Nevertheless, a rapid and highly exothermic decomposition of this compound occurs spontaneously in air that is a serious limitation for its applications.

Next step in the area was done by O. Piloty and B. G. Schwerin in 1901 [2] who prepared the first organic radical containing >N-O . The radical was named as “porphyrexide” (Fig. 1.1b). Heinrich Wieland and Moriz Offenbacher reported in

1.2 “Golden” Decade (1962–1972)

From period 1962–1972 practically all corner-stone ideas in the area of nitroxides were exposed and developed. These ideas were sustained by fundamental theoretical and experimental investigations in chemistry and physics of nitroxides. First nitroxides, presented in Fig. 1.1, though their principle importance, did not find wide application and were not be able to serve as a basis for synthesis of new paramagnetic compounds in a broad scale.

Until 1962, chemists adhered to the paradigm that the most chemically reactive portion of a radical can be a group bearing spin electron. This paradigm was broken by M. B. Neiman and E. G. Rozanzen (Figs. 1.3 and 1.4), who introduced nitroxide reactions with a nitroxide (Fig. 1.1e) without direct involvement of the spin center. A novel class of stable nitroxides radicals presented in publication [6, 7] was first met with skepticism, and even strong criticism, from qualified and very professional members of the scientific community. But, later, more and more young enthusiasts joined the ranks of scientists applying this new tool in their research, and ever increasing reports of nitroxides were published. These pioneering works have laid a chemical basis for the method of numerous nitroxide applications, spin labeling in particular. As a consequence, rapid and extensive progress in the area and a real burst of works on synthesis and application of nitroxide in chemistry, physics, biology, and even in medicine have been broken. The theoretical and experimental data presented in this book clearly demonstrate both history and the current progress within the nitroxide “empire” of about publications.

In parallel, the dependence of ESR spectra of nitroxides on their molecular dynamics in solutions was demonstrated. The radical motion leads to averaging of spin

Fig. 1.3 Professor Moisey B. Neiman (1889–1967)



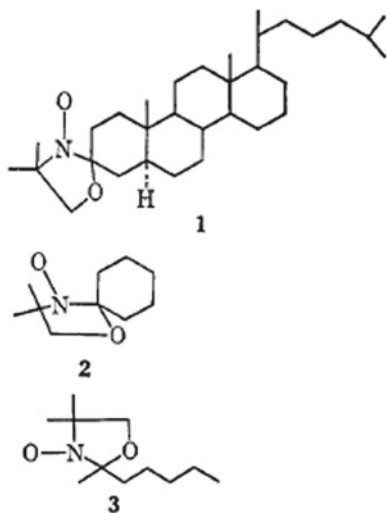


Fig. 1.4 Gertz I. Likhtenshtein, Anatoly L. Buchachenko, Eduard G. Rozanzev and Nikolay N. Semenov (1977)

electron spin nuclear interaction and to a drastic change of the ESR spectra. Correlation time for isotropic and anisotropic rotation τ_c for a nitroxide on a homogeneous media in the area of fast ($\tau_c = 10^{-9} - 10^{-10}$ s) and slow ($\tau_c = 10^{-7} - 10^{-8}$ s) motion can be estimated in the frame of theory developed by Kivelson [8] and Freed [9].

At the end of 1960 new classes of stable radicals, α -Nitronyl nitroxides [10] and Doxyl nitroxides performed by the J. F. W., Keana group Fig. 1.5 [11], possessing great potential for further wide applications, were synthesized.

Fig. 1.5 Doxyl nitroxides [11]



In the pioneering work of Golubev et al. [12], the first stoichiometric oxidation of alcohols to ketones mediated by an oxoammonium species with N^+ -oxyl fragment was demonstrated.

Decisive breakthrough in the spin-labeling area was occurred owning a whole cascade of pioneering works of Howard McConnell and his collaborators. In the first publication in this series [13], a spin label, 2,2,6,5-tetramethyl-3-isocyanatopyrrolidine-1-oxyl, was covalently tethered to bovine serum albumin and to poly-L-lysine [13]. The nitroxide ESR spectra in solution indicated sensitivity of the nitroxide segment rotation to molecular motion of the labeled compound. Binding of a spin-labeled hapten, the 2,4-dinitrophenyl hydrazone of 2,2,6,6-tetramethyl 4-piperidone nitrogen oxide to antidinitrophenyl antibody was proved by the estimation of the rotational relaxation time of the bound hapten using analysis of the nitroxide ESR spectra [14] (Fig. 1.6).

Powerful potential capacity of spin-labeling method for study conformational transitions in proteins, which are necessary for its functional activity, was illustrated by the McConnell group on example of hemoglobin. Two reactive β -93SH groups in horse hemoglobin were modified with N-(1-oxyl-2,2,5,5-tetramethyl-3-pyrrolidinyl) iodoacetamide [15]. The ESR spectra of the labeled hemoglobin labeled were dependent on the degrees of oxygenation. The Hill constant n , a measure of the cooperativity of sigmoidal oxygen binding, was found to be $n = 2.3$ for the labeled hemoglobin, as compared to $n = 3$ for native hemoglobin. It was concluded that each of subunit of the protein tetramers undergoes a substantial conformational change when that subunit binds a molecule of oxygen. To tackle the problem of allosteric interactions in enzymes and proteins not having a quaternary structure, in works of G. I. Likhtenshtein group [16–18] the enzyme lysozyme was spin labeled by the histidine-15

Fig. 1.6 Professor Harden McConnell (1927–2014)



group located at the distance 15 Å from the substrate-binding center. Addition of specific inhibitors NAG and NAG–NAG induces distinct changes in ESR spectra, which were in a good quantitative agreement with the extent of the substrate binding. Similar transglobular effect was also detected in spin-labeled myoglobin [17].

The first work on the use spin labeling in enzyme catalysis has been published by L. J. Berliner, H. M. McConnell in 1966 [19]. It was shown that the nitroxide spin-labeled substrate, DL-2,2,5,5-tetramethyl-3-carboxypyrrolidine-*p*-nitrophenyl ester, can be used to study the activity of the proteolytic enzyme α -chymotrypsin. The most conclusive work in the investigation of active serine group in proteolytic enzymes based on phosphate and nitrobenzene derivatives was carried out by Hsia et al. [20]

One of remarkable achievement of the spin-labeling methods has been quantitative characterization of flexibility of model and biological membranes. Incorporation of hydrophobic nitroxide probe 2,2,4,4-tetramethyl-1,2,3,4-tetrahydro- γ -carboline-3-oxyl into the sodium dodecyl sulfate remarkably decreased in the rate of tumbling of the probe as compare with its motion on solutions, which is quantitatively described by a rotational correlation time, τ_c [21]. Progress in the study of biological and model membranes with the use of the steroid and lipid spin probes was demonstrated in the works of Keana [11] and MacConnell [15] groups. For example, in sonicated phospholipid dispersions of the walking leg nerve fibers of *Homarus americanus*, and in erythrocytes oriented by hydrodynamic shear, the nitroxide probes motion with rotational diffusion frequencies of the order of 10^7 to 10^8 s⁻¹ was revealed. The first approach for quantitative investigation of lateral diffusion in membranes with the use of spin labels was developed by McConnell and McFarland [15], Hubbell and McConnell [22]. In a typical experiment, small drops of a lipid spin probe were inserted to films of oriented multilayers of lecithin. Because of radical diffusion, the probe ESR spectrum changes from a singlet, which is the characteristic of large local concentration, to a triplet for diluted radicals. Analysis of the process kinetics allowed to calculate the coefficient of translational lateral diffusion.

The application of nitroxide radicals to covalent modification and the study of the structure, dynamic and conformational changes of nucleic acids (poly rA, poly rU, and poly rG) were based on the principles established for proteins [23–25]. The possibilities of non-covalently bound nitroxide probes were first demonstrated in [24]. As early as in 1968, A. M. Vasserman, A. L. Buchachenko, A. L. Kovarskii, and M. B. Neiman have shown powerful potentiality of nitroxide spin-label methods in investigation molecular dynamics and microstructure of high molecular mass compounds [26]. The first observation of effect of nitroxide on radical polymerization, that is inhibition with nitroxide mono- and biradicals, was made in 1966 by the M. B. Neiman group [27]. The inhibiting effect of the nitroxides on styrene polymerization at 50 °C, initiated by azodiisobutyronitrile, was interpreted as a cross-recombination of nitroxides and polymer radicals which led to the process termination.

Synthesis and investigation of the chelate complex Cu⁺²-Schiff bases ligand derivative of TEMPO, which appeared to be the first transition metal complexes with paramagnetic ligands, were carried out in 1969 [28].

Method of double spin labeling, invented by Likhtenshtein in 1968 [29], is based on specific modification of chosen groups of the object of interest by two or several spin labels, nitroxides, or complexes of paramagnetic metal followed by the analysis of effects of the spin–spin interactions on the label ESR spectra. This approach allows to estimate the distance between the paramagnetic centers up to 2.5 nm [29–32]. Later, the higher sensitivity of spin–lattice relaxation time of a radical to interactions between the radical and paramagnetic ions up to 100 nm was demonstrated [17, 18, 33]. In parallel, the effects of spin-exchange interaction on the labels ESR spectra were used for establishment of structure of systems under investigation, such as iron–sulfur clusters in nitrogenase, ferredoxins, and non-heme protein [34].

The first version of method of spin label–spin probe method (SLSPM) proposed by Likhtenshtein and coworkers [35] was based on a dynamic exchange spin–spin interaction of a stable radical, mostly nitroxide, attached to molecular object of interest with a spin probe which are chemically inert paramagnetic species capable of diffusing freely in solution. The value of the dynamic exchange rate constant k_{ex} depends on microviscosity, steric hindrances, and distribution of electrostatic charges, and the method was intensively employed for investigating microstructure of object under interest [17, 18, 36–38]. In parallel, a variant of the SLSP method based on direct measurement of electron spin–lattice relaxation times was developed in Hyde group [39].

Principles of application of nitroxide spin-label method as a tool for experimental investigation of proteins molecular dynamics (“breathing”) have been formulated at the end of 1960 by Likhtenshtein [40, 41] and then were implemented in collaborative works. Parameters of motion of a nitroxide in the labeled protein may serve as characteristics of surrounding media dynamics. For example, the monitoring motion of hydrophobic nitroxide spin probe in binding site of human serum albumen revealed low amplitude wobbling of the probe with the correlation time $\tau_c \approx 10^{-8}$ s modulated by the binding site dynamics [41].

Protective antitumor activity of nitroxide in animals was demonstrated in pioneering work of N. P. Konovalova, M. B. Neiman, E. G. Rozanzenov, and Emanuel N. M. in 1964 [42]. Later in 1970, G. Sosnovsky and M. Konieczny have performed syntheses anticancer drugs belonging to the class of alkylating agents containing aminoxyl radicals [43].

Continuous wave electron–electron double resonance (CW ELDOR) independently reported in 1968 by the Hyde and Freed [44], Bendersky and Blumenfeld [45] groups allowed to resolve problems that are not accessible in the CW-ESR. The ELDOR spectra were shown to be sensitive to very slow rotations which may provide unique information on the details of molecular dynamics and can be used for distance estimation between centers bearing spin electron.

Thus, chemical and physical contributions within the “golden” decade have formed the basis for subsequent progress in the area. In subsequent decades, fundamentals and tendencies laid out in the “golden” period were intensively developed and number of publications in the area accelerated almost in a geometric progression [46–49] and references therein.

1.3 New Era

Starting from the pioneering works of Ya. S. Lebedev and his colleagues [50], problems of poor resolution of the 3 cm ESR have been solved by the use of the high-field–high-frequency (148 GHz), high-resolution 2-mm EPR spectroscopy. The comprehensive review on advanced biomolecular EPR spectroscopy addresses both the EPR and NMR communities has been recently published [51]. New contributions of K. Mebius and W. Lubiz groups to high-field–high-frequency EPR were summarized.

Synthesis of imidazoline and imidasolidine nitroxides (Fig. 1.7) markedly expanded ability of nitroxides for its applications as spin labels, ligands for materials with ferromagnetic properties, inhibitors in polymer processing, and initiators for “living” radical polymerization [52, 53] and references therein.

Figure 1.8 shows photography of leaders of groups involved in the nitroxide spin labeling till 1979.

Measurement of distance between spin labels by analysis of line shape of ESR spectra using new computation methods was carried out for double and multiple labeled proteins and enzymes [54]. Various aspects of spin-label magnetic resonance studies on lipid–lipid and lipid–protein interactions with integral proteins were

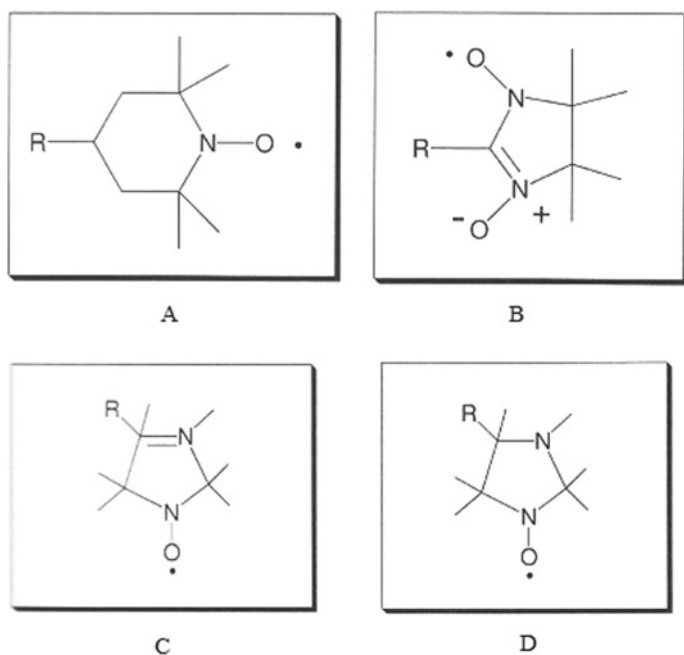


Fig. 1.7 Nitroxide derivatives: piperidine A, nitronyl B, imidasoline C, and imidasolidine D, and nitronyl D



Fig. 1.8 Leaders of groups involved in the nitroxide spin labeling till 1979. From left to right: rector of the Pech University, Leonid B. Volodarsky, Larry Berliner, Gertz Likhtenshtein, R. Rassat, John Keena, George Sosnovsky, Kalman Hideg

reviewed [55–57]. Synthesis and determination of structural characteristics of magnetic all-organic radical liquid crystals were in focus of the program developed by R. Tamura with colleagues [58].

Works of 1970–1990 on chemical modification of DNA with nitroxide derivatives and ESR examination of structure and dynamics of the labeled biopolymer have laid the basis for further detail investigations in this extremely important area of molecular biology [59, 60]. After the first publication on labeling of linear polymers such as of cotton, silk, and wool by trichlorotriazine-based nitroxide [61], a series work on the investigation of cotton fibers and cellulose was reported by Marupov and Likhtenshein groups [62] and references therein.

Hundreds of complexes transition metals with nitroxide ligands were synthesized and investigated (for review see [63] and references therein).

The CW ESR saturation techniques were employed for the investigation of depth of immersions of nitroxide spin probes radicals up to 40 Å in lipid phases of biomembranes [64]. High sensitivity of spin–lattice relaxation parameters of nitroxide was also taken into consideration at development of theory of very slow motion ($\tau_c = 10^{-3}$ – 10^{-6} s) [65].

A new impact in nitroxide-mediated polymerization has started when P. G. Griffiths, E. Rizzardo, and D. H. Solomon showed that it was possible to prepare well-controlled and living (homo-, co) polymer by radical polymerization in the presence of nitroxyl radical as a controlling agent [66–68]. Since its discovery nitroxide-mediated radical polymerization (NMP) was proved to be a powerful method to synthesize well-defined macromolecular architectures with precisely controlled topologies, compositions, microstructures, and functionalities [69–73]. A significant contribution in the area has been brought by the groups of Solomon [69], Grishin [70], Fisher [71], and Bagryanskaya [72]. Kinetic aspects of the nitroxide-mediated radical polymerization were discussed in details in comprehensive review [73].

Significant progress in the high-field–high-frequency (HFHF) ESR has been achieved [74–76] especially owing to the design of millimeter-wave quasi-optic technique, permitting the construction of a 9-Tesla, 250-GHz (1.2 mm) [55]

After remarkable invention of echo-detected ELDOR (three-pulse ELDOR, PELDOR, double electron–electron resonance DEER) by Milov et al. [77] and its first application, a real burst of development of new ESR pulse methods has been broken [78–92]. Other methods used for the study of nitroxide labeling objects are four [80, 89, 90] and five-pulse techniques [91, 92], method to determine the effective saturation factor of nitroxide radicals for dynamic nuclear polarization (DNP) experiments in liquids [83], two-dimensional ELDOR [84]), high-frequency pulsed ENDOR/EPR [85], double and multiple quantum coherence pulsed ESR (DQC ESR) [79, 81], and ESR spectra hole burning [87].

The invention and use of site-directed mutagenesis in combination with modern ESR spectroscopy gave new breath to the nitroxide spin-labeling method. Site-directed spin-labeling (SDSL) designed by Hubbell group [93] is the substitution of a selected amino acid for cysteine via the site-directed mutagenesis technique following chemical modification with a sulfhydryl reactive nitroxide radical, *S*-(1-oxyl-2,2,5,5-tetramethyl-2,5-dihydro-1H-pyrrol-3-yl) methyl methanesulfonothioate (MTSL). The main advantage of the SDSL is the possibility to overcome the limitations of a choice of amino acids suitable for the labeling in native proteins. The efficiency of combination of the site-directed spin-labeling with the advance pulse techniques can be illustrated by numerous works, for example in studies of T4 Lysozyme [94] and mutants maltose-binding protein (MBP) 09-11 [95].

Recently, new spin-labeling approaches have been shown to be an attractive alternative to the traditional method of nitroxide spin labels for pulse dipolar ESR (PD ESR). The first one, based on high-spin Gd^{3+} ($S = 7/2$) complexes, was designed and developed in Goldfarb group [96]. A combined method, utilizing NMR and EPR spectroscopies, was employed to compare different types of nitroxide-based and Gd(III) -based spin labels attached to isolated RBDs of the polypyrimidine tract-binding protein 1 (PTBP1) and to short RNA fragments [97] in complexes with short

RNAs. An idea of the use of carbon-centered triarylmethyl (trityl) radicals instead of nitroxides for nanometer distance measurements was first introduced and realized in 2012 [98]. Nowadays, triarylmethyl radicals TMA are successively used as spin labels for studies on the structure of proteins and nucleic acids utilizing site-directed spin labeling (SDSL) and pulse dipolar EPR spectroscopy [99, 100].

Spin oximetry, first reported by Subczynski and Hide [101], is a version of spin label–spin probe method [35, 39] in which molecular oxygen plays role of spin probe. A method invented for measurement of the oxygen diffusion–concentration product was based on the dependence of the spin–lattice relaxation time T_1 of the spin label, detected by using saturation recovery (SR), on the bimolecular collision rate with oxygen. Various aspects of the spin oximetry applications have been reviewed [102–104].

As it was pioneered in [105], EPR spectra of stable nitroxides of the imidazoline and imidazolidine types are sensitive to pH and can serve as spin pH probes. Data on synthesis and application of a wide set of pH-sensitive nitroxides of different sensitivity, stability to reduction, lipophilicity and its covalent-binding macromolecules have been reported [106, 107]. To quantitatively determine SH groups in high- and low-molecular weight compounds, a disulfide biradical (RS-SR), where R is imidazoline residue, has been used [108, 109]. The biradical is shown to participate in a thioldisulfide exchange reaction with compounds containing SH groups. In this case, the ESR spectra of the biradical RS-SR and the resulting monoradical R-SH are different.

Nitroxide radicals have found various applications in the field of materials science. The landmark was the discovery by M. Kinoshita group et al. in 1991 [110] who prepared the first purely organic ferromagnet with respect to a nitronyl nitroxide, 2-(4-nitrophenyl)-4,4,5,5-tetramethylimidazoline-1-oxy-3-oxide. Since then, stable nitric oxide structures have been widely used as the spin source and building block for the elaboration of organic or molecule-based magnetic materials [58, 111, 112]. In the last two decades, π -conjugated superparamagnetic organic compounds including polymer magnets with stability at ambient temperature and/or higher magnetic ordering temperatures have been attracting attention as models of multispin systems and potential magnetic devices [113]. Novel molecular magnets Cu(hfac)₂LR with nitronyl ligands were prepared and investigated in details in Ovcharenko group [114].

The spin redox probe techniques utilizing ability of nitroxides to be reacted with reducing agent to corresponding hydroxyl amine are widely used for quantitative characterization of redox processes and protection from radical damage by CW ESR spectroscopy [115–118] and references therein.

Novel methods of fast and sensitive analysis of antioxidant status of biological systems, spin redox probing and spin trapping, investigation of molecular dynamics, models for studies of photophysical and photochemical processes, and construction of new magnetic light-sensitive materials are based upon the use of dual fluorophore–

nitroxide compounds were designed and developed [119–126]. In pioneering work of Likhtenshtein and colleagues [120], three fundamental effects were first demonstrated, namely (1) The nitroxide fragment is a strong quencher of the fluorescence. (2) The radical photoreduction can lead to the decay of the EPR signal and the drastic increase of the fluorescence intensity. (3) The photoreduction kinetics strongly depends on molecular dynamics of environment. Next principle step was a series of excellent papers by Blough and Simpson [123] in which the potential of these tethered, optically switching molecules as potent redox and radical trapping probes was realized. A significant contribution to the synthesis and use of the dual compounds was made by the groups of Bottle [124] and Braslau [125]. Dual fluorescence nitroxide compounds are effectively used as convenient photochemical and photophysical models and form the basis for photoswitching magnetic materials [126] and references therein.

Stable nitroxide free radicals were utilized as antioxidants in animal models and human diseases (e.g., cancer) to protect processes of formation reactive oxygen species, ROS (O_2^- , H_2O_2 , $\cdot OH$) involving oxidative stress [127–130]. The works, in which the principle possibility of effectiveness of the spin trapping was demonstrated, came to the light in 1968 [131], later numerous theoretical and experimental studies of the spin trapping of inorganic and organic radicals were carried out [132, 133]. After cited above pioneering works [42, 43], biologically active spin-label molecules have been the focus of biophysical, biochemical, and synthetic and medicinal chemical studies [134–136]. A noticeable contribution to the theory of spin relaxation and its application was made in the works of Eaton and Eaton [137].

1.4 Concluding Remarks

Author of this review wrote in the first book on spin labeling:

Likhtenshtein G. I.: Spin-Labeling Method in Molecular Biology. Moscow, Nauka (In Russian). 1974: “It is thus our hope that spin labeling will continue to be an effective tool for solving various complicated problems in molecular biology”. Now after 45 years, it is evident that present-day reality has surpassed all optimistic expectations. As far as concern outlook for further developments, there are all reasons to believe that slow but permanent progress in the area would continue in the next decades. Nevertheless, who knows, new unexpected bright ideas would be launched and implemented and ensure vigorous success, unexpected today.

Portraits of scientists who significantly contributed in nitroxide chemistry, physics, and its miscellaneous applications are displayed in Fig. 1.9.



Rui Tamura



Albert Beth



Gareth Eaton



Sandra Eaton



Wayne Hubbell



James Hyde



Wolfgang Trimmer



Jack Freed



Igor Grigor'ev



Wolfgang Möbius



Ronald Mason



Sergey Dzuba



Alex kokorin



Harold Swartz



Gunnar Jeschke



Yury Tsvetkov



Albert Bobst



Elena Bagryanskaya



Victor Ovcharenko



Yakov Lebedev

Fig. 1.9 Gallery of scientists who significantly contributed in nitroxide chemistry, physics and its miscellaneous applications

References

1. E. Fremi, *Annales de Chimie et de Physique. Serie* **3**(15), 408–488 (1845)
2. O. Piloty, B.G. Schwerin, *Berichte den Deutschen Chemischen Gessellschaft* **34**, 1870–1877 (1901)
3. H. Wieland, M. Offenbacher, Diphenylnitric oxide, a new organic radical with tetravalent nitrogen. *Ber. Dtsch. Chem. Ges.* **47**, 2111–2115 (1914)
4. A.K. Hoffmann, A.T. Henderson, A new stable radical: Di-t-Butyl nitroxide. *Am. Chem. Soc.* **83**, 4671–4672 (1961)
5. O.L. Lebedev, M.L. Khidekel, V.A. Razuvaev, *Dokl. Acad. Nauk.* **140**, 1327–1331 (1961)
6. M.B. Neiman, E.G. Rozantzev, Y.G. Mamedova, Free radical reactions involving no unpaired electrons. *Nature* **196**, 472–474 (1962)
7. E.G. Rozantzev, *Free Nitroxyl Radicals* (Plenum Press, New York, 1970)
8. D. Kivelson, Theory of EPR line widths of free radicals. *J. Chem. Phys.* **33**, 1094–1106 (1960)
9. J.H. Freed, Theory of the ESR spectra of nitroxids, in *Spin Labeling. Theory and Applications*, vol. 1, ed. by L. Berliner (Academic Press, New York, 1976)
10. J.H. Osiecki, E.F. Ullman, Studies of free radicals. I. alpha.-Nitronyl Nitroxides, a new class of stable radicals. *J. Am. Chem. Soc.* **90**, 1078–1079 (1968)
11. J.F.W. Keana, S.B. Keana, D. Beetham, New versatile ketone spin label. *J. Am. Chem. Soc.* **89**, 3055–3056 (1967)
12. V.A. Golubev, E.G. Rozantsev, M.B. Neiman, Some reactions of free iminoxyl radicals with the participation of the unpaired electron. *Bull. Acad. Sci. USSR, Div. Chem. Sci.* **14**, 1898–1904 (1965)
13. T.J. Stone, T. Buckman, P.L. Nordio, H.M. McConnell, Spin-labeled biomolecules. *Proc. Natl. Acad. Sci.* **54**, 1010–1017 (1965)
14. L. Stryer, O.H. Griffith, A spin-labeled hapten. *Proc. Natl. Acad. Sci.* **54**, 1785–1791 (1965)
15. H.M. McConnell, B.G. McFarland, Physics and chemistry of spin labels. *Q. Rev. Biophys.* **3**, 91–136 (1970)
16. Y.D. Akhmedov, G.I. Likhtenshtein. L.V. Ivanov, Y.V. Kokhanov, Investigation of the lysozyme macromolecule by a spin-labeling method. *Dokl. Acad. Nauk. SSSR* **205**, 372–376 (1972)
17. G.I. Likhtenshtein, Spin labeling method in molecular biology (Moscow Nauka, 1974) (In Russian)
18. G.I. Likhtenshtein, Spin labeling method in molecular biology (N.Y., Wiley Interscience, 1976)
19. L.J. Berliner, H.M. McConnell, A spin-labeled substrate for α -chymotrypsin. *Proc. Natl. Acad. Sci.* **55**, 708–712 (1966)
20. J.S. Hsia, D.I. Kosman, J.S. Piette, Organophosphate spin-label studies of inhibited esterases, α -chymotrypsin and cholinesterase biochem. *Biophys. Res. Commun.* **36**, 75–78 (1969)
21. A.S. Waggoner, O.H. Griffith, C.R. Christensen, Magnetic resonance of nitroxide probes in micell-containing solutions. *Proc. Natl. Acad. Sci.* **57**, 1198–120 (1967)
22. W.L. Hubbell, H.M. McConnell, Orientation and motion of amphilic membranes. *Proc. Natl. Acad. Sci.* **64**, 20–27 (1969)
23. I.C.P. Smith, T. Yamane, Spin labeled nucleic acids. *Proc. Natl. Acad. Sci.* **58**, 884–887 (1967)
24. B.I. Sukhorukov, A.M. Wasserman, L.I. Kozlova, A.L. Buchachenko, Use the spin labeling method for study of the nucleic acid-water system. *Dokl. Acad. Nauk SSSR.* **177**, 454–457 (1967)
25. A.M. Bobst, Studies of spin-labeled polyrybo adenylic acids. *Biopolymers* **11**, 1421–1433 (1972)
26. A.M. Vasserman, A.L. Buchachenko, A.L. Kovarskii, M.B. Neiman, Study of molecular motion of polymers by method of paramagnetic probe. *Vysok. Soedin., Seriya A*, **10**, 1930–1936 (1968)
27. L.V. Ruban, A.L. Buchachenko, M.B. Neiman, Y.V. Kokhanov, Inhibition of radical polymerization with nitroxide mono-and biradicals. *Vysok. Soedin.* **8**, 1642–1646 (1966)

28. A.A. Medzhidov, L.N. Kirichenko, G.I. Likhtenshtein, *Izvestiya akademii nauk SSSR, Seriya Khimicheskaya*, 698–700 (1969)
29. G.I. Likhtenshtein, Determination of the topography of proteins groups using specific paramagnetic labels. *Mol. Biol. (Moscow)* **2**, 234–240 (1968)
30. J.C Taylor, S. Leigh, M. Cohn, The effect of dipole-dipole interaction between nitroxide radical and a paramagnetic ion on the line shape of the esr spectra of radical. *Proc. Natl. Acad. Sci.* **64**, 219–206 (1969)
31. A.V. Kulikov, G.I. Likhtenshtein, E.G. Rozantsev, V. Suskina, A. Shapiro, Nitroxide Bi- and polyradicals as standard models for distance estimation between the nitroxide moieties. *Biofizika* **17**, 42–49 (1972)
32. A.I. Kokorin, K.I. Zamaraev, G.L. Grigoryan, V.P. Ivanov, E.G. Rozantsev, Distance estimation between nitroxyl radicals. *Biofizika* **17**, 34–41 (1972)
33. A.V. Kulikov, G.I. Likhtenshtein, The use of spin-relaxation phenomena in the investigation of the structure of model and biological systems by method of spin labels. *Adv. Molecul. Relax. Proc.* **10**, 47–78 (1977)
34. L.A. Syrtsova, L.A. Levchenko, E.N. Frolov, G.I. Likhtenshtein, T.N. Pisarscaya, L.V. Vorob'ev, V.A. Gromoglasova, Structure and function of the nitrogenase components from *Azotobacter vinelandii*. *Mol. Biol. (Moscow)* **5**, 726–734 (1971)
35. G.I. Likhtenshtein, Y.B. Grebenshchikov, P. Bobodzhanov, Y.V. Kokhanov, Method of spin-labels spin probes. *Molecul. Biol. (Moscow)* **4**, 682–691 (1970)
36. G.I. Likhtenshtein, Study on the proteins microstructure by method of spin-label paramagnetic probe. *Mol. Biol. (Moscow)* **4**, 782–789 (1970)
37. G.I. Likhtenshtein, Y.B. Grebentchikov, E.G. Rosantsev, V.P. Ivanov, Study on the electrostatic charges in proteins by method of paramagnetic probes. *Mol. Biol. (Moscow)* **6**, 498–507 (1972)
38. G.I. Likhtenshtein, *New Trends in Enzyme Catalysis and Mimicking Chemical Reactions* (Kluwer Academic/ Plenum Publishers, N.Y., 2003)
39. J.S. Hyde, H.M. Swartz, W.E. Antholin, The spin probe—spin label method, in *Biological Magnetic Resonance. Spin Labeling. Theory and Application*, vol. 8, ed. by L.J. Berliner J. Reubin (Plenum Press, New York, 1979), pp. 305–339
40. G.I. Likhtenshtein, A.P. Pivovarov, P.K. Bobodzhanov, E.G. Rozantsev, N.B. Smolina, Study of dynamic structure of proteins and enzymes by specific luminescent and paramagnetic labels. *Biofizika* **13**, 396–400 (1968)
41. E.N. Frolov, G.I. Likhtenshtein, N.V. Kharakhonycheva, Investigation of dynamic structure of human serum albumin by the method of spin-probe. *Molek. Boil. (Moscow)* **8**, 886–893 (1974)
42. N.P. Konovalova, G.N. Bogdanov, V.B. Mille, M.B. Neiman, E.G. Rozantsev, G. Emanuel, N.M. Doklady Akademii nauk SSSR **157**, 707–709 (1964)
43. G. Sosnovsky, M. Konieczny, Synthesis of phosphoorganic derivatives of nitroxide radicals, *Naturforschung33b*, 792–804 (1970)
44. J.S Hyde, J.C.W. Chien, J.H. Freed, Electron–electron double resonance of free radicals in solution. *J. Chem. Phys.* **48**, 4211–4226 (1968)
45. V.A. Benderskii, L.A. Blyumenfel'd, P.A. Stunzhas, F.A. Sokolov, Double electron-electron resonance of triplet excitons in ion-radical salts. *Nature* **220**, 365–367 (1968)
46. N. Kocherginsky, H.M. Swarts, *Nitroxide spin labels: Reactions in biology and chemistry* (CRC Press, 1995)
47. L.J. Berliner (ed.), *Spin Labeling: Next Millennium, Biological Magnetic Resonance* (Book 14) (Springer, 1998)
48. G.I. Likhtenshtein, *Biophysical Labeling Methods in Molecular Biology* (Cambridge University Press, Cambridge, N.Y., 1993)
49. G.I. Likhtenshtein, J. Yamauchi, S. Nakatsuji, A.I. Smirnov, R. Tamura, *Nitroxides: Application in Chemistry, Biomedicine, and Materials Science* (WILEY-VCH, Weinheim, 2008)

50. O.Y. Grinberg, A.A. Dubinskii, V.F. Shuvalov, L.G. Oranskii, V.I. Kurochkin, Y.S. Lebedev, EPR submillimeter spectroscopy of free radicals. *Doklady Akademii Nauk SSSR* **230**, 884–887 (1976)
51. K. Moebius, W. Lubitz, N. Cox, A. Savitsky, Biomolecular epr meets nmr at high magnetic fields. *Magnetochemistry* **4**, 50 (2018)
52. L.B. Volodarsky, V.A. Reznikov, V.I. Ovcharenko, *Synthetic Chemistry of Stable Nitroxides* (CRC Press Inc, Boca Raton, FL, USA, 1994)
53. L.B. Volodarsky, I.A. Grigor'ev, R.Z. Sagdeev, Stable imidazoline nitroxides, in *Biological Magnetic Resonance*, vol. 2, ed. by L. Berliner, J. Reuben (Plenum Press, 2000), p. 73
54. E.J. Hustedt, A.H. Beth, Structural information from CW-EPR spectra of dipolar-coupled nitroxide spin-labels, in *Biological Magnetic Resonance*, vol. 19, ed. by S.S. Eaton, G.R. Eaton, L.J. Berliner (2001)
55. J.H. Freed, New technologies in electron spin resonance. *Ann. Rev. Phys. Chem.* **51**, 655–689 (2000); D. Marsh, in *Handbook of Lipid Bilayers*, 2nd edn. (CRC Press, 2013)
56. A.K. Smith, J.H. Freed, Dynamics and ordering of lipid spin-labels along the coexistence curve of two membrane phases: an ESR study. *Chem. Phys. Lipids* **165**(3), 348–361 (2012)
57. M.A. Hemminga, L. Berliner, *ESR Spectroscopy in Membrane Biophysics* (Springer, 2007)
58. A.K. Vorobiev, N.A. Chumakova, D.A. Pomogailo, Y. Uchida, K. Suzuki, Y. Noda, R. Tamura, Determination of structural characteristics of all-organic radical liquid crystals based on analysis of the dipole—dipole broadened EPR spectra. *J. Phys. Chem. B* **118**, 1932–1942 (2014)
59. B.H. Robinson, C. Mailer, G. Drobny, Site-specific dynamics in experiments DNA. *Annu. Rev. Biophys. Biomol. Struct.* **26**, 629–635 (1997)
60. R.S. Keyes, Y.Y. Cao, E.V. Bobst, J.M. Rosenberg, A.M. Bobst, Spin-labeled nucleotide mobility in the boundary of the EcoRI endonuclease binding site. *J. Biomol. Struct. Dyn.* **14**, 163–172 (1996)
61. R.M. Marupov, P.K. Bobodzhanov, I.K. Usupov, E.N. Frolov, G.I. Likhtenshtein, Study of temperature stability of cotton fibers by spin labeling. *Biofizika* **24**, 519–523 (1979)
62. I.K. Ysupov, G.I. Likhtenshtein, Study of microstructure and molecular dynamics of cotton and cellulose fibers by methods of physical labels. *Int. Res. J. Pure & Appl. Chemistry*. **6**(3), 105–119 (2015)
63. S.S. Eaton, G.R. Eaton, Interaction of spin labels with transition metals. *Coord. Chem. Rev.* **83**, 29–72 (1988)
64. A.V. Kulikov, E.S. Cherepanova, V.R. Bogatyrenko, Determination of the closest distance between a radical and a paramagnetic Ion. *Theor. Exper. Chem.* **17**, 618–626 (1981)
65. J.S. Hyde, L. Dalton, Very slowly tumbling spin labels: adiabatic rapid passage. *Chem. Phys. Lett.* **16**, 568–572 (1972)
66. G.I. Likhtenshtein, Depth of immersion of paramagnetic centers. in *Magnetic Resonance in Biology*, vol. 19, ed. by L. Berliner, S. Eaton, G. Eaton (2000), pp. 309–347
67. D.H. Solomon, E. Rizzardo, P. Cacioli, *Eur. Pat. Appl.* (1985)
68. P.G. Griffiths, P.G.E. Rizzardo, D.H. Solomon, Initiation pathways in the polymerization of alkyl methacrylates with tert-butoxy radicals. *J. Macromol. Sci., Chem. A* **17**, 45–50 (1982)
69. D.H. Solomon, Genesis of the CSIRO polymer group and the discovery and significance of nitroxide-mediated living radical polymerization. *J. Polym., Part A: Polym. Chem.* **43**(23), 5748 (2005)
70. D.F. Grishin, I.D. Grishin, Controlled radical polymerization: prospects for application for industrial synthesis of polymers (Review) *Russ. J. Appl. Chem.* **84**(12), 2021–2028 (2011)
71. H. Fisher, M. Souaille, The Persistent radical effect in living radical polymerization –border cases and side-reactions. *Macromol. Symp.* **174**, 231–240 (2001)
72. M. Edeleva, G. Audran, S. Marque, E. Bagryanskaya, Smart control of nitroxide-mediated polymerization initiators' reactivity by pH, complexation with metals, and chemical transformations. *Materials (Basel)* **12**(5), 688 (2019)
73. E.G. Bagryanskaya, S.R.A. Marque, Kinetic aspects of nitroxide mediated polymerization. in *Nitroxide Mediated Polymerization: From Fundamentals to Applications in Materials Science*, ed. by Gimes (RCS, 2015), pp. 45–113

74. V.I. Krinichny, *2-mm Wave band EPR Spectroscopy of Condensed Systems*. (CRC Press, Boca Raton, 1995)
75. S.K. Misra, J.H. Freed, Molecular motions, *Multifrequency Electron Paramagnetic Resonance*, ed. by S.K. Misra (2011), pp. 497–544
76. G.R. Eaton, S.S. Eaton, Multifrequency electron spin-relaxation times, in *Distance Measurements in Biological Systems by EPR Biological Magnetic Resonance*, vol. 19, ed. by L.J. Berliner, S. Eaton, G.R. Eaton (Springer, 2000), pp. 719–753
77. A.D. Milov, K.M. Salikhov, Y.D. Tsvetkov, *Fiz. Tverd. Tela (Leningrad)* **15**, 1187 (1973)
78. A.D. Milov, Y.D. Tsvetkov, A.G. Maryasov, M. Gobbo, C. Prinzivalli C.M. De Zotti, F. Formaggio, C. Toniolo, Conformational properties of the spin-labeled tylopeptin B and heptaibin peptaibiotics based on PELDOR spectroscopy. *Appl. Magn. Res.* **44**, 495–508 (2013)
79. P.P. Borbat, J.H. Freed, Multiple-quantum ESR and distance measurements. *Chem. Phys. Lett.* **313**, 145–154 (1999)
80. A. Schweiger, G. Jeschke, *Principles of Pulse Electron Paramagnetic Resonance* (Oxford University Press, Oxford, 2001)
81. P.P. Borbat, J.H. Freed, Double-quantum ESR and distance measurement. in *Biological Magnetic Resonance*, vol. 19, ed. by L.J. Berliner, S. Eaton, G.R. Eaton (Springer, 2001), pp. 383–460
82. A.D. Milov, R.P. Samoilova, Y.D. Tsvetkov, V.A. Gusev, F.M. Formaggio, M. Crisma, C. Toniolo, J. Raap, Spatial distribution of spin-labeled trichogin GA IV in the gram-positive bacterial cell membrane determined from PELDOR data. *Appl. Magn. Reson.* **23**, 81–95 (2002)
83. M.-T. Türke, M. Bennati, Saturation factor of nitroxide radicals in liquid DNP by pulsed ELDOR experiments. *Phys. Chem. Chem. Phys.* **13**, 3630–3633 (2011)
84. Y.-W. Chiang, A.J. Costa-Filho, B. Baird, J.H. Freed, 2D-ELDOR study of heterogeneity and domain structure changes in plasma membrane vesicles upon cross-linking of receptors. *J. Phys. Chem. B* **115**, 10462–10469 (2011)
85. T.I. Smirnova, A.I. Smirnov, S. Pachtchenko, O.G. Poluektov, Geometry of hydrogen bonds formed by lipid bilayer nitroxide probes: a high frequency pulsed ENDOR/EPR study. *J. Am. Chem. Soc.* **129**, 3476–3477 (2007)
86. S. Saxena, J.H. Freed, Theory of double quantum two-dimensional electron spin resonance with application to distance measurements. *J. Chem. Phys.* **107**, 1317–1134 (1997)
87. S.A. Dzuba, A. Kawamori, Selective hole burning in EPR: spectral diffusion and dipolar broadening. *Concepts Magn. Reson.* **8**, 49–61 (1996)
88. A.D. Milov, Y.D. Tsvetkov, A.G. Maryasov, M. Gobbo, C. Prinzivalli C, M. De Zotti, F. Formaggio, C. Toniolo, Conformational properties of the spin-labeled tylopeptin B and heptaibin peptaibiotics based on PELDOR spectroscopy. *Appl. Magn. Res.* **44**, 495–508 (2013)
89. G. Jeschke, M. Panier, H.W. Spies, Double electron-electron resonance, in *Distance Measurements in Biological Systems by EPR*, in *Biological Magnetic Resonance*, vol. 19, ed. by L.J. Berliner, S. Eaton, G.R. Eaton (Springer Verlag, 2001), pp. 493– 512
90. G. Jeschke, DEER distance measurements on proteins. *Ann. Rev. Phys. Chem.* **63**, 419–446 (2012)
91. I. Krstić, R. Hänsel, O. Romainczyk, J.W. Engels, V. Dötsch, T.F. Prisner, Long-range distance measurements on nucleic acids in cells by pulsed EPR spectroscopy. *Angew. Chem. Int. Ed. Engl.* **50**, 5070 (2011)
92. P.P. Borbat, E.R. Georgieva, J.H. Freed, Improved sensitivity for long-distance measurements in biomolecules: five-pulse double electron-electron resonance. *J. Phys. Chem. Lett.* **4**, 170–175 (2013)
93. W.L. Hubbell, R.L. Gross, M.A. Lietzow, *Curr Opin Struct Biol* **8**, 649–656 (1988)
94. P.P. Borbat, H. Mchaourab, J.H. Freed, Protein structure determination using long-distance constraints from double-quantum coherence ESR: study of T4 lysozyme. *J. Am. Chem. Soc.* **124**, 5304–5314 (2002)
95. B. Selmke, P.P. Borbat, N. Chen, V. Raghavan, J.H. Freed, W.E. Trommer, Open and closed form of maltose binding protein in its native and molten globule state as studied by electron paramagnetic resonance spectroscopy. *Biochemistry* **57**(38), 5507–5512 (2018)

96. A. Feintuch, G. Otting, D. Goldfarb, Gd³⁺ spin labeling for measuring. Distances in biomacromolecules: why and how? in *Methods in Enzymology*, vol. 563 (2015), pp. 416–457
97. C. Gmeiner, G. Dorn, F.H.T. Allain, G. Jeschke, M. Yulikov, Spin labelling for integrative structure modelling: a case study of the polypyrimidine-tract binding protein 1 domains in complexes with short RNAs. *Phys. Chem. Chem. Phys.* **19**, 28360 (2017)
98. G.W. Reginsson, N.C. Kunjir, S.T. Sigurdsson, O. Schiemann, Trityl radicals: spin labels for nanometer-distance measurements. *Chemistry* **18**, 13580–13584 (2012)
99. M.K. Bowman, C. Mailer, H.J. Halpern, The solution conformation of triarylmethyl radicals. *J. Magn. Reson.* **172**, 254 (2005)
100. O. Krumkacheva, E. Bagryanskaya, EPR-based distance measurements at ambient temperature. *J. Magn. Reson.* **280**, 117–126 (2017)
101. W.K. Subczynski, J.S. Hyde, The diffusion-concentration product of oxygen in lipid bilayers using the spin-label T₁ method. *Biochim. Biophys. Acta* **643**, 283–291 (1981)
102. R. Springett, H.M. Swartz, Measurements of oxygen in vivo: overview and perspectives on methods to measure oxygen within cells and tissues. *Antioxid. Redox Signal.* **9**, 1295–1301 (2007)
103. G. Ilangovan, J.L. Zweier, P. Kuppasamy, Oxygen sensing. *Methods Enzymol.* **381**, 747–762 (2004)
104. W.K. Subczynski, L. Mainali, T.G. Camenisch, W. Froncisz, J.S. Hyde, Spin-label oximetry at Q- and W-band. *J. Magn. Reson.* **209**, 142–148 (2011)
105. V.V. Khrantsov, L.M. Weiner, I.A. Grigor'ev, L.B. Volodarsky, Proton exchange in stable nitroxyl radicals. ESR study of the pH of aqueous solutions. *Chem. Phys. Lett.* **91**, 69–72 (1982)
106. I.A. Kirilyuk, A.A. Bobko, V.V. Khrantsov, I.A. Grigor'ev, Nitroxides with two pK values—useful spin probes for pH monitoring within a broad range”. *Org. Biomol. Chem.* **3**, 1269 (2005)
107. S. Koda, J. Goodwin, V.V. Khrantsov, H. Fujii, H. Hirata, Electron paramagnetic resonance-based pH Mapping using spectral-spatial imaging of sequentially scanned spectra. *Anal. Chem.* **84**, 3833–3837 (2012)
108. V.V. Khrantsov, V.I. Yelinova, L.M. Weiner, T.A. Berezina, V.V. Martin, L.B. Volodarsky, Quantitative determination of SH groups in low- and high-molecular-weight compounds by an electron spin resonance method. *Anal. Biochem.* **182**(1), 58–63 (1989)
109. L.M. Weiner, Quantitative determination of thiol groups in low- and high-molecular-weight compounds by an electron paramagnetic resonance. *Methods Enzymol.* **251**, 87–105 (1995)
110. M. Tamura, Y. Nakazawa, D. Shiomi, K. Nozawa, Y. Hosokoshi, M. Ishikawa, M. Takahashi, M. Kinoshita, Bulk ferromagnetism in the β -phase crystal of the *p*-Nitrophenyl nitronyl nitroxide radical. *Chem. Phys. Lett.* **186**, 401–404 (1991)
111. D.B. Amabilino, J. Veciana, Nitroxide-based organic magnet, in *Magnetism: Molecules to Materials II*, ed. by J.S. Miller, M. Drillon (Wiley-VCH, Weinheim, Germany, 2001), pp. 1–60
112. R. Tamura, Organic functional materials containing chiral nitroxide radical units, in *Nitroxides: Application in Chemistry, Biomedicine, and Materials Science*, ed. by G.I. Likhtenstein, J. Yamauchi, S. Nakatsuji, A. Smirnov, R. Tamura (Weinheim, WILEY-VCH, 2008), pp. 303–331
113. A. Rajca, From high-spin organic molecules to organic polymers with magnetic ordering. *Chem. Eur. J.* **8**, 4834–4841 (2002)
114. S.L. Veber, M.V. Fedin, K.Y. Maryunina, A. Potapov, D. Goldfarb, E. Reijerse, W. Lubitz, R.Z. Sagdeev, V.I. Ovcharenko, E.G. Bagryanskaya, Temperature-dependent exchange interaction in molecular magnets Cu(hfac) 2LR studied by EPR: methodology and interpretations. *Inorg. Chem.* **50**, 10204–10212 (2011)
115. H.M. Swartz, N. Khan, V.V. Khrantsov, Use of electron paramagnetic resonance spectroscopy to evaluate the redox state in vivo. *Antioxid. Redox Signal.* **9**, 1757–1771 (2007)
116. N. Kocherginsky, H.M. Swarts, in *Nitroxide Spin Labels. Reactions in Biology and Chemistry* (CRC Press, 1995)

117. P. Kuppusamy, M.C. Krishna, EPR imaging of tissue redox status. *Curr. Top. Biophys.* **26**, 29–34 (2002)
118. G.I. Likhtenshtein, Nitroxide redox probes and traps, nitron spin traps, in *Nitroxides: Application in Chemistry, Biomedicine, and Materials Science*, ed. by G.I. Likhtenshtein, J. Yamauchi, S. Nakatsuji, A. Smirnov, R. Tamura (WILEY-VCH, Weinheim, 2008), pp. 303–331
119. G.I. Likhtenshtein, V.R. Bogatyrenko, A.V. Kulikov, K. Hideg, H.O. Hankovsky, N.V. Lukoianov, A.I. Kotelnikov, B.S. Tanaschelchuk, Study of superflow motion in solid solutions by the method of physical probes. *Dokl. Akad. Nauk SSSR* **253**, 481–484 (1980)
120. I.M. Bystryak, G.I. Likhtenshtein, A.I. Kotelnikov, O.H. Hankovsky, K. Hideg, The influence of the molecular dynamics of the solvent on the photoreduction of nitroxyl-radicals. *Russ. J. Phys. Chem.* **60**, 1679–1983 (1986)
121. V.R. Vogel, E.T. Rubtsova, G.I. Likhtenshtein, K. Hideg, Factors affecting photoinduced electron transfer in a donor-acceptor pair (D-A) incorporated into bovine serum albumin. *J. Photochem. Photobiol. A, Chem.* **83**, 229–236 (1994)
122. E. Lozinsky, V.V. Martin, T.A. Berezina, A. Shames, A.L. Weis, G.I. Likhtenshtein, Dual fluorophore-nitroxide probes for analysis of vitamin C in biological liquids. *J. Biochem. Biophys. Meth.* **38**, 29–42 (1999)
123. N.V. Blough, D.J. Simpson, Chemically mediated fluorescence yield switching in nitroxide-fluorophore adducts, optical sensors of radical/redox reactions. *J. Am. Chem. Soc.* **110**, 1915–1917 (1988)
124. J.P. Allen, M.C. Pfrunder, J.C. McMurtrie, S.T. Bottle, J.P. Blinco, K.E. Fairfull-Smith, BODIPY-based profluorescent probes containing Meso- and β -Substituted Isoindoline Nitroxides European. *J. Org. Chem.* **3**, 476–483 (2017)
125. R. Braslau, F. Rivera III, E. Lilie, M. Cottman, Urushiol detection using a profluorescent nitroxide. *J. Org. Chem.* **78**, 238–245 (2013)
126. G.I. Likhtenshtein, K. Ishii, S. Nakatsuji, Dual chromophore-nitroxides: novel molecular probes, photochemical and photophysical models and magnetic materials. *Photochem. Photobiol.* **83**, 871–881 (2007)
127. N. Khan, B.B. Williams, H.M. Swartz, Clinical applications of in vivo EPR: rationale and initial results. *Appl. Magn. Reson.* **30**, 185–199 (2006)
128. J.B. Mitchell, M.C. Krishna, P. Kuppusamy, J.A. Cook, A. Russo, Protection against oxidative stress by Nitroxides. *Exp. Biol. Med.* **226**, 620–621 (2001)
129. V.V. Khrantsov, In vivo spectroscopy and imaging of nitroxide probes. in *Nitroxides—Theory, Experiment and Applications*, ed. by A.I. Kokorin (September, 2012), pp. 317–346
130. G.I. Likhtenshtein, Biomedical and medical application of nitroxides, in *Nitroxides: Application in Chemistry, Biomedicine, and Materials Science*, ed. by G.I. Likhtenshtein, J. Yamauchi, S. Nakatsuji, A. Smirnov, R. Tamura (WILEY-VCH, Weinheim, 2008), pp. 371–401
131. E.G. Janzen, Y.Y. Wang, R.V. Shetty, Spin trapping with alpha-pyridyl 1-oxide N-tert-butyl nitrones in aqueous solutions. A unique electron spin resonance spectrum for the hydroxyl radical adduct. *J. Am. Chem. Soc.* **100**, 2923–2925 (1978)
132. F.A. Villamena, E.J. Locigno, A. Rockenbauer, C.M. Hadad, J.L. Zweier, Theoretical and experimental studies of the spin trapping of inorganic radicals by 5, 5-dimethyl-1-pyrroline N-oxide (DMPO). 2. Carbonate radical anion. *J. Phys. Chem. A* **111**, 384–391
133. R.P. Mason, Free using anti-5, 5-dimethyl-1-pyrroline N-oxide (anti-DMPO) to detect protein radicals in time and space with immuno-spin trapping. *Radic. Biol. & Med.* **36**, 1214–1223 (2004)
134. S. Schocha, V. Senb, S. Gajewska, V. Golubev, B. Straucha, A. Hartwig, B. Köberle, Activity profile of the cisplatin analogue PN149 in different tumor cell lines. *Biochem. Pharmacol.* **156**, 109–119 (2018)
135. M. Balog, T. Kálai, J. Jekő, H.-J. Steinhoff, M. Engelhard, K. Hideg, Synthesis of New 2, 2, 5, 5-Tetramethyl-2, 5-dihydro-1H-pyrrol-1-yloxy radicals and 2-Substituted-2, 5, 5-trimethylpyrrolidin-1-yloxy radicals based α -amino acids. *Synlett* **14**, 2591 (2004)
136. O.D. Zakharova, T.S. Frolova, Y.V. Yushkova, E.I. Chernyak, A.G. Pokrovsky, M.A. Pokrovsky, S.V. Morozov, O.I. Sinitsina, I.A. Grigor'ev, G.A. Nevinsky, Antioxidant and

- antitumor activity of trolox, trolox succinate, and α -tocopheryl succinate conjugates with nitroxides. *Eur. J. Med. Chem.* **122**, 127–137 (2016)
137. S. Eaton, G. Eaton, Determination of distance based on T_1 and T_2 effects, in *Magnetic Resonance in Biology*, ed. by L. Berliner, S. Eaton, G. Eaton (Kluwer Academic Publishers, Dordrecht), pp. 348–382

Chapter 2

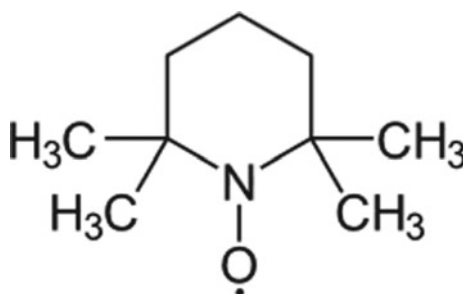
Nitroxide Basic Physical Properties



2.1 Introduction

Nitroxides belong to the class of heterocyclic compounds with typical structures of five- or six-membered heterocyclic derivatives of piperidine, pyrrolidine, imidasoline, imidasolidine, nitronyl, in particular (Figs. 1.2 and 1.7). Ninety-seven nitroxide structures were listed in a table presented in comprehensive review [1].

In a non-conjugated nitroxide



the unpaired electron is located mainly on the nitrogen and oxygen atoms and only slight delocalized for adjacent alkyl groups. The unpaired electron is considered to reside in the p orbital. According to a nitroxide molecular orbitals (MO) diagram, which is in the first approximation close to nitric oxide diagram, N–O-moiety has five fully bonding orbitals with unpaired electron resulting in one on of the fourth antibonding $\pi^*\pi^*$ -orbitals (single occupied molecular orbital (SOMO) (Fig. 2.1). The nitrogen and oxygen are held together by 2.5 bonds. Nitroxide radicals feature a $(\pi)2(\pi^*)1$ three-electron bond between a nitrogen atom and an oxygen one.

The unpaired electron in the antibonding orbitals weakens over bonding of the nitrogen to oxygen (N–O \cdot). Therefore, the transfer of the electron away from the antibonding orbital significantly stiffens the N–O \cdot^+ bond. Conversely, the transfer of

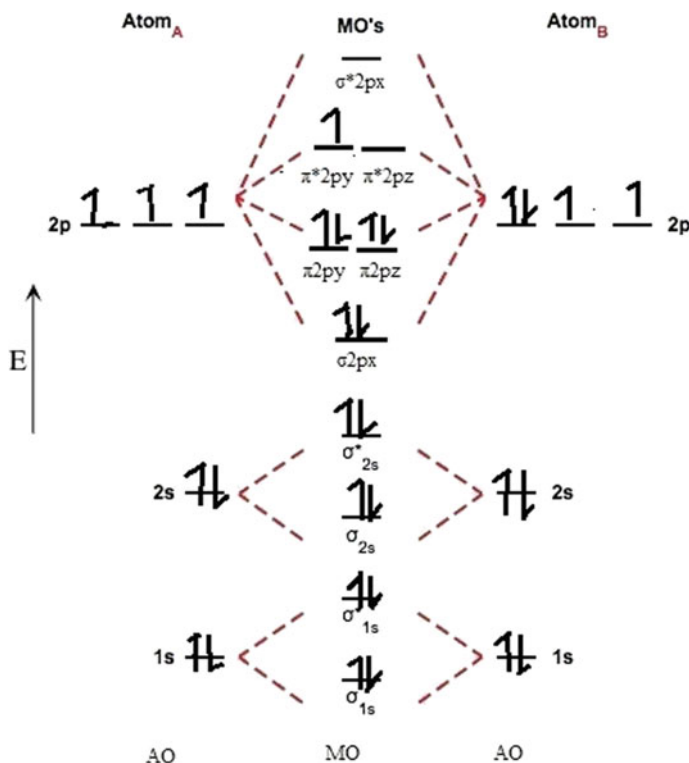


Fig. 2.1 Molecular orbitals diagram of NO fragment. https://en.wikipedia.org/wiki/Molecular_orbital_diagram

additional electron density into the antibonding additionally weakens over the N–O[−] bond. The aforementioned features of the NO molecule substantially determine its physicochemical properties and redox potential, in particular. The resulting magnetic moment is determined by the electronic spin only. The value of the intrinsic electron spin moment is a product of *g*-factor (free electron *g*-value is 2.002319) and Bohr magneton ($\beta_B = 9.274009994(57) \times 10^{-24} \text{ J T}^{-1}$).

The nitroxide radical fragments are stabilized by the steric screening imparted by its four adjacent methyl groups and by quantum mechanical interaction of the unpaired electron on oxygen and electron pair on nitrogen (three electron bond). In certain conditions, these structural features protect the radicals from reduction or other processes.

The preference for a planar (sp² hybridization) or pyramidal (sp³ hybridization) geometry around the N atom and the partitioning of the spin density between the N and O atoms are strongly dependent on the nature of the substituents. The change in hybridization of the nitrogen atom from sp² to sp³ that occurs on reduction causes

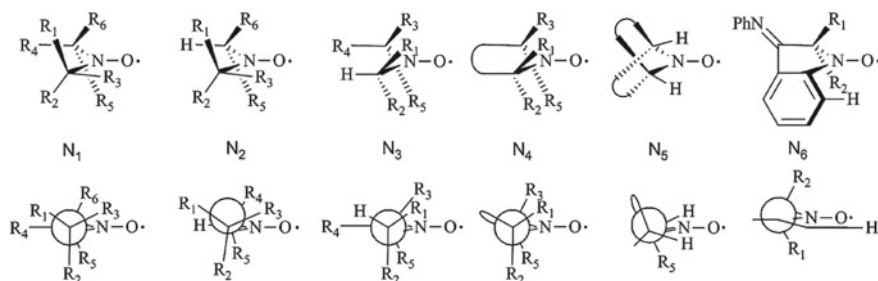


Fig. 2.2 Six deduced conformations (N1–N6) around the nitroxide center and their corresponding Newman projections: N1 (has a syn and an anti b-R group), N2 (with anti b-hydrogen atom and a syn b-R group), N3 (with an anti-R group and an anti-hydrogen atom), N4 (with an anti-ring), N5 (with two syn hydrogen atoms), and N6 (with the radical centre fused to an aromatic ring). Reprint from reference [1], Copyright 2012, American Chemical Society

change torsional strain which is small for six-membered rings, but increases for five-membered rings. Conformation N1–N6 radicals around the nitroxide center and their corresponding Newman projections are presented in Fig. 2.2 [1].

Unique chemical stability of nitroxide is partly due to the strong delocalized three-electron bond within the radical center between the nitrogen and the oxygen atoms conferring its substantial thermodynamic stability, and as a result, prohibition on dimerization between the radicals with the free energy of about 146 kJ/mol. Insignificant weight of the ionic resonant structure 95.6 kJ/mol is actually extinguished nucleophilic ability of нитроксидов [2].

2.2 Spin Electron–Spin Nuclear Interactions in Nitroxides

The total spin Hamiltonian of the system of an electron and many nuclear spins are given by [3–5]

$$\hat{H} = \hat{H}_e + \hat{H}_N + \hat{H}_{eN} + \hat{H}_{NN}, \quad (2.1)$$

and composed of the single-spin Zeeman energies, Hamiltonian for interaction in the applied magnetic field along the z -axis, the hyperfine interaction and the intrinsic nuclear–nuclear interaction, respectively. Generally, both the spin and orbital angular momentums of the electron contribute to nuclear magnetic moment. The following equation shows the total energy related to electron transitions in EPR:

$$\Delta E = g_e \mu_e S_z B + \sum g_{Ni} \mu_{Ni} I_{Ni} (1 - \sigma_i) + \sum a_i S_z I_{Ni} \quad (2.2)$$

The first two terms correspond to the Zeeman energy of the electron and the nucleus of the system, respectively. The third term is the hyperfine coupling between the electron and nucleus where a_i is the hyperfine coupling constant.

Two mechanisms with the different physical origins can contribute in coupling between electron and nuclear spins. The hyperfine interaction between the electron and the nuclear spins consists of the isotropic Fermi contact interaction and the anisotropic dipole–dipole interaction. The Fermi contact interaction is the magnetic interaction between an electron and an atomic nucleus when the electron is inside that nucleus. The electron–nuclear spin interactions for an electron in an s -symmetry orbital *non-s-symmetry orbital* are expressed as follows:

$$H_{\text{HF}} = \frac{16\pi}{3} \gamma_I \mu_B \mu_N \delta(\mathbf{r}) [\mathbf{S} \cdot \mathbf{I}], \quad l = 0 \quad (2.3)$$

where γ_I , μ_B , and μ_N are the gyromagnetic factor of the nuclear spin, the Bohr magneton, and the nuclear magneton, respectively. \mathbf{S} and \mathbf{I} are the spin operators for the electron and the nucleus, and l is the angular momentum operator for the electron. The nuclear magnetic moment m_I originating from the nuclear spin quantum number I is $m_I = 2I + 1$. Therefore, for nitrogen isotopes ^{14}N ($I = 1$), $m_I = 1, 0, -1$ and for ^{15}N ($I = 1/2$), $m_I = 1/2, -1/2$. Selection rules for ESR-transitions: $\Delta m_S = \pm 1$, $\Delta m_I = 0$.

The contact interaction is given by

$$\hat{H}_{eN} = \sum_n a_n \hat{\mathbf{S}}_e \cdot \hat{\mathbf{J}}_n, \quad (2.4)$$

where $\hat{\mathbf{S}}_e$ and $\hat{\mathbf{J}}_n$ are the spin and nucleus operators, respectively, and

$$a_n = \frac{\mu_0}{4\pi} \gamma_e \gamma_n \frac{8\pi}{3} |\Psi(\mathbf{R}_n)|^2, \quad (2.5)$$

where μ_0 is the vacuum magnetic permeability, \mathbf{R}_n denotes the coordinates of the n th nucleus, γ_n and γ_e are the nuclear gyromagnetic ratio and the electron gyromagnetic ratio, respectively; $|\Psi(\mathbf{R}_n)|^2$ is the spin density of s -electron on the nucleus ρ . The intrinsic interaction between nuclear spins includes the direct dipole–dipole interaction, the indirect interactions mediated by virtual excitation of electron–hole pairs, and the intranuclear quadrupole interaction.

The second mechanism is dipole–dipole interaction between electron and nuclear spins and is given by the term

$$\hat{H}_{NN}^d = \sum_{n < m} \frac{\mu_0}{4\pi} \frac{\gamma_n \gamma_m}{R_{n;m}^3} \left(\hat{\mathbf{J}}_n \cdot \hat{\mathbf{J}}_m - \frac{3 \hat{\mathbf{J}}_n \cdot \mathbf{R}_{n;m} \mathbf{R}_{n;m} \cdot \hat{\mathbf{J}}_m}{R_{n;m}^2} \right), \quad (2.6)$$

$$\begin{aligned} \mathcal{H}_{\text{dip}} &= -g\mu_B g_n \mu_n [\mathbf{S}_x \mathbf{S}_y \mathbf{S}_z] \cdot \begin{bmatrix} \left\langle \frac{r^2 - 3x^2}{r^5} \right\rangle & -\left\langle \frac{3xy}{r^5} \right\rangle & -\left\langle \frac{3xz}{r^5} \right\rangle \\ -\left\langle \frac{3xy}{r^5} \right\rangle & \left\langle \frac{r^2 - 3y^2}{r^5} \right\rangle & -\left\langle \frac{3yz}{r^5} \right\rangle \\ -\left\langle \frac{3xz}{r^5} \right\rangle & -\left\langle \frac{3yz}{r^5} \right\rangle & \left\langle \frac{r^2 - 3z^2}{r^5} \right\rangle \end{bmatrix} \cdot \begin{bmatrix} \mathbf{I}_x \\ \mathbf{I}_y \\ \mathbf{I}_z \end{bmatrix} \\ &= \mathbf{S} \cdot \mathbf{A}_{\text{dip}} \cdot \mathbf{I} \end{aligned}$$

Fig. 2.3 Hamiltonian for anisotropic hyperfine dipolar of anisotropic electron spin with anisotropic nuclear spin [4]

where $\mathbf{R}_{n;m}$ is the distance between electron and nucleus. $\hat{\mathbf{J}}_m$ (S_e) and $\hat{\mathbf{J}}_n$ are the spin and nucleus operators.

For asymmetric molecules, the dipolar interaction depends on the electron spin–electron nuclei distances and on their orientations, which links interacting spins referred to the direction of the applied magnetic field. This interaction can be described by a matrix of parameters A_{xx} , A_{yy} , and A_{zz} , corresponding to the principal axes of the radical. The appearance of the spectrum will change depending on the orientation of the molecule relative to the magnetic field.

For anisotropic hyperfine dipolar of anisotropic electron spin with anisotropic nuclear spin, Hamiltonian is shown in Fig. 2.3 [4].

$$\begin{aligned} \mathcal{H}_{\text{dip}} &= -g\mu_B g_n \mu_n [\mathbf{S}_x \mathbf{S}_y \mathbf{S}_z] \cdot \begin{bmatrix} \left\langle \frac{r^2 - 3x^2}{r^5} \right\rangle & -\left\langle \frac{3xy}{r^5} \right\rangle & -\left\langle \frac{3xz}{r^5} \right\rangle \\ -\left\langle \frac{3xy}{r^5} \right\rangle & \left\langle \frac{r^2 - 3y^2}{r^5} \right\rangle & -\left\langle \frac{3yz}{r^5} \right\rangle \\ -\left\langle \frac{3xz}{r^5} \right\rangle & -\left\langle \frac{3yz}{r^5} \right\rangle & \left\langle \frac{r^2 - 3z^2}{r^5} \right\rangle \end{bmatrix} \cdot \begin{bmatrix} \mathbf{I}_x \\ \mathbf{I}_y \\ \mathbf{I}_z \end{bmatrix} \\ &= \mathbf{S} \cdot \mathbf{A}_{\text{dip}} \cdot \mathbf{I} \end{aligned}$$

2.3 Relationships Between the Structure and Properties of Nitroxide

Review [6] described the relationships between the structure and properties of nitroxide spin labels, methods for their synthesis, advances in methods for their incorporation into biomolecules, and selected examples of applications in biomolecule structural investigations. Various aspects in this area are covered in the original articles.

Density functional and ab initio (MP2) coupled cluster methods indicated that the spin density is distributed roughly evenly between the oxygen and nitrogen atoms except for $(\text{CF}_3)_2$.

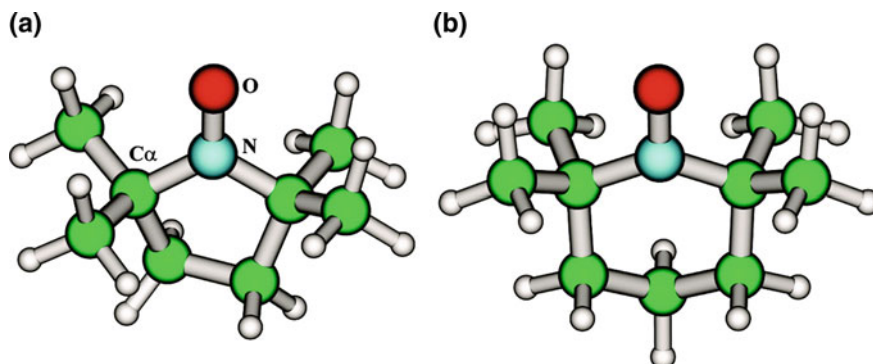


Fig. 2.4 Structure and label of the Proxyl **a** and Tempo **b** spin-probe molecules Michele Pavone [8]. Reprint from reference [8], Copyright 2010, American Chemical Society

- Synthesis and properties of diradicals in which nitronyl nitroxide fragments and a fused-thiophene bridge lie in the range $2.6\text{--}8.5^\circ$ were described [7]. The planarity of **nitroxides** makes the Kekulé-type coupler units effective bridges to transmit magnetic interactions by a spin polarization mechanism. According to the magnetic susceptibility measurements, supported by density functional theory calculations, the singlet–triplet energy splitting ($2J/k_B$) ranges from -130 to -80 K. The singlet diradicals **D** demonstrated two one-electron reversible electrochemical oxidation peaks and two-electron quasi-reversible reduction peaks resulting in the formation of the corresponding bis(oxoammonium) dication or bis(aminooxidane) dianion.

Stereoelectronic, environmental, and dynamical effects in the proxyl and TEMPO (Fig. 2.4) were investigated in [8]. The parameter-free PBE023 density functional, which includes an amount of exact exchange, and the polarized double-basis set N07D tailored for DFT-based calculations of magnetic parameters were employed.

According to the calculation, in the planar NO moiety of Proxyl, both N and O atoms exhibit a sp^2 hybridization, whereas in the non-planar case of TEMPO, the N hybridization is close to sp^3 . It was shown that pyramidalization at the nitrogen center allows for the direct involvement of the nitrogen s-type orbital in the SOMO (Fig. 2.5), leading to a large direct contribution to the Fermi contact term.

The following findings were also pointed out: (1) Vibrational effects are relevant in the case of Proxyl, with a shift of -2 G, whereas they are negligible in the case of TEMPO. (2) Dynamical effects are not markedly affected by the presence of the solvent; i.e., the $hccN$ shifts from the minimum energy structure are -2 G in the case of Proxyl and smaller than 1 G for TEMPO. (3) The isotropic nitrogen hyperfine coupling constant ($hccN$) experimental values in nonpolar solvents were found to be 14.2 and 15.28 G for Proxyl and TEMPO, respectively. (4) The $hccN$ value increases when going from a planar to a pyramidal nitroxide conformation. (5) The planar structure is the minimum energy configuration for Proxyl, while in the case of TEMPO it corresponds to a transition state governing inversion between two equivalent pyramidal energy minima. (6) Calculating the $hccN$ and Δg_{iso} values

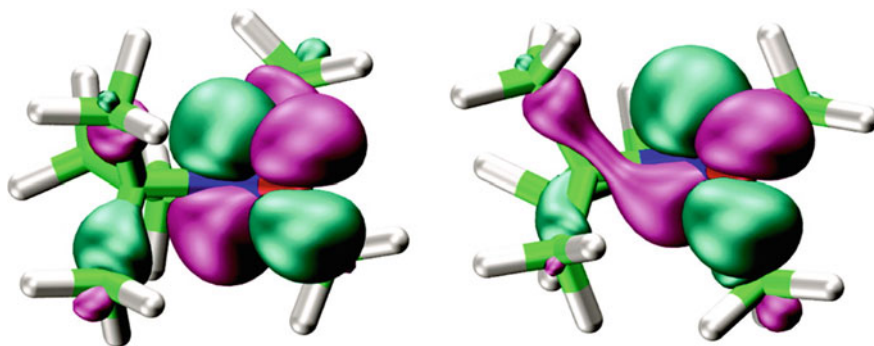


Fig. 2.5 Isodensity surface of Proxyl's SOMO from a planar configuration (left) to a pyramidal one (right) [8]. Reprint from reference [8], Copyright 2010, American Chemical Society

for the Proxyl and TEMPO is close. (7) The hccN shift, when going from gas phase to nonpolar solution, is in qualitative agreement with the experimental observations regarding a similar nitroxide (-1 G). Three tables summarized data on structural and magnetic parameters of proxyl and TEMPO in the gas phase, structural and magnetic parameters of proxyl and TEMPO in DMSO and isotropic nitrogen hyperfine coupling constant.

The calculation of large nitroxides in condensed phases based on geometries, vibrational frequencies, and potential energy surfaces computed at the DFT level was carried out employing AMBER force-field program [9]. Environmental and short-time dynamic effects on the hyperfine and gyromagnetic g -factor tensors of Proxyl, TEMPO, and (2-methyl-3-oxo-2-phenyl-2,3-dihydro-1H-indol-1-yl)oxidanyl molecule (INDCO) were taken in consideration. The partial atomic charges were calculated with the restrained electrostatic potential (*RESP*) procedure, by fitting an electrostatic potential grid computed for the nitroxide molecules. The HF/6-31 G (d) level of theory was used for study the partial atomic charges. The suggested model is based on a least squares fitting of the electrostatic potential with the addition of hyperbolic restraints on the charges of non-hydrogen atoms, which reduce the charges on buried carbons. Molecular dynamic calculations for Proxyl led to the following sequence in the values of hcc (in G): 13.4 (vacuum), 13.9 (toluene), 15.3 (water), while experimental a_N are 14.2 and 16.4 for toluene and water, respectively. For TEMPO, hcc (in G) are 14.6, (vacuum), 15.0 (toluene), 16.4 (water), and experimental values are 15.5 and 17.3 for toluene and water, respectively. The minima and transition state together with their relative energies for structures of DTBN, Proxyl, and TEMPO were also calculated. For PROXYL, transition state energy calculated at AMBER level was found to be $2.56 \text{ kcal mol}^{-1}$, and for TEMPO, the correspondent value is $5.11 \text{ kcal mol}^{-1}$. The average number of solvent molecules coordinating the NO moiety is two in aqueous solution and one in methanol. For Proxyl, both water molecules lie in the molecular plane approximately along the directions of the two lone pairs. The calculation showed that the behavior of the g tensor is dominated

by component g_{xx} , and that Δg_{iso} and g_{xx} have parallel trends while g_{yy} and g_{zz} are almost unchanged, and dynamical effects do not influence the g tensor.

A systematic study of structure and physical properties of the INDCO has been undertaken [10]. Geometry optimization of INDCO performed by the QM (PBE0/N07D) or MM (AMBER) level produces an almost flat structure. A nitrogen isotropic hyperfine coupling constant (a_N) of 7.9 Gauss was calculated. Hyperfine coupling constants (in G) of the nitrogen and hydrogen atoms in the INDCO molecule were also calculated on the minimum structure in gas phase and in benzene and were listed in the table. The overall vibrational correction of a_N amounts 1.2 G. Calculated a_N values were found to be 9.1 G in gas phase and 9.3 G in benzene which is in agreement with experiment (9.25 G). The values of the g tensor computed on the energy minimum and those averaged along the MD trajectories (2.00593) are close to the experimental value of 2.00598.

Density functional and ab initio (MP2, coupled cluster) methods were used to obtain insight into the molecular structures, harmonic vibrational frequencies, inversion barriers, and hyperfine coupling constants of nitroxides: (i) acyclic: dimethylaminoxyl (Me_2NO), bis(trifluoromethyl)aminoxyl ($\text{CF}_3)_2\text{NO}$, and di-*tert*-butyl nitroxyl [$(\text{Me}_3\text{C})_2\text{NO}$]; (ii) cyclic: aziridine-N-oxyl, azetidine-N-oxyl, pyrrolidine-N-oxyl and piperidine-N-oxyl; and (iii) imino nitroxides [11]. Scheme of the optimized structures of several nitroxides studied in this work is shown in Fig. 2.6. The cyclic aziridine-N-oxyl exhibits an inversion barrier of $\sim 3500\text{ cm}^{-1}$ compared to

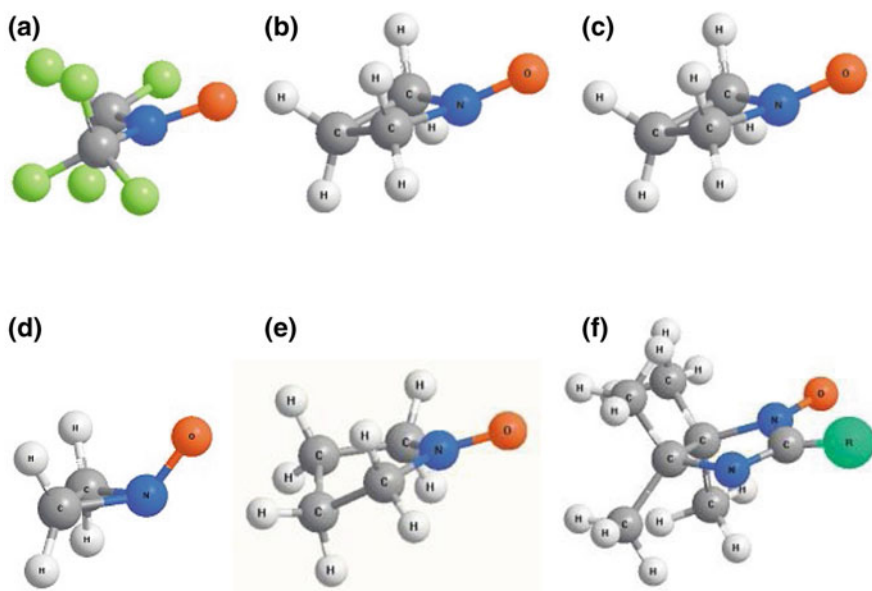
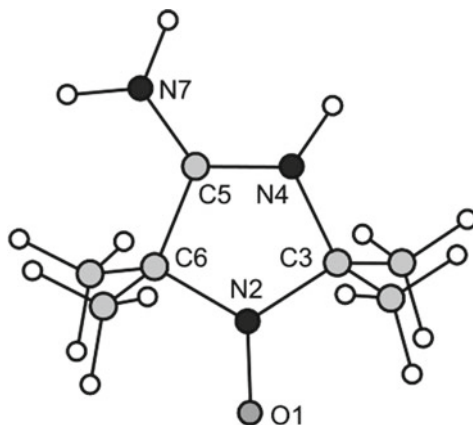


Fig. 2.6 Scheme of the optimized structures of **a** bis(trifluoromethyl)aminoxyl $(\text{CF}_3)_2\text{NO}$, **b** aziridine-N-oxyl, **c** azetidine-N-oxyl, **d** pyrrolidine-N-oxyl, **e** piperidine-N-oxyl, **f** imino nitroxide [11]. Reprint from reference [8], Copyright 2010, Schweizerische Chemische Gesellschaft

only $\sim hc\ 500\text{ cm}^{-1}$ for the other nitroxides. The possibilities that some of the chiral derivatives may be dominated by molecular parity violation in their dynamics were discussed.

Effects of solvent on structural and electronic characteristics of 4-amino-2,2,5,5-tetramethyl-3-imidazoline-N-oxyl (ATP)



were evaluated in detail, employing the density functional theory (DFT) [12]. All calculations were carried out with the use of the original program Priroda. The calculation an aqueous sphere around a spin label protonated at the position of the ring nitrogen N4, $\text{ATI}(\text{H}^+)$, was started with a small system ($\text{ATI}(\text{H}^+) + 2\text{H}_2\text{O}$) and then expanded to 41 water molecules when a complete hydrogen-bonded water network surrounding $\text{ATI}(\text{H}^+)$ was formed (Fig. 2.7). Calculations showed that (1) ATI protonation occurs at the nitrogen atom of the imidazoline ring rather than at the amino group. (2) Direct proton transfer between the amino group and N4 atom is hindered kinetically. (3) Spin density on the nitrogen atom of the nitroxide fragment increased with an extension of a water shell around ATI. (4) Protonation of ATI leads to a decrease in a spin density on the nitrogen atom of the nitroxide fragment $> \text{N}-\text{O}\cdot$. (5) The ring nitrogen N4 is characterized by higher affinity to proton, as compared to the amino group. (6) The energy of the transition state $[\text{ATI}-\text{H}^+]$ of the interconversion process $\text{ATI}(\text{H}^+) \rightleftharpoons \text{ATI}(-\text{NH}_3^+)$ is higher than the energies of $\text{ATI}(\text{H}^+)$ and $\text{ATI}(-\text{NH}_3^+)$ by 55.2 and 23.8 kcal/mol, respectively (Fig. 2.8). (7) The energy difference between $\text{EATI}(-\text{NH}_3^+)-(\text{H}_2\text{O})_{41}$ and $\text{EATI}(\text{H}^+)-(\text{H}_2\text{O})_{41}$ is 19.1 kcal/mol, which is smaller than E_{gas} . (8) Both protonation and hydration of ATI caused certain changes in calculated bond lengths and valence angles. The authors concluded that a hydrogen-bonded cluster of $\text{HO} n \geq 41$ water molecules could be considered as an appropriate model for simulation of ATI hydration effects.

The calculation also revealed the following peculiarities of the hydration process (Fig. 2.9): (1) The most significant changes in charge distribution occur in the nitroxide fragment $\text{N2}-\text{O1}$ and in the amino group and $\text{N4}-\text{H}$ bond. (2) Hydration of ATI and $\text{ATI}(\text{H}^+)$ molecules causes a rise in the positive charges on their N2 atoms.

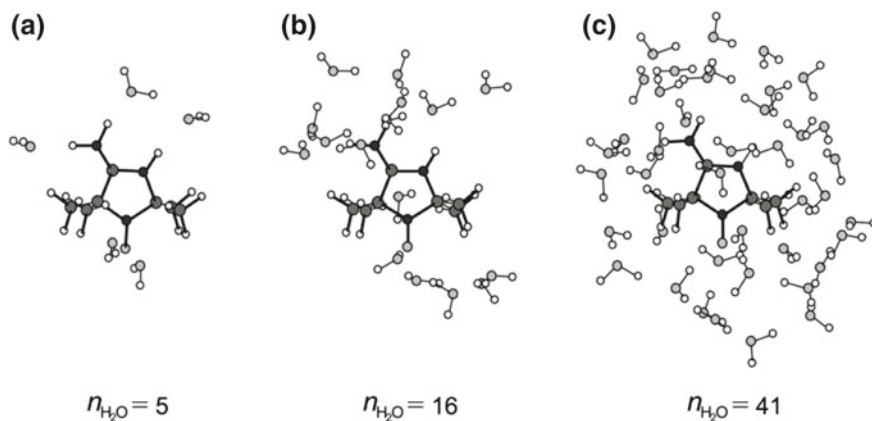
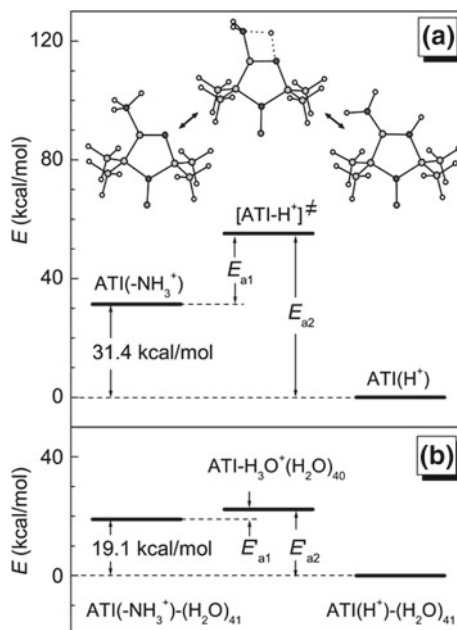


Fig. 2.7 Chemical structures of protonated 4-amino-2,2,5,5-tetramethyl-3-imidazoline-*N*-oxyl, ATI(H⁺), surrounded by water molecules: **a** ATI(H⁺) surrounded by five H₂O molecules; **b** ATI(H⁺) surrounded by 16 H₂O molecules; **c** ATI(H⁺) surrounded by 41 H₂O molecules [12]. Reprint from reference [12], Copyright 2004, American Chemical Society

Fig. 2.8 Energy diagrams characterizing proton transfer between the amino group and the ring nitrogen N4 of ATI molecule: **a** ATI in the gas phase; top figures show calculated structures of ATI molecule protonated either at the amino group (left) or at the ring nitrogen atom N4 (right) [12]; **b** ATI in water. Reprint from reference [12], Copyright 2004, American Chemical Society



(3) The negative charges on O1 atoms become smaller. (4) Effects of water-induced redistribution of charges on the N4-H bond and amino group are different in cases of protonated and deprotonated ATI.

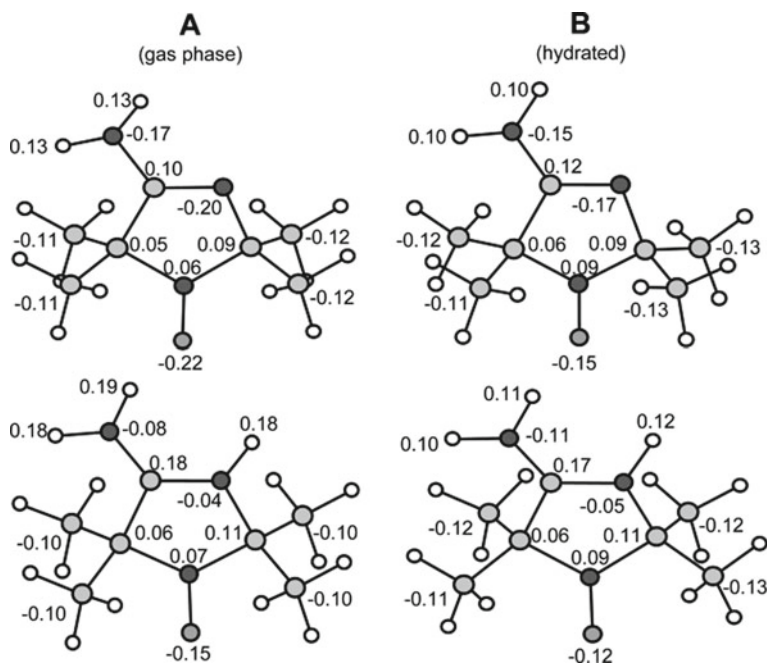


Fig. 2.9 Electric charges on atoms of deprotonated (top pictures) and protonated (bottom pictures) ATI molecules: **a** spin-labels in the gas phase; **b** spin-labels surrounded by 41 water molecules. For deprotonated form, negative charges of the nitrogen atoms N4 and N7 decrease after a spin-label hydration, while the hydration of $\text{pe ATI(H}^+)$ results to a certain increase in the values of negative charges of N4 and N7 atoms. Calculation also revealed positive charges of hydrogens in the amino group and the positive charge of the hydrogen atom bound to the N4 atoms [12]. Reprint from reference [12], Copyright 2004, American Chemical Society

Figure 2.10 presents the distribution of spin densities over the atoms of protonated and deprotonated ATI molecules in the gas phase or surrounded by 41 water molecules.

The electronic structure of nitronyl nitroxide 2-phenyl-4,4,5,5-tetramethyl-4,5-dihydro 1H-imidazole-1-oxyl-3-oxide (NitPh) was investigated by conventional and polarized neutron diffraction and compared to those obtained by various theoretical *ab initio* calculations [13]. It was found that in the O-N-C-N-O fragment, most of the spin density the O-N-C-N-O fragment is equally shared between the four atoms of the two NO groups: 0.27 (O) and 0.27 (N). In addition, the bridging sp^2 carbon atom carries a significant negative spin density (-0.11), while delocalization of the unpaired spin onto the phenyl fragment is weak.

Modulating spin delocalization in conjugated nitroxides, 2-(N-aminoxyl-N-tert-butyl)-benzothiazols, was carried out using UB3LYP/cc-pVDZ//UB3LYP/6-31G [14]. In solvent CH_2Cl_2 , this radical exhibits UV-Vis absorbances at 476, 512, and 558 nm and solution ESR hyperfine coupling constants (hfc) of $a_{\text{N}}(\text{NO}) = 9.16$, (ring N) 2.67 G, $a_{\text{H}} = 1.05, 1.31, 0.33, 0.43$ G. In the same conditions, the nitroxide

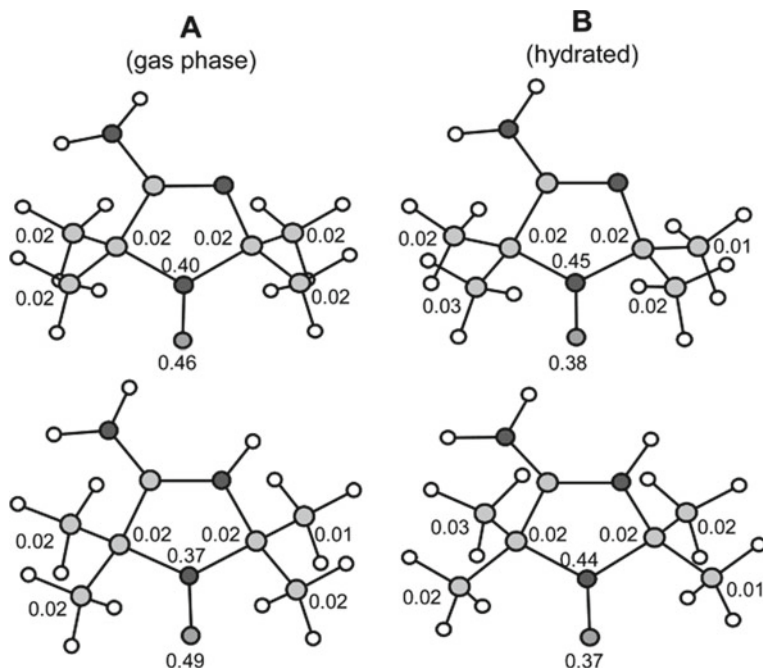


Fig. 2.10 Spin densities on atoms of ATI (top pictures) and ATI(H⁺) (bottom pictures) molecules: **a** spin-labels in the gas phase; **b** spin-labels surrounded by 41 water molecules [12]. Reprint from reference [12], Copyright 2004, American Chemical Society

hcc observed for isoelectronic 2-(N-aminoxyl-N-tert-butyl)-benzimidazole is 10.0–10.2 G. Distribution of spin densities was estimated from ESR hyperfine coupling (a) using the formulae $a_{(H-[p-C])} = (-22 \text{ G})\rho(\pi-[C])$ and $a_{(N)} = 30 \text{ G})\rho[N]$, where ρ are the estimated spin densities for p-carbons and nitrogens. The hyperfine constants showed that spin density throughout the benzothiazole ring is about 10% from the total value and the sp³ carbons attached to the nitroxide nitrogen has ≤ 1 –2% spin density. The optimized structure with the N–O group syn to the thiazole nitrogen was found to be lower in energy than the anticonformer by 7.5 kcal/mol.

The analysis of the high-resolution W-band (95 GHz) pulsed ELDOR-detected NMR (EDNMR) and 244 GHz cw EPR spectra yielded precise electron Zeeman parameter, g_{xx} , ^{14}N hyperfine, A_{zz} , and ^{14}N quadrupole, P_{zz} , tensor components for the perdeuterated nitroxide radical 3-hydroxymethyl-2,2,5,5-tetramethylpyrrolin-1-oxyl dissolved in deuterated frozen solvents of polar or unpolar, protic, or aprotic character (*ortho*-terphenyl, methanol, propanol, glycerol, aniline, phenol, and water) [15]. The results, obtained on the basis of semi-empirical and DFT quantum chemical calculations, indicated that the principal values of all the magnetic interaction parameters primarily depend on the nitroxide hydrogen-bond situation and the type of hydrogen-bond donor group of the solvent. To characterize the heterogeneity of the nitroxide local environment A_{zz} hyperfine and P_{zz} quadrupole values of the

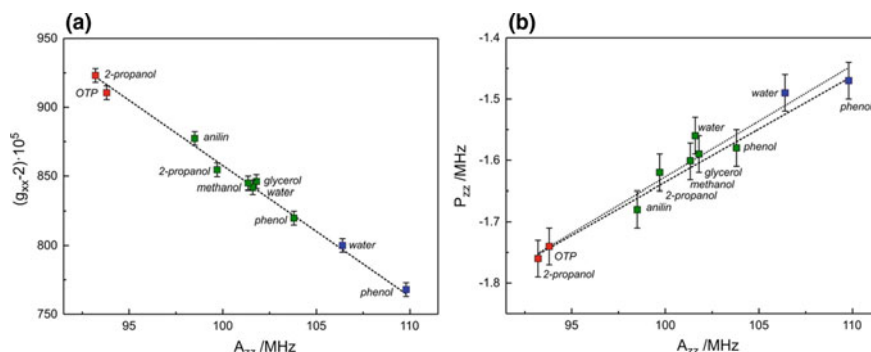


Fig. 2.11 **a** The g_{xx} versus A_{zz} plot showing g_{xx} values extracted from the analysis of the 244 GHz cw EPR spectra and A_{zz} values obtained from W-band EDNMR recordings. The dashed line shows the best linear least squared fit with a slope of $(-9.5 \pm 0.3) \times 10^{-5} \text{ MHz}^{-1}$ (or $-2.59 \pm 0.07 \text{ T}^{-1}$). **b** The P_{zz} versus A_{zz} plot using values obtained from W-band EDNMR experiments. The dotted and dashed lines show best linear least-square fits (with the slopes of $(18 \pm 2) \times 10^{-3}$ and $(17 \pm 1) \times 10^{-3}$) including and excluding data for water, respectively. The red-, green- and blue-colored squares denote nitroxide fractions assigned to nitroxide forming zero, one, or two H-bonds with the solvent molecule, respectively (color figure online) [15]

perdeuterated nitroxide radical in different matrices, W-band EDNMR spectra were recorded. Figure 2.11 demonstrates perfect linear correlation between the hyperfine A_{zz} and g-tensor g_{xx} components with an R -squared coefficient $R^2 = 0.994$.

According to the author's discussion, A_{zz} is expected to react to polarity changes in non-bonding as well as H-bonding situations through changes in the spin density distribution of the N–O bond as a consequence of charge displacements between N and O in the N–O bond. The effective g_{xx} value of nitroxide radicals is, among other perturbations, significantly affected by additional matrix perturbations of the n - π energy gap of the O-atom in H-bonding situations.

References

1. E.G. Bagryanskaya, S.R. Marque, Y.P. Tsentalovich, Alkoxyamine re-formation reaction. Effects of the nitroxide fragment: a multiparameter analysis. *J. Org. Chem.* **77**, 4996–5005 (2012)
2. E.G. Bagryanskaya, S.R.A. Marque, Scavenging of organic C-centered radicals by nitroxides. *Chem. Rev.* **114**, 5011–5056 (2014)
3. G.R. Eaton, S.S. Eaton, D.P. Barr, R.T. Weber, *Quantitative EPR* (Springer, 2010)
4. G.I. Likhtenstein, J. Yamauchi, S. Nakatsuji, A. Smirnov, R. Tamura, *Nitroxides: Application in Chemistry, Biomedicine, and Materials Science* (WILEY-VCH, Weinheim, 2008)
5. W.R. Hagen, *Biomolecular EPR Spectroscopy* (CRC, 2008)
6. M.M. Haugland, E.A. Andersona, J.E. Lovet, Tuning the properties of nitroxide spin labels for use in electron paramagnetic resonance spectroscopy through chemical modification of the nitroxide framework, in *Electron Paramagnetic Resonance*, vol. 25 (Royal Chemical Society, 2017), pp. 1–34

7. E. Tretyakov, K. Okada, S. Suzuki, M. Baumgarten, G. Romanenko, A. Bogomyakov, V. Ovcharenko, Synthesis, structure and properties of nitronyl nitroxide diradicals with fused-thiophene couplers. *J. Phys. Org. Chem.* **29**(12) (2016). <https://doi.org/10.1002/poc.3561>
8. M. Pavone, M. Biczysko, N. Rega, V. Barone, Magnetic properties of nitroxide spin probes: reliable account of molecular motions and nonspecific solvent effects by time-dependent and time-independent approaches. *J. Phys. Chem. B*, **114**, 11509–11514 (2010)
9. E. Stendardo, A. Pedone, P. Cimino, M.C. Menziani, O. Crescenzi, V. Barone, Extension of the AMBER force-field for the study of large nitroxides in condensed phases: an ab initio parameterization. *Phys. Chem. Chem. Phys.* **12**(37), 11697–11709 (2010)
10. P. Cimino, A. Pedone, E. Stendardo, V. Barone, Interplay of stereo-electronic, environmental, and dynamical effects in determining the EPR parameters of aromatic spin-probes: INDCO as a test case. *Phys. Chem. Chem. Phys.* **12**, 3741 (2010)
11. L. Horný, F. Mariotti, M. Quack, Ab initio study of some persistent nitroxide radicals. *CHIMIA* **62**, 256–259 (2008)
12. L.N. Ikryannikova¹, L.Y. Ustynyuk, A.N. Tikhonov, DFT study of nitroxide radical 1. Effects of solvent on structural and electronic characteristics of 4-amino-2,2,5,5-tetramethyl-3-imidazoline-N-oxyl. *J. Phys. Chem. A*, **108**(21), 4759–4768 (2004)
13. A. Zheludev, V. Barone, M. Bonnet, B. Deuy, A. Grand, E. Ressouche, P. Rey, R. Subra, J. Schweizer, Spin density in a nitronyl nitroxide free radical. Polarized neutron diffraction investigation and ab initio calculations. *J. Am. Chem. Soc.* **116**, 2019–2027 (1994)
14. P.S. Taylor, P. Ghalsasi, P.M. Lahti, Modulating spin delocalization in conjugated nitroxides: 2-(N-aminoxyl-N-tert-butyl)-benzothiazole. *Tetrahedron Lett.* **45**, 6295–6298 (2004)
15. A. Nalepa, K. Möbius, M. Plato, W. Lubitz, A. Savitsky, Nitroxide spin labels—magnetic parameters and hydrogen-bond formation: a high-field EPR and EDNMR study. *Appl. Magn. Reson.* **50**, 1–16 (2019)

Chapter 3

Nitroxide Chemical Reactions



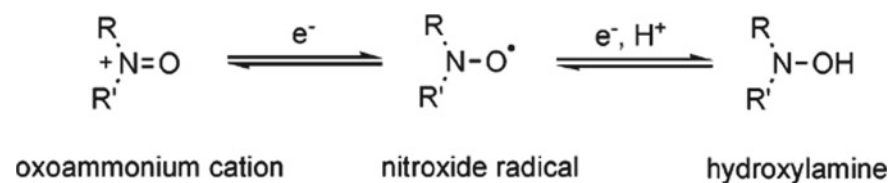
3.1 Introduction

After the pioneering work of Neiman et al. [1], the possibilities of modifying nitroxides without affecting the free valence appeared to be practically unlimited. Modern synthetic chemistry represents a rich and wide arsenal for carrying out almost any projects in these fields.

Nitroxides possess unique properties and chemical reactivity. A radical power of the N-oxyl moiety is partially redeemed due to the formation of a three-electron bond. This property provides chemical inertness with respect to many biological and other molecules under ambient conditions. The chemical activity increases with increasing temperature, which in particular is used in syntheses and living polymerization. On the other hand, nitroxides readily react with active radicals, which allows them to be used as antioxidants and intermediate agents in the living polymerization. Another avenue is the use of nitroxyls for analyzing antioxidants and establishing the antioxidant status in biological systems objects. Nitroxides are very weak nucleophilic reagent.

Nitroxyl radicals, oxoammonium cations, and hydroxylamines form a stable organic redox triad with efficient one- and two-electron transfer (Scheme 3.1).

In the pioneering work of Golubev et al. [3], the first stoichiometric oxidation of alcohols to ketones mediated by an oxoammonium species with N⁺-oxyl fragment was performed. Since then, numerous applications of aminoxyl radicals in organic



Scheme 3.1 Redox triad: oxoammonium cations, nitroxyl radicals, and hydroxylamine anion [2]. Reprinted from [2], Copyright 2007 American Chemical Society

oxidation reactions have focused on catalytic methods in which the oxoammonium species is (re)generated by a stoichiometric secondary oxidant. The chemical activity of the N-oxyl and N⁺-oxyl moieties is mainly determined by their redox potential.

3.2 Nitroxide Redox Potential

The standard redox potential of nitroxides dictates the thermodynamic possibility and, to a large extent, the kinetics of the reactions with the participation of these compounds. Tables presented in review [4] listed the following data on: (1) experimental aminoxyl/oxoammonium and N-hydroxyimide/imidoxyl redox potentials, (2) effect of ring structure on the calculated one-electron potentials for oxidation of cyclic aminoxyl radicals, (3) redox potential of the aminoxyl to oxoammonium redox process for various N-oxyl radicals, (4) redox potentials (V vs. NHE) of N-aryl hydroxylamines, hydroxyamic acids, and other acyclic N-hydroxy derivatives as determined by cyclic voltammetry (CV) or differential pulse voltammetry, and (5) second-order rate constants of the reaction of phthalimide N-oxyl (PINO) with substrates containing activated C–H bonds.

The value of the midpoint potentials ($E_{1/2}$), for 48 nitroxyl/oxoammonium pairs varies in the range from 0.67 to 1.31 eV, for 16 N-hydroxyimide/imidoxyl pairs from 0.57 to 1.12 eV, and for 18 redox potential of the nitroxyl to oxoammonium redox process for various N-oxyl radicals in a range 0.57–1.20 eV. The following general conclusions were made regarding the redox potential data presented: (1) The change of potentials for oxidation of cyclic nitroxyl radicals was explained by the change in hybridization of the nitrogen atom from sp² to sp³ that occurs on reduction and causes change torsional strain; (2) this change is small for six-membered rings, but increases for five-membered rings; (3) an attachment of aromatic groups to the radical rings leads to the significant increase of the potential; and (4) replacing the group t-Bu by SO₃[−] leads to a substantial decrease in the nitroxide redox potential.

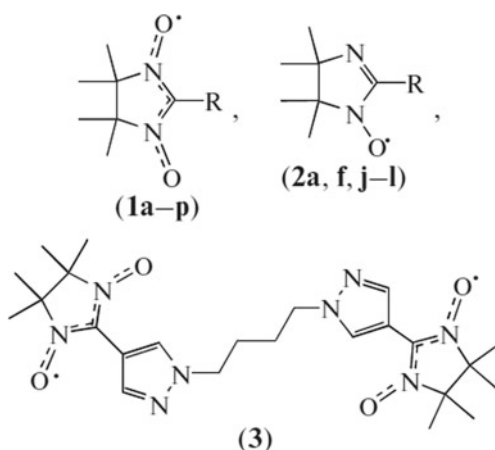
The oxidation and reduction potentials of 54 piperidine, pyrrolidine, isoindoline, and azaphenalene nitroxides, substituted with COOH, NH₂, NH₃⁺, OCH₃, OH, and NO₂ groups nitroxides were calculated using G3(MP2)-RAD//B3-LYP/6-31G(d) gas-phase energies and PCM solvation calculations at the B3-LYP/6-31G(d) level [2]. This approach gave theoretical values of oxidation and reduction potentials within 40 mV of experimental values. Effects of level of the theory used for geometry optimization on the adiabatic ionization energies, on the adiabatic electron affinities, and on the oxidation potentials of various nitroxides were listed in corresponding tables. As a result of the calculation, the following conclusions were drawn: (1) The overall ring structure has more effect on the electrode potentials than the inclusion of substituents; (2) piperidine and pyrrolidine derivatives have intermediate oxidation potentials but on average pyrrolidine derivatives display more negative reduction potentials; (3) isoindoline derivatives show higher oxidation potentials and more negative reduction potentials; (4) within a ring, the substituents have a relatively small effect with electron donating groups such as amino and hydroxy

groups; (5) the oxidized species and electron-withdrawing groups such as carboxy groups stabilize the reduced species; and (6) azaphenylene derivatives display the lowest oxidation potentials and negative reduction potentials. In addition, the calculations revealed the following patterns: (1) the five-membered cyclic nitroxides (pyrrolidine and isoindoline derivatives) have reduction potentials centered around -1570 mV; (2) the six-membered cyclic nitroxides (piperidine and azaphenylene derivatives) have reduction potentials centered at -1370 mV; (3) piperidine and pyrrolidine derivatives show oxidation potentials centered around 830 mV; (4) the highest for the isoindoline derivatives centered around 1020 mV; and (5) the lowest oxidation potentials are seen for the azaphenylene. Derivatives centered around 510 mV. It was suggested that azaphenylene derivatives show even lower oxidation potentials than piperidines due to the fact that the positive charge in the cation species can be delocalized onto the ring by hyperconjugation.

The redox potential of piperidine nitroxides and *N*-oxoammonium cation couples modified at the C4 position was measured, and the nitroxide structure–reactivity relationship was evaluated [5]. It was concluded that the superoxide dismutase activity of a nitroxide can be controlled based on its redox potential.

Redox potentials of a wide group of nitronyl (NN) and imino nitroxides with methyl, phenyl, iodo, and cyanosubstituents (Fig. 3.1) were determined by CV [6]. Nitronyls studied underwent reversible one-electron reduction, which formed the oxoammonium cation. The oxidation potentials E_{ox} of NNs were calculated as the mean potentials of the anode (E_p^{ai}) and cathode (E_p^{ci}) peaks. The reduction potentials E_{red} of NNs were calculated by the equation $E_{\text{red}} = (E_p^{\text{a2}} + E_p^{\text{c2}})/2$. The experiments revealed the following trends in the values E_{red} depending on the structure of the nitroxides: (1) The highest potential, $E_{\text{red}} = 1.41$ V, is required for the reduction of pyrazol-4-yl-substituted **1a**, (2) the alkyl derivatives **1b–1e** and **1i** of this nitroxide

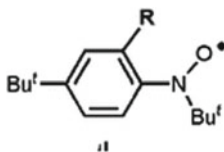
Fig. 3.1 Nitroxides used in [6]



were reduced at slightly lower potentials $E_{\text{red}} \sim 1.23\text{--}1.26$, (3) the stronger electron-accepting substituent in **1l**, **1n**, and **1o** led to a decrease in E_{red} to ~ 1.2 V, and (4) the lowest $E_{\text{red}} \sim 0.9$ V is inherent in **1f**, **1j**, **1k**, and **1p**.

In the case of the oxidation potential, the tendency is as follows: (1) Pyrazol-4-yl-substituted NNs **1a–1e** and **1i**, pyrazol-3-yl-substituted NN **1g**, imidazole-4-yl-substituted NNs **1j** and **1k**, and methyl-substituted NN **1m** are characterized by the lowest values of $E_{\text{ox}} \sim 0.35\text{--}0.40$ V, (2) as the electron-accepting properties of substituents increased in the series **1n**, **1o** < **1l** < **1f**, **1h**, E_{ox} gradually increased 0.55 and 0.81 V on passing to **1p**, (3) changes in E_{ox} correlate with the ability of the N–O group to act as a Lewis base in reactions with transition metal ions, and (4) imino nitroxides are oxidized irreversibly.

The redox potentials of seven aromatic nitroxides derived from *tert*-butyl phenyl nitroxide



were determined by CV in non-aqueous solution, and the first oxidation potential to the formation of the corresponding N-oxo ammonium cation was assigned [7]. The electrochemical experiments were conducted in a three-electrode glass cell. A platinum wire and a saturated calomel electrode (SCE) were used as a counter and a reference electrode, respectively. The following general conclusions were made: (1) The electrochemical reduction of the aromatic nitroxides reveals an irreversible wave, and (2) the first oxidation potential as well as the reduction potential strongly depend on the electron-donating and withdrawing substituents of the compounds. The experimental values of oxidation and reduction potentials of the studied nitroxides were tabulated. The following experimental results and their explanation were reported: (1) The reduction potentials of the aromatic nitroxides (1.13–1.40 eV) are relatively low compared to TEMPO (1.61 eV) probably due to the mesomeric effect of the aromatic cycle, stabilizing the negative charge on the oxygen; (2) for the neutral nitroxides having the ester and sulfonate ester electron-withdrawing groups a shift of 150 mV toward less negative potentials took place; (3) the negatively charged nitroxides are more prone to reduction than their corresponding neutral nitroxides with potential shifts of 150 and 220 mV, respectively; (4) the observed high-potential shift from 0.918 to 0.358 mV in the case of the carboxylate was explained by charge effect; and (5) the proximity of the carboxylate group in the ortho position and the rigid structure of compound allow for a cyclic conformation of the corresponding N-oxo ammonium via an intramolecular electrostatic interaction, which can stabilize the nitroxide structure.

The redox potentials of 25 cyclic nitroxides from four different structural classes (pyrrolidine, piperidine, isoindoline, and azaphenalene) (Fig. 3.2) determined experimentally by cyclic voltammetry in acetonitrile were found to be influenced by the

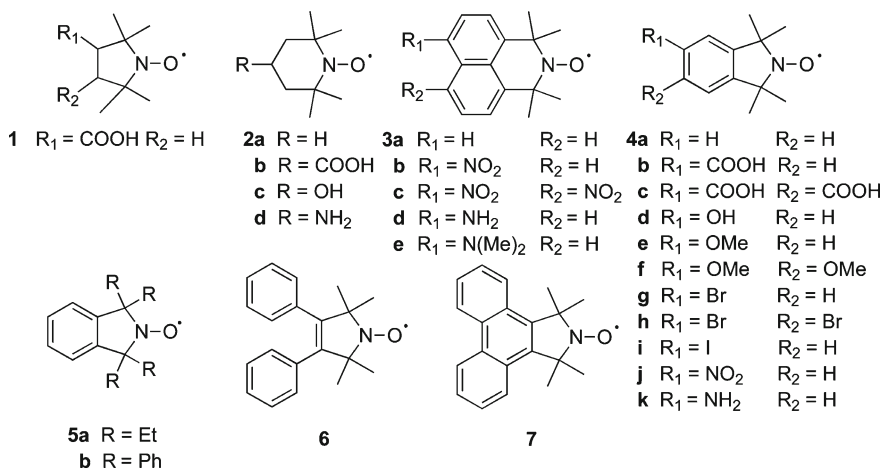


Fig. 3.2 Nitroxides investigated in cyclic voltammetry and theoretical studies [8]. Reprint from [8], Copyright 2008, American Chemical Society

type of ring system, ring substituents and/or groups surrounding the radical moiety [8]. The redox potentials, E_o of the oxidation of the nitroxide, were estimated as half the sum of the anodic (E_{pa}) and cathodic (E_{pc}) peak potentials. In addition, the potential values were calculated by high-level ab initio molecular orbital calculations with agreements with experimental data. Exceptions are the azaphenalenenes, for which is an extraordinary discrepancy (mean absolute deviation of 0.60 V). It was found that for investigated nitroxides, the peak separation, $E_{pa} - E_{pc}$, ranged from 65 to 109 mV and for the unsubstituted ring systems, the order of oxidation from most easily oxidized to least easily oxidized is: piperidine (**2a**, 0.577 V), azaphenalene (**3a**, 0.736 V) > isoindoline (**4a**, 0.771 V). Azaphenalenenes were more easily oxidized than the piperidine derivatives, which was attributed to the ability of the aromatic ring of the azaphenalene to stabilize the cation.

Orbital diagrams showing the singly occupied molecular orbital (SOMO) of the parent nitroxide radicals and the highest occupied molecular orbital (HOMO) of the oxidized species are presented in Fig. 3.3. Oxidation potentials of monosubstituted isoindoline nitroxides plotted with respect to the Hammett constant of the functional group (σ_p), an empirical constant based on the electronic effect of the substituent, showed the linear correlation.

The kinetics and thermodynamics of comproportionation of eight pairs of oxoammonium and hydroxyammonium salts $3H^+$ were investigated, and the effect of substituents and heterocyclic ring structure on the comproportionation equilibrium constant K_4 was revealed [9]. The following finding was shown: (1) Experimental values of the reduction potentials $E_{2/1}$, dissociation constants of $R_2\text{NO}^+$ and $R_2\text{NOH}$ to $R_2\text{NO}\cdot$ hydroxyammonium cations $\text{p}K_{3H^+}$, the equilibrium constant K_4 ; (2) the values of bond dissociation energies $D(\text{O}-\text{H})$ for hydroxylamines in water (0.972–0.734 V vs. NHE), (3) pH dependences of reduction potentials of nitroxyl radicals; (4) linear

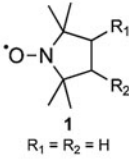
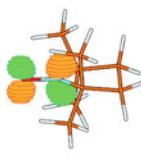
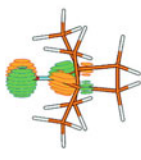
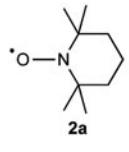
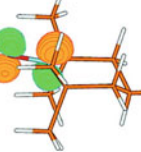
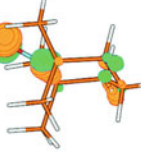
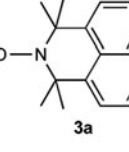
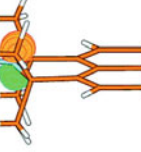
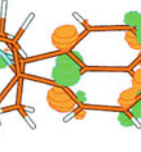
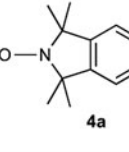
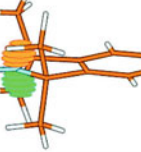

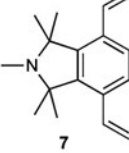
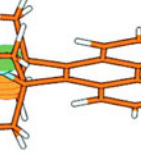
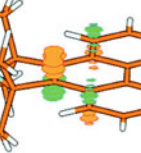
Nitroxide	SOMO of radical species	HOMO of oxidised species (cation)
 1 $R_1 = R_2 = H$		
 2a		
 3a		
 4a		
 7		

Fig. 3.3 B3LYP/6-311+G(3df,2p) orbital diagrams showing the singly occupied molecular orbital (SOMO) of the parent nitroxide radicals and the highest occupied molecular orbital (HOMO) of the oxidized species [8]. Reprint from [8], Copyright 2008, American Chemical Society

free energy relationships between redox potentials ($E_{1/2}$), dissociation constants of hydroxyammonium cations K_{3H^+} , and the equilibrium constant K_4 ; (5) correlations with the inductive substituent constants σ_I for the radicals of piperidine and pyrrolidine series, values of pK_{3H^+} and $E_{1/2}$, (6) increasing in $-I$ -effects of substituents which reduces the overall equilibrium constant of the reaction K_4 ; (7) dissociation energies for hydroxylamines in water; and (8) correlation between the Pauling Group Electronegativity (E_g) of substituents versus redox potentials ($E_{1/2}$) for the 5-membered ring hydroxylamine/aminoxyl radicals in MeOH (0.1 M Bu_4NClO_4) and phosphate buffer (0.1 M, pH 7.4) was also established [10].

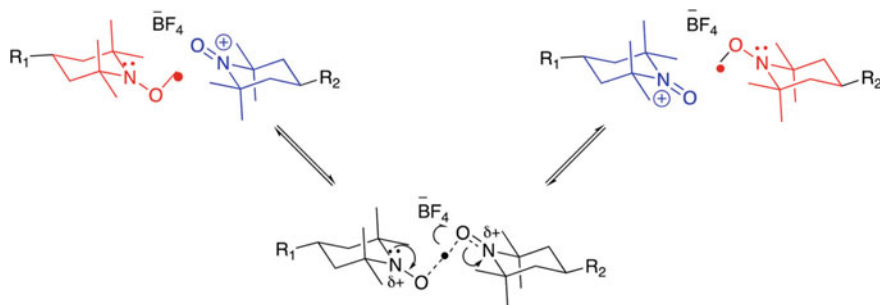


Fig. 3.4 A redox equilibrium between oxoammonium salts and trace amounts of corresponding nitroxide [12]. Reprint from [12], Copyright 2017, American Chemical Society

The influence of the structure of 21 nitroxyl radicals on the thermodynamics and the kinetics of the reverse comproportionation reaction of R_2NO^+ and R_2NOH to $R_2NO\cdot$ in aqueous H_2SO_4 was investigated [11]. pH dependences of reduction potentials of nitroxyl radicals $E_{1/2}$ and bond dissociation energies $D(O-H)$ for hydroxylamines in water were determined. The experiments indicated: (1) the linear free energy relationships between the reduction potentials $E_{2/1}$, dissociation constants of hydroxyammonium cations $K3H^+$, and the equilibrium constant $K4$; (2) for the radicals of piperidine and pyrrolidine series, values of $pK3H^+$ and $E_{2/1}$ correlate with the inductive substituent constants σ_1 ; and (3) a correlation between the basicity of nitroxyl groups and reduction potentials of oxoammonium cations takes place.

Three new homologous TEMPO oxoammonium salts and three homologous nitroxide radicals have been prepared, and their oxidation properties of the salts have been explored [12]. Overall paramagnetism in the oxoammonium salt solutions revealed by EPR spectroscopy was explained by a redox equilibrium between oxoammonium salts and trace amounts of corresponding nitroxide (Fig. 3.4). This equilibrium was confirmed by electron interchange reactions between nitroxides with an N-acetyl substituent and oxoammonium salts with longer acyl side chains.

Nitronyl nitroxides (NNs) are capable of scavenging physiologically relevant reactive oxygen (ROS) and nitrogen (RNS) species, namely superoxide, nitric oxide (NO), and nitroxyl (HNO). The redox properties of 2-(4-carboxyphenyl),-4,5-dihydro-4,4,5,5-tetramethyl-1H-imidazolyl-1-oxy-3-oxide monopotassium salt, cPTIO, 4,4,5,5-tetramethyl-2-[4-trimethylammoniophenyl]-2-imidazoline-3-oxide-1-yloxy methyl sulfate (NN^+), and 4,4,5,5-Tetramethyl-2-[4-trimethylammoniophenyl]-2-imidazoline-1-yloxy methyl sulfate (IN^+), including determination of the equilibrium and rate constants of their reduction by HNO and ferrocyanide, and reduction potential of the couple NN/hydroxylamine of nitronyl nitroxide (hNN), were investigated [13]. The reduction potential of the NNs and iminonitroxides (Ins), product of NNs reaction with NO were calculated based on their reaction constants with ferrocyanide. The values of the reduction potential were found to be for NN/hNN ($E'_0 \approx 285$ mV) and IN/hIN ($E' \approx 495$ mV). Obtained data on equilibrium and bimolecular rate and constants for the redox reactions of

NNs and Ins were tabulated. A correlation between the reduction potential of cyclic oxoammonium derivatives and substituent Hammett σ^* constants was established. In addition, the rate constants of the reaction of the NNs with HNO were measured to be equal to $(1-2) \times 10^4 \text{ M}^{-1} \text{ s}^{-1}$.

N-tert-Butyl-*N*-2-pyridylhydroxylamines were characterized using NMR, electrochemistry, and density functional theory [14]. Substitution of the pyridyl ring in the 3-, 4-, and 5-positions was used to vary the reduction potential (E_{red}) of the nitroxyl/oxoammonium redox couple by 0.95 V. The values were found to follow Hammond's correlation. DFT computations of the electrochemical properties agreed with experiment. Electrochemical studies of the reduction and oxidation reactions of five different organic nitroxyls have been performed across a wide pH range (0–13) [15]. The hydroxylammonium $\text{p}K_{\text{a}}$ was determined by NMR. The resulting Pourbaix diagrams illustrate structural effects on their various redox potentials and on pH (Fig. 3.5). Evidence was also given for the reversible formation of a hydroxylamine *N*-oxide when nitroxyls are oxidized in alkaline media. Several conclusions have been drawn from the Pourbaix diagram: (1) the oxoammonium reduction potential is pH insensitive, (2) the potential is insensitive to the identity of the buffering electrolyte, and (3) the nitroxyl reduction potential is pH-dependent and has a break in slope, corresponding to the hydroxylammonium $\text{p}K_{\text{a}}$.

3.3 Oxoammonium Cation Reactions

The oxoammonium species can be commonly generated by a stoichiometric secondary oxidant such as NaOCl, bromine, NO_x/O_2 , hypervalent iodide species, or electrochemically. The species may be isolated as a stable salt, and it serves as two-electron oxidant in a number of organic oxidation reactions. The first reaction of the oxidation of alcohols by oxoammonium cation was demonstrated by Golubev et al. [2]. Primary alcohols were oxidized to corresponding aldehydes, while secondary alcohols were oxidized to ketone. This approach has been commonly used for alcohol oxidation including in industrial scale what attracts particular interest [16–19].

Oxidation of alcohols containing a β -oxygen atom, using 4-acetylamino-2,2,6,6-tetramethylpiperidine-1-oxoammonium tetrafluoroborate, in the presence of pyridine, yielded dimeric esters, while in the presence of 2,6-lutidin, the product is aldehyde [20]. The betaine is oxidized by the oxoammonium salt to give an *N*-acylpyridinium ion that serves as an acylating agent for ester formation. A suggested mechanism for oxoammonium cation oxidations premised on nucleophilic additions to the oxygen atom of the positively charged nitrogen–oxygen double bond. The rates of oxidation of a series of primary, secondary, and benzylic cycle of alcohols oxidation oxoammonium salt with CF_3 moiety have been found to oxidize alcohols more rapidly than does with CH_3 (Fig. 3.6). The rate of oxidation of meta- and para-substituted benzylic alcohols displays a strong linear correlation to Hammett parameters ($r > 0.99$) with slopes (ρ) of -2.7 and -2.8 , respectively (Fig. 3.7). It was

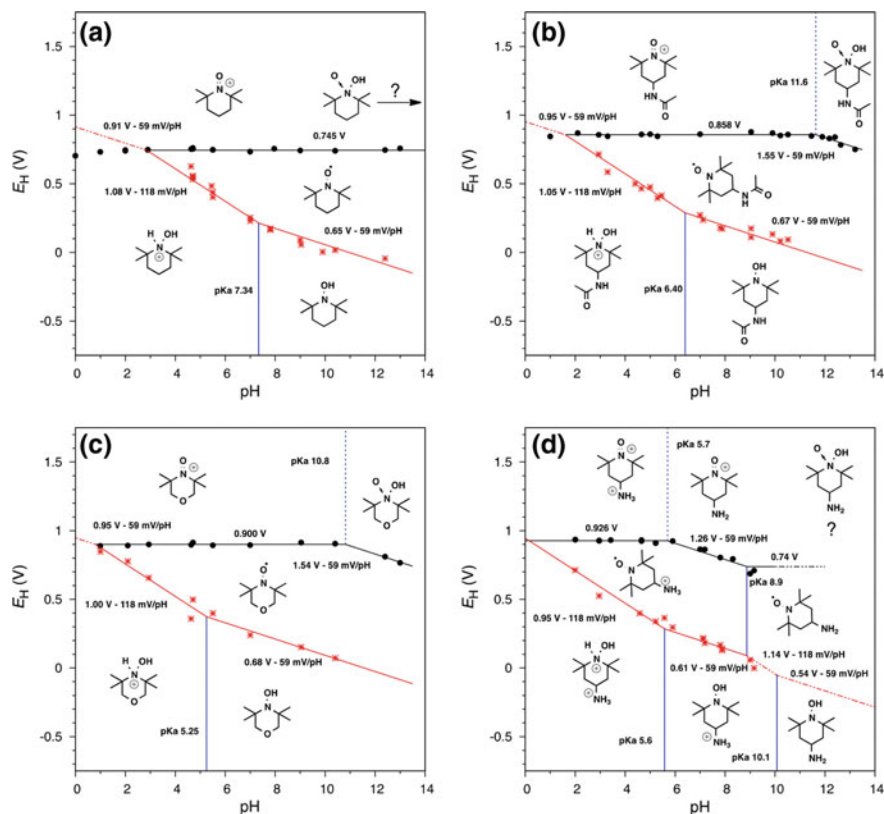
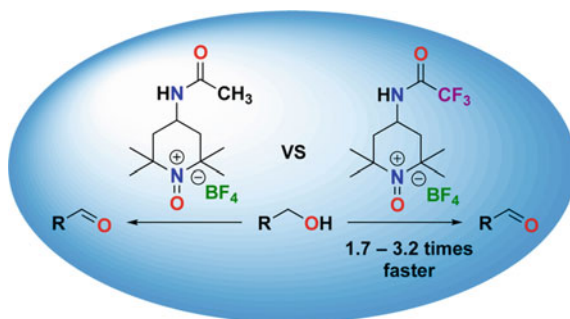


Fig. 3.5 Line fits have been constrained to have slopes corresponding to 0, 1, or 2 H^+/e^- and to intersect at points. Black circles and lines correspond to oxoammonium reduction to the nitroxyl, red stars and solid lines correspond to aminoxyl reduction, and the dashed red line corresponds to the theoretical $2e^-/2H^+$ oxidation of hydroxylammonium to oxoammonium. E_H denotes redox potential referenced to NHE. Reprint from [15], Copyright 2018, American Chemical Society

Fig. 3.6 Illustration of effect of structure of oxoammonium cation on an alcohol oxidation [21]. Reprint from [21], Copyright 2017, American Chemical Society



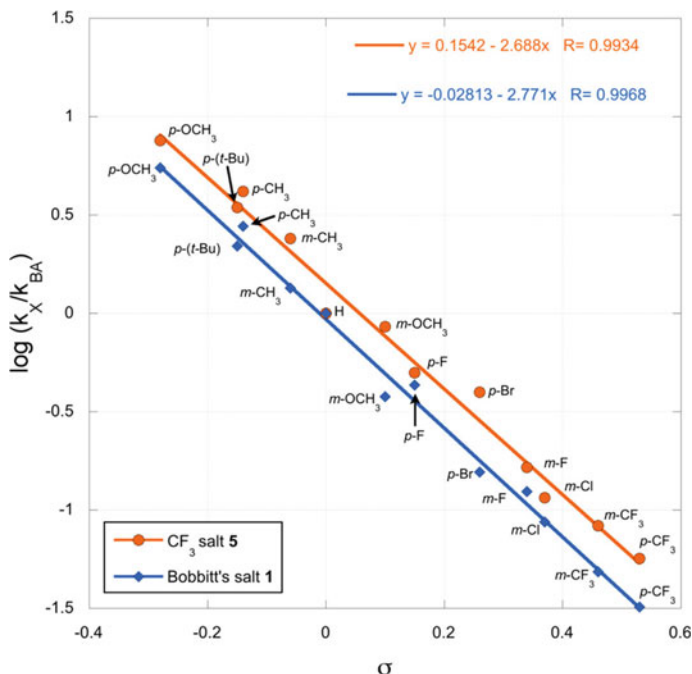


Fig. 3.7 Hammett plot of the rates of oxidation of substituted benzyl alcohols by 1 and 5; k_{BA} is the rate constant for oxidation of benzyl alcohol, and k_X is the rate constant for oxidation of substituted benzyl alcohol [21]. Reprint from [21], Copyright 2017, American Chemical Society

suggested that the rate-limiting step in the oxidations involves hydride abstraction from the carbinol carbon of the alcohol substrates.

A novel TEMPO-based oxoammonium salt, 2,2,6,6-tetramethyl-4-(2,2,2-trifluoroacetamido)-1-oxopiperidinium tetrafluoroborate, and its corresponding nitroxide were synthesized and characterized [21]. The rates of oxidation of primary, secondary, and benzylic alcohols by the nitroxide in acetonitrile solvent at room temperature have been determined. The rate of oxidation of meta- and para-substituted benzylic alcohols displayed a linear correlation to Hammett parameters ($r > 0.99$) with slopes (ρ) of -2.7 and -2.8 , respectively. This finding indicated that the rate-limiting step in the oxidations involves hydride abstraction from the carbinol carbon of the alcohol substrate.

The mechanism of an NO_x -assisted, nitroxide-catalyzed aerobic oxidation of alcohols was evaluated using a set of sterically and electronically modified nitroxides with azaadamantane nucleus [i.e., TEMPO, AZADO (1), 5-F-AZADO (2), 5,7-DiF-AZADO (3), 5-MeO-AZADO (4), 5,7-DiMeO-AZADO (5), oxa-AZADO (6), TsN-AZADO (7), and DiAZADO (8)]. s [i.e., TEMPO, AZADO (1), 5-F-AZADO (2), 5,7-DiF-AZADO (3), 5-MeO-AZADO (4), 5,7-DiMeO-AZADO (5), oxa-AZADO (6), TsN-AZADO (7), and DiAZADO (8)] [22]. The introduction of an F atom at a remote position from the nitroxyl radical moiety on the azaadamantane nucleus

enhanced the catalytic activity under typical NO_x -mediated aerobic oxidation conditions. The kinetic profiles of the azaadamantane-*N*-oxyl-[AZADO-, 5-F-AZADO-, and 5,7-DiF-AZADO]-catalyzed aerobic oxidations were investigated, revealing that: (1) AZADO showed a high initial reaction rate compared to 5-F-AZADO and 5,7-DiF-AZADO (Fig. 3.8), (2) AZADO-catalyzed oxidation exhibited a marked slowdown, resulting in $\sim 90\%$ conversion, (3) 5-F-AZADO-catalyzed oxidation smoothly reached completion. Experiments with Oxa-AZADO, TsN-AZADO, and DiAZADO supported evidence for the electronic effect on the catalytic efficiency of F atom at a remote position from the nitroxyl radical moiety on the azaadamantane nucleus to enhance the catalytic activity under NO_x -mediated aerobic oxidation conditions.

4-acetamido-2,2,6,6-tetramethylpiperidine-1-oxoammonium tetrafluoroborate (1) in wet CH_3CN at room temperature oxidatively cleaved benzylic ethers and related ArCH_2OR substrates to give the corresponding aromatic aldehyde and alcohol in high yield (Fig. 3.9) [20]. Primary or secondary alcohol products are further oxidized by 1 to give carboxylic acids and ketones, respectively. The oxidation likely involves a hydride abstraction from the benzylic carbon. In addition, the following findings were reported: (1) oxidation of alcohols containing a β -oxygen atom in the presence of pyridine by 1 yields dimeric esters; (2) in the presence of 2,6-lutidine the product is a simple aldehyde; (3) the betaine is oxidized by the oxoammonium salt to give an *N*-acetylpyridinium ion; and (4) a series of alcohols containing a β -oxygen

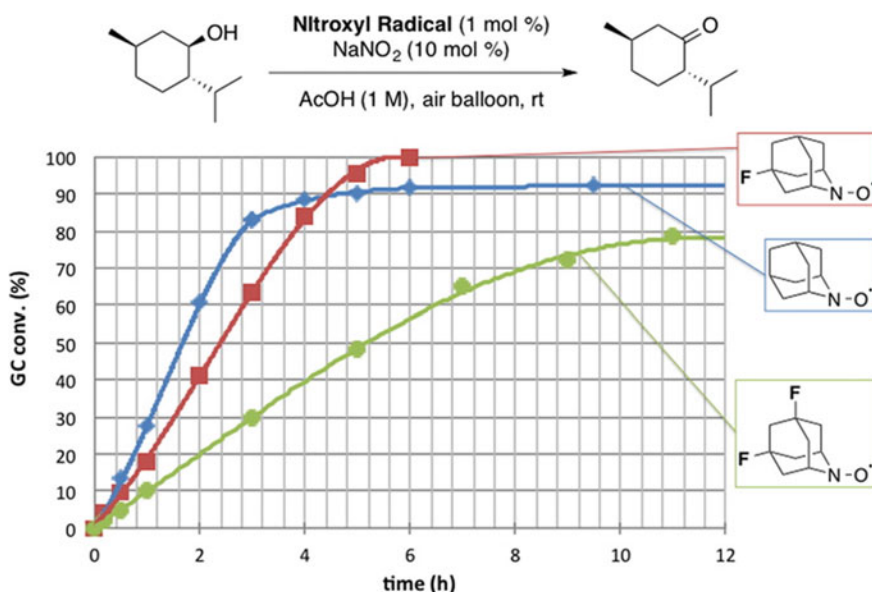


Fig. 3.8 Illustration of the electronic effect on the catalytic efficiency of the heteroatoms under NO_x -assisted aerobic oxidation conditions [22]. Reprint from [22], Copyright 2014, American Chemical Society

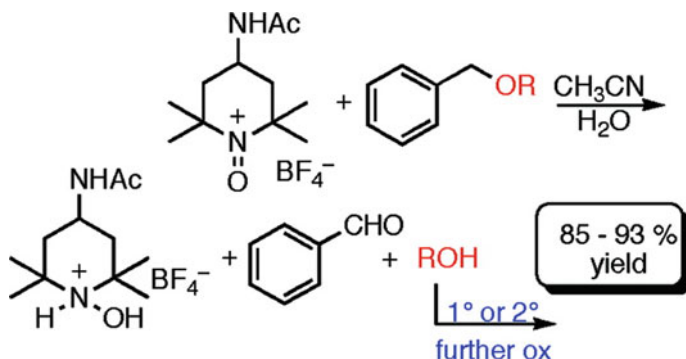


Fig. 3.9 Benzylic ethers and related ArCH_2OR substrates are oxidative cleavage of enzylic ethers [20]. Reprint from [21], Copyright 2014, American Chemical

substituent were oxidized to aldehydes in the presence of 2,6-lutidine. Suggested mechanism for oxoammonium cation oxidations premised on nucleophilic additions to the oxygen atom of the positively charged nitrogen–oxygen double bond (Fig. 3.9).

Facile oxidation of primary amines to nitriles using a stoichiometric quantity of 4-acetamido-2,2,6,6-tetramethylpiperidine-1-oxoammonium tetrafluoroborate I was performed in CH_2Cl_2 – pyridine solvent at room temperature with yield of 75–95% (Fig. 3.10) [23].

At room temperature, benzylic amines bearing electron-withdrawing substituents were oxidized in 12 h, while aliphatic amines in 24–36 h. The detailed oxidation mechanism, taking ethylamine as the substrate and the 2,2,6,6-tetramethylpiperidine-1-oxoammonium cation ($\text{TEMP}\cdot\text{O}^+$) as the oxidant, was computationally investigated using the B3LYP/6-311+G* level of DFT theory (Fig. 3.11). The mechanism involves a hydride transfer from the amine to the oxygen atom of I as the rate-limiting step.

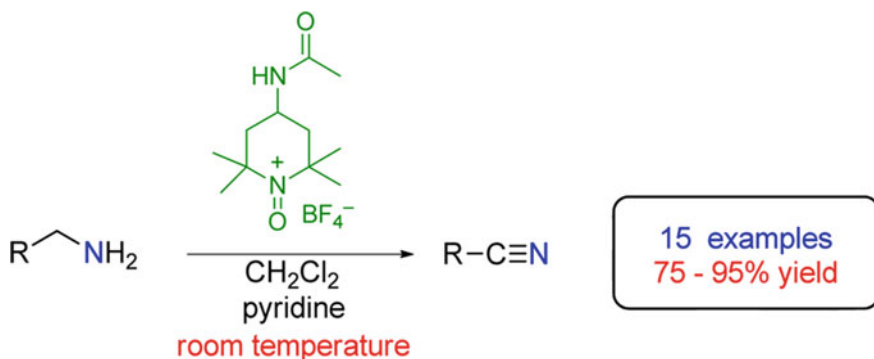


Fig. 3.10 Oxidation of primary amines to nitriles (Scheme 3.1, 1) a% [23]. Reprint from [23], Copyright 2017, American Chemical Society

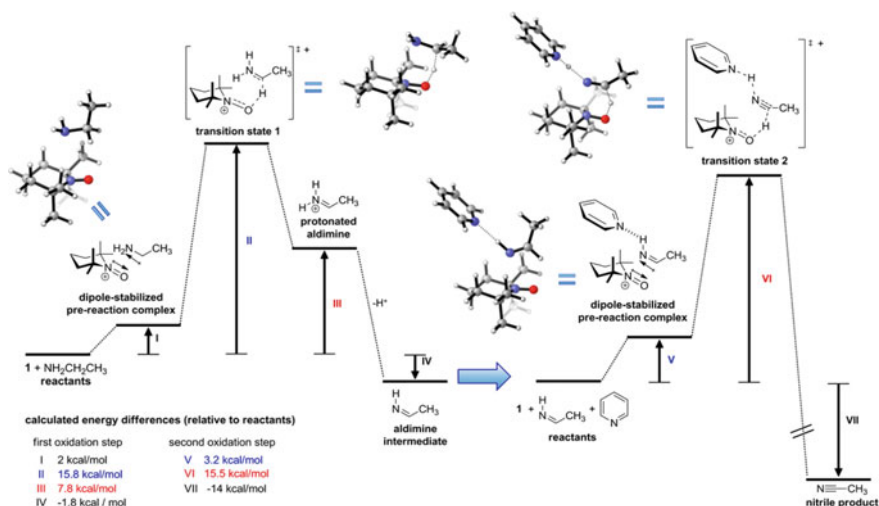


Fig. 3.11 Computed profile (B3LYP/6-311+G*) for the oxidation of primary amines to nitriles [23]. Reprint from [23], Copyright 2017, American Chemical Society

Efficient reduction of O_2 to water is a challenge in energy conversion and many aerobic oxidation reactions. It was demonstrated that the electrochemical oxygen reduction reaction (ORR) can be achieved at high potentials by using soluble organic nitroxyl and nitrogen oxide (NO_x) mediators [24]. The combination of nitroxyl/ NO_x species, such as 2,2,6,6-tetramethyl-1-piperidiny-N-oxyl (TEMPO), or sodium nitrite, mediated sustained O_2 reduction with overpotentials as low as 300 mV in acetonitrile containing trifluoroacetic acid. The nitrogen oxide catalyst drives aerobic oxidation of a nitroxyl mediator to an oxoammonium species, and the electrolysis potential is dictated by the oxoammonium/nitroxyl reduction potential. The oxoammonium species are reduced by cathode. The overpotentials accessible to this ORR system were found to be significantly lower than widely studied molecular metal-macrocycle ORR catalysts.

3.4 Nitroxide Cross-Coupling Reactions

Cross-coupling reactions of nitroxides with organic C-centered radicals (OCCR) (Fig. 3.12) comprehensively reviewed by Bagryanskaya and Marque [25] are attracted special interest. The review discussed the data on 75 carbon- and heteroatoms-centered active radicals and 100 nitroxides. Numerous examples of the involving of the cross-coupling stages in various chemical processes and methods of the processes investigation were described. General trends and specific effects in the frame of the multiparameter approach were also discussed in detail.

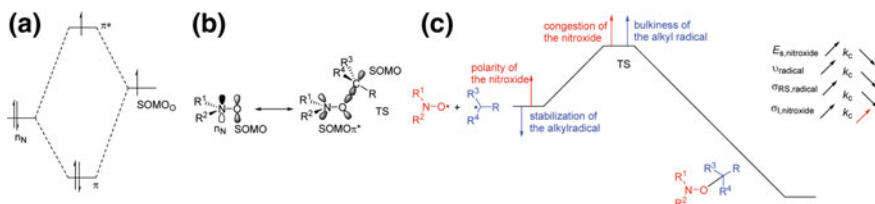


Fig. 3.12 Orbital diagram for the SOMO interactions and the energy profile of the cross-coupling reaction between a nitroxide and a C-centered radical [26]. Reprinted from [26] Copyright 2012 American Chemical Society

Orbital diagram for the SOMO interactions and the energy profile of the cross-coupling reaction between a nitroxide and a C-centered radical are presented in Fig. 3.12 [26].

In Fig. 3.12, the SOMO of the nitroxide is described as a three-electron bond orbital with the odd electron located in the π^* orbital. Factors affected on the efficiency of the cross-coupling reaction are: (1) the energy gap, (2) the overlapping between the SOMOs of the nitroxide (SOMO π^*) and the alkyl radical, (3) the spin density in the SOMOs, (4) strength of stabilization of the alkyl sRS (low electron density on the coupling sites), (5) bulkiness of the alkyl radical ν (large steric hindrance) that increases the activation energy of the process, and (6) the polarity (electron-withdrawing groups modifying the stabilization, matching of electrophilic/nucleophilic character) of the radicals. Quantitative experimental data on reactions in which the cross-coupling plays a key role were summarized in tables: (1) values of rate constant k_c at room temperature for various active radicals and nitroxides and in various solvent ranging from 9.5 to 520 M⁻¹S⁻¹; (2) data on Arrhenius parameters, pre-exponent factor A_c , energy activation E_{ac} and values of bond dissociation energies [BDEs(C-H)] for the cross-coupling reaction of nitroxides and C-centered radicals; (3) values of bond dissociation energies [BDEs(C-H)] and stabilization (σ_{RS}), polarity (σ_I), and steric (ν); (4) descriptors for selected C-centered radicals corresponding re-evaluated rate constants k_c for the cross-coupling with nitroxides; (5) correlation of log k_c at room temperature with a linear combination of the molecular descriptors; (6) values of polarity (σ_I) and steric (ν) molecular descriptors for selected nitroxides; and (7) steric effect accounted for by ν takes into account both the hampered approach of the nitroxide by the congested radical center and the rehybridization $sp^2 \rightarrow sp^3$ impeded by the bulkiness of the groups attached to the radical center [26].

To determine the cross-coupling rate constant (k_c), several pathways for the constant determination were suggested [25–28]. The reaction rate of cross-coupling after photo homolysis can be measured by methods of time domain absorption spectroscopy or EPR [25]. Radical clock reactions involve a competition between a unimolecular radical reaction with a known rate constant and a bimolecular radical reaction with an unknown rate constant to produce unrearranged and rearranged products [27]. In the C-centered radical nitroxide trapping (competitive method), scavenging

of the C-centered radicals in the presence of two nitroxides, $N\alpha$ (k_c unknown) and $N\beta$ (k_c known) provides indirect measurement of k_c [28]. Time-Resolved Chemically Induced Dynamic Nuclear Polarization (TR CIDNP) has been proved to be a powerful method for investigation of radical processes [29, 30]. In TR CIDNP, the NMR spectra of emission or absorption of reactants and products are detected. The analysis of the spectra yielded information on the intermediate radical pairs and mechanism of the reaction studied. For example, the measurements of the CIDNP intensity of the alkoxyamine in the absence and in the presence of nitroxide and at different time delays between the laser pulse and radio frequency pulse τ_0 provide the observed alkoxyamine formation rate constant k_{obsd} . The dependence of k_{obsd} on the nitroxide concentration gives the value of cross-coupling rate constant k_c .

A key role of the radical cross-coupling in a chemical reaction can be illustrated by an example of reaction of hindered amine light stabilizers (HALSs), which includes the generation of nitroxides from amines [31]. Thermodynamically favored proposed cycle for the nitroxide regeneration and competitive amine formation via H-atom abstraction from an alkoxyamine and subsequent aminyl radical formation are schematically illustrated in Fig. 3.13.

Along with the effects of the electron structure of nitroxides in various solvent, values of the dipole moment (μ), dielectric constant (ϵ_r), cohesive pressure (c), normalized Reichardt solvent polarity constant (E_T^N), EPR nitrogen hyperfine coupling constant (a_N) (spin density on the NO moiety) can also affect on values of the cross-coupling rate constant k_c . [25]. For example, linear trends were observed between k_c the cohesive pressure c , the normalized Reichardt solvent polarity constant E_T^N , [32] and the nitrogen hyperfine coupling constant a_N .

Effects polarity and sterics on the rate constant of cross-coupling of alkyl radicals were investigated in detail [33]. The analysis of the experimental data led to the following conclusions: (1) congestion around the nitroxide moiety and the bulkiness of the alkyl radical destabilize the transition state (TS) and cause the decrease in k_c .

Fig. 3.13 HALS mechanism [31]. Reprinted from [31], Copyright 2012 American Chemical Society [31]



(2) the increase in the polarity of the substituents on the nitroxide moiety destabilizes the reactant state, increasing k_c , and (3) the steric effect is better ascribed to an entropy effect, which is in turn affected by the stabilization/polarity effect.

3.5 Nitroxides in Electrocatalysis

N-Oxyl compounds represent a diverse group of reagents that find widespread use as electro catalysts for the selective oxidation of organic molecules in both laboratory and industrial applications [34–62].

In pioneering research Semmelhack and co-workers, it was found that TEMPO can act as an electrocatalyst for alcohol electrooxidation [34]. The reaction between electrogenerated TEMPO^+ with primary alcohols in the presence 2,6-lutidine, as a base, was fast, even at -60°C , and up to 40 catalytic turnovers were achieved. Secondary alcohols were oxidized at significantly slower rates. On the basis of deuterium kinetic isotope effects and Hammett relationship, four potential routes TEMPO-catalyzed alcohol oxidation were considered: (1) direct hydride abstraction from the alcohol by the oxoammonium to afford hydroxylamine and an oxocarbenium ion that undergoes subsequent deprotonation, (2) electron/proton transfer from alcohol to oxoammonium, generating TEMPO, H^+ , and an alkoxyl radical, (3) nucleophilic attack of an alkoxide at the nitrogen atom of TEMPO^+ to generate a reactive N–O adduct, and (4) nucleophilic attack of the alkoxide at the oxygen atom of TEMPO^+ to generate a reactive O–O adduct.

In the past decades, numerous works on electrocatalysis with nitroxides as catalysts have been carried out. Among them: electrooxidation of menthol [35], [6 β -Methyl-3 β ,5 α -dihydroxy-16 α ,17 α -cyclohexanopregnan-20-one [36], carbohydrates and carboxylated cellulose [37], racemic SEC-benzylic alcohols [38] lignin β -O-4 model compound [39], oxidation of primary and secondary amines to give the corresponding nitrile or carbonyl [40], oxidation of tertiary amines catalyzed by 4-BzO-TEMPO [41], oxidation tetrahydroisoquinolines and related compounds [42], electrochemically induced C–H functionalization sing bromide ion/ 2,2,6,6-Tetramethylpiperinyl-N-oxyl dual redox catalysts in a two-phase electrolytic system [43], synthesis of nitriles from aldehydes dehydrogenation of saturated N-heterocycles [44], propargyl acetates to provide α,α -dihaloketone [45], terminal alkenes by $\text{Pd}(\text{OAc})_2$ catalysis with Co-catalytic TEMPO [46], oxidation of thioamides to benzothiazoles and thiazolopyridines [47], oxidation of glycerol to 1,3-Dihydroxyacetone [48], and 5) electrocatalytic oxidation of L-tyrosine by a nitroxide [49]. However, the reactions of alcohols and their derivatives attract particular attention.

A comprehensive survey of the electrochemical properties and wide electrocatalytic applications of aminoxyls, imidoxyls, and related reagents were reviewed [4]. The following aspects of electrocatalytic systems were described: (1) electrochemistry of TEMPO and other aliphatic cyclic aminoxyl derivatives; (2) electrochemical properties of TEMPO; (3) structural effects on the electrochemical

properties of cyclic aminoxyl radicals; (4) electrochemical reactions mediated by TEMPO and related cyclic aminoxyl radicals; (5) alcohol oxidation mechanism of aminoxyl-mediated process; (6) performance of aminoxyl derivatives, (7) cooperative copper/aminoxyl catalysis; (8) oxidation of synthetic alcohol; (9) amine oxidation; (10) C–H functionalization; (11) palladium co-catalyzed reactions; (12) alkene aminooxygenation; (13) alkyne hydroxybromination; (14) oxidation of sulfur-containing compounds; (15) electrochemistry and electrochemical applications of imidoxyl derivatives including electrochemical properties of N-Hydroxyphthalimide in alcohol oxidation and other NHPI-mediated electrooxidation reactions, and (16) electrochemistry of other N-oxyl radicals.

Numerous quantitative experimental data were tabulated: (1) experimental aminoxyl/oxoammonium redox potentials, (2) redox leveling in the $1\text{ e}^-/\text{H}^+$ hydroxylamine/aminoxyl redox couple, (3) effect of ring structure on the calculated e^- potentials for oxidation of cyclic aminoxyl radicals, (4) experimental N-hydroxyimide/imidoxyl redox potentials versus NHE (5) redox potential of the aminoxyl to oxoammonium redox process for various N-oxyl radicals potentials, (6) redox potentials (V vs. NHE) of N-aryl hydroxylamines, hydroxyamic acids, and other acyclic N-hydroxy derivatives as determined by CV or differential pulse voltammetry, (7) redox potential of heterocyclic N-hydroxy derivatives, (8) second-order rate constants of the reaction of phthalimide N-oxyl (PINO) with alcohol substrates, and (9) second-order rate constants of the reaction of PINO with substrates containing activated C–H bonds.

Figure 3.14 demonstrates an example of electrochemical processes involving TEMPO and phthalimide N-oxyl (PINO).

Fig. 3.14 Example of nitroxide redox reactions [4].
Reprinted from [4],
Copyright 2012 American Chemical Society

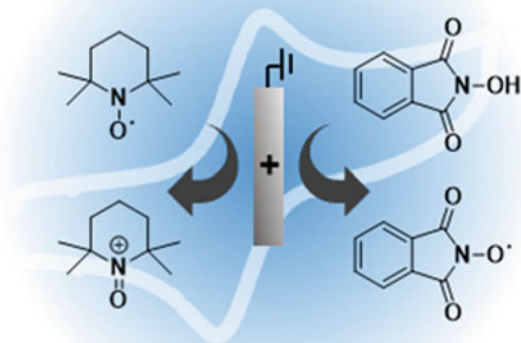
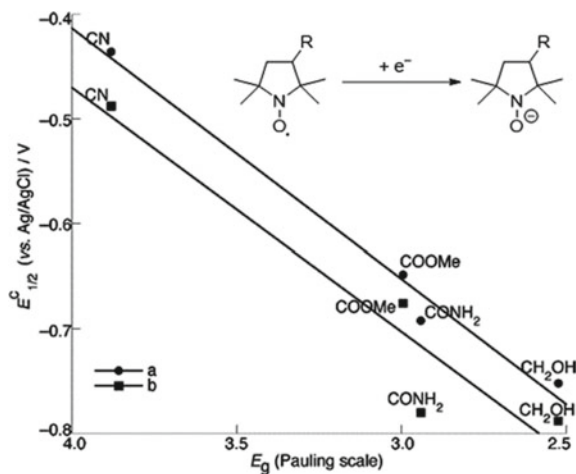


Fig. 3.15 Correlation between the Pauling group electronegativity (E_g) of substituents versus redox potentials ($E_{1/2}$) for the five-membered ring NUTIG hydroxylamine/aminoxyl radicals in **a** MeOH (0.1 M Bu_4NClO_4) and **b** phosphate buffer (0.1 M, pH 7.4) [4]. Reprinted from [4], Copyright 2012 American Chemical Society

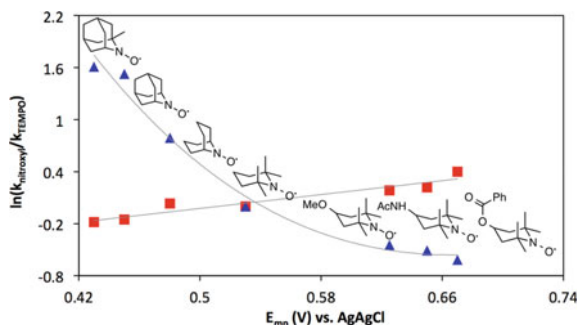


A linear relationship between the Pauling group electronegativity of the substituent and the hydroxylamine/aminoxyl redox potential of the corresponding PROXYL derivative is shown in Fig. 3.15.

The voltammetric technique was used to determine the catalytic activity for TEMPO-mediated electrooxidation of a series of primary and secondary alcohols, for example, benzyl alcohol [50]. A mechanism for electrocatalytic oxidation of benzyl alcohol by TEMPO was proposed. Alcohol electrooxidation in CH_3CN with TEMPO as electron–proton transfer mediators and N-methylimidazole as an added base was carried out [51]. A series of TEMPO analogs and bi- and polycyclic nitroxides with a range of redox potentials for the oxidation of alcohols under basic conditions was examined using chronoamperometry and CV techniques [52]. In addition, catalytic rate constants for the oxidation of butanol in both chemical (by NaOCl) and electrochemical oxidation processes were obtained. The experiments showed that reaction rates exhibit opposite trends with respect to the nitroxide/oxoammonium redox potential. Specifically, it was found that: (1) for the less hindered nitroxides, which exhibit comparatively low redox potentials, the reaction run much faster than TEMPO derivatives when NaOCl is used as the oxidant; (2) the rates are faster with higher-potential TEMPO derivatives under electrochemical conditions; (3) low-potential nitroxide mediators are more rapidly oxidized by NaOCl and exhibited higher steady-state concentration of the oxoammonium relative to high-potential nitroxides; (4) the increased rate of alcohol oxidation by low-potential aminoxyl mediators under chemical oxidation conditions correlates with the more rapid generation of the corresponding oxoammonium species under these conditions; (5) the reaction driving force is more significant than steric effects in nitroxide-mediated electrochemical oxidation of alcohols; and (6) linear free energy correlations for aminoxyl-catalyzed oxidation of 1-butanol takes place (Fig. 3.16).

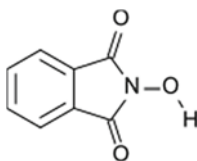
Immobilization of nitroxyl mediators on electrode surfaces significantly enhanced rates of alcohols oxidation and facilitates isolation of products as compare with

Fig. 3.16 Linear free energy correlations for aminoxyl-catalyzed oxidation of 1-butanol with NaOCl as a chemical oxidant (blue solid triangles) and under electrochemical conditions (red solid squares) [52]. Reprinted from [52], Copyright 2015 American Chemical Society



methods that use dissolved nitroxide mediators [53]. For example, pyrene-tethered TEMPO derivative was noncovalently immobilized at electrodes coated with multi-walled carbon nanotubes [54]. In preparative electrolysis experiments with a series of alcohol substrates and the immobilized catalyst, turnover numbers and frequencies approached 2000 and 4000 h⁻¹, respectively. The reaction conversion was almost 100% and less 5% for the immobilized and free nitroxides, respectively. The oxidation of a sterically hindered hydroxymethylpyrimidine precursor to the blockbuster drug, Rosuvastatin, was also demonstrated.

In paper [55], it was shown that *N*-Hydroxyphthalimide (NHPI)



which generates phthalimide *N*-oxyl (PINO) radical is an effective mediator for the oxidation of alcohols by electrolysis. NHPI undergoes one-electron oxidation to form PINO. In CH₃CN, the e⁻/H⁺ NHPI/PINO couple exhibits a redox potential of 1.44 V versus SCE which is quasi-reversible. It was also found that electrogenerated PINO catalytically oxidizes benzyl alcohols [56]. The NHPI/PINO couple was applied to electrocatalytic oxygenation of various compounds including lignin models [57], native lignin [58], benzylic and allylic bonds [59], and allylic C–H bonds oxidation [60]. A mechanism of NHPI-mediated electrooxidation of alcohols was suggested.

The first use of *N*-hydroxyphthalimide as an electrochemical mediator for C–H oxidation to non-oxygenated products provided the basis for direct (in situ) or sequential benzylation of diverse nucleophiles using methylarenes as the alkylating agent [61]. The proposed hydrogen-atom transfer mechanism for C–H iodination allows C–H oxidation to proceed with minimal dependence on the substrate electronic properties and at electrode potentials 0.5–1.2 V lower than that of direct electrochemical C–H oxidation.

The use of NHPI as an electrochemical mediator for iodination of methylarenes was reported [62]. It was found that electrochemical generation of PINO is followed



Fig. 3.17 **a** Electrochemical NHPI/PINO-mediated iodination/functionalization of methyl arenes, **b** iodination, and **c** in situ methylarene iodination/alkylation of pyridine [62]. Reprinted from [62], Copyright 2018 American Chemical Society

by H-atom abstraction, and the resulting radical is trapped rapidly by I_2 (Fig. 3.17). Values of experimental N-hydroxyimide/imidoxyl redox potentials versus NHEa of the aminoxyl to oxoammonium redox process for various N-oxyl radicals, N-aryl hydroxylamines, hydroxyamic acids, and other acyclic N-hydroxy derivatives, as determined by CV or differential pulse voltammetry, were listed in separate tables. In addition, the following schemes were described: (1) NHPI-mediated electrochemical oxidation of alcohol substrates, (2) NHPI-mediated electrooxidation of lignin models, (3) electrooxidation and photochemical cleavage of native lignin, benzylic and allylic oxygenation mediated by NHPI, (4) electrochemical NHPI/PINO-mediated oxygenation of benzylic and allylic bonds, (5) comparison of the benzylic oxygenation of heteroaromatic species by NHPI-mediated aerobic and electrochemical method, (6) scope of the oxygenation of allylic C–H bonds mediated by Cl4–NHPI257, (7) NHPI-mediated oxidation of aldehyde acetals, and (8) electrochemical NHPI/PINO-mediated iodination/functionalization of methyl arenes. The electrochemical mediation of iodination reaction was illustrated in Fig. 3.17.

3.6 Nitroxides as Radical Scavenger

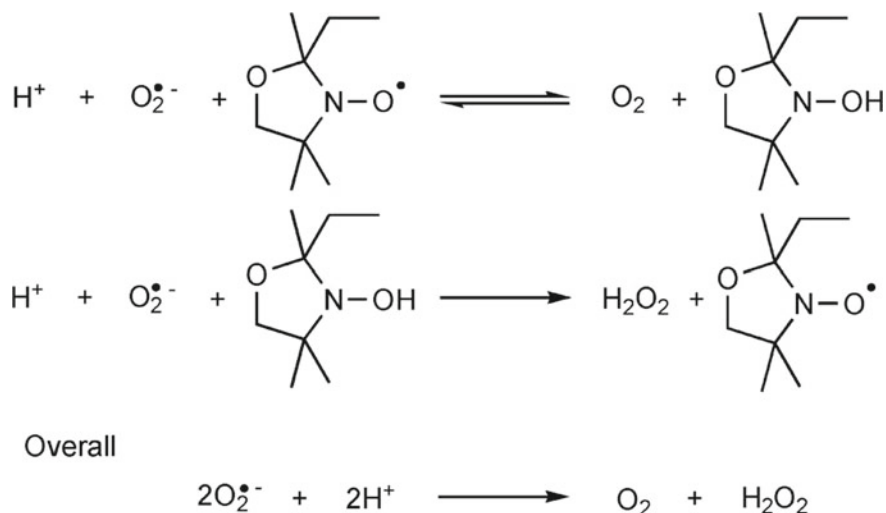
Oxidative/nitrosative stress contributes to the etiology of various disorders and associates with the destruction of key macromolecules and inactivation of antioxidant enzymes by reactive oxygen species (ROS) or reactive nitrogen species (RNS). The excess of reactive radicals generated in biological organisms can lead to the damage of vital cellular components such as lipids, proteins, and nucleic acids. These radicals can produce secondary reactive species and then induce a series of cellular response or severely endanger cell health and viability, ultimately leading to irreparable cell damage. Nitroxides have long been ascribed antioxidant activity to underly their chemopreventive and antiaging properties (Chap. 10). The reaction of nitroxides with ascorbate and glutathione (GSH) in solution and biological systems have great importance and been thoroughly studied [63–69]. For most nitroxides, the reaction follows the second-order kinetics law with the only product of nitroxide reduction being hydroxylamine. Nevertheless, when the rate constant of this reaction is low, the reversibility of the first steps may contribute to the kinetics. It is obvious that the

biological activity of nitroxides is linked to their electron transfer rates and redox potentials.

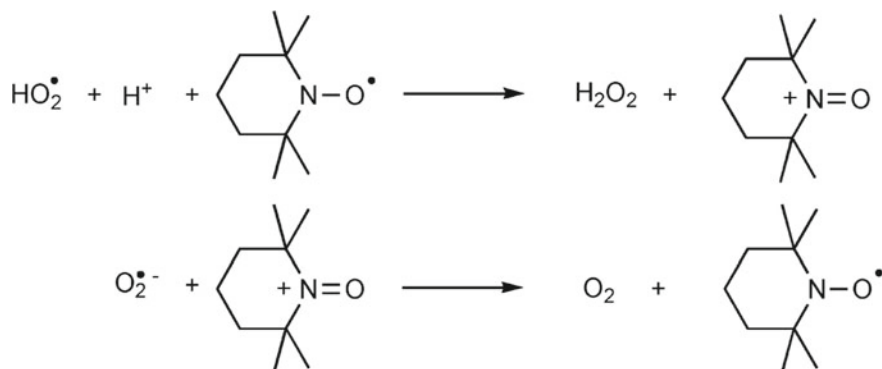
Reactivity of nitroxides to quench superoxide radicals as superoxide dismutase (SOD) mimics (Scheme 3.2) was first established by Samuni, Krishna, Goldstein, and co-workers [63].

In the case of oxazolidines (e.g., 2-ethyl-2,5,5-trimethyl-3-oxazolidin-1-yloxy, OXANO) Scheme 3.2 and its corresponding hydroxylamine, they react with superoxide [64]. The sequence of the SOD mimics reactions for TEMPO is indicated in Scheme 3.3. 2-ethyl-2,5,5-trimethyl-3-oxazolidin-1-yloxy, OXANO). Within the framework of this mechanism, a nitroxide undergoes repeated reductions and oxidations allowing in catalytic fashion the dismutation of superoxide to oxygen and hydrogen peroxide. Piperidine derivatives such as TEMPO undergo oxidation and reduction reactions to yield the corresponding oxoammonium cation, which then oxidizes superoxide to molecular oxygen. However, this mechanism is not likely physiologically relevant in all cases in cell with cells higher level of SOD enzymes [65]. Employing pulse radiolysis, Goldstein and Samuni demonstrated that nitroxides react readily with peroxy radicals [66]. Nitroxides can undergo acid-promoted reactions with peroxy radicals and then be recycled from the resultant oxoammonium ion by reduction with a substrate-derived radical eventually acting as a catalytic radical-trapping antioxidants.

The kinetics and mechanisms of the reactions of TEMPO, as well as an *N*-arylnitroxide and an *N,N*-diarylnitroxide, with alkylperoxy radicals, the propagating species in lipid peroxidation, were characterized [67]. Inhibited autoxidations of THF in aqueous buffers revealed that nitroxides reduce peroxy radicals by electron transfer with rate constants ($k \approx 10^6$ to $> 10^7 \text{ M}^{-1} \text{ s}^{-1}$) that correlate with the standard potentials of the nitroxides ($E^\circ \approx 0.75\text{--}0.95 \text{ V vs. NHE}$) and that this



Scheme 3.2 SOD-mimicking behavior of OXANO [2]. Reprinted from [2], Copyright 2007 American Chemical Society



Overall



Scheme 3.3 SOD-mimicking behavior of TEMPO [2]. Reprinted from [2], Copyright 2007 American Chemical Society

activity is catalytic regarding nitroxide. Regeneration of the nitroxide was suggested to occur by a two-step process involving hydride transfer from the substrate to the nitroxide-derived oxoammonium ion followed by H-atom transfer from the resultant hydroxylamine to a peroxy radical. In the presence of a hydride donor (NADPH for example) (Fig. 3.18), TEMPO⁺ is converted to TEMPOH which can trap another peroxy radical via H-atom transfer, thereby regenerating TEMPO. Figure 3.19 indicates calculated transition state structure for the reaction of TEMPO⁺ with THF.

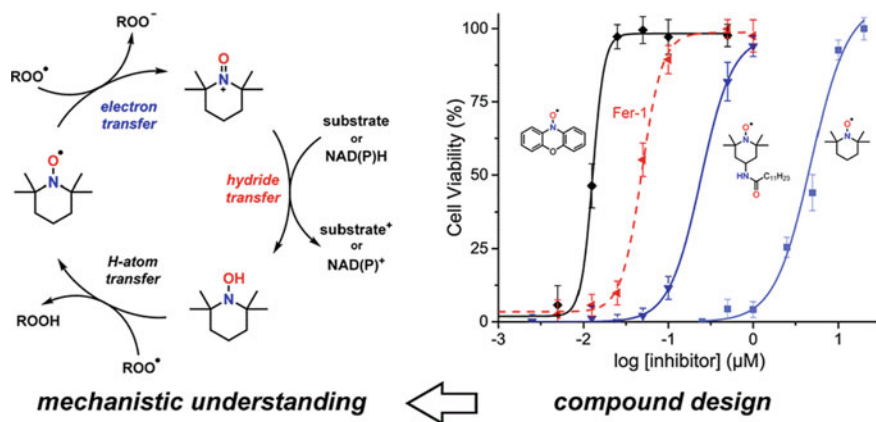
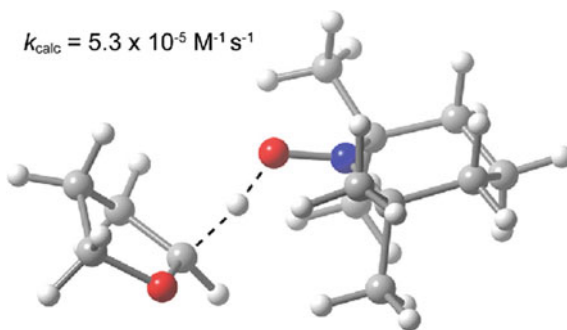


Fig. 3.18 Mechanisms of the reactions of TEMPO, *N*-arylnitroxide *N,N*-diarylnitroxide, with alkylperoxy radicals and its effect on cell viability [67]. Reprinted from [67], Copyright 2018 American Chemical Society

Fig. 3.19 CBS-QB3—calculated transition state structure for the reaction of TEMPO+ with THF [67]. Reprinted from [67], Copyright 2018 American Chemical Society



It was determined that TEMPO can be regenerated from its oxoammonium ion by reaction with alkyl radicals, and this reaction was proposed to be a key step in TEMPO-catalyzed synthetic transformations. Because this process occurs with $k \sim 1\text{--}3 \times 10^{10} \text{ M}^{-1} \text{ s}^{-1}$, it enables to compete with O_2 for alkyl radicals [68]. The addition of weak acids facilitates this reaction, whereas the addition of strong acids slows it by enabling back electron transfer. Another mechanism invoked to account for the biological activity of nitroxides involves the scavenging of alkyl radicals [69]. This reaction is too slow ($k \approx 1\text{--}3 \times 10^8 \text{ M}^{-1} \text{ s}^{-1}$) to compete with the formation of peroxy radicals from the combination of alkyl radicals and O_2 ($k \approx 3 \times 10^9 \text{ M}^{-1} \text{ s}^{-1}$). Nevertheless, a competition can be more unlikely because O_2 is generally present in much higher concentration than nitroxide (mM vs. μM to nM).

Autoxidations of unsaturated hydrocarbons are efficiently inhibited by nitroxides and/or compounds which react readily to produce nitroxides under autoxidative conditions. For example, diarylamines and hindered aliphatic amines comprise two of the three key types of radical-trapping antioxidants (RTAs) to preserve hydrocarbon-based materials (Fig. 3.1a) [64]. Diarylamines can trap peroxy radicals at ambient temperatures by a catalytic mechanism involving the formation of diarylnitroxide intermediates (the “Korcek Cycle”) (Fig. 3.20) [70]. At elevated temperatures, nitroxides trap radicals in still catalytic manner (the “Denisov Cycle”) (Fig. 3.20) [71]. Hindered aliphatic reaction nitroxides do not react with alkylperoxy radicals, while aryl nitroxides react by addition to the aryl rings [64].

Thermodynamically favored proposed cycle for nitroxide regeneration and competitive amine formation: via H-atom abstraction from an alkoxyamine and subsequent aminyl radical formation is summarized in Fig. 3.21 [31]. Alternative literature mechanisms of nitroxide regeneration were also discussed.

Radical scavenging activity of aromatic and aliphatic mono- and bis-nitroxides was investigated in the presence of alkyl and peroxy radicals generated from thermal decomposition of 2,20-azobis(2,4-di-methylvaleronitrile) using EPR and UV–Vis spectroscopy [72]. Antioxidant activity of the nitroxides was evaluated by monitoring conjugated dienes formation during methyl linoleate micelles peroxidation and by measuring carbonyl content in oxidized bovine serum albumin. Suggested scheme showing the scavenging of alkyl ($\text{R}\cdot$) and peroxy radicals

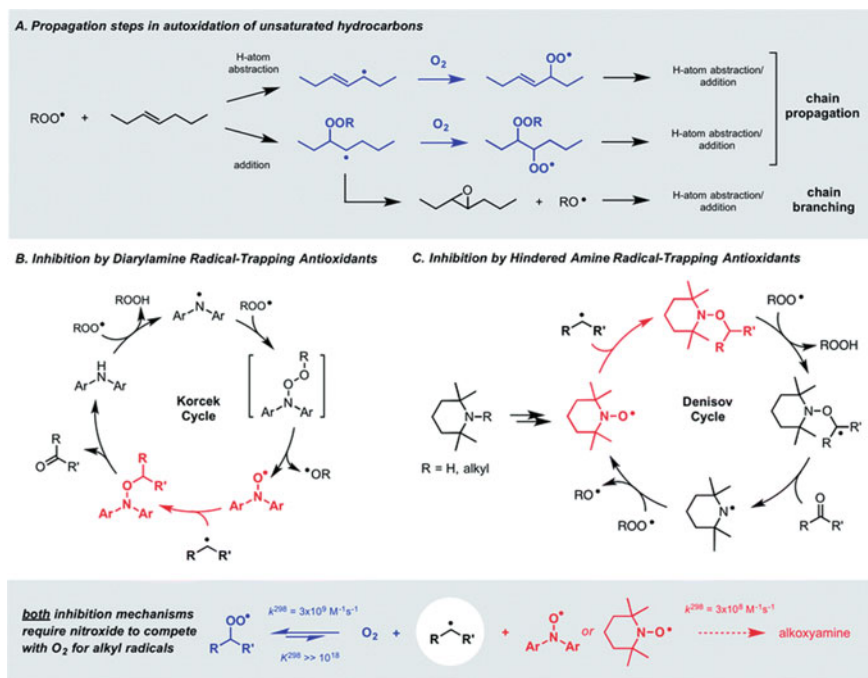


Fig. 3.20 **a** Key propagation steps in the autoxidation of unsaturated hydrocarbons. **b** and **c** The Korcek and Denisov mechanisms believed responsible for the catalytic inhibition of hydrocarbon autoxidation by diarylamine and hindered amine antioxidants [64]. Reprinted from [64], Copyright 2018 RSC

(ROO•) by aromatic and aliphatic nitroxides was proposed. According to the scheme, (1) indolinonic aromatic nitroxides react with peroxy radical, (2) aliphatic nitroxides react, (3) bis-nitroxides are roughly twice more efficient at inhibiting lipid peroxidation compared to their corresponding mono-derivatives, and (4) aromatic nitroxides are more effective antioxidants than aliphatic ones.

3.7 Nitroxide Reaction with Typical Antioxidants

Within recent two decades, nitroxides are widely used for an analysis antioxidants in biological systems [73–88]. First application of nitroxide for quantitative analysis ascorbic acid in biological liquids was performed in Likhtenshtein group using dual fluorophore–nitroxide probes [77].

It was revealed [73] that tetracarboxylate pyrroline nitroxides are reduced by ascorbate/glutathione (GSH) with second-order rate constants that five orders of magnitude greater than those for gem-diethyl pyrroline nitroxide.

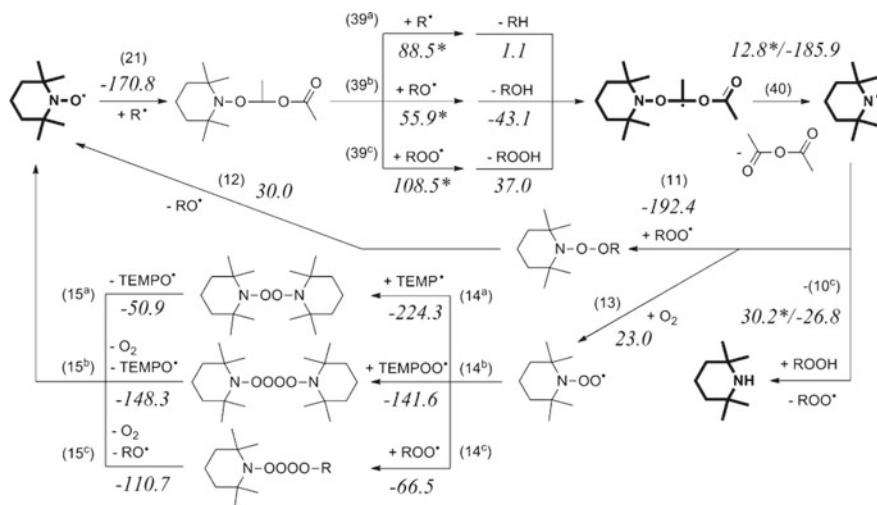
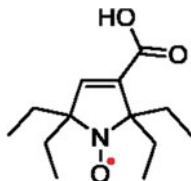


Fig. 3.21 Proposed cycle for nitroxide regeneration and competitive amine formation via H-atom abstraction from an alkoxyamine and subsequent aminyl radical formation. Numbers in italics are calculated as Gibbs free energies (kJ mol^{-1} , gas phase, 25 °C) of the reactions and activation (denoted by an asterisk) [31]. Reprinted from [31], Copyright 2018 American Chemical Society



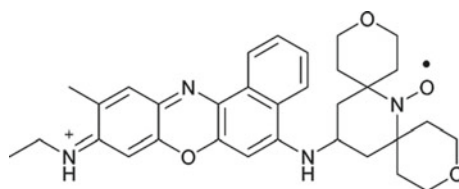
For these nitroxides, the electrochemical reduction potential was found to be less negative (by about 0.8 V), compared with the corresponding gem-diethyl nitroxides, while the oxidation potentials become more positive (by about 0.7 V). Electrochemical potentials as well as rates of reduction with ascorbate/GSH correlate via simple regressions with field/inductive parameters such as Swain/Lupton F-parameters (and/or Charton σ_I -parameters). Rates of reduction with ascorbate/GSH similarly correlate with four pyrroline nitroxides. Exception is the slowest reducing gem-diethyl nitroxide. These results suggest that the electron-withdrawing groups adjacent to the nitroxide moiety have a strong accelerating impact on the reduction rates.

The effects of substitution on nitroxides stability using five different classes of radicals, specifically, piperidine-, imidazolidine-, pyrrolidine-, isoindoline-based nitroxides, and as well as the Finland trityl radical were evaluated [74]. The rate of nitroxide reduction in the presence of ascorbate, cellular extracts, and after injection into oocytes cytoplasmic extracts from *X. laevis* oocytes was measured by continuous-wave EPR spectroscopy. Main results of the study are as follows: (1) Introduction of bulky ethyl groups next to a nitroxide group leads to significant stabilization against reduction by both ascorbic acid and the reductants present in living cells, (2) these

radicals are more stable in cells than trityl radical, (3) superior stability against reduction is due to combination of sterical shielding, ring size, and charge, (4) charged and neutral radicals showed different relative stabilities in cell extracts than in cells, and (5) the trityl radical exhibited considerable stability toward reduction, especially in cells. Thermodynamic parameters of nitroxide reduction determined by cyclic voltammetry were tabulated.

With a goal to improve stability of nitroxides to reduction by ascorbic acid, a series of 2,6-substituted nitroxyl radicals was prepared [75]. It was found that tetraethyl-substituted imidazolidine nitroxide is the most stable nitroxide in respect to reduction in ascorbate solutions ($k_1 = 0.02 \text{ M}^{-1} \text{ s}^{-1}$). The role of substituents on the stability of new synthesized several nitroxides with different substituents which vary the steric and electronic environment around the N–O moiety the radicals was investigated [76]. Results indicated that: (1) the nitroxide reactivity toward ascorbate correlates with the redox potential of the derivatives, (2) the electronic factors largely determine the radicals' stability, and (3) *ab initio* calculations confirmed a correlation between the reduction rate and the computed singly occupied molecular orbital–lowest unoccupied molecular orbital energy gap.

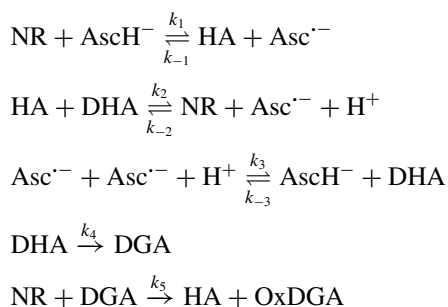
To increase the reactivity and selectivity toward the detection of ascorbic acid, the dual fluorophore–nitroxide probe 15-((9-(Ethylimino)-10-methyl-9*H*benzo[*a*]phenoxazin-5-yl)amino)-3,11-dioxo-7-azadispiro hexadecan-7-ylloxyl, (Nile-DiPy)



Nile-DiPy

was synthesized and characterized [78]. This fluorophore–nitroxide probe rapidly reacted with ascorbic acid and showed in parallel fluorescence enhancement in PBS at pH 7.4, containing 5% (v/v) DMSO, while other biological reductants, including uric acid, glutathione, NADH, catechin, 2,2,5,7,8-pentamethyl-6-chromanol did not react with the nitroxide in these conditions. In the presence of ascorbic acid, the fluorescence intensity of Nile-DiPy increased in a dose-dependent manner concentrations of ascorbic acid (0.13–8.0 mM). The second-order rate constant for the reaction of Nile-DiPy and of Nile-TEMPO with ascorbic acid was calculated as $246 \text{ M}^{-1} \text{ s}^{-1}$ and ($17.4 \text{ M}^{-1} \text{ s}^{-1}$), respectively. The kinetic isotope effect (KIE) for the detection of ascorbic acid was determined to be 9.77, indicating that Nile-DiPy reacts with ascorbic acid via hydrogen atom transfer. The limit of detection of this fluorometric method was estimated to be 9.72 nM. The usefulness of Naph-DiPy nitroxide for the measurement of ascorbic acid in the plasma of osteogenic disorder Shionogi rats of healthy and streptozotocin-induced diabetic animals was demonstrated.

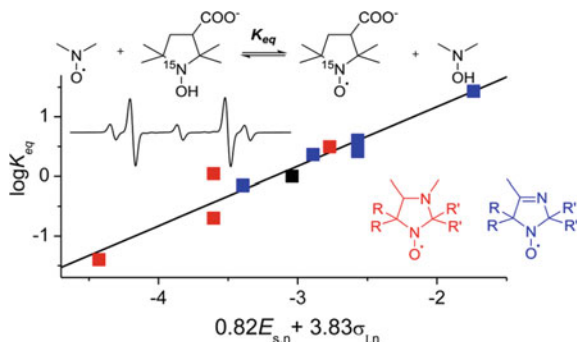
Mechanistic studies of the reduction of TEMPO and other nitroxides in deaerated solutions of ascorbate were performed [79]. In the kinetics studies, the peak intensity of the low-field component of the triplet EPR spectrum was monitored using an EMX X-band spectrometer. Quantitative kinetics analysis of the nitroxide reduction by ascorbate and hydroxylamine oxidation monitored using an EMX X-band spectrometer was carried out taken into account the following stages:



where *NR* and *HA* denote nitroxyl radical and its hydroxylamine, respectively; AscH^- , $\text{Asc}^{\bullet-}$, *DHA*, *DGA*, and *OxDGA* denote ascorbate anion, ascorbate radical, dehydroascorbic acid, diketogulonic acid, and product of oxidation of diketogulonic acid by *NR*, respectively. Finally, it was summarized that: (1) The bimolecular rate constants of ascorbate-induced reduction are significantly higher for six-membered ring *NR* of piperidine types ($k_1 = 3.5 \text{ M}^{-1} \text{ s}^{-1}$ for TEMPO and $k_1 = 7 \text{ M}^{-1} \text{ s}^{-1}$ for TEMPOL) than for the five-membered ring *NR* of pyrrolidine ($k_1 = 0.07\text{--}0.3 \text{ M}^{-1} \text{ s}^{-1}$), and imidazolidine ($k_1 = 0.85 \text{ M}^{-1} \text{ s}^{-1}$) types; (2) a presence of the double bond at the position 3 in the five-membered ring *NR* of pyrroline ($k_1 = 0.64\text{--}1.6 \text{ M}^{-1} \text{ s}^{-1}$) and imidazoline ($k_1 = 5.6 \text{ M}^{-1} \text{ s}^{-1}$) types increases their reduction rates by ascorbate, (3) carboxyproxyl *NR* **1** is resistant against reduction by ascorbate ($k_1 = 0.1 \text{ M}^{-1} \text{ s}^{-1}$), and (4) tetraethyl-substituted imidazolidine *NR* **4** is the most stable *NR* in respect to reduction in ascorbate solutions (e.g., $k_1 = 0.02 \text{ M}^{-1} \text{ s}^{-1}$). The equilibrium constants for one-electron reduction of the tetraethyl-substituted *NR* by ascorbate were found to be in the range from 2.65×10^{-6} to 10^{-5} which is significantly lower than corresponding values for the tetramethyl-substituted *NR* (more or about 10^{-4}). The reduction of ascorbate radicals by GSH with the rate constant $10 \text{ M}^{-1} \text{ s}^{-1}$ was examined.

The importance of effect of sterical shielding on the redox properties has been also revealed for various types of nitroxides, including those of isoindoline, 4 imidazoline, imidazolidine, piperidine, pyrroline, and pyrrolidine series [80]. Direct measurements of the rate constants of nitroxide of reduction with ascorbate and equilibrium constant K_{eq} in the mixture of the reference isotopically labeled (^{15}N) hydroxylamine ((3-carboxy-1-hydroxy-2,2,5,5-tetramethylpyrrolidine-1-oxyl-1- ^{15}N) and the nitroxides of the imidazoline and midazolidine series were carried out. For example, the 2,2,5,5-tetraethyl-substituted pyrrolidine nitroxides demonstrate the highest stability inside cells, exceeding that of trityl radicals. The nitroxide electrochemical

Fig. 3.22 Correlation of $\log(K_{eq})$ versus $f(E_s, \sigma_I)$ [80]. Reprinted from [80], Copyright 2015 American Chemical Society



reduction was also studied. Results showed that increase in the number of bulky alkyl substituents leads to a decrease in the rate of reduction with ascorbate. Oxidant properties of the nitroxides determined by steric and 'electronic effects of the substituents were quantitatively characterized by means of multiple regression using the Fujita steric constant E_s and the inductive Hammett constant σ_I (Fig. 3.22).

In order to improve the stability of the radicals through steric and to strength electrostatics shielding, two new pyrrolidine nitroxide radicals, *cis/trans*-2,5-bis(carboxymethyl)-2,5-diethylpyrrolidine 1-oxyl and 2-(carboxymethyl)-2,5,5-triethylpyrrolidine 1-oxyl, were prepared [81]. An ascorbic acid reduction assay proved that the newly synthesized radicals exhibit higher reductive stability than 3-carboxy-PROXYL and 4-carboxy-TEMPO.

Synthesis and antioxidant activity and reactive oxygen species (ROS) scavenging of nitroxides, that is, *N*-[2-(*p*-vinylbenzylidene)benzothiazole] 4-amino-2,2,6,6-tetramethyl-1-piperidinyloxy (3a) and *N*-[2-(*p*-vinylbenzylidene)benzoxazole] 4-amino-2,2,6,6-tetramethyl-1-piperidinyloxy (3b), *N*-[2-(*p*-vinylbenzyl)benzoxazole]4-amino-2,2, 6,6-tetramethyl-1-piperidinyloxy (4a), and *N*-[2-(*p*-vinyl, benzyl)benzoxazole]4-amino-2,2,6,6-tetramethyl-1-piperidinyloxy (4b), were performed [82]. The activities were assayed by the reduction of nitroblue tetrazolium (NBT). The superoxide radical was generated in the *N*-methylphenazonium (PMS) and nicotinamide adenine dinucleotide (reduced form, NADH). The hydroxyl radicals were generated in the reaction of H_2O_2 - $FeSO_4$ and colored substance produced by reacting $\bullet OH$ with salicylic acid.. IC50 values of the studied compounds which characterized their effect on ROS scavenging activity were tabulated. The results indicated that the novel compounds exhibit improved antioxidant activity and the superoxide radical scavenging activity which is related to redox property of the compounds.

3.8 Nitroxide Redox Behavior in Biological Systems

The scavenging activities of dual fluorophore–nitronyl compound for superoxide and hydroxyl radicals are described in Section X. Methamphetamine (METH)-induced neurotoxicity is associated with mitochondrial dysfunction and enhanced oxidative stress. The aims of study [83], conducted in the mouse brain repetitively treated with METH, were to examine the redox status using the redox-sensitive imaging probe 3-methoxycarbonyl-2,2,5,5-tetramethylpiperidine-1-oxyl (MCP), and non-invasively visualize the brain redox status with electron paramagnetic resonance imaging. Measurements of the rate of reduction of MCP in a mouse head measured from a series of temporal EPR images were used to construct a two-dimensional map of rate constant. The obtained redox map illustrated the change in redox balance in the METH-treated mouse brain as result of oxidative damage. Enhancement of the reduction reaction of MCP resulted from enzymatic reduction in the mitochondrial respiratory chain and blood-brain barrier (BBB) dysfunction after treatment with METH for 7 days was also revealed.

In vivo physiological ligand citrate can bind iron(II) ions to form the iron(II) citrate complex. EPR and fluorescence spectroscopies were employed to study that TEMPO inhibited $\cdot\text{OH}$ production from the Fenton-like reaction of iron(II) citrate with H_2O_2 by up to 90% [84]. The $\cdot\text{OH}$ production from the Fenton-like reaction was monitored using the fluorescence probe APF. Reaction of spin-trap DMPO with the generated $\cdot\text{hydroxyl}$ was studied employing EPR spectrometer. The spectrophotometrical experiments indicated that this inhibition was due to oxidation of the iron(II) citrate by TEMPO with a stoichiometry of Tempo:Iron(III) citrate 1.1:1.0.

The TEMPO-conjugated gold nanoparticles (Au NPs, Au-PEG-TEMPO NPs) (Fig. 3.23) were used for the culture of hMSCs to investigate their effect on ROS scavenging, proliferation, and osteogenic and adipogenic differentiation of hMSCs [85]. Au NPs with an average size of 40 nm were conjugated with 2,2,6,6-tetramethylpiperidine *N*-oxyl (TEMPO) to endow them with ROS scavenging capacity while holding the beneficial biological effect of Au NPs. The work results indicated that the TEMPO-conjugated Au NPs had high scavenging capacity for overproduced ROS and maintained the promotive effect of Au NPs on osteogenic differentiation of hMSCs without the inhibitory effect of free TEMPO.

A nitroxide radical-containing polymer (NRP), which is composed of poly(4-methylstyrene) possessing nitroxide radicals as a side chain via amine linkage, was coated onto cigarette filters, and its ROS scavenging activity from streaming cigarette smoke was evaluated [86]. The intensity of electron spin resonance signals of the NRP in the filter decreased after exposure to cigarette smoke. It was also demonstrated that the extract of cigarette smoke passed through the NRP-coated filter has a lower cellular toxicity than smoke passed through poly[4 (cyclohexylamino)methylstyrene]- and poly(acrylic acid)-coated filters. Schematic illustrations of the NRP and smoking device were presented. NRP was suggested as a promising material for ROS scavenging from cigarette smoke.

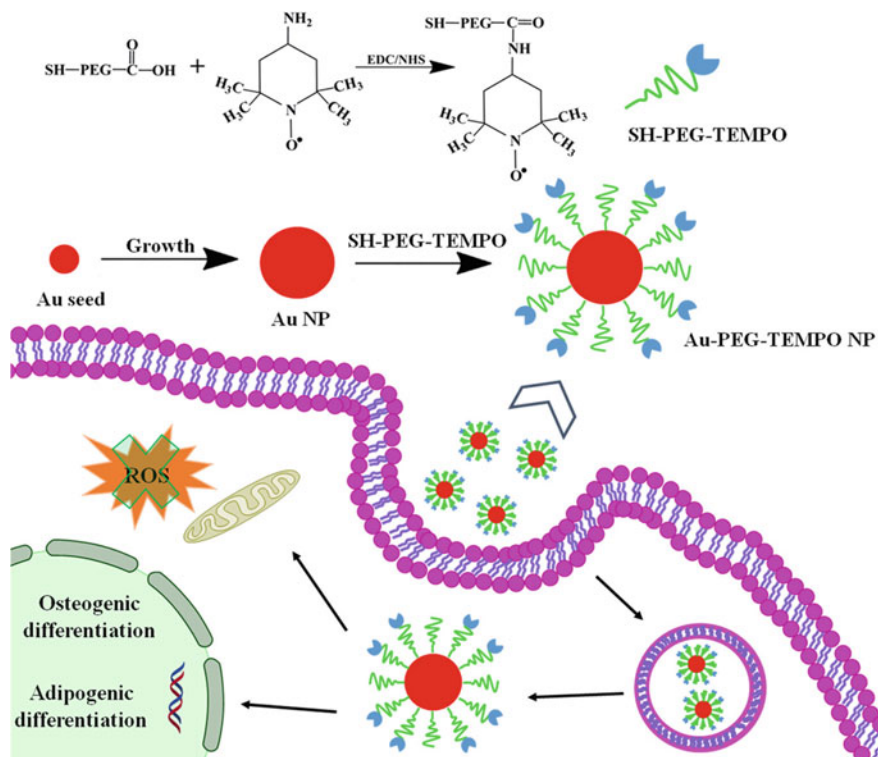


Fig. 3.23 TEMPO-conjugated Au NPs (Au-PEG-TEMPO NPs) [85]. Reprinted from [85], Copyright 2018 American Chemical Society

Pyrrolidine nitroxides, 3,4-bis-(acetoxymethoxycarbonyl)-proxyl (DCP-AM2) and 3-(2-(bis(2-(acetoxymethoxy)-2-oxoethyl)amino)acetamido)-proxyl (DCAP-AM2) which can undergo hydrolysis by cellular esterases to hydrophilic carboxylate derivatives were studied in human aortic endothelial cells (HAEC) using EPR method [87]. EPR measurements in the isolated mitochondrial fraction indicated that mitochondria is the main place where DCP was finally accumulated. TEMPO derivatives showed much faster decay of EPR signal in the cellular fraction, compared to pyrrolidine nitroxides. It was found that (1) supplementation of endothelial cells with 50 nM of DCP-AM2 completely normalized the mitochondrial superoxide level, (2) administration of DCP-AM2 to mice (1.4 mg/kg/day) resulted in substantial nitroxide accumulation in the tissues and significantly reduced hypertension, (3) hydroxylamine derivatives of dicarboxyproxyl nitroxide DCP-AM-H can be used for the detection of superoxide in vivo in angiotensin II model of hypertension, and (4) infusion of DCP-AM-H in mice leads to accumulation of persistent EPR signal of nitroxide in the blood. Thus, the data demonstrate that acetoxymethoxycarbonyl group containing nitroxides accumulate in mitochondria and indicated site-specific antioxidant activity.

The therapeutic and research studies of nitroxide compounds, biologically relevant effects of nitroxides, including their ability to degrade **superoxide** and peroxide, inhibit Fenton reactions, and undergo radical–radical recombination, were reviewed [88].

References

1. M.B. Neiman, É.G. Rozantsev, Y.G. Mamedova, Free radical reactions involving no unpaired electrons. *Nature* **196**, 472 (1962)
2. J.L. Hodgson, M. Namazian, S.E. Bottle, M.L. Coote, One-electron oxidation and reduction potentials of nitroxide antioxidants: a theoretical study. *J. Phys. Chem. A* **111**, 13595–13605 (2007)
3. V.A. Golubev, E.G. Rozantsev, M.B. Neiman, Some reactions of free iminoxyl radicals with the participation of the unpaired electron. *Bull. Acad. Sci. USSR Div. Chem. Sci.* **14**, 1898–1904 (1965)
4. J.E. Nutting, M. Rafiee, S.S. Stahl, Tetramethylpiperidine *N*-Oxyl (TEMPO), Phthalimide *N*-Oxyl (PINO), and related *N*-Oxyl species: electrochemical properties and their use in electrocatalytic reactions. *Chem. Rev.* **118**, 4834–4885 (2018)
5. T. Yamasaki, Y. Matsuoka, F. Mito, M. Yamato, K. Yamada, Redox potential of nitroxides is an index to evaluate superoxide dismutase mimic activity. *Asian J. Org. Chem.* **2**(5), 388–391. <https://doi.org/10.1002/ajoc.201300011>
6. Y.G. Budnikova, T.V. Gryaznova, M.K. Kadirov, E.V. Tret'yakov, K.V. Kholin, V.I. Ovcharenko, R.Z. Sagdeev, O.G. Sinyashin, Electrochemistry of nitronyl and imino nitroxides. *Russ. J. Phys. Chem. A* **83**(11), 1976–1980 (2009)
7. L. Marx, B. Schöllhorn, Intramolecular charge effects in the electrochemical oxidation of aminoxyl radicals. *New J. Chem.* **30**, 430–434 (2006)
8. J.P. Blinco, J.L. Hodgson, B.J. Morrow, J.R. Walker, G.D. Will, M.L. Coote, S.E. Bottle, Experimental and theoretical studies of the redox potentials of cyclic nitroxide. *J. Org. Chem.* **73**(17), 6763–6771 (2008)
9. V.D. Sen', I.V. Tikhonovb, L.I. Borodinb, E.M. Plissb, V.A. Golubev, M.A. Syroeshkinc, A. Rusakov, Kinetics and thermodynamics of reversible disproportionation–comproportionation in redox triad oxoammonium cations–nitroxyl radicals–hydroxylamines. *J. Phys. Org. Chem.* **28**, 17–24 (2015)
10. S. Manda, I. Nakanishi, K. Ohkubo, H. Yakumaru, K.-I. Matsumoto, T. Ozawa, N. Ikota, S. Fukuzumi, K. Anzai, Nitroxyl radicals: electrochemical redox behavior and structure-activity relationships. *Org. Biomol. Chem.* **5**, 3951–3955 (2007)
11. I.V. Tikhonov, V.D. Sen, L.I. Borodin, E.M. Pliss, V.A. Golubev, A.I. Rusakov, Kinetics and thermodynamics of reversible disproportionation–comproportionation in redox triad oxoammonium cations–nitroxyl radicals–hydroxylamines. *J. Phys. Org. Chem.* **27**, 114–120 (2014)
12. J.M. Bobbitt, N.A. Eddy, X. Cady, J. Jin, J.A. Gascon, S. Gelpí-Dominguez, J. Zakrzewski, M.D. Morton, Preparation of some homologous TEMPO nitroxides and oxoammonium salts; notes on the NMR spectroscopy of nitroxide free radicals; observed radical nature of oxoammonium salt solutions containing trace amounts of corresponding nitroxides in an equilibrium relationship. *J. Org. Chem.* **82**(18), 9279–9290 (2017)
13. A. Bobko, V.V. Khramtsov, Redox properties of the nitronyl nitroxide antioxidants studied via their reactions with nitroxyl and ferrocyanide. *Free Radical Res.* **49**(8), 919–926 (2015)
14. J.A. Bogart, H.B. Lee, M.A. Boreen, M. Jun, E.J. Schelter, Fine-tuning the oxidative ability of persistent radicals: electrochemical and computational studies of substituted 2-pyridylhydroxylamines. *J. Org. Chem.* **78**, 6344–6349 (2013)

15. J.B. Gerken, Y.Q. Pang, M.B. Lauber, S.S. Stahl, Structural effects on the pH-dependent redox properties of organic nitroxyls: Pourbaix diagrams for TEMPO, ABNO and three TEMPO analogs. *J. Org. Chem.* **83**(14), 7323–7330 (2018)
16. S. Caron, R.W. Dugger, S.G. Ruggeri, J.A. Ragan, D.H.B. Ripin, Large scale oxidations in the pharmaceutical industry. *Chem. Rev.* **106**, 2943–2989 (2006)
17. R. Ciriminna, M. Pagliaro, Industrial oxidations with organocatalyst TEMPO and its derivatives. *Org. Process Res. Dev.* **14**(1), 245–251 (2010)
18. J.M. Bobbitt, C. Brückner, N. Merbouh, Oxoammonium- and nitroxide-catalyzed oxidations of alcohols, in *Organic Reactions* (Wiley: Hoboken, NJ, 2010), pp. 103–424
19. S. Wertz, A. Studer, Nitroxide-catalyzed transition-metal-free aerobic oxidation processes. *Green Chem.* **15**, 3116–3134 (2013)
20. J.M. Bobbitt, A.L. Bartelson, W.F. Bailey, T.A. Hamlin, C.B. Kelly, Oxoammonium salt oxidations of alcohols in the presence of pyridine bases. *J. Org. Chem.* **79**(3), 1055–1067 (2014)
21. K.M. Lambert, Z.D. Stempel, S.M. Kiendzior, A.L. Bartelson, W.F. Bailey, Enhancement of the oxidizing power of an oxoammonium salt by electronic modification of a distal group. *J. Org. Chem.* **82**(21), 11440–11446 (2017)
22. M. Shibuya, S. Nagasawa, Y. Osada, Y. Iwabuchi, Mechanistic insight into aerobic alcohol oxidation using NO_x–nitroxide catalysis based on catalyst structure–activity relationships. *J. Org. Chem.* **79**(21), 10256–10268 (2014)
23. K.M. Lambert, J.M. Bobbitt, S.A. Eldirany, K.B. Wiberg, W.F. Bailey, Facile oxidation of primary amines to nitriles using an oxoammonium salt. *Org. Lett.* **16**(24), 6484–6487 (2014)
24. J.B. Gerken, S.S. Stahl, High-potential electrocatalytic O₂ reduction with nitroxyl/NO_x mediators: implications for fuel cells and aerobic oxidation catalysis. *ACS Cent. Sci.* **1**(5), 234–243 (2015)
25. E.G. Bagryanskaya, S.R.A. Marque, Scavenging of organic C-centered radicals by nitroxides. *Chem. Rev.* **114**, 5011–5056 (2014)
26. E.G. Bagryanskaya, S.R.A. Marque, Y.P. Tsentalovich, Alkoxyamine re-formation reaction. Effects of the nitroxide fragment: a multiparameter analysis. *J. Org. Chem.* **77**, 4996–5005 (2012)
27. A.L.J. Beckwith, V.W. Bowry, K.U. Ingold, Kinetics of nitroxide radical trapping. 1. Solvent effects. *Am. Chem. Soc.* **114**, 4983 (1992)
28. V.W. Bowry, K.U. Ingold, Kinetics of nitroxide radical trapping. 2. Structural effects. *Am. Chem. Soc.* **114**, 4992 (1992)
29. R.J. Kaptein, Simple rules for chemically induced dynamic nuclear polarization. *J. Chem. Soc. D* 732–733 (1971)
30. L.J. Berliner, E. Bagryanskaya, in *Multifrequency Electron Paramagnetic Resonance*, ed. by S.K. Misra (Wiley-VCH, Weinheim, Germany, 2011), p. 947
31. G. Gryn'ova, K.U. Ingold, M.L. Coote, New insights into the mechanism of amine/nitroxide cycling during the hindered amine light stabilizer inhibited oxidative degradation of polymers. *J. Am. Chem. Soc.* **134**(31), 12979 (2012)
32. C. Reichardt, T. Welton, *Solvent and Solvent Effect in Organic Chemistry*, 4th edn. (Wiley-VCH, Weinheim, Germany, 2011)
33. D. Bertin, P.-E. Dufils, I. Durand, D. Gimes, B. Giovanetti, Y. Guillaneuf, S.R.A. Marque, T. Phan, P. Tordo, Effect of the penultimate unit on the C–ON bond homolysis in SG1-based alkoxyamines. *Macromol. Chem. Phys.* **209**, 220 (2008)
34. M.F. Semmelhack, C.S. Chou, D.A. Cortes, Nitroxyl-mediated electrooxidation of alcohols to aldehydes and ketones. *J. Am. Chem. Soc.* **105**, 4492–4494 (1983)
35. Y. Demizu, H. Shiigi, T. Oda, Y. Matsumura, O. Onomura, Efficient oxidation of alcohols electrochemically mediated by Azabicyclo-*N*-oxyls. *Tetrahedron Lett.* **49**, 48–52 (2008)
36. Y.N. Ogibin, I.S. Levina, A.V. Kamernitsky, G.I. Nikishin, A highly efficient, indirect electrooxidation of 6β-Methyl-3β, 5α-dihydroxy-16α,17α-cyclohexanopregnan-20-one to the corresponding 5α-Hydroxy-3,20-dione using a mediatory couple of sodium bromide and substituted 2,2,6,6-Tetramethylpiperidine-*N*-oxyl (TEMPO). *Mendeleev Commun.* **5**, 184–185 (1995)

37. P. Parpot, K. Servat, A.P. Bettencourt, H. Huser, TEMPO mediated oxidation of carbohydrates using electrochemical methods. *Cellulose* **17**, 815–824 (2010)
38. Y. Kashiwagi, F. Kurashima, C. Kikuchi, J.-I. Anzai, T. Osa, J.M. Bobbitt, Enantioselective electrocatalytic oxidation of racemic sec-alcohols using a chiral 1-azaspiro [5.5] undecane-N-oxyl radical. *Tetrahedron Lett.* **40**, 6469–6472 (1999)
39. Y. Sannami, H. Kamitakahara, T. Takano, TEMPO-mediated electro-oxidation reactions of non-Phenolic β -O-4-type lignin model compounds. *Holzforschung* **71**, 109–117 (2017)
40. P.-Y. Blanchard, O. Alévêque, T. Breton, E. Levillain, TEMPO mixed SAMs: electrocatalytic efficiency versus surface coverage. *Langmuir* **28**, 13741–13745 (2012)
41. Y. Kashiwagi, J.-I. Anzai, Selective electrocatalytic oxidation of N-Alkyl-N-ethylanilines to N-alkylformanilides using nitroxyl radical. *Chem. Pharm. Bull.* **49**, 324–326 (2001)
42. C. Li, C.-C. Zeng, L.-M. Hu, F.-L. Yang, S.J. Yoo, D. Little, Electrochemically induced C-H functionalization using bromide ion/2,2,6,6-tetramethylpiperidiny-N-oxyl dual redox catalysts in a two-phase electrolytic system. *Electrochim. Acta* **114**, 560–566 (2013)
43. Q. Chen, C. Fang, Z. Shen, M. Li, *Electrochem. Commun.* **64**, 51–55 (2016)
44. Y. Wu, H. Yi, A. Lei, Electrochemical acceptorless dehydrogenation of N-heterocycles utilizing TEMPO as an organo-electrocatalyst. *ACS Catal.* **8**, 1192–1196 (2018)
45. T. Breton, D. Liaigre, E.M. Belgsir, Allylic oxidation: easy synthesis of alkenones from activated alkenes with TEMPO. *Tetrahedron Lett.* **46**, 2487–2490 (2005)
46. K. Mitsudo, T. Kaide, E. Nakamoto, K. Yoshida, H. Tanaka, Electrochemical generation of cationic Pd catalysts and application to Pd/TEMPO double-mediatory electrooxidative Wacker-type reactions. *J. Am. Chem. Soc.* **129**, 2246 (2007)
47. X.-Y. Qian, S.-Q. Li, J. Song, H.-C. Xu, TEMPO-catalyzed electrochemical C–H thiolation: synthesis of benzothiazoles and thiazolopyridines from thioamides. *ACS Catal.* **7**, 2730–2734 (2017)
48. R. Ciriminna, G. Palmisano, C. DellaPina, M. Rossi, M. Pagliaro, One-pot electrocatalytic oxidation of glycerol to DHA. *Tetrahedron Lett.* **47**, 6993–6995 (2006)
49. X.L. Wen, Y.H. Jia, L. Yang, Z.L. Liu, Electrocatalytic oxidation of L-tyrosine by a nitroxide. *Talanta* **53**(5), 1031–1036 (2001)
50. M. Rafiee, B. Karimi, S. Alizadeh, Mechanistic study of the electrocatalytic oxidation of alcohols by TEMPO and NHPI. *ChemElectroChem* **1**, 455–462 (2014)
51. A. Badalyan, S.S. Stahl, Cooperative electrocatalytic alcohol oxidation with electron-proton-transfer mediators. *Nature* **535**, 406–410 (2016)
52. M. Rafiee, K.C. Miles, S.S. Stahl, Electrocatalytic alcohol oxidation with TEMPO and bicyclic nitroxyl derivatives: driving force trumps steric effects. *J. Am. Chem. Soc.* **137**, 14751–14757 (2015)
53. R. Ciriminna, G. Palmisano, M. Pagliaro, Electrodes functionalized with the 2,2,6,6-Tetramethylpiperdinyloxy radical for the waste-free oxidation of alcohols. *ChemCatChem* **7**, 552–558 (2015)
54. A. Das, S.S. Stahl, Noncovalent immobilization of molecular electrocatalysts for chemical synthesis: efficient electrochemical alcohol oxidation with a Pyrene–TEMPO conjugate. *Angew. Chem. Int. Ed.* **56**, 8892–8897 (2017)
55. M. Masui, T. Ueshima, S.N. Ozaki, Electrolysis. *J. Chem. Soc. Chem. Commun.* 479–480 (1983)
56. S. Kishioka, S.A. Yamada, Kinetic study of the catalytic oxidation of benzyl alcohols by phthalimide-N-oxyl radical electrogenerated in acetonitrile using rotating disk electrode voltammetry. *J. Electroanal. Chem.* **578**, 71–77 (2005)
57. T. Shiraishi, T. Takano, H. Kamitakahara, F. Nakatsubo, Studies on the electro-oxidation of lignin and lignin model compounds. Part 2: N-Hydroxyphthalimide (NHPI)-mediated indirect electrooxidation of non-phenolic lignin model compounds. *Holzforschung* **66**, 311–315 (2012)
58. I. Bosque, G. Magallanes, M. Rigoulet, M.D. Karkas, C.R.J. Stephenson, Redox catalysis facilitates lignin depolymerization. *ACS Cent. Sci.* **3**, 621–628 (2017)
59. F. Recupero, F. Punta, Free radical functionalization of organic compounds catalyzed by N-hydroxyphthalimide. *Chem. Rev.* **107**, 3800–3842 (2007)

60. E.J. Horn, B.R. Rosen, Y. Chen, J. Tang, K. Chen, M.D. Eastgate, P.S. Baran, Scalable and sustainable electrochemical allylic C–H oxidation. *Nature* **533**, 77–81 (2016)
61. W.F. Bailey, J.M. Bobbitt, K.B. Wiberg, Mechanism of the oxidation of alcohols by oxoammonium cations. *J. Org. Chem.* **72**(12), 4504–4509 (2007)
62. M. Rafiee, F. Wang, D.P. Hruszkewycz, S.S. Stahl, *N*-hydroxyphthalimide-mediated electrochemical iodination of methylenes and comparison to electron-transfer-initiated C–H functionalization. *J. Am. Chem. Soc.* **14**, 22–25 (2018)
63. A. Samuni, C.M. Krishna, P.E. Riesz, E. Finkelstein, A. Russo, *J. Biol. Chem.* **263**(34), 17921–17924 (1988)
64. K.A. Harrison, E.A. Haidasz, M. Griessera, D.A. Pratt, Inhibition of hydrocarbon autoxidation by nitroxide-catalyzed cross-dismutation of hydroperoxyl and alkylperoxyl radicals. *Chem. Sci.* **9**, 6068–6079 (2018)
65. T. Fukai, M. Ushio-Fukai, Superoxide dismutases: role in redox signaling, vascular function, and diseases. *Antioxid. Redox Signal.* **15**(6), 1583–1606 (2011)
66. S. Goldstein, A. Samuni, Kinetics and mechanism of peroxyl radical reactions with nitroxides. *J. Phys. Chem. A* **111**(6), 1066–1072 (2007)
67. M. Griesser, R. Shah, A.T. Van Kessel, O. Zilka, E.A. Haidasz, D.A. Pratt, The catalytic reaction of nitroxides with peroxyl radicals and its relevance to their cytoprotective properties. *J. Am. Chem. Soc.* **140**(10), 3798–3808 (2018)
68. E.A. Haidasz, D. Meng, R. Amorati, A. Baschieri, K.U. Ingold, L. Valgimigli, D.A. Pratt, Acid is key to the radical-trapping antioxidant activity of nitroxides. *J. Am. Chem. Soc.* **138**(16), 5290–5298 (2016)
69. Y. Ishida, Y. Okamoto, Y. Matsuoka, A. Tada, J. Janprasit, M. Yamato, N.P. Morales, K.-I. Yamada, Detection and inhibition of lipid-derived radicals in low-density lipoprotein. *Free Radical Biol. Med.* **113**, 487–493 (2017)
70. R.K. Jensen, S. Korcek, M. Zinbo, J.L. Gerlock, Regeneration of amine in catalytic inhibition of oxidation. *J. Org. Chem.* **60**, 5396 (1995)
71. E.T. Denisov, *Polymer Deg. Stab.* **25**, 209 (1989)
72. E. Damiani, R. Castagna, P. Astolfi, L. GRECI Aromatic and aliphatic mono- and bis-nitroxides: a study on their radical scavenging abilities. *Free Radical Res.* **39**(3), 325–336 (2005)
73. S. Huang, H. Zhang, J.T. Paletta, S. Rajca, A. Rajca, Reduction kinetics and electrochemistry of tetracarboxylate nitroxides. *Free Radical Res.* **52**(3), 327–333 (2018)
74. A.P. Jagtap, I. Krstic, N.C. Kunjir, R. Hänsel, T.F. Prisner, S.T. Sigurdsson, Sterically shielded spin labels for in-cell EPR spectroscopy: analysis of stability in reducing environment. *Free Radic. Res.* **49**(1), 78–85 (2015)
75. Y. Kinoshita, K. Yamada, T. Yamasaki, H. Sadasue, K. Sakai, H. Utsumi, Development of novel nitroxyl radicals for controlling reactivity with ascorbic acid. *Free Radical Res.* **43**, 565–571 (2009)
76. T. Yamasaki, F. Mito, Y. Ito, S. Pandian, Y. Kinoshita, K. Nakano, R. Murugesan, K. Sakai, H. Utsumi, K.J., Yamada, Structure-reactivity relationship of piperidine nitroxide: electrochemical, ESR and computational studies. *J. Org. Chem.* **76**, 435–440 (2011)
77. E. Lozinsky, V.V. Martin, T.A. Berezina, A.I. Shames, A.L. Weis, G.I. Likhtenshtein, Dual fluorophore–nitroxide probes for analysis of vitamin C in biological liquids. *J. Biochem. Biophys. Methods* **38**(1), 29–42 (1999)
78. Y. Matsuoka, M. Yamato, T. Yamasaki, F. Mito, K. Yamada, Rapid and convenient detection of ascorbic acid using a fluorescent nitroxide switch. *Free Radical Biol. Med.* **53**, 2112–2118 (2012)
79. A.A. Bobko, I.A. Kirilyuk, I.A. Grigor’ev, J.L. Zweier, V.V. Khramtsov, Reversible reduction of nitroxides to hydroxylamines: the roles for ascorbate and glutathione. *Free Radical Biol. Med.* **42**(3), 404–412 (2007)
80. I.A. Kirilyuk, A.A. Bobko, S.V. Semenov, D.A. Komarov, I.G. Irtogova, I.A. Grigor’ev, E. Bagryanskaya, Effect of sterical shielding on the redox properties of imidazoline and imidazolidine nitroxides. *J. Org. Chem.* **80**, 9118–9125 (2015)

81. L. Lamp, U. Morgenstern, K. Merzweiler, P. Imming, R.W. Seidel, Synthesis and characterization of sterically and electrostatically shielded pyrrolidine nitroxide radicals. *J. Mol. Struct.* **1182**, 87–94 (2019)
82. H. Zhao, J. Wu, X. Meng, S. Zuo, W. Wang, H. Yuan, Novel piperidine nitroxide derivatives: synthesis, electrochemical and antioxidative evaluation. *J. Heterocycl. Chem.* **45**(2), 371–376 (2008)
83. M.C. Emoto, M. Yamato, H. Sato-Akaba, K. Yamada, Y. Matsuoka, H.G. Fujii, Brain imaging in methamphetamine-treated mice using a nitroxide contrast agent for EPR imaging of the redox status and a gadolinium contrast agent for MRI observation of blood-brain barrier function. *Free Radical Res.* **49**(8), 1038–1104 (2015)
84. F. Shi, P. Zhang, Y. Mao, C. Wang, M. Zheng, Z. Zhao, The nitroxide Tempol inhibits hydroxyl radical production from the Fenton-like reaction of iron(II)-citrate with hydrogen peroxide. *Biochem. Biophys. Res. Commun.* **483**, 159–164 (2017)
85. J. Li, J. Zhang, Y. Chen, N. Kawazoe, G. Chen, Tempol-conjugated gold nanoparticles for reactive oxygen species scavenging and regulation of stem cell differentiation. *ACS Appl. Mater. Interfaces* **9**, 35683–35692 (2017)
86. T. Yoshitomi, K. Kuramochi, L. Binh Vong, Y. Nagasaki, Development of nitroxide radicals-containing polymer for scavenging reactive oxygen species from cigarette smoke. *Sci. Technol. Adv. Mater.* **15**, 035002 (2014)
87. S.I. Dikalov, A.E. Dikalova, D.A. Morozov, I.A. Kirilyuk, Cellular accumulation and antioxidant activity of acetoxymethoxycarbonyl pyrrolidine nitroxides. *Free Radical Res.* **52**(3), 339–350 (2018)
88. B.P. Soule, F. Hyodo, K. Matsumoto, N.L. Simone, J.A. Cook, M.C. Krishna, J.B. Mitchell, The chemistry and biology of nitroxide compounds. *Free Radical Biol. Med.* **42**(11), 1632–1650 (2007)

Chapter 4

ESR and NMR as Tools for Nitroxides Studies



4.1 Introduction

The electron spin resonance (ESR) phenomena involve the resonance absorption or dispersion of a microwave frequency (0.3–250 GHz) of electromagnetic field (ν) by a system of particles with the intrinsic spin moment of an unpaired electron in a constant magnetic field of strength H_0 [1–5]. The absorption leads to magnetization in the excited state of the system. Accordingly, the electron magnetic resonance condition is

$$h\nu = g_e\beta_B H_0, \quad (4.1)$$

where g_e is a g -factor, characterizing the value of the intrinsic electron spin moment (free electron g -value is 2.002319), and β_B is the Bohr magneton ($9.27400968 \times 10^{-24} \text{ J T}^{-1}$). The values of g -factors and magnetic field strength H_0 dictate the position of resonance frequencies in ESR spectra. The hyperfine interaction between the electron and the nuclear spins consists of the isotropic Fermi contact interaction and the anisotropic dipole–dipole interaction. The hyperfine interaction is manifested by characteristic splittings of ESR spectra (Fig. 4.1).

The main ESR features are [1–5]: (1) integral intensity and amplitude of the ESR spectrum, (2) the position of the spectral features depending on the value of the g -factor according to the resonance condition, (3) the ESR spectral line shape which can be either homogenous (single spin packet) or heterogeneous (overlap of packets), (4) spin–lattice (T_1) and spin–spin (T_2) relaxation times, (5) the ESR spectra hyperfine splitting (hfs) attributed to the contact and dipolar interactions of electron spin with nuclear spin I , (6) the ESR spectral fine splitting (fs) caused by electron spin–electron spin exchange and dipolar interactions, and (7) the response of the ESR signal to progressive saturation; and (8) The degree of electron spin polarization.

Equation 4.1 predicts a dependence of position of EPR spectra on g -factor value and improvement of the resolution of the spectra for species of different g -factor with increasing frequency (Fig. 4.1). One of the most important advances has been

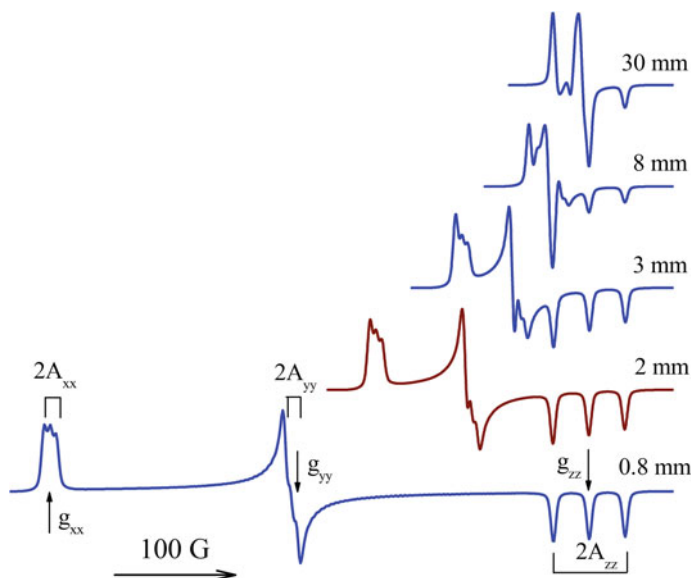


Fig. 4.1 EPR spectra of nitroxide radical calculated for different spin precession frequencies (microwave linewidths) [14]. <http://hf-epr.awardspace.us/index.htm>

the extension of ESR to high magnetic fields and high frequencies. High-frequency–high-field EPR (HF–HF EPR) was pioneered by Lebedev group [6]. Since then, theoretical and experimental bases of the method were essentially developed and found numerous applications [7–10]. The utilization of quasi-optical methods, especially above 150 GHz markedly expanded the HF–HF EPR efficiency [8].

Spin relaxations times are important parameters in many aspects of electron spin resonance theory and application. Spin–lattice relaxation time (T_1) characterizes the recovery of the induced magnetization to the ground state on account of a transfer of magnetic energy to energy of media (lattice). Another type of relaxation, spin–spin time (T_2), is related to time of return of the spin system to equilibrium in the excited magnetic state as a result of spin–spin interaction with environment. The second approach to the electron spin relaxation is based on the properties of the spin electron Larmor precession, which is the precession of the magnetic moments of electrons about external magnetic field. In the frame of Bloch model [11] after the microwave resonance absorption, the dynamic of spin magnetization $M = (M_x, M_y, M_z)$ is a function of longitudinal relaxation times T_1 and transverse relaxation time or spin phase memory time (T_m, T_2) which are synonyms of spin–lattice and spin phase memory relaxation time, respectively.

The two fundamental phenomena, spin exchange and dipole–dipole coupling, constitute the basis of the spin electron–spin electron and spin electron–spin nuclear interactions. Electrons and nuclei can be thought as tiny magnets and interact with

each other through space. The exchange process occurs via direct or indirect overlap of the orbitals of the interacting species.

An arsenal of experimental ESR methods including conventional, electrically, and optically detected ESR (CW ESR, ED ESR, and OD ESR, respectively) and advanced pulse techniques is widely used in chemistry and biology [1–10]. The CW technique is employed for collecting information of interest through the analysis of ESR spectra, saturation curves, electron–electron double resonance (ELDOR) or double electron–electron resonance (DEER), electron–nuclear double-resonance (ENDOR) multifrequency ESR (MF ESR), two-dimensional ESR (2D ESR), two-dimensional electron–electron double resonance (2D-ELDOR), ENDOR with circularly polarized radiofrequency fields (CP-ENDOR), electron–nuclear–nuclear resonance (double ENDOR), proton–electron double-resonance imaging (PEDRI), time-domain ESR, and electron–nuclear–nuclear triple resonance (TRIPLE), reaction yield detection magnetic resonance (RYDMR), and magnetically affected reaction yield (MARY).

The more important developments of pulse EPR include [1–5]: Fourier transform ESR (FT ESR), two-dimensional Fourier transform ESR (2D FT ESR), electron spin echo (ESE), electron spin echo envelope modulation (ESEEM), hyperfine sublevel correlation spectroscopy (HYSCORE), double nuclear coherence transfer hyperfine sublevel correlation electron spin echo (DONUT-HYSCORE), dynamic nuclear polarization (DNP), electron spin echo-detected magnetization transfer (ESE MT), two-dimensional electron spin echo correlation spectroscopy (2D SECSY), pulse electron–nuclear double resonance (pulse ENDOR), pulse electron–electron double resonance (PELDOR), electron spin transient nutation (ESTN), two-dimensional electron spin transient nutation (2D ESTN), phase-inverted echo-amplitude detected nutation (PEANUT), saturation recovery ESR (SR ESR), pulse multifrequency ESR (PMF ESR), magnetic isotope effect (MEF), quantum beats effect (QBE), double quantum coherence pulsed ESR (DQC ESR), ESR spectra hole burning, A “211” electron spin echo method, relaxation enhancement (RE), the pulsed triple electron resonance (TRIER), pulse ESR-based electron spin nutation (ESN) spectroscopy, two-dimensional (2D-ESN) spectroscopy, relaxation-induced dipolar modulation enhancement (RIDME), and hyperfine-correlated electron–nuclear double-resonance spectroscopy (HYEND).

4.2 Spin Electron–Spin Electron Interactions. Distance Determination

The method of double spin labeling (DSL), pioneered by Likhtenshtein in 1968 [12, 13], is based on specific modification of chosen groups in the object of interest by two or several spin labels, nitroxides, or complexes of paramagnetic metal, followed by the analysis of the effects of the spin–spin interactions on the label ESR spectra or spin relaxation times. Nowadays, various modifications of the double labeling

method and their modifications are widely employed for solving numerous problems of structure and molecular dynamics of biological molecules [13–55, 57–68].

The first applications of dipole–dipole spin–spin interactions to the investigation of protein surface topography were based on the changes in the line shape of nitroxide radical ESR spectra arising from interactions with a second nitroxide radical or a paramagnetic ion [12–17]. This approach allows one to estimate distances between the paramagnetic centers up to 2.5 nm. Later, the higher sensitivity of power saturation curves of a radical to interactions between the radical and paramagnetic ions up to 10 nm was demonstrated [18–22]. The effects of the spin–spin-exchange interaction on the ESR spectra and spin relaxation were first used in the Likhteshtein group for establishing the structure of systems under investigation, such as nitrogenase and non-heme protein [23].

Methods of determination of spin electron–spin electron distance based on analysis the CW EPR spectra were described in comprehensive reviews [24, 25]. A detailed description of the continuous wave microwave saturation recovery technique which allows to measure spin relaxation times, T_1 and T_2 and corresponding theory was presented in [26–28].

Factors affecting dipolar interaction between two spins in a static magnetic field (H_0) are [18, 30–36]: (i) magnetic moments, (ii) interspin distance, (iii) the angle between the interspin vector and the external field, (iv) the spin–spin (transverse, phase memory, T_2 T_m) and spin–lattice (T_1) relaxation times, the ESR frequencies (ω) of both interacting paramagnetics. When the product of relaxation time T_1 for the second center and the interaction energy ($\Delta\omega$) expressed in frequency units $\Delta\omega^2 T_1^2 \gg 1$, the effect of the second spin may be regarded as an interaction with a permanent dipole moment (slow relaxing spin). When $\Delta\omega^2 T_1^2 \ll 1$, the interaction may be considered as a weak perturbation because of the fast relaxation (fast relaxing spins).

The Hamiltonian that describes the interaction between two permanent spins in a point-dipole approximation is given by

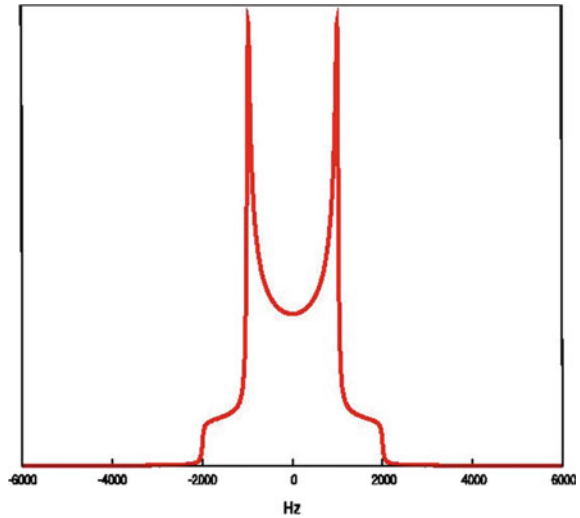
$$\hat{H}_{ss} = \frac{g_e^2 \alpha^2}{8} \sum_{i \neq j} \left[\frac{\hat{s}(i)\hat{s}(j)}{r_{ij}^3} - 3 \frac{(\hat{s}(i)\mathbf{r}_{ij})(\hat{s}(j)\mathbf{r}_{ij})}{r_{ij}^5} \right] \quad (4.2)$$

here, $\mathbf{r}_{ij} = \mathbf{r}_i - \mathbf{r}_j$ for electrons i and j at positions \mathbf{r}_i and \mathbf{r}_j , and with spins $\hat{s}(i)$ and $\hat{s}(j)$, g_e is the free electron g -value. The dipolar coupling between two spin leads to splitting of the NMR and ESR lines with formation of the Pake doublet (Fig. 4.2) [37].

In high magnetic fields, the dipole–dipole interaction is expressed with the secular dipole–dipole coupling constant d_{12} including the angle Θ between the axis connecting the two spins and the external magnetic field vector \mathbf{B}_0 as follows:

$$d_{12} = b_{12} \frac{1}{2} (3 \cos^2 \Theta_{12} - 1) \quad (4.3)$$

Fig. 4.2 Pake doublet
https://en.wikipedia.org/wiki/Pake_doublet



where

$$b_{12} = -\frac{\mu_0}{4\pi} \frac{\gamma_1 \gamma_2 \hbar}{r_{12}^3} \quad (4.4)$$

and μ_0 is the vacuum magnetic permeability.

Within the Larmor precession model, in the laboratory frame, the static magnetic field B is assumed to be parallel to the z -axis and an applied microwave field B_1 parallel to the x -axis. In the rotating frame, the B_1 component rotating with frequency ω_0 can be on resonance with the precessing magnetization vector M_0 if $\omega_L = \omega_0$. The magnetization vector will rotate around the x -axis in the zy -plane for the duration of the applied B_1 field. The tip angle α by which M_0 is rotated is given by

$$\alpha = -\gamma |B_1| t_p \quad (4.5)$$

Thus, the desirable angle can be regulated.

For the two-pulse primary echo experiment and the three-pulse stimulated echo-detected (ED) experiments, the EPR line shape is obtained when the magnetic field B is scanned across the resonance line [38]. The two-pulse ED spectra (pulse sequence: $\pi/2-\tau-\pi-\tau$ -echo) experiment is used to detect processes, on the timescale of the phase memory time (T_m), in the nanosecond regime. Echo-detected spectra from the three-pulse stimulated spin echo (pulse sequence: $\pi/2-\tau-\pi/2-T_0-\pi/2-\tau$ -echo) experiment are used to detect slower processes, due to its dependence on the longer T_1 process.

Since the pioneer work of Milov, Salikhov, and Tsvetkov based on instantaneous diffusion that arises from dipolar spin–spin interactions between different spins [39], the use of pulse electron paramagnetic resonance (Echo-detected ELDOR, pulse

ELDOR, PELDOR, double electron–electron resonance DEER) for long distance spin–spin interaction has been essentially developed and widely applied for the distance determination up to 10 nm [40–55, 57–68]. In a system of two spins (observed and pumped), the effects of diffusion coupled with the action of the applied pulse on the precession frequency of the observed spin were detected [39, 40]. In three-pulse PELDOR, the ESR spectrum is excited by two electron spin echo (ESE) pulses and an additional pumping pulse. For a system of two spins A and B, coupled by the dipole–dipole interaction the experiment consists of two $\pi/2$ – π -pulse electron ESE subsequence with a mixed interpulse delay τ at the observer frequency ω_a for the spin A and a pump π pulse at frequency ω_b for the spin B. For these spins A and B, coupled by the dipole–dipole interaction at a distance R and given the angle between the direction of the external magnetic field and the vector which connects the paramagnetic centers (θ), the ratio of the primary echo signal amplitude $V_p(2\tau)$ with the pumping pulse to the ESE signal amplitude $V_0(2\tau)$ without the pumping pulse is

$$V(T) = \frac{V_p(2\tau)}{V_0(2\tau)} = 1 - p_B[1 - \cos(DT)]. \quad (4.6)$$

where p_B is the probability of a spin B flip under the action of the pumping pulse; D is the splitting (in rad/s) of the resonance spin A line due to interaction with spin B and has the analytical form

$$D = \frac{\gamma^2 \hbar}{R^3} (1 - 3 \cos^2 \theta) + J, \quad (4.7)$$

which includes the dipolar and J exchange interaction.

A “211” electron spin echo method developed by Raitsimring and Tsvetkov is complementary to the pulse ELDOR [41]. The difference between the PELDOR and “2 + 1” methods consists in the choice of the carrier frequency of the second microwave pulse. The “2 + 1” pulse train allows to measure the dipole–dipole interactions between paramagnetic centers which are substantially weaker than those that can be measured by the ordinary two-pulse train and between spins with overlapping EPR spectra.

In the four-pulse PELDOR experiment invented by the Jeschke group, the detection sequence $\pi/2$ – τ_1 – π – τ_1 –echo $_1$ – τ_2 – π is applied at a microwave frequency ν_A (Fig. 4.3) [42]. The four-pulse techniques allow one to avoid a number of artifacts.

In a five-pulse DEER sequence, an extra pulse at the pump frequency is added and compared with standard four-pulse DEER (Fig. 4.4) [43]. The position of the extra pulse is fixed relative to the three pulses of the detection sequence. This procedure significantly reduces the effect of nuclear spin diffusion on the electron spin phase relaxation, thereby enabling longer dipolar evolution times that are required to measure longer distances.

Using spin-labeled T4 lysozyme at a concentration less than 50 μM , as an example, it was shown that the evolution time increases by a factor of 1.8 in protonated solution and 1.4 in deuterated solution to 8 and 12 μs , respectively (Fig. 4.5).

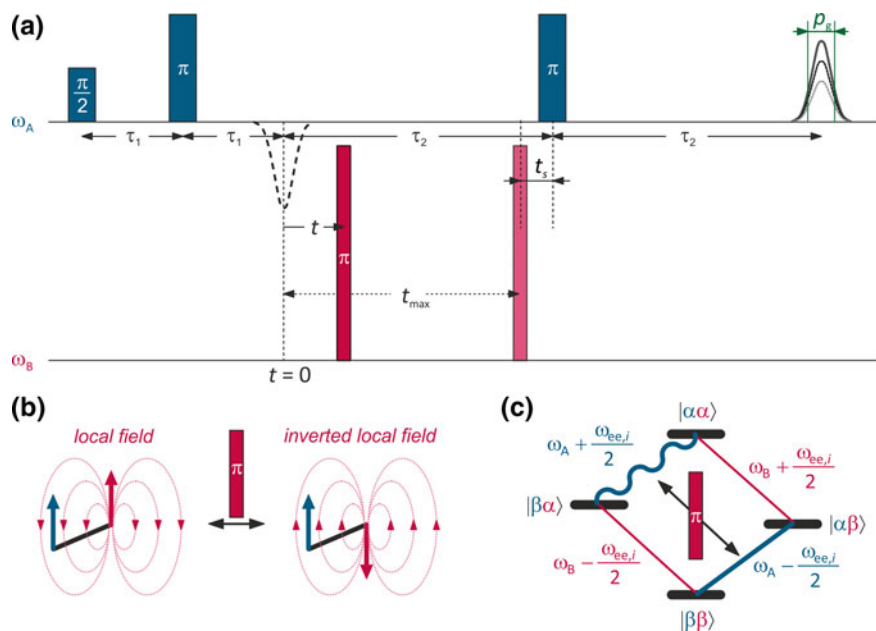


Fig. 4.3 Four-pulse DEER experiment. **a** Pulse sequence. Time t is varied from $t < 0$ to t_{\max} , and variation of the integral echo intensity in the window of length p_g is recorded. **b** Local field picture. The π pump pulse at frequency ω_B inverts the state of spin B (gray), thus inverting the local field imposed by spin B at the site of spin A (black). **c** Energy level diagram. Inversion of the local field at spin A exchanges coherence between the two transitions of spin A that differ in frequency by $\omega_{ee,i}$ [42]. Private communication from Prof. Jeschke

A Refocused Out-Of-Phase DEER (ROOPh-DEER) seven-pulse sequence detection scheme which acquires only the modulated fraction of the dipolar DEER signal was recently proposed for a case when Zeeman splitting is small [45]. The application of seven-pulse ROOPh-DEER sequence to a model biradical yielded the interspin distance identical to the one obtained with the conventional four-pulse DEER, however, without the unmodulated background present as a dominant fraction in the latter signal. The four-pulse DEER-RELOAD scheme applied to two membrane protein complexes labeled with nitroxide may improve SNR by a factor of >3 as it has been demonstrated for one of these two membrane proteins.

Compared to four-pulse DEER, five-pulse DEER suffers from additional artifacts that stem from pulse imperfection and excitation band overlap. To eliminate experimentally the artifacts in five-pulse DEER due to partial excitation and excitation band overlap at frequencies, a data post-processing method was introduced [46]. The method removes the partial excitation artifact without relying on previous knowledge of its amplitude and without sensitivity loss on acquisition of two traces with shifted positions of the artifact and computation of the artifact shape from the difference of the two traces. Experimental conditions that suppress additional artifact

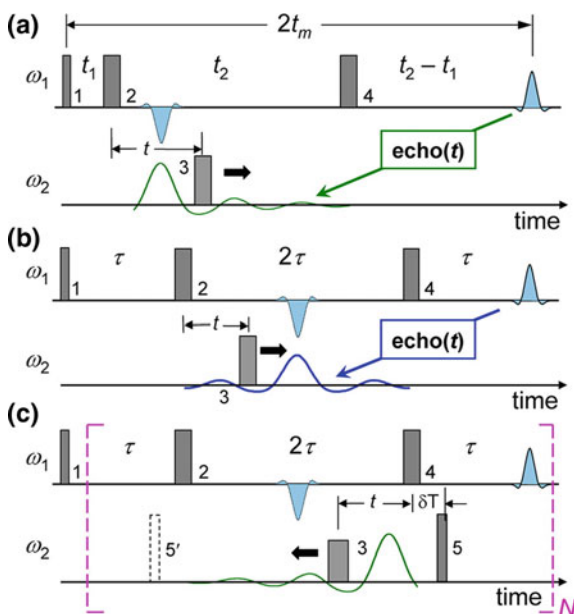


Fig. 4.4 **a** Standard four-pulse DEER sequence with the respective dipolar modulation pattern plotted in green. **b** The four-pulse sequence modified for $t_{2-2}t_{1-2}\tau$ to minimize nuclear spin diffusion, thus increasing the signal, but this shifts the dipolar modulation (in blue) to the middle of the second interval, thereby losing half of the dipolar modulation because the halves are identical. **c** Placing the second pump pulse, 5, after the pulse 4 shifts dipolar modulation toward pulse 4, thereby recovering the full time span, 2τ . The dipolar modulation (green) is reversed in time compared with panel a. Pulse 5 could also be placed at position 5' before pulse 2, reversing the modulated time trace. Note that time period, t_m , available for recording the dipolar signal is **a** t_2 and **(b, c)** 2τ [43]. Reprint from [43], Copyright 2013, American Chemical Society

contributions stemming from overlap between the excitation bands of the microwave pulses that introduce additional dipolar evolution pathways were analyzed in detail.

An ESR version of multiple quantum coherence (ESR MQC) was predicted by Tang and Noris [47] and observed in experiments on spin-correlated pairs formed by laser-induced dissociation by Dzuba et al. [48]. A novel six-pulse pulsed ESR technique for the detection of double quantum coherence (DQC), which yields high-quality dipolar spectra for distance measurements, was developed by Freed with coworkers [49, 50]. The suggested six-pulse DQC sequence is shown in Fig. 4.6. The detection of double quantum coherence (DQC) yields high-quality dipolar spectra for distance measurements allow one to extract distance distributions. The main virtues of DQC ESR are (1) detection of weak dipolar interactions between paramagnetic molecules in the ESR signal and reliable measurement of distances and distance distributions between them up to 80 Å, (2) determination of the angular geometry of the biradical, (3) determination of the asymmetric g -factor and hyperfine tensors, (4) characterization of many body spin systems, and (5) investigation of conformers.

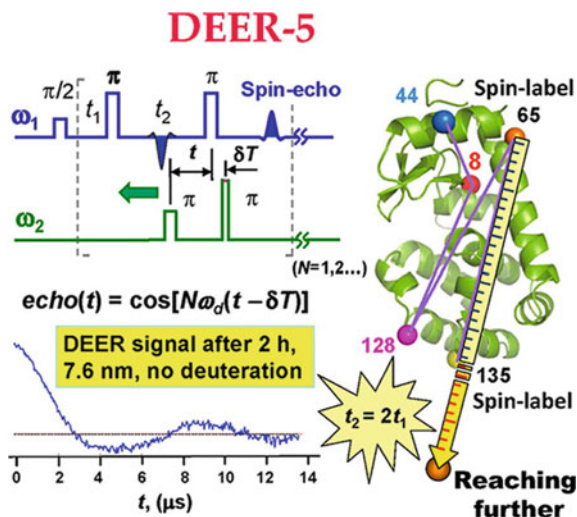


Fig. 4.5 Schematic illustration five-pulse DEER application to spin-labeled T4 lysozyme [43]. Reprint from [43], Copyright 2013, American Chemical Society

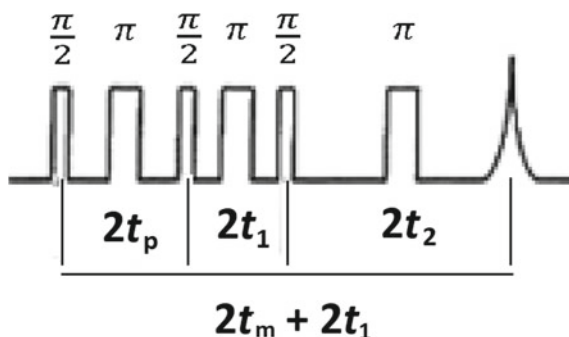


Fig. 4.6 Six-pulse DQC sequence **a** is shown with the corresponding coherence pathways [49]

Two-dimensional electron–electron double-resonance (2D-ELDOR) technique was invented, developed, and applied by the Freed group [51]. The following time periods in a three-pulse 2D-ELDOR experiment are defined as follows: (1) the preparation period, (2) the mixing period, and (3) the final $\pi/2$ pulse. 2D-ELDOR has proven to be a technique that is sensitive to the fast and slow dynamics processes.

The hole burning method has been invented by Schweiger et al. [52] and developed by Dzuba and Kawamori [53]. For inhomogeneously broadened electron paramagnetic resonance spectra of solids and viscous liquids, spectral diffusion can be studied by selective hole burning of homogeneous linewidth (0.5–0.05 G) using a free-induction decay (FID). The pulse sequence for the hole-burning experiment is $\pi - \tau - \pi/2 - \tau - \pi/2$. Sources of spectral diffusion which can be investigated by these

methods are as follows: (1) chemical exchange which can be induced by chemical reactions, by transitions between different molecular conformations or isomers, and by rotation about some particular molecular bond, (2) molecular tumbling in a viscous liquid, (3) spin–lattice relaxation, and (4) spin diffusion, a process of mutual flip-flops in the spin system leading to a spatial diffusion of the Zeeman energy. For selective hole-burning relaxation-induced dipolar modulation enhancement (RIDME) experiments with stable nitroxide biradical in a frozen solution, it allowed to eliminate the major unwanted contributions to the FID modulation originating from spectral diffusion and from excitation of forbidden electron-nuclear spin transitions by mw pulses [54]. The proposed method can be employed to measure interspin distances in the range of $13 \text{ \AA} \leq r \leq 25 \text{ \AA}$.

A method of distance measurement up to 150 nm based on effect of fast relaxation spin on slow relaxation spin was proposed by Kulikov and Likhtenshtein in 1974 [18, 19, 56] in parallel of invention of the pulse ELDOR [39]. According to the Solomon and Bloembergen theory [55], the electron relaxation enhancement depends on magnetic moments μ , and interspin distance (r), electron spin (S), the spin-phase (T_2) and spin–lattice (T_1) relaxation times, the ESR frequencies (ω) of both interacting paramagnetics, the angle (θ) between the interspin vector and the external field (H_0), and the interaction energy expressed in frequency units ($\Delta\omega$).

For estimation of distances between paramagnetic centers using the Solomon-Bloembergen theory, it is necessary to know T_{1f} and T_{2f} for the radical. A method of estimation of the relaxation times by analysis of CW power saturation curves in solids from saturation curves recorded under conditions of rapid passage was applied to nitroxide radicals [18–21]. These values can be determined directly by pulse methods. In the case of nitroxide TEMPOL in ethanolic solution at 77 K, the obtained relaxation rates were reasonably agreed with direct measurements by pulse saturation and spin echo measurements [57]. In solids, T_{1f} usually decreases monotonically with increasing temperature, so one can find experimentally the temperature at which the dipolar contribution is maximum. At this temperature, $1/T_{1s} = \omega$ and the Solomon-Bloembergen theory predicted dipolar contribution given by (4.8)

$$\Delta\left(\frac{1}{T_{1s}}\right) = \frac{\mu_f^2 \gamma^2}{15r^6 \Delta\omega} \quad (4.8)$$

The theoretical maximum distances (r_{\max}) to a second paramagnetic center with spin S_f that could be determined were estimated as $r_{\max} = 100 \text{ \AA}$ for $S_f = 1/2$ and $r_{\max} = 150 \text{ \AA}$ for $S_f = 5/2$ [18, 21]. The effect of a rapidly relaxing spin on T_1 of a slowly relaxing spin also was considered in [44, 58]. Application of this method was illustrated by the estimation of distances between the heme group of human hemoglobin and the nitroxide fragment of three spin labels attached covalently to the α -93 SH-group [21]. The determined values of r (in \AA with an accuracy 5–6%) between heme and the nitroxide fragment are in reasonable agreement with each other and with the x-ray diffraction structure of hemoglobin [59].

In work [60], the relaxation enhancement (RE) value Δk was defined as the difference of the inverse relaxation times of a slowly relaxing species in the presence T_{1f} and absence of a fast relaxing species $T_{1f,0}$. Specifically, the final intermolecular RE time traces employing the nitroxide echo-detected (ED) EPR were rescaled and fitted by multiexponential fit curves to extract T_1 times that were used as a measure of the average relaxation enhancement Δk , which is related to the spin–spin distance (r) (4.9).

$$\Delta k = \frac{CT_{1f}}{r^6} \quad (4.9)$$

The approach was tested on a water-soluble *T4* lysozyme labeled by nitroxide and lanthanide complex and showed the spin–spin distance value of about 3.2 nm.

Pulse-ESR-based electron spin nutation (ESN) spectroscopy was suggested as a tool to determine relatively short distances between weakly exchange-coupled electron spins [61, 62]. Two-dimensional (2D-ESN) spectroscopy was used to determine spin dipolar interactions for spin distances within 2.0 nm in a system of weakly exchange-coupled molecular spins in non-oriented media. Thus, ESN spectroscopy has been proved to be a useful complement to other modern pulse-ESR methods.

A method of singular value decomposition (SVD) to determine distance distributions in pulsed dipolar electron spin resonance was invented [63]. Even very small amounts of noise (e.g., signal-to-noise ratio $\text{SNR} \approx 850$) are sufficient to corrupt measurement of spin–spin distance distribution. SVD can be employed directly on the denoised data, using pulse dipolar electron spin resonance experiments as an example. This method is useful in measuring distances and their distributions, $P(r)$, between spin labels on proteins. SVD can be employed directly on the denoised data using pulse dipolar electron spin resonance experiments. A new wavelet transform-based method of denoising experimental signals to pulse-dipolar electron spin resonance spectroscopy (PDS) was developed [64]. The method allowed to reduce the signal averaging times of the time-domain signals by as much as two orders of magnitude, while retaining the fidelity of the underlying signals, and to achieve excellent signal recovery when the initial noisy signal has an $\text{SNR} \gtrsim 3$. The authors expected that the method can be applicable to other time-domain spectroscopies.

The “chirp-induced dipolar modulation enhancement” (CIDME) six-pulse sequence was introduced in [65]. CIDME eliminates limitation of frequency-swept pump pulses in DEER experiments associated with a need for the pump pulses to be short in comparison with dipolar evolution periods by means of longitudinal storage during the application of one single or two consecutive pump pulses. In pulse EPR correlation techniques, the monochromatic excitation often cannot uniformly excite the entire spectrum. Restrictions in pulse EPR correlation techniques were alleviated for nitroxide spin labels at Q-band microwave frequencies around 35 GHz T by substitution of monochromatic pulses by frequency-swept chirp pulses tailored for uniform excitation [66]. The dipole–dipole interaction can be separated by a constant-time Zeeman-compensated solid echo sequence called SIFTER. EPR-correlated dipolar spectra can be obtained when the four pulses are replaced by chirp

pulses. These two-dimensional spectra encode additional information on the geometrical arrangement of the two spin labels. In a new approach to DEER for distance determination involving nitroxide spin labels at dilute concentrations (nDEER), non-selective chirp pulses that refocus all relevant spin pairs are combined with DEER [67]. A key advantage of nDEER is the high fidelity of the chirp refocusing pulses, which is important for nDEER schemes that incorporate dynamical decoupling to access longer distances.

The pulsed triple electron resonance (TRIER) experiment, which correlates dipolar frequencies of molecules with three electron spins, was introduced [68]. These correlation patterns in combination with DEER allow to interpret distance distributions of biological systems that exist in more than one conformation. This method is able to obtain two-dimensional distance correlation maps of the previously investigated model compounds as well as of spin-labeled proteins by application of two-dimensional approximate Pake transformation to TRIER data. This enabled to get distance correlation plots from two triple-labeled protein samples that were in good agreement with DEER data and simulations.

4.2.1 Spin Electron–Spin Nuclear Interactions

The electron-nuclear spin interaction appears from the coupling of the nuclear magnetic moment to the magnetic field generated by the electron magnetic moment or equivalently from the coupling of the electron magnetic moment to the magnetic field generated by the nuclear magnetic moment [69, 70]. This interaction causes superfine splitting in EPR spectra and effects on nucleus NMR properties. The nuclear magnetic moment m_I originating from the nuclear spin quantum number I is $m_I = 2I + 1$.

The total Hamiltonian of the system of an electron and many nuclear spins is given by

$$\hat{H} = \hat{H}_e + \hat{H}_N + \hat{H}_{eN} + \hat{H}_{NN}, \quad (4.10)$$

and composed of the single spin Zeeman energies, Hamiltonian for interaction in the applied magnetic field along the z -axis, the hyperfine interaction, and the intrinsic nuclear–nuclear interaction, respectively. The electron-nuclear spin dipole–dipole interactions for an electron in an s -symmetry orbital and in a non- s -symmetry orbital are expressed as follows:

$$\begin{aligned} H_{\text{HF}} &= \frac{16\pi}{3} \gamma_I \mu_B \mu_N \delta(\mathbf{r}) [\mathbf{S} \cdot \mathbf{I}], \quad I = 0 \\ H_{\text{HF}} &= \frac{2\gamma_I \mu_B \mu_N}{r^3} \left[(\mathbf{L} - \mathbf{S}) \cdot \mathbf{I} + 3 \frac{(\mathbf{S} \cdot \mathbf{r})(\mathbf{I} \cdot \mathbf{r})}{r^2} \right], \quad I \neq 0. \end{aligned} \quad (4.11)$$

where μ_I , μ_B , and μ_N are the gyromagnetic factor of the nuclear spin, the Bohr magneton, and the nuclear magneton, respectively. \mathbf{S} and \mathbf{I} are the spin operators

for the electron and the nucleus, and L is the angular momentum operator for the electron.

The contact Fermi electron–nucleus interaction, which is caused by the probability to find the electron spin at the same point in space as the nuclear spin, is given by

$$\hat{H}_{eN} = \sum_n a_n \hat{\mathbf{S}}_e \cdot \hat{\mathbf{J}}_n, \quad (4.12)$$

where $\hat{\mathbf{S}}_e$ and $\hat{\mathbf{J}}_n$ are the spin and nucleus operators, respectively, and

$$a_n = \frac{\mu_0}{4\pi} \gamma_e \gamma_n \frac{8\pi}{3} |\Psi(\mathbf{R}_n)|^2, \quad (4.13)$$

where μ_0 is the vacuum magnetic permeability, \mathbf{R}_n denotes the coordinates of the n th nucleus, γ_n and γ_e are the nuclear gyromagnetic ratio, and the electron gyromagnetic ratio, respectively; $|\psi(R_n)|^2$ is the spin density of s-electron on the nucleus.

The main sources of information on the electron–nucleus interactions are CW EPR spectra, electron–nuclear double resonance (ENDOR), two-dimensional electron–electron double resonance (2D-ELDOR), electron spin echo (ESE), electron spin echo envelope modulation (ESEEM), ENDOR with circularly polarized radiofrequency fields (CP-ENDOR), electron–nuclear–nuclear resonance (double ENDOR), proton–electron double-resonance imaging (PEDRI), time-domain ESR, and electron–nuclear–nuclear triple resonance (TRIPLE), hyperfine sublevel correlation spectroscopy (HYSCORE), double nuclear coherence transfer hyperfine sublevel correlation spectroscopy (DONUT-HYSCORE), magnetic isotope effect (MEF), ESR nutation spectroscopy (ESN), and two-dimensional ESN (2D-ESN).

In a continuous wave electron–nuclear double resonance (CW-ENDOR) introduced by Feher [71], an EPR transition is partly saturated by microwave radiation of amplitude B_1 , and, in parallel, a driving radio frequency (rf) field of amplitude B_2 induces nuclear transitions. While the magnetic field is swept through the EPR spectrum, the rf frequency follows the Zeeman frequency of the nucleus. Transitions occur at frequencies ν_1 and ν_2 obeying the NMR selection rules $\Delta M_I = \pm 1$ and ESR selection rule $\Delta M_S = 0$. The ENDOR spectrum can reveal both the hyperfine coupling constant (a) and the nuclear Larmor frequencies (ν_n), using EPR which is markedly more sensitive than that NMR [71–74]. Thus, the hyperfine enhancement effect manifests itself both in CW and pulse ENDOR.

With the aim to identify by CW EPR techniques electron–nuclear dipolar and contact interaction, and electron spin–electron spin dipolar and exchange interactions, a method based on the phenomenon of continuous wave electron–electron double resonance (CW ELDOR) was independently introduced in 1968 by Hyde and Freed [72–75] and Bendersky and Blumenfeld [76] groups. In the CW ELDOR technique, one part of the EPR spectrum of a paramagnetic sample is irradiated with an intense saturating microwave pump field, and the effect of this intense field on other parts of the spectrum is assessed by a second weak microwave probe field. The EPR signals

detected by the weak microwave probe field are reduced in intensity due to saturation transfer effects when the two frequencies are separated either by an integral number of hyperfine energy differences or by a g -factor difference of two or more paramagnetic species.

Electron spin echo envelope modulation (ESEEM) arises from a coupling between the EPR-active electron being probed and nuclei [77]. ESEEM contains information on the type of nuclei, on the distances between nuclei, on the spin density distribution (hyperfine interaction), and on the electric field gradient at the nuclei (nuclear quadrupole interaction). Pulse-ENDOR techniques make use of a combination of microwave and radiofrequency pulses. ESEEM is suited for measuring weak hyperfine couplings, e.g., of the order of the free nuclear Larmor frequency, while continuous wave ENDOR is better suited for strong hyperfine couplings [77–80]. The two most common forms of ESEEM experiments use either a two-pulse ($\pi/2$ – τ – π – τ –echo) or three-pulse ($\pi/2$ – τ – $\pi/2$ – T – $\pi/2$ – τ + T –echo) sequences. In ESEEM experiments, the modulation of the echo intensity is monitored as a function of the delay between the microwave pulses. Electron spin echoes, as created by the two-pulse ESEEM sequence, are a superposition of Hahn echoes [78] arising from allowed and forbidden nuclear transitions. This leads to a non-oscillatory or unmodulated part. Coherence transfer echoes, whose amplitude oscillates at the sum and difference frequencies of the (weakly coupled) local nuclei, form the modulated part. T Anisotropy of g -, hyperfine anisotropy, field inhomogeneities g -, and A -strains caused an extreme inhomogeneous broadening in the solid state can be revealed by these methods.

In the frame of a three-pulse sequence ($\pi/2$ – τ – $\pi/2$ – T – $\pi/2$ – τ –echo), a set of stimulated ESEEM patterns is recorded as a function of time T [80, 81]. The four-pulse method ESEEM, which exploits additional filtering of the relevant signal, is advantageous for measuring combination lines compared to two-pulse ESEEM. To improve the ESEEM modulation depth, five-pulse ESEEM, with the sequence ($\pi/2$ – τ_1 – π – τ_1 – $\pi/2$ – T – $\pi/2$ – τ_2 – π – τ_2 –echo) has been proposed. In Davies ENDOR of an $S = 1/2$, $I = 1/2$ system a microwave (mw) inversion recovery pulse sequence (π – T – $\pi/2$ – τ – π – τ –echo) was used. Davies ENDOR is useful for systems with large hfs while applications of Mims ENDOR are limited to relatively small hfs. constants ($B_1 > a$) 0.13 [81].

A time-domain pulsed method in which polarization transfer ENDOR occurs can be performed with selective as well as non-selective mw pulses. In these experiments, the mixing period consists of two rf $\pi/2$ pulses separated by a variable time interval T^* [82]. Hyperfine-correlated electron-nuclear double-resonance spectroscopy (HYEND), where the nuclear transition frequencies are correlated with the corresponding hyperfine frequencies, can be used for considerable simplification of the interpretation of the spectra.

The HYSCORE is a two-dimensional ESEEM method first published by Hofer et al. in 1986 [83]. The following pulse sequence of a HYSCORE experiment is used: $p/2$ – t – $p/2$ – t_1 – p – t_2 – $p/2$ – t –echo. The experiment can be separated into three steps:

generation of nuclear coherence, the evolution time with inversion pulse, and the detection sequence. After 2D Fourier transformation, the HYSORE spectrum is a 2D plot related to nuclear frequencies of different spin manifolds of the paramagnetic system for a certain orientation [83]. Due to the high spectral resolution and reasonable number of pulses, HYSORE experiments can be performed on samples with a low concentration of paramagnetic species. DONUT-HYSORE (double nuclear coherence transfer hyperfine sublevel correlation) is a two-dimensional experiment, which was designed to obtain correlations between nuclear frequencies belonging to the same electron spin manifold [84]. The sequence employed is $\pi/2-\tau_1-\pi/2-t_1-\pi-\tau_2-\pi-t_2-\pi/2-\tau_1$ -echo. The echo is in turn measured as a function of t_1 and t_2 ; whereas, τ_1 and τ_2 are held constant. The DONUT-HYSORE experiment was designed to improve the resolution of the ESEEM frequencies and to resolve the assignment of ESEEM frequencies for the case of an electron spin, $S = 1/2$, interacting with a number of nuclear spins with $I \geq 1$ (e.g., ^{14}N nuclei) with non-negligible nuclear quadrupole interactions.

Two-dimensional electron–electron double-resonance (2D-ELDOR) technique was invented, developed, and applied by the Freed group [85]. The FID, obtained during the evolution period, t_1 is collected as a function of t_2 . The experiments are repeated for a series of mixing time, T_m , at several temperatures. The signals are then doubly Fourier transformed and can be presented as magnitude spectra. 2D-ELDOR is sensitive to the dynamical processes affecting spin labels in complex fluid environments. In ordered fluids, such as membrane vesicles, the 2D-ELDOR experiment is affected by the molecular tumbling in the locally ordered environment.

Two-dimensional Fourier transfer ESR approach includes correlation spectroscopy (COSY) and spin echo correlation spectroscopy (SECSY) [86]. In the standard COSY experiment, the first $\pi/2$ pulse creates transverse magnetization (± 1 coherences). The signal is measured after a second $\pi/2$ pulse. The SECSY signal is related to the COSY signal by the transformation $t_2 \rightarrow t_2 + t_1$, and inhomogeneities are refocused in t_1 . In the SECSY experiment with a hard pulse, the homogeneous linewidth (T_2^{-1}) across the spectrum can be obtained in a single experiment. The linear dependence T_2^{-1} versus τ_R^a was τ_R which is the rotational correlation time and allows one to determine τ_R in the slow motion region (10^{-7} – 10^{-8} s).

Effects of electron spin on nuclear spins on NMR spectra and nuclear spins relaxation were widely investigated [87]. The total observed NMR chemical shift (δ_{tot}) includes both a diamagnetic or orbital contribution (δ_{dia}) from paired electrons and a hyperfine contribution (δ_{hf}) from unpaired electrons of the electron-nuclear term of Hamiltonian. Effects of electron spin on nuclear spins on position of NMR spectra are revealed in Fermi contact (δ_{FC})

$$\delta_{\text{FC}} = m(S + 1)\rho_{\alpha\beta}/T \quad (4.14)$$

depending on the spin state (S) of the system, the spin density at the nucleus ($\rho_{\alpha\beta}$), temperature and a collection of fundamental physical constants, and pseudocontact (δ_{pc}) term:

$$\delta^{\text{PCS}} = \frac{1}{12\pi r^3} \left[\Delta\chi_{\text{ax}}(3\cos^2\theta - 1) + \frac{3}{2}\Delta\chi_{\text{rh}}\sin^2\theta\cos 2\varphi \right]$$

$$\Delta\chi_{\text{ax}} = \chi_{zz} - \frac{\chi_{xx} + \chi_{yy}}{2} \text{ and } \Delta\chi_{\text{rh}} = \chi_{xx} - \chi_{yy} \quad (4.15)$$

where r is the distance between observed nuclei and electron, $\Delta\chi_{\text{ax}}$ and $\Delta\chi_{\text{rh}}$ are the axial and rhombic anisotropy parameters of the magnetic susceptibility tensor of the system, and θ and φ are the polar coordinates of the nucleus in the frame of the electronic magnetic susceptibility tensor.

The unpaired electron–nucleus dipolar interaction causes R_1 (longitudinal) and R_2 (transverse) nuclear relaxation because of its modulation. For the Solomon and Curie contributions, proton relaxation enhancement (PRS) is described by equations [87]

$$R_2^{\text{PRE}} = \frac{k_{\text{Solomon}} + k_{\text{Curie}}}{r^6} \quad (3)$$

$$k_{\text{Solomon}} = \left(\frac{\mu_0}{4\pi}\right)^2 \frac{\gamma_1^2 g_e^2 \mu_B^2 S(S+1)}{15} \left[4\tau_c + \frac{\tau_c}{1 + (\omega_1 - \omega_S)^2 \tau_c^2} \right. \\ \left. + \frac{3\tau_c}{1 + \omega_1^2 \tau_c^2} + \frac{6\tau_c}{1 + (\omega_1 + \omega_S)^2 \tau_c^2} + \frac{6\tau_c}{1 + \omega_S^2 \tau_c^2} \right]$$

$$k_{\text{Curie}} = \frac{1}{5} \left(\frac{\mu_0}{4\pi}\right)^2 \frac{\omega_1^2 g_e^4 \mu_B^4 S^2(S+1)^2}{(3kT)^2} \left[4\tau_{\text{Curie}} + \frac{3\tau_{\text{Curie}}}{1 + \omega_1^2 \tau_{\text{Curie}}^2} \right] \quad (4.16)$$

As it is seen from (4.16), the interaction depends on the nuclear Larmor frequency, electron Larmor frequency, electron–nucleus distance, electron g -factor, electron Bohr magneton, nuclear magnetogyric ratio, Boltzmann constant, temperature, and the electron spin quantum number. In certain conditions, (4.14–4.16) allow to estimate spin density on nucleus and determine electron–nucleus distances. Recently, a new method for extracting probability densities from pseudocontact shift (PCS) data that relies on Tikhonov-regularised 3D reconstruction was described [89].

Dynamic nuclear polarization (DNP) [88, 92–94] results from transferring spin polarization from electrons to nuclei, thereby enhancing the nuclear spin polarization. Electrons at a given magnetic field and temperature in thermal equilibrium can be aligned to a higher degree by chemical reactions (Chemical-induced DNP, CIDNP), optical pumping and spin injection. The polarization transfer between electrons and nuclei can occur spontaneously when electron spin polarization deviates from its thermal equilibrium value through electron-nuclear cross-relaxation and/or spin-state mixing among electrons and nuclei. The general static DNP Hamiltonian can be written as [90, 91]

$$H = H = H_E + H_N + H_{EN} = \omega_{0E} E_z - \omega_{0N} N_z + H_{EN}^{is} + H_{EN}^{di} \\ = \omega_{0Z} E_z - \omega_{0N} N_z + K_{SE}(E_Z N_Z + E_X N_X + E_Y N_Y) + K_{PSE} E_X N_Z \quad (4.17)$$

where H_E and H_N are the Hamiltonians for the electron and nucleus, respectively; H_{EN} is the hyperfine coupling, which is separated into the isotropic hyperfine interaction H_{EN}^{is} and the anisotropic dipolar coupling H_{EN}^{di} between the electron and the nucleus; the coefficients K_{SE} and K_{PSE} denote the secular and pseudosecular hyperfine interactions. ω_{0E} and ω_{0N} are the electron and nuclear Larmor frequencies. The nuclear Overhauser effect (NOE), the solid effect (SE), the cross-effect (CE), and thermal mixing (TM) can be mechanisms for microwave-driven DNP processes. The Overhauser effect accounts for the perturbation of nuclear spin level populations observed in free radicals when electron spin transitions are saturated by the microwave irradiation [96]. The solid effect occurs when an electron–nucleus mutual spin flip transition in an electron–nucleus two spin system is excited by microwave irradiation [97]. The cross-effect requires two unpaired electrons as the source of high polarization [87]. The thermal mixing effect is an energy exchange phenomenon between the electron spin ensemble and the nuclear spin, using the electron spin ensemble as a whole to provide hypernuclear polarization.

An important advantage of the DNP-NMR method is the ability to significant NMR signal enhancement [98, 99]. For example, the technique of dynamic nuclear polarization (DNP) can significantly improve the sensitivity of solid state NMR spectroscopy by transferring the large electron spin polarization to the nuclear spin system, through microwave irradiation at or near the electron paramagnetic resonance frequency. Studies of the temperature, magnetic field, and microwave power dependence of the DNP enhancement can optimize the signal enhancements. In some cases, magnetic or chemical interactions between the radicals and the target molecules can lead to attenuation of the NMR signal through paramagnetic quenching and/or radical decomposition [99]. To avoid this problem, polarizing materials incorporating nitroxide radicals of the solids to minimize interactions between the radicals and the solute were introduced. For example, these materials can hyperpolarize pure pyruvic acid.

A prepared series of 37 dinitroxide biradicals was used as polarizing agents in cross-effect DNP-NMR experiments at 9.4 T and 100 K in 1,1,2,2-tetrachloroethane [100]. It was observed that in this regime the DNP: (1) Performance is strongly correlated with the substituents on the polarizing agents. (2) Electron and nuclear spin relaxation times, with longer relaxation times lead to better enhancements. (3) Deuteration of the radicals generally leads to better DNP enhancement with longer build up time. To avoid suffering many polarizing agents from an unfavorable field and magic angle spinning (MAS) frequency dependence, a series of new hybrid biradicals, α,γ -bis(diphenylene- β -phenylallyl) (BDPA), tethered to a broad line nitroxide was prepared and investigated [95]. By tuning the distance between the two electrons and the substituents at the nitroxide moiety, correlations between the electron–electron interactions and the electron spin relaxation times on the one hand and the BDPA DNP enhancement factors on the other hand were established. The best radical in this series has a short methylene linker and bears bulky phenyl spirocyclohexyl ligands.

References

1. W.R. Hagen, *Biomolecular EPR Spectroscopy* (CRC, 2008)
2. G.R. Eaton, S.S. Eaton, D.P. Barr, R.T. Weber, *Quantitative EPR* (Springer, Berlin, 2010)
3. A. Savitsky, K. Mobius, *High-Field EPR Spectroscopy on Proteins and their Model Systems* (Wiley-VCH Verlag GmbH, 2009)
4. J. Jarmauci, Fundamentals of electron spin resonance, in *Nitroxides: Application in Chemistry, Biomedicine, and Materials Science*, ed. by G.I. Likhtenshtein, J. Yamauchi, S. Nakatsuji, A. Smirnov, R. Tamura (WILEY-VCH, Weinheim, 2008), pp. 71–120
5. G.I. Likhtenshtein, *Electron Spin in Chemistry and Biology: Fundamentals, Methods, Reactions Mechanisms, Magnetic Phenomena, Structure Investigation* (Springer, Berlin, 2016)
6. O.Ya. Grinberg, A.A. Dubinskii, V.F. Shuvalov, L.G. Oranskii, V.I. Kurochkin, Ya.S. Lebedev, EPR submillimeter spectroscopy of free radicals. *Doklady Akademii Nauk SSSR* **230**, 884–887 (1976)
7. M. Malferrari, A. Savitsky, W. Lubitz, K. Mobius, G. Venturoli, Protein immobilization capabilities of sucrose and trehalose glasses: the effect of protein/sugar concentration unraveled by high-field EPR. *J. Phys. Chem. Lett.* **7**(23), 4871–4877 (2016)
8. J.H. Freed, New technologies in electron spin resonance. *Ann. Rev. Phys. Chem.* **51**, 655–689 (2000)
9. K. Moebius, A.N. Savitsky, *High-Field EPR spectroscopy of Proteins and their Model Systems: Characterization of Transient Paramagnetic States* (Royal Society of Chemistry, 2009)
10. A.I. Smirnov, Recent advantages in ESR techniques used in nitroxide application, in G.I. Likhtenshtein, J. Yamauchi, S. Nakatsuji, A. Smirnov, R. Tamura, *Nitroxides: Application in Chemistry, Biomedicine, and Materials Science* (WILEY-VCH, Weinheim, 2008), pp. 121–160
11. F. Bloch, Nuclear induction. *Phys. Rev.* **70**, 460–473 (1946)
12. G.I. Likhtenshtein, Determination of the topography of proteins groups using specific paramagnetic labels. *Mol. Biol. (Moscow)* **2**, 234–240 (1968)
13. G.I. Likhtenshtein, *Spin Labeling Method in Molecular Biology* (Wiley Interscience, New York, NY, 1976)
14. J.C. Taylor, J.S. Leigh, M. Cohn, The effect of dipole-dipole interaction between nitroxide radical and a paramagnetic ion on the line shape of the ESR spectra of radical. *Proc. Natl. Acad. Sci. U.S.A.* **64**, 206–219 (1969)
15. G.I. Likhtenshtein, Study on the proteins microstructure by method of spin-label paramagnetic probe. *Mol. Biol. (Moscow)* **4**, 782–789 (1970)
16. A.V. Kulikov, G.I. Likhtenshtein, E.G. Rozantsev, V. Suskina, A.V. Shapiro, Nitroxide bi- and polyradicals as standard models for distance estimation between the nitroxide moieties. *Biofizika* **17**, 42–49 (1972)
17. A.I. Kokorin, K.I. Zamaraev, G.L. Grigoryan, V.P. Ivanov, E.G. Rozantsev, Distance estimation between nitroxyl radicals. *Biofizika* **17**, 34–41 (1972)
18. A.V. Kulikov, G.I. Likhtenshtein, Application of saturation curves for evaluating distances in biological objects by the method of double spin-labels. *Biofizika* **19**, 420–424 (1974)
19. G.I. Likhtenshtein, Depth of immersion of paramagnetic centers, in *Magnetic Resonance in Biology*, ed. by L. Berliner, S. Eaton, G. Eaton (Kluwer Academic Publishers, Dordrecht, 2000), pp. 1–36
20. G.D. Case, J.S. Leigh, Intramitochondrial position of cytochrome haem groups determined by dipolar interaction with paramagnetic cations. *Biochem. J.* **160**, 769–783 (1976)
21. A.V. Kulikov, G.I. Likhtenshtein, The use of spin-relaxation phenomena in the investigation of the structure of model and biological systems by method of spin labels. *Adv. Mol. Relax Proc.* **10**, 47–78 (1977)
22. M.K. Bowman, J.R. Norris, Cross relaxation of free radicals in partially ordered solids. *J. Phys. Chem.* **86**, 3385–3390 (1982)

23. L.A. Syrtsova, L.A. Levchenko, E.N. Frolov, G.I. Likhtenshtein, T.N. Pisarscaya, L.V. Vorob'ev, V.A. Gromoglasova, Structure and function of the nitrogenase components from *Azotobacter vinelandii*. *Mol. Biol. (Moscow)* **5**, 726–734 (1971)
24. E.J. Hustedt, A.H. Beth, Structural information from CW-EPR spectra of dipolar coupled nitroxide spin label, in *Biological Magnetic Resonance: Distance Measurements in Biological Systems by EPR*, vol. 19, ed. by L.J. Berliner, G.R. Eaton, S.S. Eaton (Kluwer Academic, New York, 2000), pp. 155–184
25. W. Xiao, Y.K. Shin, EPR spectroscopic ruler: the deconvolution method and its application, in *Biological Magnetic Resonance: Distance Measurements in Biological Systems by EPR*, vol. 19, ed. by L.J. Berliner, G.R. Eaton, S.S. Eaton (Kluwer Academic, New York, 2000), pp. 249–276
26. J.H. Freed, S. Wang, Theory of relaxation, applied to saturation and double resonance in ESR spectra. VI. Saturation recovery. *J. Phys. Chem.* 1155–1157 (1974)
27. M. Huisjen, J.S. Hyde, Saturation recovery measurements of electron spin relaxation time of free radicals in solution. *J. Chem. Phys.* **60**, 1682–1683 (1974)
28. S.S. Eaton, G.R. Eaton, Relaxation times of organic radicals and transition metal ions, in *Biological Magnetic Resonance: Distance Measurements in Biological Systems by EPR*, vol. 19, ed. by L.J. Berliner, G.R. Eaton, S.S. Eaton SS, (Kluwer Academic, New York, 2000), pp. 29–154
29. G.M. Smith, D.J. Keeble, O. Schiemann (eds.), *Introduction to Modern EPR Spectroscopy* (CRC, 2010)
30. S.S. Eaton, G.R. Eaton, L.J. Berliner (eds.), Biomedical EPR—part B: methodology, instrumentation, and dynamics, in *Biological Magnetic Resonance*, vol. 24 (Springer, Berlin, 2005)
31. L.J. Berliner, S.S. Eaton S, G.R. Eaton (eds.), Distance measurements in biological systems by EPR, in *Biological Magnetic Resonance*, vol. 19 (Springer, Berlin, 2001)
32. G.R. Eaton, S.S. Eaton, K.M. Salikhov, *Foundations of Modern EPR* (World Scientific, 1998)
33. G.I. Likhtenstein, *Biophysical Labeling Methods in Molecular Biology* (Cambridge University Press, New York, Cambridge, 1993), pp. 46–79
34. G. Jeschke, Dipolar spectroscopy—double-resonance methods. *eMagRes* **5**(3), 1459–1476 (2016)
35. O. Krumkacheva, E. Bagryanskaya, EPR-based distance measurements at ambient temperature. *J. Magn. Reson.* **280**, 117–126 (2017)
36. A. Feintuch, G. Otting, D. Goldfarb, Gd^{3+} spin labeling for measuring distances in biomacromolecules: why and how? in *Methods in Enzymology*, vol. 563 (2015), pp. 416–457
37. G.E. Pake, Nuclear resonance absorption in hydrated crystals: fine structure of the proton line. *J. Chem. Phys.* **16**, 327–336 (1948)
38. S.A. Dzuba, E.S. Salnikov, L.V. Kulik, CW EPR, echo-detected EPR, and field-step ELDOR study of molecular motions of nitroxides in o-terphenyl glass: Dynamical transition, dynamical heterogeneity and β -relaxation. *Appl. Magn. Resn.* **30**, 637–650 (2006)
39. A.D. Milov, K.M. Salikhov, Y.D. Tsvetkov, Phase relaxation of hydrogen atoms stabilized in an amorphous matrix. *Sov. Phy. Solid State* **15**, 802–806 (1973)
40. A.D. Milov, R.I. Samoilova, Y.D. Tsvetkov, M. De Zotti, C. Toniolo, J. Raap, PELDOR conformational analysis of bis-labeled Alamethicin aggregated in phospholipid vesicles. *J. Phys. Chem. B* **112**, 13469–13472 (2008)
41. V.V. Kurshev, A.M. Raitsimring, Yu.D. Tsvetkov, Selection of dipolar interaction by the “2+1” pulse train ESE. *J. Magn. Reson.* **81**, 441 (1989)
42. G. Jeschke, DEER distance measurements in proteins. *Annu. Rev. Phys. Chem.* **63**, 419–446 (2012)
43. P.P. Borbat, E.R. Georgieva, J.H. Freed, Improved sensitivity for long-distance measurements in biomolecules: five-pulse double electron-electron resonance. *J. Phys. Chem. Lett.* **4**, 170–175 (2013)
44. G.I. Likhtenshtein, Depth of immersion of paramagnetic centers, in *Magnetic Resonance in Biology*, ed. by L. Berliner, S. Eaton, G. Eaton (Kluwer Academic Publishers, Dordrecht, 2000), pp. 309–347

45. S. Milikisiyants, M.A. Voinov, A.I. Smirnov, Refocused Out-Of-Phase (ROOPh) DEER: a pulse scheme for suppressing an unmodulated background in double electron-electron resonance experiments. *J. Magn. Reson.* **293**, 9–18 (2018)
46. F.D. Breitgoff, Y.O. Polyhach, G. Jeschke, Reliable nanometre-range distance distributions from 5-pulse double electron electron resonance. *Phys. Chem. Chem. Phys.* **19**(24), 15754–15765 (2017)
47. J. Tang, J.R. Norris, Multiple quantum EPR coherence in a spin correlated pair system. *Chem. Phys. Lett.* **233**, 192–200 (1995)
48. S.A. Dzuba, M.K. Bosh, A.Y. Hoff, Electron and spin-echo detection of quantum beats and double quantum coherence in spin-correlated pairs of protonated photosynthetic reaction centers. *Chem. Phys. Lett.* **248**, 427–433 (1996)
49. P.P. Borbat, J.H. Freed, Double-quantum ESR and distance measurements, in *Distance Measurements in Biological Systems by EPR*, Part of the Biological Magnetic Resonance book series, vol. 19 (Springer, Boston, 2002), pp. 383–459
50. P.P. Borbat, J.H. Freed, Multiple-quantum ESR and distance measurements. *Chem. Phys. Lett.* **313**, 145–154 (1999)
51. Y.-W. Chiang, A.J. Costa-Filho, B. Baird, J.H. Freed, 2D-ELDOR study of heterogeneity and domain structure changes in plasma membrane vesicles upon cross-linking of receptors. *J. Phys. Chem. B* **115**, 10462–10469 (2011)
52. A. Schweiger, C. Gemperle, R.R. Ernst, Soft pulse electron-spin-echo-envelope modulation spectroscopy (Soft ESEEM). *J. Magn. Reson.* **86**, 70–81 (1990)
53. S.A. Dzuba, A. Kawamori, Selective hole burning in EPR: spectral diffusion and dipolar broadening. *Concepts Magn. Reson.* **8**, 49–61 (1996)
54. K.B. Konov, A.A. Knyazev, Y.G. Galyametdinov, N.P. Isaev, L.V. Kulik, Selective hole-burning in RIDME experiment: dead-time free measurement of dipolar modulation. *Appl. Magn. Reson.* **44**(8), 949–966 (2013)
55. J. Solomon, N. Bloembergen, Nuclear magnetic interaction in HF molecule. *J. Chem. Phys.* **25**, 261–266 (1956)
56. A.V. Kulikov, Determination of distance between the nitroxide label and a paramagnetic center in spin-labeled proteins from the parameters of the saturation curve of the ESR spectrum of the label at 77K. *Mol. Biol. (Moscow)* **10**, 109–116 (1976)
57. K.M. Salikhov, A.G. Semenov, Yu.D. Tsvetkov, *Electron Spin Echo and Its Application* (Nauka, Novosibirsk, 1976)
58. S. Eaton, G. Eaton, Determination of distance based on T_1 and T_2 effects, in *Magnetic Resonance in Biology*, ed. by L. Berliner, S. Eaton, G. Eaton (Kluwer Academic Publishers, Dordrecht), pp. 348–382
59. M.F. Perutz, Mechanisms of cooperativity and allosteric regulation in proteins. *Quart. Rev. Biophys.* **22**, 139–236 (1989)
60. S. Razzaghi, E.K. Brooks, E. Bordignon, W.L. Hubbell, M. Yulikov, G. Jeschke, EPR relaxation-enhancement-based distance measurements on orthogonally spin-labeled T4-lysozyme. *Chembiochem* **14**(14), 1883–1890 (2013)
61. S. Weber, G. Kothe, J.R. Norris, Transient nutation electron spin resonance spectroscopy Transient nutation electron spin resonance spectroscopy on spin-correlated radical pairs: a theoretical analysis on hyperfine-induced nuclear modulations. *J. Chem. Phys.* **106**, 6248–6261 (1997)
62. K. Ayabe, K. Sato, S. Nishida, T. Ise, S. Nakazawa, K. Sugisaki, Y. Morita, K. Toyota, D. Shiomi, M. Kitagawa, T. Takui, Pulsed electron spin nutations spectroscopy of weakly exchange-coupled biradicals: a general theoretical approach and determination of the spin dipolar interaction. *Phys. Chem. Chem. Phys.* **14**, 9137–9148 (2012)
63. M. Srivastava, J.H. Freed, Singular value decomposition method to determine distance distributions in pulsed dipolar electron spin resonance: II Estimating uncertainty. *J. Phys. Chem. A* **123**(1), 359–370 (2019)
64. M. Srivastava, E.R. Georgieva, J.H. Freed, A new wavelet denoising method for experimental time-domain signals: pulsed dipolar electron spin resonance. *J. Phys. Chem. A* **121**(12), 2452–2465 (2017)

65. A. Doll, M. Qi, A. Godt, G. Jeschke, CIDME: short distances measured with long chirp pulses. *J. Magn. Reson.* **273**, 73–82 (2016)
66. A. Doll, G. Jeschke, EPR-correlated dipolar spectroscopy by Q-band chirp SIFTER. *Phys. Chem. Chem. Phys.* **18**(33), 23111–23120 (2016)
67. A. Doll, G. Jeschke, Double electron-electron resonance with multiple non-selective chirp refocusing. *Phys. Chem. Chem. Phys.* **19**(2), 1039–1053 (2017)
68. M. Sajid, M. Hulsman, A. Godt, G. Jeschke, Two-dimensional distance correlation maps from pulsed triple electron resonance (TRIER) on proteins with three paramagnetic centers. *Appl. Magn. Reson.* **49**(11), 1253–1279 (2018)
69. H.M. McConnell, R.E. Robertson, Isotropic nuclear resonance shifts. *J. Chem. Phys.* **29**, 1361–1366 (1958)
70. M. Karplus, Contact electron-spin coupling of nuclear magnetic moments. *J. Chem. Phys.* **30**, 11–16 (1959)
71. G. Feher, Observation of nuclear magnetic resonances via the electron spin resonance line. *Phys. Rev.* **103**(3), 834–835 (1956)
72. J.S. Hyde, ENDOR of free radicals in solution. *J. Chem. Phys.* **43**, 1806–1812 (1965)
73. H. Kurreck, B. Kirste, W. Lubitz, *Electron Nuclear Double Resonance Spectroscopy of Radicals in Solution* (VCH Publishers, New York, 1988)
74. D.V. Murphy, R.D. Farley, Principles and applications of ENDOR spectroscopy for structure determination in solution and disordered matrices. *Chem. Soc. Rev.* **35**, 249–268 (2006)
75. J.S. Hyde, J.C.W. Chien, J.H. Freed, Electron–electron double resonance of free radicals in solution. *J. Chem. Phys.* **48**, 4211 (1968)
76. V.A. Benderskii, L.A. Blyumenfel'd, P.A. Stunzhas, F.A. Sokolov, Double electron-electron resonance of triplet excitons in ion-radical salts. *Nature* **220**, 365–367 (1968)
77. W.B. Mims, Amplitudes of superhyperfine frequencies in electron-spin-echo-envelope. *Phys. Rev. B* **6**, 3543–3545 (1973)
78. E.L. Hahn, Spin echoes. *Phys. Rev.* **80**, 580–594 (1950)
79. B. Kasumaj, H. Dube, N. Zoelch, F. Diederich, G. Jeschke, Relaxation and modulation interference effects in two-pulse electron spin echo envelope modulation (ESEEM). *J. Magn. Reson.* **223**, 187–197 (2012)
80. L.V. Kulik, I.A. Grigor'ev, E.S. Salnikov, S.A. Dzuba, Y.D. Zvetkov, Electron spin–echo envelope modulation induced by slow intramolecular motion. *J. Phys. Chem. A* **107**, 3692–3695 (2003)
81. A. Schweiger, G. Jeschke, *Principles of Pulse Electron Paramagnetic Resonance* (Oxford University Press, Oxford, 2001)
82. M. Mehring, P. Hofer, A. Grupp, Pulsed electron nuclear double and triple resonance schemes. *Ber. Bunsenges. Phys. Chem.* **91**, 1132–1137 (1987)
83. P. Hofer, A. Grupp, H. Nebenfuhr, M. Mehring, Hypern sublevel correlation (HYSCORE) spectroscopy—a 2D ESR investigation of the squaric acid radical. *Chem. Phys. Lett.* **132**, 279–282 (1986)
84. D. Goldfarb, V. Kofman, J. Libman, A. Shanzer, R. Rahmatouline, S. Van Doorslaer, A. Schweiger, Double nuclear coherence transfer (DONUT)-HYSCORE: a new tool for the assignment of nuclear frequencies in pulsed EPR experiments. *J. Am. Chem. Soc.* **120**, 7020–7029 (1998)
85. B. Fresch, D. Frezzato, G.J. Moro, G. Kothe, J.H. Freed, Collective fluctuations in ordered fluids investigated by two-dimensional electron-electron double resonance spectroscopy. *J. Phys. Chem. B* **110**, 24238–24254 (2006)
86. S. Lee, D. Budil, J.H. Freed, Theory of two-dimensional Fourier transform electron spin resonance for ordered and viscous fluids. *J. Chem. Phys.* **101**, 5529 (30 pages) (1994)
87. I.A. Solomon, Relaxation processes in a system of two spins. *Phys. Rev.* **99**, 559–565 (1955)
88. I. Bertini, C. Luchinat, M. Nagulapalli, G. Parigi, E. Ravera, Paramagnetic relaxation enhancement for the characterization of the conformational heterogeneity in two-domain proteins. *Phys. Chem. Chem. Phys.* **14**, 9149–9156 (2012)

89. E.A. Suturina, D. Haussinger, K. Zimmermann, L. Garbuio, M. Yulikov, G. Jeschke, I. Kuprov, Model-free extraction of spin label position distributions shift data from pseudocontact. *Chem. Sci.* **8**(4), 2751–2757 (2017)
90. Y.N. Molin (ed.), *Spin Polarization and Magnetic Effects in Radical Reactions* (Elsevier, Amsterdam, 1984)
91. L.J. Berliner, E. Bagryanskaya, Chemically induced electron and nuclear polarization, in *Multifrequency Electron Paramagnetic Resonance*, ed. by S. Misra (Wiley-VCH, 2011), pp. 947–992
92. A. Abragam, M. Goldman, Principles of dynamic nuclear polarisation. *Rep. Prog. Phys.* **41**, 395–467 (1976)
93. C. Griesinger, M. Bennati, H.M. Vieth, C. Luchinat, G. Parigi, P. Höfer, F. Engelke, S.J. Glaser, V. Denysenkov, T.F. Prisner, Dynamic nuclear polarization at high magnetic fields in liquids. *Prog. Nucl. Magn. Reson. Spectrosc.* **64**, 4–28 (2012)
94. H. Hayashi, *Introduction to dynamic spin chemistry* (World Scientific, Singapore, 2004)
95. D. Wiser, G. Karthikeyan, A. Lund, G. Casano, H. Karoui, M. Yulikov, G. Menzildjian, A.C. Pinon, A. Pura, F. Engelke, S.R. Chaudhari, D. Kubicki, A.J. Rossini, I.B. Moroz, D. Gajan, C. Copéret, G. Jeschke, M. Lelli, L. Emsley, A. Lesage, O. Ouari, BDPA-nitroxide biradicals tailored for efficient dynamic nuclear polarization enhanced solid-state NMR at magnetic fields up to 21.1 T. *J. Am. Chem. Soc.* **140**(41), 13340–13349 (2018)
96. A.W. Overhauser, Polarization of nuclei in metals. *Phys. Rev.* **92**, 411–415 (1953)
97. A.A. Smith, B. Corzilius, A.B. Barnes, T. Maly, R.G. Griffin, Solid effect dynamic nuclear polarization and polarization pathways. *J. Chem. Phys.* **136**(1), 015101 (2012)
98. K.H. Sze, Q. Wu, H.S. Tse, G. Zhu, Dynamic nuclear polarization: new methodology and applications. *Top. Curr. Chem.* **326**, 215–242 (2012)
99. D.L. Silverio, H.A. van Kalker, T.C. Ong, M. Baudin, M. Yulikov, L. Veyre, P. Berruyer, Chaudhari, G. Sachin, D. Gajan, D. Baudouin, C. Matthieu, V. Basile, G. Jeschke, G. Bodenhausen, A. Lesage, L. Emsley, S. Jannin, C. Thieuleux, C. Copéret. Tailored polarizing hybrid solids with nitroxide radicals localized in mesostructured silica walls. *Helv. Chim. Acta* **100**(6) (2017)
100. D. Kubicki, G. Casano, M. Schwarzwald, S. Abel, C. Sauvee, K. Ganesan, M. Yulikov, A.J. Rossini, G. Jeschke, C. Coperet, A. Lesage, P. Tordo, O. Ouari, L. Emsley, Rational design of dinitroxide biradicals for efficient cross-effect dynamic nuclear polarization. *Chem. Sci.* **7**(1), 550–558 (2016)

Chapter 5

Nitroxide Biradicals



Alexander I. Kokorin

Abstract This chapter is devoted to the current state in the area of nitroxide biradicals shortly describing their history, effects of the electron spin exchange in nitroxide biradicals, structural investigations including comparing the X-ray structure with DFT calculations, features of the intramolecular dynamics in biradicals, and their possible applications.

5.1 Introduction—Historical Notes

The first information about nitroxide biradicals (NB) has appeared in press [1–4] less than in a year after classical papers by Rozantsev and Neiman [5, 6]. Afterward, the number of publications on this item increased exponentially and a lot of them were cited in many books and reviews, e.g., in [7–17]. The figures presented in these articles revealed the wide diversity of EPR spectra of different biradicals and their variability on chemical composition, temperature and solvent nature, which initiated discussions concerning the mechanisms of the intramolecular spin exchange in such systems with two stable unpaired electrons. In principle, any biradical molecule can be reproduced as $R'-Z-R'$, where R' means a paramagnetic radical group (e.g., see Fig. 5.1), and Z denotes organic or metal-organic bridge connecting two radical fragments [15].

Evidently, the “world” of stable nitroxide radicals centers which were involved to constructing NB molecules is much more diversified including such groups as are shown in Fig. 5.2.

These compounds were synthesized and described, and their properties were investigated, e.g., in: (A) [18], (B) [19], (C) [20, 21], (D) [21], (E) [22], (F) [23], (G) [24], (H) [25]. Also, such interesting works as [26, 27] should be mentioned in which ferromagnetic interactions in a crystalline nitroxide biradical: 1,3,5,7-tetramethyl-2,6-diazaadamantane N,N' -dioxyI [26] and the structure–properties’ relationships

A. I. Kokorin (✉)

N.N. Semenov Federal Research Center for Chemical Physics, Russian Academy of Sciences,
Moscow, Russian Federation

e-mail: alex-kokorin@yandex.ru; kokorin@chph.ras.ru

© Springer Nature Switzerland AG 2020

G. I. Likhtenshtein, *Nitroxides*, Springer Series in Materials Science 292,
https://doi.org/10.1007/978-3-030-34822-9_5

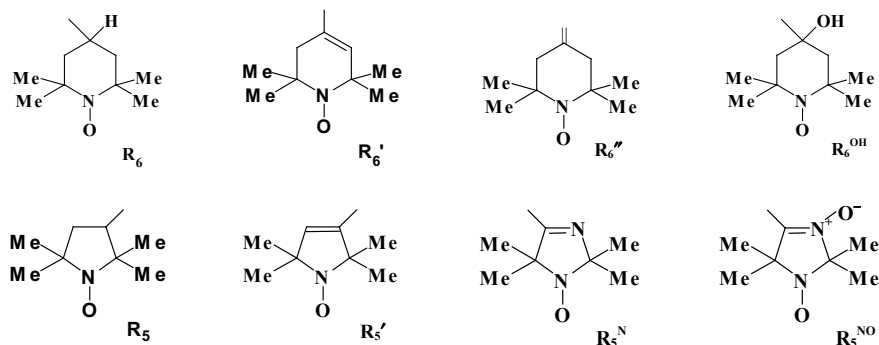


Fig. 5.1 Schematic structures of some nitroxide rings

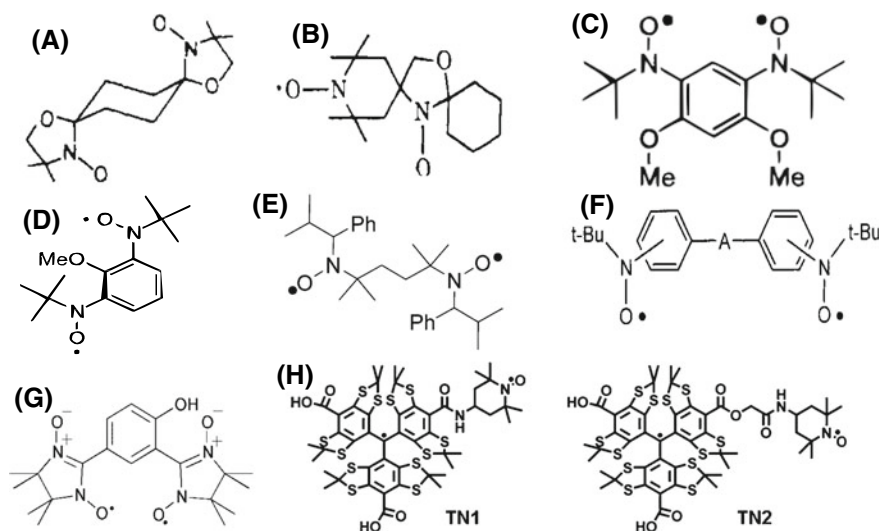


Fig. 5.2 Structures of some novel nitroxide groups

were analyzed in trimethylenemethane-type biradicals which were synthesized and studied by EPR spectral characterization of biradicals [27].

A lot of publications were devoted to a huge class of nitronyl nitroxide biradicals, their structure, and properties, e.g., [13, 17, 24, 28–30] and many others. As an example, magnetic properties of phenol- and phenoxide-substituted nitronyl nitroxide biradicals were revealed to be perspective as building blocks of organic-salt ferrimagnets [28], and some nitronyl nitroxide biradicals and their copper (II) complexes showed interesting structures, and magnetic properties in a solid state [29]. A nice family of stable organic triradicals with quartet ground states, which consisted of different nitroxide radicals, their syntheses, and magnetic properties were described in [31].

During the last decade, a new class of mixed biradicals, first of all, trityl-nitroxide biradicals as unique molecular probes which exhibited enhanced sensitivity and stability for rapid and simultaneous measurement of redox status and oxygenation by EPR spectroscopy [25]. First results showed that these biradical probes provided an opportunity for the design of new spin probes with the sensitivity of nitroxides to measure redox status while the narrow singlet signal of the trityl group enhanced sensitivity and speed of detection for greatly increased resolution of EPR imaging. Such new probes have high potential for the simultaneous EPR measurement of redox status and oxygenation in a wide variety of chemical and biological systems.

The value of exchange interaction J in organic biradicals strongly depends on their composition and can be modulated by changing the linker. In [32], for the first time the effect of chiral configurations of radical parts on the J value was demonstrated in the case of trityl-nitroxide biradicals (TN, Fig. 5.2h). Four diastereoisomers were synthesized and purified by the conjugation of a racemic nitroxide with the racemic trityl radical via *l*-proline. The absolute configurations of these diastereoisomers were assigned by comparing experimental and calculated electronic circular dichroism (ECD) spectra. EPR spectra showed that the configuration of the nitroxide part instead of the trityl part was dominant in controlling the exchange interaction and the order of the J value at room temperature. Measured $|J|$ values clearly showed this effect, and in some cases, the $|J|$ values varied with temperature and the polarity of the solvent due to their flexible linker, whereas the J values of another biradical were almost insensitive to these factors due to the rigidity of their linkers [32].

Simultaneous evaluation of redox status and oxygenation in biological systems is of great importance for the understanding of biological functions, and an approach of their measuring using EPR spectroscopy using nitroxide radicals has already interesting applications but were still limited by rather low oxygen sensitivity and low EPR resolution due to the moderately broad EPR triplet and spin quenching through biochemical processes. Authors of [33] showed that these problems can be overcome by the use of new trityl-nitroxide biradicals (TNB) contained ^{14}N pyrrolidinylnitroxide and a trityl and its isotopically labeled by ^{15}N analog. Both TNB exhibited much stronger spin–spin interaction with $|J| > 40$ mT compared with that of the previously synthesized TNB with longer linker chain length. The enhanced stability of new TNB was confirmed, and the effect of different types of cyclodextrins on its stability was also studied. New biradicals are sensitive to redox status, and their corresponding trityl-hydroxylamines formed from the reduction of the biradicals by ascorbate shared the same oxygen sensitivity. The ^{15}N -labeled TNB exhibited higher EPR signal amplitude as compared with that of ^{14}N analog. Cyclic voltammetric studies verified the electrochemical behavior of these TNB [33].

Several trityl-nitroxide biradicals (TNB) with highly asymmetric exchange coupling revealed specific magnetic properties provided new possibilities for the application in physicochemical, biophysical, and biological studies [34]. The effect of the linker length on the spin–spin interaction in TNB was investigated. It was shown that the magnitude of the spin–spin coupling $|J|$ could be easily tuned from ~ 0.4 mT to over 120 mT using various linkers separated two radical moieties and under varying temperatures. Computer simulation of EPR spectra was carried out to estimate $|J|$

values in TNB. The spin–spin interaction in TNB, their hyperfine splitting (hfs) constants g , and zero-field splitting D were measured at 220 K. Changes of the spin–spin coupling with variation of linker length and temperature provide a way to develop new TNB for applications in relevant fields [34].

TN biradicals were successfully used to study supramolecular host–guest interactions of TNB with methyl- β -cyclodextrin, hydroxypropyl- β -cyclodextrin, and γ -cyclodextrin [35]. EPR spectroscopy showed that in the presence of cyclodextrins, host–guest complexes were formed where the nitroxide and linker parts could interact with the cyclodextrins' cavities. Complexation with cyclodextrins led to the suppression of the intramolecular through-space spin–spin-exchange coupling allowing the determination of the through-bond spin–spin-exchange coupling value which was calculated as 0.16 mT using EPR simulations. Different types of cyclodextrins had various binding affinities with TNB. The effect of the linker in TNB on the host–guest forming was studied. The complexes of TNB with cyclodextrins could noticeably change the spin–spin-exchange coupling due to the size of linkers, and the stability of TNB toward ascorbate ions was significantly enhanced after the attaching to cyclodextrins. This approach seems to be a useful method to modulate the magnitude of the spin–spin interaction and redox sensitivity of TNB.

5.2 Electron Spin Exchange in Nitroxide Biradicals

Theory of the electron spin exchange in stable nitroxide biradicals with explanation of the changes observed in the EPR spectra has been developed and published in several independent papers practically at the same time [3, 4, 36–38], was detailed in papers [39, 40], and then enhanced to both areas of fast and slow exchange coupling by Parmon et al. in [41, 42]. A bit later, all data concerning physical–chemical and EPR spectroscopy features of nitroxide biradicals were collected and critically analyzed in [11, 12].

In liquid solutions with a low viscosity, the spin Hamiltonian \hat{H} comprises the isotropic hyperfine interactions, the Zeeman splitting, and the exchange coupling. In those cases when both radical fragments are identical and each bears only one nucleus with a nonzero nuclear spin I , the following equation is valid [37, 38]:

$$\hat{H} = \gamma_e H_0 (S_z^{(1)} + S_z^{(2)}) + a (S_z^{(1)} I_z^{(1)} + S_z^{(2)} I_z^{(2)}) + J S^{(1)} S^{(2)} \quad (5.1)$$

The spin Hamiltonian here is written in frequency units; superscripts 1 and 2 denote different radical fragments; $S^{(k)}$ are electron spin operators; $S_z^{(k)}$ and $I_z^{(m)}$ are projections of the electron and nuclear spins to the z -axis, respectively; γ_e is the electron magnetogyric ratio; H_0 is the external magnetic field; a is the ^{14}N isotropic hfs constant of the radical fragments, and J is the exchange integral. In a low-viscous solvent, the dipole–dipole coupling tensor is averaged to zero owing to the fast rotational motion of the biradical molecules [12, 42]. For any individual conformation, only one value $|J|$ should correctly describe the position and integral

intensity of each line in the EPR spectrum. In some cases, J in (5.1) is the mean value of two rather similar exchange integrals corresponding to two conformations, which one cannot distinguish in the experimental setup because of very fast hopping between them, e.g., [43–45].

The manifestation of exchange interaction in EPR spectra is caused by the ratio between the exchange integral J and the isotropic hfs constant a . If $|J| \ll |a|$, the hyperfine components of the spectrum can be split; in the zero approximation, a value of $|J|$ can be calculated by the parameter $|J/a|$; and in this case, an exchange integral value is easily determined. With increasing of $|J/a|$, the splitted lines become asymmetric relating to hfs lines at $J = 0$, and their intensities are no longer equal. All such changes at different $|J/a|$ values are schematically shown in many papers for the case of ^{14}N - ^{14}N nitroxide biradicals [X, Y, Z, 12, 46]. At high J values, a five lines' spectrum with the ratio 1:2:3:2:1 is observed, $|J| \gg a$, and precise determination of the J value is not available from the EPR spectrum.

An example of changes experimentally observed in the row of homological nitroxide biradicals containing only acetylene or *para*-phenylene groups in the bridge connecting two identical radical rings is shown in Fig. 5.3. R_6' is shown in Fig. 5.1.

$|J|$ values determined from these spectra from parameter $|J/a|$ presented in the related articles according to recommendations given in [12, 46] and confirmed by EPR spectra and DFT calculations are listed in Fig. 5.3. One can conclude that upon increasing the length of the bridge between two nitroxide rings, the value of the

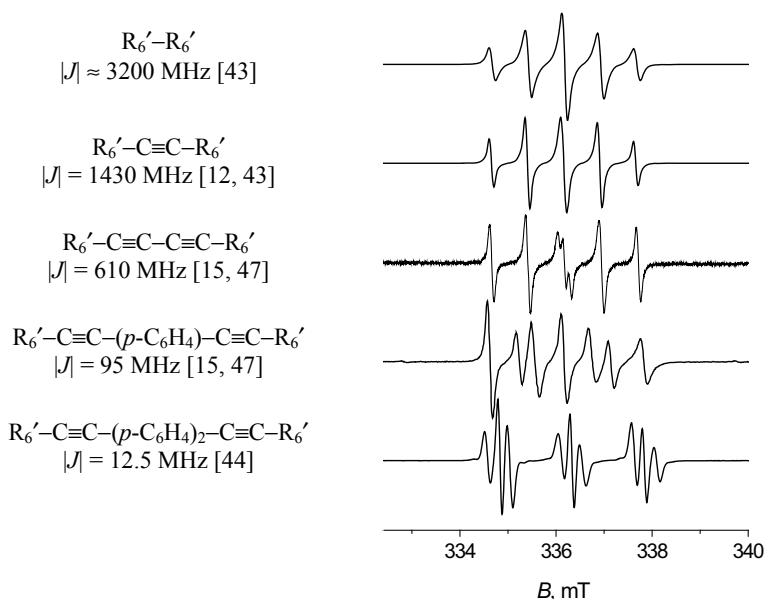


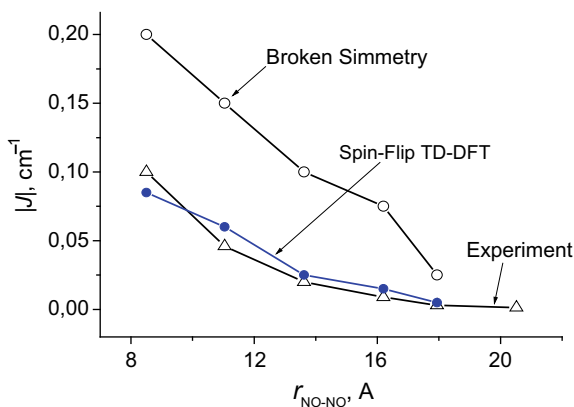
Fig. 5.3 Structures and the corresponding EPR spectra of some conjugated NB with acetylene and *p*-phenylene groups in the bridge dissolved in toluene at 313 K

exchange integral is noticeably decrease. A logical question arises: What is the reason of such changes? This could be caused either by the geometric elongation of the bridge or because of inserting various chemical groups in the bridge, their nature, and mutual orientation. In many theoretical works, old ones [48, 49], and much newer [50, 51], authors tried to distinguish two different mechanisms of the intramolecular spin exchange: “direct,” via straight collisions of two paramagnetic centers, and “indirect,” by delocalization of the electron spin density through the bridge of atoms and bonds [12]. In flexible long-chain biradicals, the direct mechanism should be realized, and in rigid stick-like molecules, one would assume that the indirect mechanism of spin exchange can occur. In the case of short-chain biradicals without conjugation, choosing of the mechanism is much more complicated as it was discussed, e.g., in [52, 53].

For the set of homological biradicals shown in Fig. 5.3 and such ones as $R_6'-(C\equiv C)_3-R_6'$ and $R_6'-C\equiv C-p-C_6H_4-C\equiv C-C\equiv C-R_6'$ [12], the dependence of the exchange integral $|J|$ as a function of the distance r_{NO-NO} between the unpaired electrons has been calculated. It follows from Fig. 5.4 that calculations carried out using the spin-flip TD-DFT method show very nice agreement with the experimental data while the broken symmetry calculations showed the tendency only qualitatively.

EPR spectra of biradicals with several acetylene and *p*-phenylene groups in the spacer linking two nitroxide rings (Fig. 5.3) are weakly temperature dependent. $|J|/a$ values measured for all of them allowed authors to suggest that the efficiency of spin density delocalization of unpaired electrons should be described with the use of the “coefficient of attenuation” $\gamma_k = |J_i/J_k|$ for the biradicals with $(|J_k/a|)$ and without $(|J_i/a|)$ a certain group or atom in the bridge [12]. In such linear biradicals, the intramolecular spin exchange can be realized only via the mechanism without straight collisions of the two N-O \cdot groups but rather due to overlapping of spin orbitals of two unpaired electrons by the indirect mechanism. $|J_k/a|$ and $|J_i/a|$ values should both be measured at the same temperature and in the same solvent [11, 12]. This attenuation coefficient γ_k is a characteristic parameter of the functional group or atom, which does not depend on other groups forming the bridge. This fact was

Fig. 5.4 Electron spin-exchange integral value $|J|$ as a function of the distance r_{NO-NO} between the unpaired electrons in biradicals' X-Y: experimental and DFT calculated



discussed in detail in [12] and then confirmed and enlarged with new examples in [15, 44, 45]. Many γ_k coefficients were determined and are listed in [15].

$$|J_{RR}| = |J_{Bir}| \cdot \gamma_k \cdot \gamma_l \cdot \gamma_m \cdot \dots, \quad (5.2)$$

where $\gamma_k, \gamma_l, \gamma_m$ are the attenuation coefficients for k-, l-, or m-atom or a group in the bridge between two R_6' or other radical fragments in a real biradical with its $|J_{Bir}|$. These γ_k values were experimentally measured for many biradicals with different nitroxide rings, e.g., $R_6', R_5, R_5', R_5^N, R_5^{NO}$ (Fig. 5.1), and various compositions of the linker [15]. Note that knowledge of all γ_k values for all groups in the bridge makes it possible to estimate the spin density ρ_C localized on the carbon atom in the fourth position of the piperidine ring connected with the first atom of the biradical bridge [44, 45]. Thus, the exchange integral value $|J_{RR}|$ for a biradical $R_6'-R_6'$ (the first one in Fig. 5.3) can be easily calculated by (5.2) knowing the $\gamma_k, \gamma_l, \gamma_m$, and $|J_{Bir}|$ parameters for a certain biradical.

As an example, using this procedure and keeping in mind that $|J/a| = 2.2$ and 14.5 for $R_6'-C\equiv C-p-C_6H_4-C\equiv C-R_6'$ and $R_6'-C\equiv C-C\equiv C-R_6'$ at 298 K in toluene, respectively [54], one can calculate $\gamma_{Ph} = 6.6$ (Ph is the same as $p-C_6H_4$) which is close to the values published earlier [47, 54]. Thus, the electron spin-exchange integral $|J|$ decreases by *ca.* a factor of 6.6 passing through the $p-C_6H_4$ group. It is known from [15] that a value of $\gamma_{C\equiv C} = 2.2 \pm 0.15$; therefore, one can calculate a value of $|J_{RR}| \approx 113$ mT, which is close to $|J_{RR}| \approx 122$ mT estimated in [44] and is in a good correlation with $|J_{RR}| \approx 0.12 \text{ cm}^{-1} \approx 128.5$ mT obtained in [43]. The similarity between these values obtained independently using various pairs of nitroxide biradicals confirms the correctness and universality of the approach envisaged by (5.2).

Similar estimating the spin density ρ_C localized on the carbon atom in the fourth position of the piperidine or in the third position of the five-membered ring connected with the nearest (first) atom of the biradical bridge, or the exchange integral value $|J_{RR}|$ for biradicals $R_{5,6}-Z-R_{5,6}$, real or hypothetical, was calculated and is given in Table 5.1.

It follows from the table that $|J_{RR}|$ parameters, hence, the ρ_C values, essentially depend on the structure of the radical ring. Indeed, in the case of $R_5'-R_5'$ biradical this value exceeds that of the $R_6'-R_6'$ analog because the C3 atom in a five-membered ring with a double bond is located much closer to the paramagnetic N-O \cdot group than the C4 atom in the six-membered ring in $R_6'-R_6'$ [44]. In $R_5^{NO}-Z-R_5^{NO}$ biradicals

Table 5.1 $|J_{RR}|$ values estimated from the data given in Tables 1–3 in [15] for $R_6'-R_6'$ and some other hypothetical nitroxide biradicals

Biradical	$R_6'-R_6'$	$R_6''-R_6''$	R_5-R_5	$R_5'-R_5'$	$R_5^N-R_5^N$	$R_5^{NO}-R_5^{NO}$
$ J_{RR} $, MGz	3400	750 ^a	1100	4500	42	3600

The precision of calculations is *ca.* $\pm 10\%$

^aCalculated by data from [40, 55]

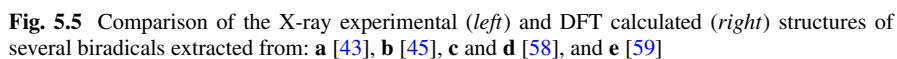
[13, 15], the spin density is more delocalized by the imidazolium ring comparing to similar $R_5^N - Z - R_5^N$ structures; therefore, $|J_{RR}|$ values of the latter are *ca.* 80–100 times smaller than in those containing R_5^{NO} rings. In the case of $R_6''=N-N=R_6''$ biradical [40, 55], the $|J_{RR}|$ value (Table 5.1) is sufficiently less comparing to that of the $R_6'-R_6'$ system due to (i) the geometry of the R_6' ring is a semi-chair and R_6'' ring is a twisted-form [56, 57], and (ii) the presence of a double bond in the R_6' ring helps to realize better conjugation between nitroxide groups and the bridge.

5.3 X-Ray Structures and DFT Calculations

One of the most important and informative characteristics of a nitroxide biradical is its structure obtained usually from the X-ray analysis data [56, 57]. Knowledge of the exact geometry allows understanding and prediction of some features of a biradical molecule and its behavior in liquid solutions. X-ray studies report often about geometries of a few conformers existing even in a solid state, in a crystal: see, e.g., [58, 59].

A very valuable advantage for evaluating structural, physical–chemical and dynamic properties of biradicals in a liquid phase can be obtained by the use of quantum chemical and especially the density functional theory (DFT) computations [60–63]. DFT calculations became very popular during the last 10–15 years due to increasing the calculation possibilities of new computer clusters and further development of specialized program packages. DFT calculations permit not only to predict the geometry of the molecule but also to determine correctly the spin Hamiltonian parameters such as a *g*-tensor, hyperfine splitting (hfs) *A*-tensor, the dipole–dipole coupling constant *D*, the intramolecular electron spin-exchange integral *J* and to characterize the dynamic behavior of the intramolecular motions in a biradical as well as transitions between different conformations [43–45, 64]. Figure 5.5 illustrates a comparison between the X-ray and calculated DFT structural parameters for several biradicals.

Numerical comparison geometries (bond lengths and angle) for these and more nitroxides demonstrated perfect agreement of the X-ray and DFT results which were represented in the tables (see references above). At several examples, we will describe the abilities of the DFT method. Relating to the structure of the $R_6'-C\equiv C-R_6'$ biradical obtained by DFT calculations is shown in Fig. 5.5a [43]. The effect of toluene as a solvent calculated in the scope of COSMO model did not reveal any significant changes in bond lengths, angles, or the r_{NO-NO} distance in the biradical comparing to the X-ray results. The zero-field splitting parameter *E* was not observed as well as in the case of $R_6'-R_6'$ biradical and was not taken into consideration at EPR spectra simulations. DFT calculation predicted *E* to be about three orders smaller than *D* parameter. The *g*-tensor axes were oriented along the N–O bond and were assumed to be collinear in both radical rings. Angles which represent the internal rotation around the main molecular axis connecting two N–O groups were included in fitting



procedure. Parameters D calculated by DFT were in perfect agreement with experimental ones. The COSMO model slightly increased the delocalization of the spin density, and the calculation taken into account the solvent influence allowed obtaining the D parameters in a better agreement with the experiment. $r_{\text{NO-NO}}$ distances calculated using the point-dipole approximation from EPR spectra for both biradicals differed both from the X-ray data and DFT-calculated $r_{\text{NO-NO}}$ distances and that implied assuming some delocalization of the electron spin density though the major part of the spin density is localized on the N and O atoms of the N-O \cdot bond [43].

The geometry of biradical $\text{R}_6'-p-\text{C}_6\text{H}_4-\text{R}_6'$ calculated at the UDFT/B3LYP level with a split valence basis set cc-PVDZ [65] is shown in Fig. 5.5b. Comparing the computational results with the X-ray pattern (Fig. 5.5 and Table 2 in [45]), one can conclude that DFT calculations provide correct information on the biradical molecular structure with a precision comparable with X-ray diffraction data. DFT calculations revealed the presence of several conformers of $\text{R}_6'-p-\text{C}_6\text{H}_4-\text{R}_6'$ biradical which were characterized by identical $r_{\text{NO-NO}}$ distances and identical zero-field splitting values D [45]. $|J|$ values were likely to be varied for these conformations due to significantly different mutual orientations of the two nitroxide moieties; see below in detail.

DFT calculations were applied to a model mixed-valence system presented a double-exchange phenomenon [62]. Due to the intrinsic multireference character of the spin states, it was shown that the couplings involved in the double-exchange model cannot be extracted from the DFT energies as it is usually done, but it was possible to extract the interactions of a generalized Hubbard Hamiltonian from different DFT single determinant energies, from which then the double-exchange spectrum could be evaluated. The problems generated by the charge and spin polarization were discussed in both symmetric and non-symmetric geometries [62].

The most important advantage of DFT method consists in the possibility to characterize not only structural peculiarities of the biradical molecule but also in distinguishing different conformations in which biradicals can exist, energetic features of transitions between them, calculating the spin Hamiltonian parameters, evaluating the spin density distribution in the system, etc. For example, characteristics such as the g -tensor, hyperfine splitting A -tensor, D , and $r_{\text{NO-NO}}$ values for biradicals $\text{R}_6'-\text{R}_6'$, $\text{R}_6'-\text{C}\equiv\text{C}-\text{R}_6'$, $\text{R}_6'-\text{C}\equiv\text{C}-\text{C}\equiv\text{C}-\text{R}_6'$, $\text{R}_6'-p-\text{C}_6\text{H}_4-\text{R}_6'$, $\text{R}_6'-\text{C}\equiv\text{C}-p-\text{C}_6\text{H}_4-\text{C}\equiv\text{C}-\text{R}_6'$, $\text{S}(\text{OR}_6)_2$, $\text{O}=\text{S}(\text{OR}_6)_2$, $\text{O}=\text{P}(\text{C}_6\text{H}_5)(\text{OR}_6)_2$, and others were calculated with high precision and demonstrated very good agreement with experimental results [43–45, 58, 59, 64]. At the same time, estimating exchange integral values seems to be rather more complicated problem: If $|J| > 1000$ MHz, its magnitude and sign can be determined with high accuracy; at $150 < |J| < 1000$ MHz, discrepancy with the experiment can achieve two- or threefold, and at $|J| \leq 100$ MHz, its evaluation is usually impossible due to very small energy magnitudes.

It should be noted that while calculations of the dipolar components of the hfs tensor can be systematically tuned by going to a much larger basis set of common use, isotropic hfs constants a are usually reproduced better using a specialized basis set described in [66]. Two important results were pointed out in [45]: First, specialized basis sets, such as N07 family or EPR family, enable much better agreement with

the experimental data than the conventional basis sets even in the case of very small hfs coupling. Second, for some reasons, PBE0 functional gives better agreement of calculated ^{13}C isotropic hfs constant with the experimental one in the particular case of ^{13}C -labeled $\text{R}_6'-\text{C}\equiv\text{C}-p-\text{C}_6\text{H}_4-\text{C}\equiv\text{C}-\text{R}_6'$ biradical [45], while the functional B3LYP, in turn, underestimates it, though both approaches yield results which are within the experimental error limits and agree well with the experiment. It was concluded that combination of PBE0/N07D or PBE0/EPR-II can be recommended as a cheap and precise way to compute small hfs couplings in nitroxide biradicals. A more detailed comparison of the experimental results obtained in different solvents with calculated ones taking into account various polarities were obtained and discussed in [67].

Concerning the number of conformations in which biradical molecules can exist in solutions: Fig. 5.6 demonstrates basing on DFT results that biradical $\text{R}_5'-\text{C}\equiv\text{C}-(p-\text{C}_6\text{H}_4)_2-\text{C}\equiv\text{C}-\text{R}_5'$ (**B**₅) realizes cis and trans conformations $\text{R}_6'-\text{C}\equiv\text{C}-(p-\text{C}_6\text{H}_4)_2-\text{C}\equiv\text{C}-\text{R}_6'$ (**B**₆) biradical has 8 energy equivalent conformers with the angle between SOMOs varying from 0°, this conformer corresponds to the maximal $|J|$ value, to ~60° at conformers with much lower $|J|$ values [44]. It makes a simple two-conformational model [12, 15, 36–39] inapplicable in a case of the latter biradicals **B**₅ and **B**₆. Biradical **B**₅ exhibited fast inversions of R_6' ring and internal rotations around the axis passing through the main molecular axis of the bridge even at low temperatures, averaging the $|J/a|$ values. Low barriers' activation energy E_a allows “mixing,” i.e., averaging the conformer's spectral parameters at high temperatures effectively as have been demonstrated in [43, 47].

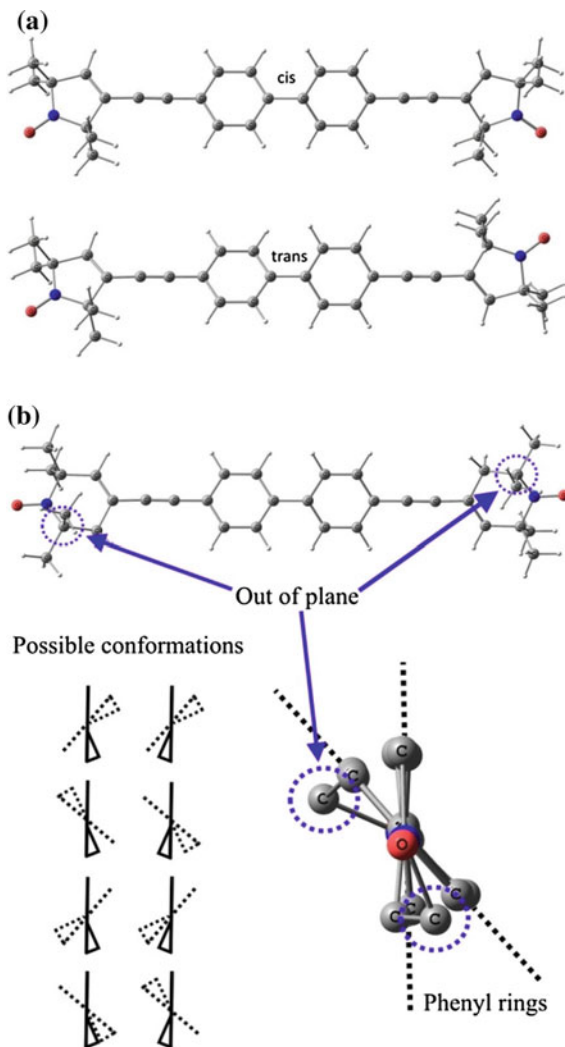
Another important for biradicals' result of DFT method is calculating the spin density distribution in nitroxide radicals and polyradicals. Figure 5.7 presents several examples of spin density distribution in $\text{R}_6'-\text{R}_6'$, $\text{R}_6'-\text{C}\equiv\text{C}-\text{R}_6'$, and $\text{O}=\text{P}(\text{C}_6\text{H}_5)(\text{OR}_6)_2$ biradicals in triplet and singlet states.

One can see that spin densities of biradicals shown in Fig. 5.8 are strongly localized at the N–O groups and the spin density value at the nitrogen atom is equal to 0.43 in both cases [47].

Very important from theoretical, spectroscopic, and application points of view results were reported in [53] where authors have synthesized new stable radical 2,5-di(*tert*-butyl)-3-ethoxycarbonyl-4-hydroxy-1-pyrroloxyl (**R**), and biradical 2,2',5,5'-tetra(*tert*-butyl)-4,4'-bis(ethoxycarbonyl)-3,3'-bipyrrolyl-1,1'-dioxyl (**BR**), in which the unpaired electrons were highly delocalized by the pyrroloxyl rings. Both were investigated using X-ray crystallography, EPR spectroscopy, and quantum chemical calculations. Besides, using this radical **R** and several linkers of various lengths, saturated and unsaturated, a group of new biradical products was also synthesized and studied using EPR and DFT methods.

To study the electronic structure, the localized SOMOs were calculated for three configurations: two coplanar at 0° and 180° and a perpendicular one at –90°. In all configurations, the SOMOs were π -orbitals delocalized over the N–O group and the parent ring system [53]. It was revealed that in the coplanar configurations even the localized SOMOs had significant contributions on the neighboring atoms: The population of the SOMOs on the N–O fragments was estimated as 91% and up to

Fig. 5.6 Calculated geometries of biradicals $R_5'-C\equiv C-(p-C_6H_4)_2-C\equiv C-R_5'$ (a) in cis and trans conformations (a) and $R_6'-C\equiv C-(p-C_6H_4)_2-C\equiv C-R_6'$ (b)



9% delocalization, and in the perpendicular configuration, the SOMOs showed small tails into the σ -system of $\sim 2\%$.

For three biradicals differed only by their bridges: (i) a saturated one with a $-C_{10}H_{20}$ linker, (ii) the unsaturated (conjugated) $-C_{10}H_{10}$ linker, and (iii) for the partially saturated linker $-C_{10}H_{12}$ localized SOMOs were calculated [53]. Note that all structures with the allyl linkers are planar. DFT results obtained were astonishing: The ratio between spin density in the nitroxide ring to that by the linker was equal to (i) 97:3%, (ii) 74:26%, and (iii) 78:22%, correspondingly. These results are very important for solving an old problem of spin-exchange coupling: “through bonds” or “through space” as well as for correct determining the dipole–dipole coupling

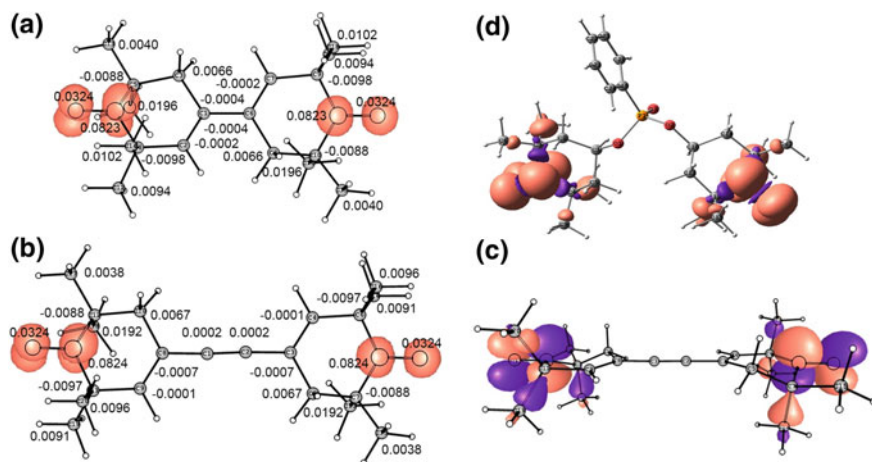


Fig. 5.7 Spin density distribution in biradicals $R_6'-R_6'$ (a) and $R_6'-C\equiv C-R_6'$ in triplet (b) and in singlet (c) state including atomic spin densities at the C, N, O nuclei (a.u.). d shows spin densities distribution in biradical $O=P(C_6H_5)(OR_6)_2$ in the open-shell triplet state [59]. Contour value of 0.01 a.u. was used in all cases

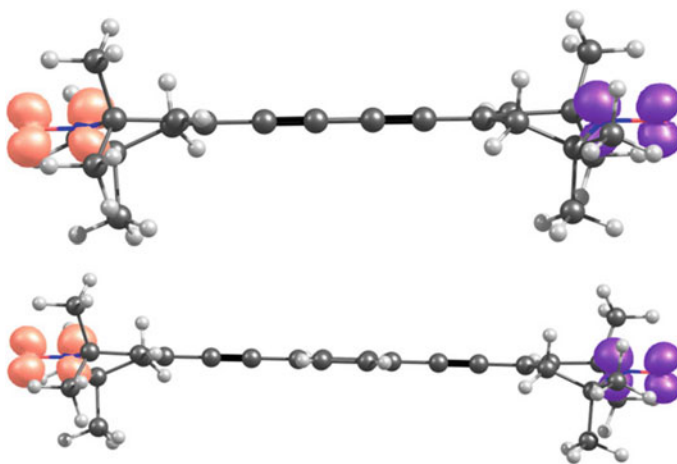


Fig. 5.8 Spin densities' distribution in biradicals $R_6'-C\equiv C-C\equiv C-R_6'$ and $R_6'-C\equiv C-p-C_6H_4-C\equiv C-R_6'$ in open-shell singlet states [47]

parameter D and the distance r_{NO-NO} between unpaired electrons from EPR spectra. Concerning the influence of unsaturated (or conjugated) groups in a linker, we have already discussed above.

The analysis presented in [53] suggests that the point-dipole approximation for dinitroxide **BR** is not completely correct due to the close proximity of the two electronic systems and the significant electron delocalization, which leads to large

quantum mechanical corrections to the point-dipole approximation, and the authors could estimate at what distance and separation of two spin systems does the native point-dipole approximation become accurate.

It was understood when the delocalization of the spin density strongly affects the D value and led to errors in the interspin distances obtained using the point-dipole model. Spins at closer distances much stronger depend on the dipole–dipole interaction operator than larger distances, and even small delocalization affects to errors in derived distances and become dramatic for aromatic nitroxides or if there are conjugated groups between radical centers. In this case, the D value deviates from the expected behavior becoming significantly sensitive to the relative orientation of the two radical fragments. If the spin label or the bridge separated two paramagnetic centers is rather unsaturated, it is better to avoid the point-dipole approximation, and quantum chemical calculations could be of great help in the analysis of actual experiments.

A nitroxide biradical $R_6'-^{13}C\equiv C-p-C_6H_4-C\equiv^{13}C-R_6'$ has been investigated by X-band EPR and electron-nuclear double-resonance (ENDOR) spectroscopy [64]. Spin density distribution and hfs constant value on ^{13}C atoms in the bridge were calculated using B3LYP and PBE0 functionals and several different basis sets including N07 family. These results were compared with the experimental value of the hfs constant on ^{13}C atoms measured from ENDOR spectra. A few recommendations concerning the calculation of electron spin density distribution and the isotropic hfs constant values in nitroxide biradicals were given, and the results presented in that paper confirmed the fact that intramolecular electron spin exchange in this biradical is realized by the indirect mechanism [64].

An isotope-labeling approach has been continued with a specially synthesized nitroxide $R_6'-C\equiv^{13}C-(p-C_6H_4)_2-^{13}C\equiv C-R_6'$ biradical which was investigated using X- and W-band EPR, echo-detected EPR and W-band ENDOR spectroscopy in comparison with two radicals: $R_6'-C\equiv^{13}C-p-C_6H_4$ and $R_6'-C\equiv^{13}CH$ [69]. DFT calculations were performed with ORCA 3.0.3 program package [70]. The biradical and radical geometries were optimized on UKS/B3LYP/cc-pVDZ level and showed a good agreement with previously reported results [44]. Hfc constants were calculated using density functional theory with PBE0 functional and N07D full electron basis set [66]. Fine Lebedev 770 angular grid and 10^{-10} Eh SCF convergence tolerance were used. Solvent effects were simulated with the COSMO model [71].

The hyperfine splitting constants on ^{14}N , 1H , and ^{13}C atoms were experimentally determined and compared with those obtained for previously investigated $R_6'-^{13}C\equiv C-p-C_6H_4-C\equiv^{13}C-R_6'$ biradical [64]. It was concluded that the current quantum chemical approaches do not allow determining precise values of the hfs constants on the β - ^{13}C atoms in the bridge connecting two paramagnetic nitroxide rings in the biradical, though it gave good results in calculating hfs constants on α - ^{13}C atoms.

We can conclude that in the case of quantum chemical calculations of rather short-spacer biradicals such as $R_6'-C\equiv C-R_6'$ or $O=S(OR_6)_2$ [43, 58, 67], the parameters $|D|$, r_{NO-NO} , and A_{zz} correlate well with experimental ones, while the hfs constants A_{xx} , A_{yy} , and a_{iso} differ significantly. On the other hand, the results

presented in [43–45, 64, 68, 69] regarding calculations of the geometry, dipolar coupling, and intramolecular dynamics confirm the fact that the electron spin exchange in all polyacetylene-poly-*para*-phenylene biradicals is realized via the indirect mechanism.

5.4 Intramolecular Dynamics in Biradicals

Evidently, nitroxide biradicals can be absolutely rigid only in solid crystals or in a frozen state at temperatures around or below 77 K. In liquid solutions at low biradical concentrations, when *intermolecular* collisions and interactions become negligible [72], one can distinguish three different types of *intramolecular* motions and transitions [12, 43, 67]: (i) in short-linked flexible biradicals, (ii) in long-chain flexible ones, and (iii) in so-called linear (conjugated) rather chemically rigid structures.

The typical temperature changes in EPR spectra of several biradicals $R_6'-(CH_2)_4-R_6'$ (**BA**); $R_6-(CH_2)_4-R_6$ (**BB**), $S[(CH_2)_4-COOR_6]_2$ (**BC**), and $S(OR_6)_2$ (**BD**) are shown in Fig. 5.9, which presents two essentially different types of spectral changes for biradicals **BA** and **BB** of similar composition, the structure of the bridge and slightly different nitroxide rings. In the case of **BB**, the multilinear spectrum is observed providing the exact measurement of the $|J_1|$ value in one conformation while for **BA** it is only possible to estimate that $|J_1| \gg a$. Temperature behavior of EPR spectra for both biradicals shows that they exist in solution in two conformations with fast transitions between them [12]. For both **BA** and **BB**, $J = 0$ [73].

Theory for correct quantitative description of both biradicals **BA** and **BB** has been given in [12, 41, 42] connected experimental parameters $\ln|J/a|$ or $\ln(\Delta B_2 - \Delta B_3)$, where ΔB_2 is shown in Fig. 5.9C, and ΔB_3 is the line width of the corresponding central line, with temperature, T^{-1} [74–77]. EPR spectra in Fig. 5.9C look very similar to those presented in Fig. 5.9A, but there is a principle difference between them: Since all changes in EPR spectra of **BA** are completely described by two-conformational mode, a quantitative description of **BC** could be done the more complex system of fast and slow transitions among three conformations [11, 74–77]. Correction of the three-conformational model has been confirmed in many papers of different research groups. Bridges linked two nitroxide rings were varied widely, e.g., $-(CH_2)_n-$, $-OOC-(CH_2)_n-COO-$, $-NHCO-(CH_2)_n-CONH-$, $-(OCH_2CH_2)_n-$, $-COO(OCH_2CH_2)_n-OOC-$, $S[(CH_2)_m-COO-]_2$, $-[O-(SiCH_2)_2]_n-O-$. [7, 12, 13, 78]. The most attractive in such long-chain biradicals is that they are nicely modeling structural and dynamic properties of oligomers in liquid solutions including room temperature ionic liquids [79–81].

Figure 5.9D illustrates changes in the EPR spectra of a short and very flexible $S(OR_6)_2$ biradical at different temperatures which were nicely confirmed by theoretical calculations [58]. Such changes are characteristic for fast transitions between two conformers with values of the differences in enthalpies, ΔH , and entropies, ΔS , of these conformations equal to 13.3 ± 1.1 kJ/mol and 37.2 ± 4 J/mol K respectively, calculated by (5.3) and (5.4) [58]:

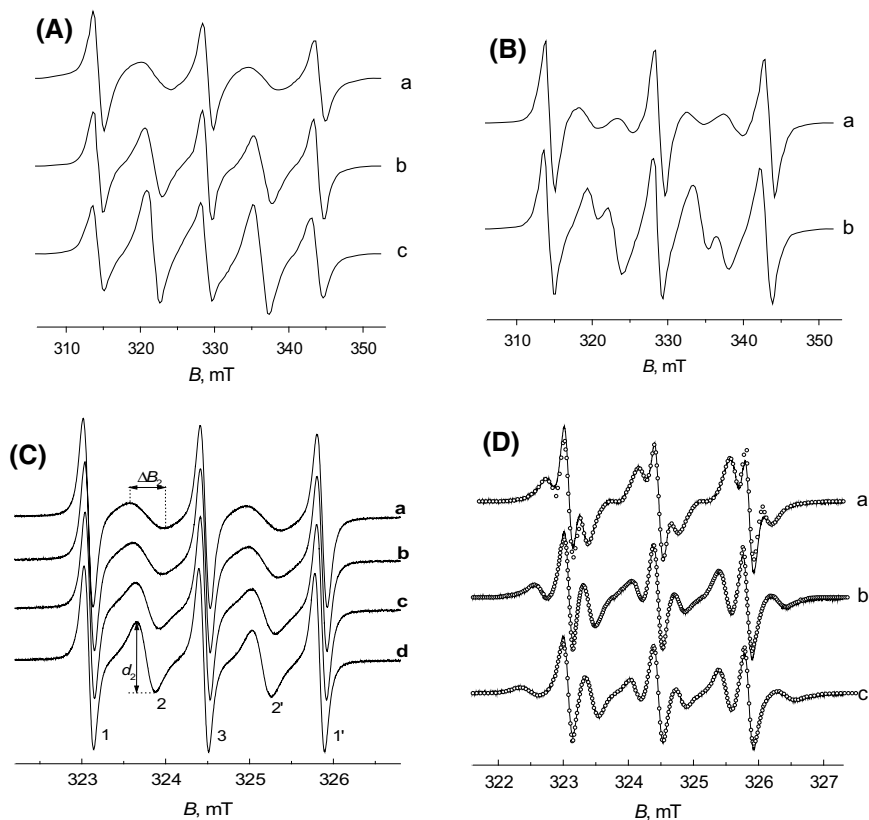


Fig. 5.9 Experimental (lines) and calculated (open circles) EPR spectra of biradicals in toluene solutions: **A** $R_6'-(CH_2)_4-R_6'$ at 250 (a), 291 (b), and 345 K (c); **B** biradical $R_6-(CH_2)_4-R_6$ at 287 (a) and 348 K (b) [73]. **C** biradical $S[(CH_2)_4-COOR_6]_2$ at 295 (a), 304 (b), 324 (c), and 344 K (d) [74]. **D** biradical $S(OR_6)_2$ at 293 (a), 323 (b), and 343 K (c) [58]

$$\ln J^*/a = \Delta S/R - \Delta H/RT, \quad (5.3)$$

$$J^* = (J_1\tau_1 + J_2\tau_2)/(\tau_1 + \tau_2), \quad (5.4)$$

where J^* is the experimentally measured from EPR spectra effective (averaged in time) value of the exchange integral; $|J_1| < |J_2|$; J_1 , J_2 , and τ_1 , τ_2 are exchange integrals and the characteristic lifetimes of these conformations, respectively. In the case of $S(OR_6)_2$, $J_1 = 0$, hence, (5.4) becomes even simpler.

Another type of intramolecular rotational mobility has been observed for biradicals of the polyacetylene line (Fig. 5.3). The slight decrease of $|J/a|$ values with the increase of temperature for these biradicals cannot be explained by the population of distinct conformations with lower $|J|$, but rather a higher accessibility of larger

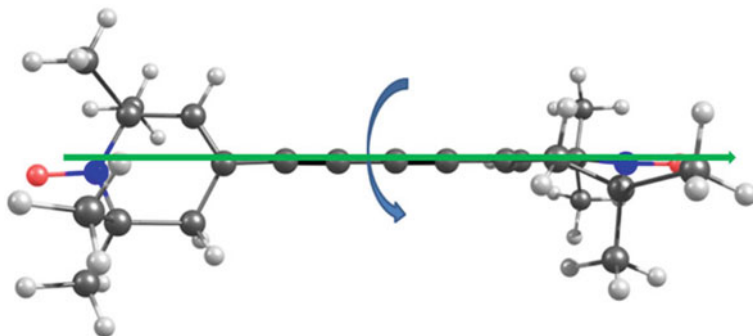


Fig. 5.10 Rotational conformers of biradical $R_6'-C\equiv C-C\equiv C-R_6'$

deviations from equilibrium geometries leading to lowering of the exchange coupling. Such probable rotational movements are shown in Fig. 5.10. Obviously, this type of rotations is also possible for $R_6'-C\equiv C-p-C_6H_4-C\equiv C-R_6'$ and $R_6'-C\equiv C-(p-C_6H_4)_2-C\equiv C-R_6'$ biradicals. In the case of polyacetylene biradicals, the idea that $|J/a|$ changes on temperature are caused by temperature changes of the hfs constant on ^{14}N a is also not correct. Indeed, it was shown in [15] that a values decrease with temperature in the case of all studied piperidine-type radicals and biradicals except $O=R_6$ radical [15], but a increases with temperature for five-membered pyrroline- and pyrrolidine-type nitroxides [15, 82]. Thus, $|J/a|$ value dependences vs temperature are similar to those of a . Values of the enthalpy ΔH and activation energy E_a , as results from the DFT calculations, in the range of 0–8 kJ/mol [44, 47], are responsible for practically free rotation or librations of the nitroxide rings around the bridge axis; i.e., the EPR spectra and measured values of $|J/a|$ do not characterize individual conformations of such linear biradicals but an averaged pattern with very fast transitions between several rotamers, and the measured value of $|J/a|$ is averaged by all these conformations.

It has been reported above that nitroxide biradicals of the $R_6'-(C\equiv C)_n-(p-C_6H_4)_m-(C\equiv C)_n-R_6'$ series, where $n = 0, 1, \dots$ and $m = 1, 2, \dots$ undergo fast internal rotations with low barriers. In the case of $R_6'-p-C_6H_4-R_6'$, two types of barriers of approximately 5 and 10 kJ/mol were revealed as one can see in Fig. 5.11 [45]. One can identify up to 10 possible conformers of $R_6'-p-C_6H_4-R_6'$ biradical schematically shown in Fig. 5.11, by changing the bend direction between the two planes in the nitroxide ring (see Fig. 5.11); the respective barrier was estimated to ~15 kJ/mol in [44].

These conformations can be divided into three groups by their energy: The most low-lying conformers are nos. 6, 8, 9, and 10 in Fig. 5.11. The energy of conformers nos. 2, 4, 5, and 7 with respect to the lowest energy conformers is higher by *ca.* 1.5 kJ/mol and that of conformers nos. 1 and 3 is higher by *ca.* 3.0 kJ/mol [45]. The full potential energy surface (PES) projection on the C5–C4–C1–C3A dihedral angle coordinate (Fig. 5.12B) is equivalent to a rotation about one of the Ph– R_6' bonds. It may include three sets of conformations: No. 1–2–3–4, No. 4–8–2–6, and No.

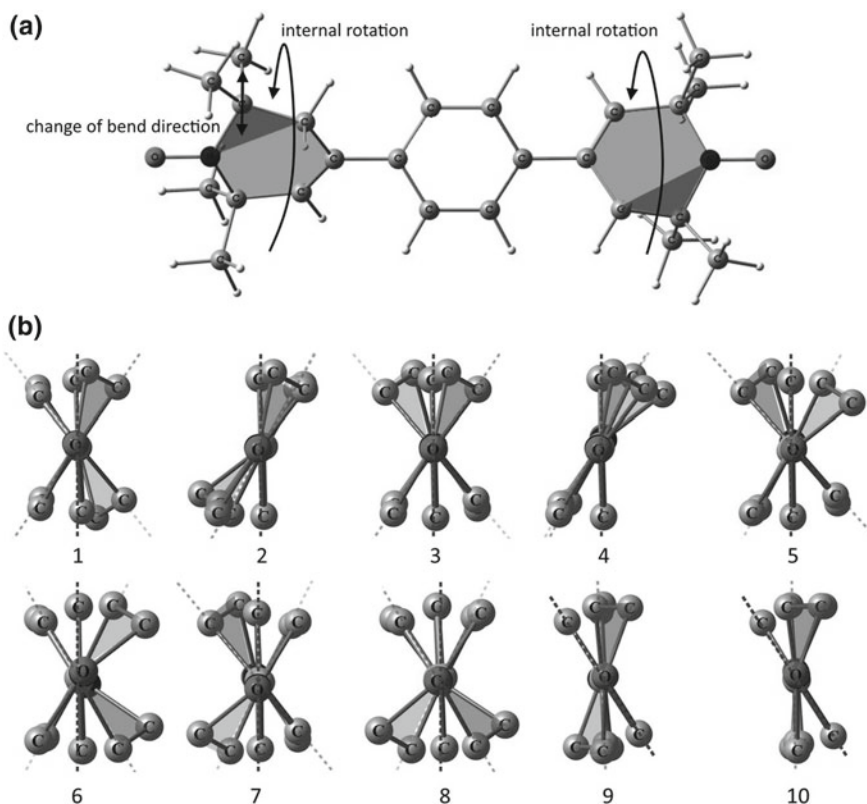


Fig. 5.11 **a** Conformation "1" of biradical $R_6'-p-C_6H_4-R_6'$ with color designation of 1-oxyl-2,2,6,6-tetramethyl-1,2,5,6-tetrahydropyridine ring planes: N1–C2–C3–C4–C5 (by IUPAC nomenclature, colored in light gray) plane and N1–C5–C6 (colored in dark gray) plane. **b** Possible conformers of the biradical [45]

5–10–7–9 (see Fig. 5.11). Transitions between trajectories No. 1–2–3–4 and No. 4–8–2–6 require additional rotation about the second Ph– R_6' bond. Transitions among trajectories No. 1–2–3–4 and No. 5–10–7–9 need changing the ring bend direction of one of the $-R_6'$ groups [45].

All the conformers of the discussed biradical were characterized by identical r_{NO-NO} distances and identical zero-field splitting values D . The $|J|$ value is likely to be varied for these conformations due to significantly different mutual orientations of the two nitroxide moieties. Its value may range from *ca.* zero in conformers 6 and 8 up to 0.00124 cm^{-1} in conformers 9 and 10 (Fig. 5.11).

One can see from Fig. 5.12 that the internal rotation over the angle θ in $R_6'-R_6'$ should be hindered due to steric factors; the calculated barriers are 17.6 kJ/mol for the perpendicular orientation of two nitroxide rings and 19.2 kJ/mol for a $\sim 180^\circ$ rotation from the equilibrium [45]. The energy difference between the equilibrium geometry and the local minimum at $\theta = -54^\circ$ is equal to ~ 9 kJ/mol. Including the acetylene

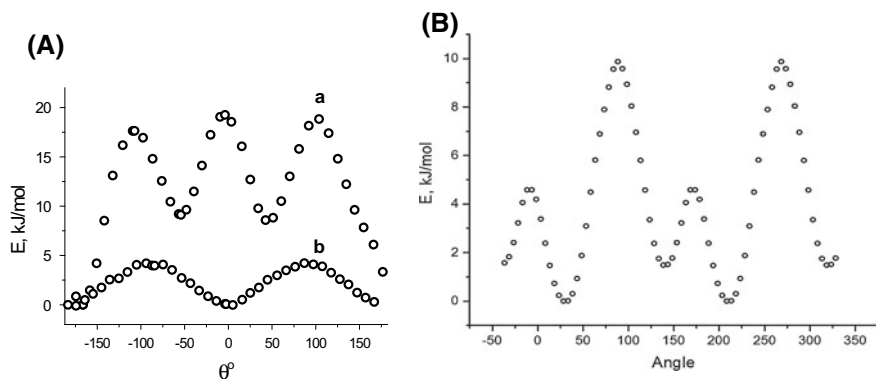


Fig. 5.12 Relaxed PES scan over θ in biradicals **A**: $R_6'-R_6'$ (**a**) and $R_6'-C\equiv C-R_6'$ (**b**) in triplet state, and **B** for biradical $R_6'-p-C_6H_4-R_6'$ over C5–C4–C1–C3A (for atoms numerated in Fig. 5.5b) dihedral angle equivalent to the rotation about one of the Ph– R_6' bonds

spacer into the bridge reduces the rotation barrier in $R_6'-C\equiv C-R_6'$ significantly: The steric factors are almost vanished, and it becomes difficult to locate the transition states (TSs) at $\theta = 0^\circ$. TS at $\sim 90^\circ$ is still existing, but the barrier is equal to only 4.0 kJ/mol. Both minima at $R_6'-C\equiv C-R_6'$ PES are equal within hundredth of kJ/mol [45]. In the case of $R_6'-C\equiv C-C\equiv C-R_6'$, the barrier is less than 1.0 kJ/mol, i.e., becomes negligible [47]. This result reveals an almost free internal rotation in two latter biradicals at room temperature, and the exchange integral value $|J|$ measured by EPR spectroscopy can be averaged by the internal rotation.

Very subtle effects can be understood by combined usage of X-, Q-, and W-band EPR (operating frequencies are 9.74 GHz, 34.18 GHz, and 94.21 GHz, respectively), supplied with the standard commercially available flexline cavities, X-ray diffraction, and DFT calculations [67]. A short nitroxide biradical $O=S(OR_6)_2$ (**BS**) has been studied by EPR spectroscopy in liquid and frozen toluene, ethanol, and ionic liquid solutions. Variations of the intramolecular dynamics and conformational transitions in **BS** as a function of temperature in the wide range of 240–420 K, polarity and the ionic strength were characterized by the changes in the isotropic ^{14}N hyperfine splitting constant a , values of the exchange integral $|J|$, and the empirical parameter γ_3 , the ratio between conformations with slow and fast transitions, and thermodynamic parameters of the conformational rearrangements were calculated [67].

The obtained EPR results were compared with the X-ray structural data and quantum chemical calculations of the geometry and intramolecular transitions of biradical **BS**. Three different groups of conformers with large exchange coupling, with $|J| \ll a$, and with an intermediate value of $|J|$ revealed from DFT calculations were also observed experimentally by EPR measurements at three effective conformations, “1,” “2,” and “E” with $|J_1| \ll a$, $|J_2| \gg a$, and $|J_E| \approx 10.0$ mT correspondingly, in solutions with high polarity or with rather high ionic strength [67]. It was concluded that conformation “E” presents more or less always in both non-polar and polar

solutions. There were discussed possible mechanisms of the polarity and the ionic strength effecting on the biradical **BS** behavior in solutions of different types.

Distances $r_{\text{NO-NO}}$ were close to the data obtained from X-ray analysis, but were ~ 1.2 to 1.3 Å longer than values obtained from EPR measurements in frozen solutions. Inclusion of dispersion correction to DFT calculations resulted in $r_{\text{NO-NO}}$ values slightly shorter than observed in EPR experiment, but the absolute error is reduced to 0.1 – 0.5 Å. Changes in $r_{\text{NO-NO}}$ distances in **BS**, due to media polarity, were also smaller than the experimentally observed values, but changes in mutual orientations of nitroxide rings caused by introducing polar media were more pronounced. These changes in geometry, according to calculations carried out in [67], could lead to the increase of the isotropic spin-exchange coupling. Although energy differences between various conformers were close to typical errors of DFT calculations, data allowed satisfactorily explained the experimental observations. Relative stability of conformers in polar media differed significantly: In non-polar media, the lowest energy conformer was stabilized by two intramolecular hydrogen bonds between $\text{O}=\text{S} < \text{oxygen atom}$ and 4-H protons of the R_6 rings. This conformer had the highest $|J|$ value and the shortest $r_{\text{NO-NO}}$ distance.

In polar media, the most stable conformers have $r_{\text{NO-NO}}$ distance very close to measured experimentally in the ionic liquid at low temperature. These conformers have only one short intramolecular $\text{O} \cdots \text{H}$ bond and thus are stabilized by polar media. The $|J|$ value in these conformers is smaller than in non-polar solvents. Hence, in polar media, a relatively low $|J|$ value should be observed at low temperatures, while at higher temperatures the admixture of that conformer should grow up along with observed $|J|$. Indeed, this behavior of the **BS** biradical in solutions has been observed in [67]. Note that in polar media, this conformer had a larger $|J|$ value than in non-polar media due to slight changes in a mutual orientation of the nitroxide rings.

5.5 Applications of Biradicals

Numerous publications, original papers, books, and reviews, devoted to fundamental and practical applications of nitroxide mono- and polyradicals [10, 12, 83, 84] (and references therein). The main interest to biradicals as spin probes and labels, in the area of structural biology, for controlling processes of radical polymerization, in biomedicine, etc. Such studies started only in one–two years after opening chemical reactions without involving the unpaired electrons in several countries at once. At the first stage, researchers paid attention to the qualitative characterization of changes in the system based on measuring hfs constants and rotational correlation time τ_c . Quantitative studies in EPR of nitroxides started from measuring distances $r_{\text{NO-NO}}$ between unpaired electrons in biradicals and obtained results were extrapolated to spin-labeled proteins, enzymes [85–88], and later to nucleic acids and biomembranes.

As an example, the influence of the ionic strength and pH of the solution on intramolecular spin dynamics has been studied [89, 90] for the biradicals containing the ionizable groups $-\text{COO}^-$ or $-\text{NH}^+(\text{CH}_3)_2$. The changes in the ESR spectra are

discussed within the framework of the model of rapid exchange and it is suggested that biradicals of this kind can be used for the study of pH-dependent conformational changes in membranes and other biological media. This work was developed in [70].

Very important direction of further study was devoted to correct determination of $r_{\text{NO-NO}}$ at long distances using various approaches and advantages of EPR spectroscopy [91–98]. A lot of papers were published concerning binitroxide-mediated radical polymerization: biradical initiation and controlling of polymerization processes [22, 99–102].

At last, nitroxide biradicals containing disulfide group in the bridge were used as specific spin probes in in vivo EPR spectroscopy and imaging application for measuring pH, pO_2 , redox status, and concentrations of phosphate and glutathione in tumor microenvironment and in tumor-bearing mice tissues [103–106].

References

1. E.G. Rozantsev, V.A. Golubev, M.B. Neiman, First kinetically stable individual iminoxyl biradical. *Izv. AN SSSR, Ser. Khim.*, No. 2, 393–394 (1965)
2. E.G. Rozantsev, V.A. Golubev, M.B. Neiman, Y.V. Kokhanov, On new stable iminoxyl biradicals. *Izv. AN SSSR, Ser. Khim.*, No. 2, 572–573 (1965)
3. R. Briere, R.-M. Dupeyre, H. Lemaire, C. Morat, A. Rassat, P. Rey, Nitroxides: XVIIIBiradicaux stables du type nitroxides. *Bull. Soc. chim. France* 3290–3297 (1965)
4. A.L. Buchachenko, V.A. Golubev, A.A. Medzhidov, E.G. Rozantsev, EPR spectra of biradicals with weak exchange coupling. *Theor. Exper. Khimia* **1**, 249–253 (1965)
5. E.G. Rozantsev, M.B. Neiman, Organic radical reactions involving no free valence. *Tetrahedron* **20**(1), 131–137 (1964)
6. E.G. Rozantsev, On free organic radicals with a hydroxy group. *Izv. AN SSSR, Ser. Khim.*, No. 12, 2187–2191 (1964)
7. E.G. Rozantsev, *Free Nitroxyl Radicals* (Plenum Press, New York, 1970)
8. A. Rassat, Application of electron spin resonance to conformational analysis. *Pure Appl. Chem.* **25**, 623–634 (1971)
9. A.L. Buchachenko, A.M. Vasserman, *Stable Radicals* (Khimia, Moscow, 1973)
10. L.J. Berliner (ed.), *Spin Labeling: Theory and Applications* (Academic Press, New York, 1976)
11. V.N. Parmon, A.I. Kokorin, G.M. Zhidomirov, Conformational structure of Nitroxide biradicals. Use of biradicals as spin probes. *Russ. J. Struct. Chem.* **18**, 104–147 (1977)
12. V.N. Parmon, A.I. Kokorin, G.M. Zhidomirov, *Stable Biradicals* (Nauka, Moscow, 1980)
13. L.B. Volodarsky (ed.), *Imidazoline Nitroxide. Synthesis, Properties, Applications*, vol. 1, 2 (CRC Press, Boca Raton, 1988)
14. A. Rassat, Magnetic properties of nitroxide multiradicals. *Pure Appl. Chem.* **62**, 223–227 (1990)
15. A.I. Kokorin, Regularities of the spin exchange coupling through a bridge in nitroxide biradicals. *Appl. Magn. Reson.* **26**(1–2), 253–274 (2004)
16. M. Abe, Diradicals. *Chem. Rev.* **113**, 7011–7088 (2013)
17. M. Baumgarten, High spin organic molecules, in *World Scientific Reference on Spin in Organics*, vol. 4, ed. by J.S. Miller (World Sci. Publ. Co., Singapore, 2017), pp. 1–93
18. P. Michon, A. Rassat, Nitroxides. LXIX. 1,4-Bis(4',4'-dimethyloxazolidine-3'-oxy)cyclohexane structure determination by electron spin resonance and nuclear magnetic resonance. *J. Am. Chem. Soc.* **97**(4), 696–700 (1975)

19. J. Michon, A. Rassat, Nitroxides. LIX. Rotational correlation time determination of nitroxide biradical application to solvation studies. *J. Am. Chem. Soc.* **96**(2), 335–337 (1974)
20. Y. Liao, C. Xie, P.M. Lahti, R.T. Weber, J. Jiang, D.P. Barr, 3,5-Di-tert-butyl-3 ϵ -(N-tert-butyl-N-aminoxy)-4-oxybiphenyl: a heterospin diradical with temperature dependent behavior. *J. Org. Chem.* **64**, 5176–5182 (1999)
21. J. Fujita, M. Tanaka, H. Suemune, N. Koga, K. Matsuda, H. Iwamura, Antiferromagnetic exchange interaction among the three spins placed in an isosceles triangular configuration in 2,4-dimethoxy-1,3,5-benzenetriyltris(N-tert-butyl nitroxide). *J. Am. Chem. Soc.* **118**, 9347–9351 (1996)
22. J. Ruehl, N.L. Hill, E.D. Walter, G. Millhauser, R. Braslau, A proximal bisnitroxide initiator: studies in low-temperature nitroxide-mediated polymerizations. *Macromolecules* **41**, 1972–1982 (2008)
23. T. Iida, J. Ohshita, T. Uemura, H. Fukuoka, N. Ohta, K. Komaguchi, Y. Itagaki, M. Shiotani, S. Yamanaka, A. Kunai, Spin-spin interaction between phenyl nitroxides through the σ - π system. *Silicon Chem.* **1**, 383–389 (2002)
24. S. Hase, D. Shiomi, K. Satob, T. Takui, Phenol-substituted nitronyl nitroxide biradicals with a triplet ($S \sim 1$) ground stat. *J. Mater. Chem.* **11**, 756–760 (2001)
25. Y. Liu, F.A. Villamena, A. Rockenbauer, J.L. Zweier, Trityl-nitroxide biradicals as unique molecular probes for the simultaneous measurement of redox status and oxygenation. *Chem. Commun.* **46**, 628–630 (2010)
26. R. Chiarelli, A. Rassat, P. Rey, Ferromagnetic interactions in a crystalline nitroxide biradical: 1,3,5,7-tetramethyl-2,6-diazaadamantane N,N'-dioxyl. *J. Chem. Soc. Chem. Commun.* 1081–1082 (1992)
27. D.A. Shultz, A.K. Boal, H. Lee, G.T. Farmer, Structure-property relationships in trimethylenemethane-type biradicals. 2. Synthesis and EPR spectral characterization of dinitroxide biradicals. *J. Org. Chem.* **64**, 4386–4396 (1999)
28. S. Hase, D. Shiomi, K. Sato, T. Takui, Magnetic properties of phenol-substituted nitronyl nitroxide biradicals as building blocks of organic salt ferrimagnets. *Polyhedron* **20**, 1403–1409 (2001)
29. A. Caneschi, P. Chiesi, L. David, F. Ferraro, D. Gatteschi, R. Sessoli, Crystal structure and magnetic properties of two nitronyl nitroxide biradicals and of their Copper(II) complexes. *Inorg. Chem.* **32**, 1445–1453 (1993)
30. D. Wang, Y. Ma, A.I. Kokorin, M. Baumgarten, Temperature dependent intramolecular spin coupling interactions of a flexible bridged nitronyl nitroxide biradical in solution. *J. Phys. Chem. A* **122**(3), 574–581 (2018)
31. M. Tanaka, K. Matsuda, T. Itoh, H. Iwamura, Syntheses and magnetic properties of stable organic triradicals with quartet ground states consisting of different nitroxide radicals. *J. Am. Chem. Soc.* **120**, 7168–7173 (1998)
32. W. Zhai, Y. Feng, H. Liu, A. Rockenbauer, D. Mance, S. Li, Y. Song, M. Baldus, Y. Liu, Diastereoisomers of l-proline-linked trityl-nitroxide biradicals: synthesis and effect of chiral configurations on exchange interactions. *Chem. Sci.* **9**(19), 4381–4391 (2018)
33. Y. Liu, F.A. Villamena, Y. Song, J. Sun, A. Rockenbauer, J.L. Zweier, Synthesis of ^{14}N - and ^{15}N -labeled trityl-nitroxide biradicals with strong spin-spin interaction and improved sensitivity to redox status and oxygen. *J. Org. Chem.* **75**(22), 7796–7802 (2010)
34. Y. Liu, F.A. Villamena, A. Rockenbauer, Y. Song, J.L. Zweier, Structural factors controlling the spin-spin exchange coupling: EPR spectroscopic studies of highly asymmetric trityl-nitroxide biradicals. *J. Am. Chem. Soc.* **135**, 2350–2356 (2013)
35. T. Xiaoli, S. Yuguang, L. Huiqiang, Z. Qinwen, A. Rockenbauer, Supramolecular host-guest interaction of trityl-nitroxide biradicals with cyclodextrins: modulation of spin-spin interaction and redox sensitivity. *Org. Biomol. Chem.* **14**, 1694–1701 (2016)
36. G.R. Luckhurst, Alternating linewidths. A novel relaxation process in the electron resonance of biradicals. *Mol. Phys.* **10**, 543–550 (1966)
37. S.H. Glarum, J.H. Marshall, Spin exchange in nitroxide biradicals. *J. Chem. Phys.* **47**, 1374–1379 (1967)

38. H. Lemaire, Nitroxides XX. Résonance paramagnétique électronique d'un biradical nitroxyde; détermination du signe de l'échange. *J. Chim. Phys.* **64**, 559–571 (1967)
39. J.H. Marshall, Spin exchange in the carboxylic acid dimer of nitroxide monoradical. *J. Chem. Phys.* **54**, 2762–2763 (1971)
40. A. Nakajima, H. Ohya-Nishiguchi, Y. Deguchi, Magnetic properties of some iminoxyl polyradicals. III. Exchange interaction in iminoxyl biradicals. *Bull. Chem. Soc. Japan* **45**, 713–716 (1972)
41. V.N. Parmon, A.I. Kokorin, G.M. Zhidomirov, K.I. Zamaraev, Evidence for slow exchange in ESR spectra of nitroxide biradicals. *Mol. Phys.* **26**, 1565–1569 (1973)
42. V.N. Parmon, G.M. Zhidomirov, Calculation of the E.S.R. spectrum shape of the dynamic biradical system. *Mol. Phys.* **27**, 367–375 (1974)
43. O.I. Gromov, E.N. Golubeva, V.N. Khrustalev, T. Kálai, K. Hideg, A.I. Kokorin, EPR, the X-ray structure and DFT calculations of the nitroxide biradical with one acetylene group in the bridge. *Appl. Magn. Reson.* **45**(10), 981–992 (2014)
44. A.I. Kokorin, O.I. Gromov, T. Kálai, K. Hideg, Peculiarities of spin exchange in nitroxide biradicals containing two *para*-phenylene groups in the bridge. EPR investigation and DFT calculations. *Appl. Magn. Reson.* **47**(11), 1283–1293 (2016)
45. A.I. Kokorin, O.I. Gromov, P.V. Dorovatovskii, V.A. Lazarenko, V.N. Khrustalev, K. Hideg, T. Kálai, The structure and internal dynamics of R6-p-C6H4-R6 biradical: EPR, X-ray crystallography and DFT calculations. *Appl. Magn. Reson.* **50**(1–3), 425–439 (2019)
46. A.I. Kokorin, V.N. Parmon, A.A. Shubin, *Atlas of Anisotropic EPR Spectra of Nitroxide Biradicals* (Nauka, Moscow, 1984)
47. A.I. Kokorin, E.N. Golubeva, B. Mladenova, V.A. Tran, T. Kálai, K. Hideg, G. Grampp, Behaviour of nitroxide biradicals with acetylene bridges in organic solvents and ionic liquids. *Appl. Magn. Reson.* **44**(9), 1041–1051 (2013)
48. P.V. Shashev, K.M. Salikhov, Spin polarization and exchange interaction of the multyelectron systems. *Teor. Eksper. Khim.* **9**, 291–299 (1973)
49. G.M. Nedlin, To the theory of the exchange interaction. *Fiz. Tverd. Tela (Leningrad)* **15**, 3048–3052 (1973)
50. S.Ya. Umanskiy, E.N. Golubeva, B.N. Plakhutin, Combined calculation method of weak exchange interactions in biradicals. *Russ. Chem. Bull., Intern. Ed.* **62**(7), 1511–1518 (2013)
51. S.Ya. Umanskiy, Weak exchange interactions in biradicals: a pseudopotential for unpaired electrons and an asymptotic methods for calculating the exchange integral. *Russ. J. Phys. Chem. B* **9**(1), 1–8 (2015)
52. D.A. Shultz, R.M. Fico Jr., H. Lee, J.W. Kampf, K. Kirschbaum, A.A. Pinkerton, P.D. Boyle, Mechanisms of exchange modulation in trimethylenemethane-type biradicals: The roles of conformation and spin density. *J. Am. Chem. Soc.* **125**, 15426–15432 (2003)
53. C. Riplinger, J.P.Y. Kao, G.M. Rosen, V. Kathirvelu, G.R. Eaton, S.S. Eaton, A. Kutateladze, F. Neese, Interaction of radical pairs through-bond and through-space: Scope and limitations of the point-dipole approximation in electron paramagnetic resonance spectroscopy. *J. Am. Chem. Soc.* **131**, 10092–10106 (2009)
54. A.I. Kokorin, V.A. Tran, K. Rasmussen, G. Grampp, Effect of solvent nature on spin exchange in rigid nitroxide biradicals. *Appl. Magn. Reson.* **30**, 35–42 (2006)
55. A. Nakajima, J. Yamauchi, Magnetic interactions in TEMPAD biradical. *Bull. Inst. Chem. Res. Kyoto Univ.* **54**(4), 234–247 (1976)
56. J. Lajzerowicz, Molecular Structures of nitroxides. Ch. 6, in: *Spin Labeling. Theory and Applications*, L.J. Berliner (ed.), (Academic Press, New York, 1976)
57. R.P. Shibaeva, Structure of organic paramagnetics of nitroxide radicals. *Zh. Strukt. Khimii* **16**, 330–348 (1975)
58. A.I. Kokorin, V.N. Khrustalev, E.N. Golubeva, The structure and EPR behavior of short nitroxide biradicals containing sulfur atom in the bridge. *Appl. Magn. Reson.* **45**(4), 397–409 (2014)
59. A.I. Kokorin, V.N. Khrustalev, O.I. Gromov, The structure and EPR behavior of nitroxide biradical containing phosphorus atom in the bridge. *Appl. Magn. Reson.* **46**(12), 1429–1442 (2015)

60. F. Neese, *ORCA—an ab initio, density functional and semiempirical program package. Version 2.8–20* (Max-Planck Institute for Bioinorganic Chemistry, Mülheim an der Ruhr, 2010)
61. V. Barone, I. Cacelli, P. Cimino, A. Ferretti, S. Monti, G. Prampolini, Magnetic interactions in phenyl-bridged nitroxide diradicals: Conformational effects by multireference and broken symmetry DFT approaches. *J. Phys. Chem. A* **113**, 15150–15155 (2009)
62. C. Boilleau, N. Suaud, R. Bastardis, N. Guihéry, J.P. Malrieu, Possible use of DFT approaches for the determination of double exchange interactions. *Theor. Chem. Acc.* **126**(3), 231–241 (2010)
63. M.F. Ottaviani, A. Modelli, O. Zeika, S. Jockusch, A. Moscatelli, N.J. Turro, EPR analysis and DFT computations of a series of polynitroxides. *J. Phys. Chem. A* **116**, 174–184 (2012)
64. A.I. Kokorin, R.B. Zaripov, O.I. Gromov, A.A. Sukhanov, T. Kálai, É. Lamberth, K. Hideg, Spin density distribution in a nitroxide biradical containing ^{13}C -enriched acetylene groups in the bridge: DFT calculations and EPR investigation. *Appl. Magn. Reson.* **47**(9), 1057–1067 (2016)
65. T.H. Dunning Jr., Gaussian basis sets for use in correlated molecular calculations. I. The atoms boron through neon and hydrogen. *J. Chem. Phys.* **90**, 1007–1017 (1989)
66. V. Barone, P. Cimino, E. Stendardo, Development and validation of the B3LYP/N07D computational model for structural parameter and magnetic tensors of large free radicals. *J. Chem. Theor. Comput.* **4**, 751–764 (2008)
67. A.I. Kokorin, B.Y. Mladenova-Kattnig, O.I. Gromov, A.A. Shubin, R.B. Zaripov, G. Grampp, Influence of polarity and ionic strength on intramolecular spin exchange in a short nitroxide biradical containing sulphur atom in the bridge. *Appl. Magn. Reson.* **49**, 1059–1073 (2018)
68. A.V. Bogdanov, A.K. Vorobiev, Orientation order and rotation mobility of nitroxide biradicals determined by quantitative simulation of EPR spectra. *Phys. Chem. Chem. Phys.* **18**(45), 31144–31153 (2016)
69. A.I. Kokorin, R.B. Zaripov, O.I. Gromov, K. Hideg, T. Kálai, Tailored nitroxide radicals and biradical containing ^{13}C enriched acetylene groups: ENDOR and DFT investigation. *Appl. Magn. Reson.* **49**, 137–149 (2018)
70. F. Neese, The ORCA program system. *Wires Comput. Mol. Sci.* **2**, 73–78 (2012)
71. S. Sinnecker, A. Rajendran, A. Klamt, M. Diedenhofen, F. Neese, Calculation of solvent shifts on electronic g -tensors with the conductor-like screening model (COSMO) and its self-consistent generalization to real solvents (Direct COSMO-RS). *J. Phys. Chem. A* **110**, 2235–2245 (2006)
72. Y.N. Molin, K.M. Salikhov, K.I. Zamaraev, *Spin Exchange* (Springer, Berlin, 1980)
73. G. Grampp, S. Landgraf, I.A. Grigor'ev, A.B. Shapiro, A.I. Kokorin, Conformational dynamics of some short-chain biradicals in solutions. *Appl. Magn. Reson.* **19**(2), 187–196 (2000)
74. V.A. Tran, K. Rasmussen, G. Grampp, A.I. Kokorin, The solvent effect on spin exchange in long-chain nitroxide biradicals. *Appl. Magn. Reson.* **32**(3), 395–406 (2007)
75. V.N. Parmon, A.I. Kokorin, G.M. Zhidomirov, K.I. Zamaraev, On the mechanism of spin exchange in long-chain nitroxide biradicals. *Mol. Phys.* **30**, 695–701 (1975)
76. G. Ionita, G.A. Vorobieva, V. Chechik, A.I. Kokorin, Intramolecular spin exchange in flexible PEG-based nitroxide biradicals in aqueous solutions. *Appl. Magn. Reson.* **46**, 251–260 (2015)
77. B. Mladenova-Kattnig, G. Grampp, A.I. Kokorin, Influence of pressure on intramolecular dynamics in a long-chain flexible nitroxide biradical. *Appl. Magn. Reson.* **46**, 1359–1366 (2015)
78. S.V. Kozlov, A.I. Kokorin, A.B. Shapiro, E.G. Rozantsev, Chained nitroxide biradicals—a model for investigating of oligomers in solutions. *Vysokomol. Soed. Ser. B* **23**, 322–327 (1981)
79. V.A. Tran, A.I. Kokorin, G. Grampp, K. Rasmussen, Features of spin exchange in nitroxide biradicals in the ionic liquid bmimPF₆. *Appl. Magn. Reson.* **35**(3), 389–398 (2009)
80. A.I. Kokorin, B. Mladenova, E.N. Golubeva, G. Grampp, Behavior of short nitroxide biradical in room temperature ionic liquids. *Appl. Magn. Reson.* **41**, 353–362 (2011)

81. A.I. Kokorin, Peculiarities of intramolecular motions, in ionic liquids, in *Ionic Liquids. Theory, Properties, New Applications*, ed. by A.I. Kokorin (InTech Publ, Rijeka, 2011), pp. 183–200
82. A. Weber, O. Schiemann, B. Bode, T.F. Prisner, PELDOR at S- and X-band frequencies and the separation of exchange coupling from dipolar coupling. *J. Magn. Reson.* **157**, 277–285 (2002)
83. G.I. Likhtenshtein, *The Method of Spin Labeling in Molecular Biology* (Nauka, Moscow, 1974); *Spin labeling methods in molecular biology* (Wiley, New York, 1976)
84. G.I. Likhtenstein (ed.), *Nitroxides: Applications in Chemistry, Biomedicine, and Materials Science* (Wiley VCH, New York, 2008)
85. A.V. Kulikov, G.I. Likhtenstein, E.G. Rozantsev, V.I. Suskina, A.B. Shapiro, On possible determination of distances between functional groups of protein by the method of spin labels. *Biofizika* **17**(1), 42–48 (1972)
86. A.I. Kokorin, K.I. Zamaraev, G.L. Grigoryan, V.P. Ivanov, E.G. Rozantsev, Measurement of the distances between the paramagnetic centres in solid solutions of nitroxide radicals, biradicals and spin-labeled proteins. *Biofizika* **17**(1), 34–41 (1972)
87. A.V. Kulikov, Evaluation of the distance between spins of the spin label and paramagnetic centre in spin-labeled proteins from the parameters of saturation curve of EPR spectra of labels at 77 K. *Russ. Molek. Biol.* **10**(1), 132–141 (1976)
88. A.I. Kokorin, Forty years of the d_1/d parameter, in *Nitroxides: Theory, Experiment and Applications*, ed. by A.I. Kokorin (InTech Publ, Rijeka, 2012), pp. 113–164
89. P. Ferruti, D. Gill, M.P. Klein, M. Calvin, Correlation between conformation and pairwise spin exchange in flexible biradicals in solution. Control of conformation by pH-dependent ionic forces. *J. Am. Chem. Soc.* **91**, 7765–7766 (1969)
90. P. Ferruti, D. Gill, M.P. Klein, H.H. Wang, G. Entine, M. Calvin, Synthesis of mono-, di-, and polynitroxides. Classification of electron spin resonance spectra of flexible ninitroxides dissolved in liquids and glasses. *J. Am. Chem. Soc.* **92**, 3704–3713 (1970)
91. P.P. Borbat, J.H. Freed, Double quantum ESR and distance measurements, in *Biological Magnetic Resonance*, vol. **19**, *Distance Measurements in Biological Systems by EPR*, ed. by L.J. Berliner, S.S. Eaton, G.R. Eaton (Kluwer Acad./Plenum Pub, New York, 2000)
92. P. Gajula, S. Milikisyants, H.-J. Steinhoff, M. Huber, A short note on orientation selection in the DEER experiments on a native cofactor and a spin label in the reaction center of *Rhodobacter sphaeroides*. *Appl. Magn. Reson.* **31**, 99–104 (2007)
93. A. Savitsky, A.A. Dubinskii, H. Zimmermann, W. Lubitz, K. Moebius, High-field dipolar electron paramagnetic resonance (EPR) spectroscopy of nitroxide biradicals for determining three-dimensional structures of biomacromolecules in disordered solids. *J. Phys. Chem. B* **115**, 11950–11963 (2011)
94. M. Drescher, G. Jeschke (eds.), *EPR Spectroscopy: Applications in Chemistry and Biology* (Springer, Berlin, Heidelberg, 2012)
95. Y.D. Tsvetkov, Nitroxide radicals in pulsing double electron-electron resonance spectroscopy (PELDOR). *Russ. J. Strukt. Khimii* **54**, S46–S75 (2013)
96. G. Jeschke, The contribution of modern EPR to structural biology. *Emerg. Topics Life Sci.* **2**, 9–18 (2018)
97. Y.D. Tsvetkov, M.K. Bowman, Y.A. Grishin, *Pulsed Electron-Electron Double Resonance: Nanoscale Distance Measurement in the Biological, Materials and Chemical Sciences* (Springer, Cham, 2019)
98. S. Pribitzer, L.F. Ibáñez, C. Gmeiner, I. Ritsch, D. Klose, M. Sajid, M. Hülsmann, A. Godt, G. Jeschke, Two-dimensional distance correlation maps from pulsed triple electron resonance (TRIER) on proteins with three paramagnetic centers. *Appl. Magn. Reson.* **49**, 1253–1279 (2018)
99. W. Huang, R. Chiarelli, B. Charleux, A. Rassat, J.-P. Vairon, Unique behavior of nitroxide biradicals in the controlled radical polymerization of styrene. *Macromolecules* **35**, 2305–2317 (2002)
100. K. Pietrasik, O. Swiatkowska, A. Kaim, New difunctional mediators based on 4-amino-TEMPO derivatives for controlling free radical polymerization of styrene. *Polimery* **55**, 812–816 (2010)

101. A. Kaim, J. Szydłowska, K. Pietrasik, The effect of the spacer length on binitroxide mediated radical polymerization of styrene. *Macromol. Res.* **19**, 1041–1047 (2011)
102. J. Nicolas, Y. Guillaneuf, C. Lefay, D. Bertin, D. Gigmes, B. Charleux, Nitroxide-mediated polymerization. *Progr. Polym. Sci.* **38**, 63–235 (2013)
103. V.V. Khramtsov, I.A. Grigor'ev, D.J. Luried, M.A. Foster, J.L. Zweier, P. Kuppusamy, Spin pH and SH probes: enhancing functionality of EPR-based techniques. *Spectroscopy* **18**, 213–225 (2004)
104. G.I. Roshchupkina, A.A. Bobko, A. Bratasz, V.A. Reznikov, P. Kuppusamy, V.V. Khramtsov, In vivo EPR measurement of glutathione in tumor-bearing mice using improved disulfide biradical probe. *Free Rad. Biol. Med.* **45**, 312–320 (2008)
105. V.V. Khramtsov, In vivo molecular EPR-based spectroscopy and imaging of tumor microenvironment and redox using functional paramagnetic probes. *Antiox. Redox Signaling* **28**, 1365–1377 (2018)
106. A.A. Bobko, T.D. Eubank, B. Driesschaert, V.V. Khramtsov, In-vivo EPR assessment of pH, pO₂, redox status and concentrations of phosphate and glutathione in tumor microenvironment. *J. Vis. Exp.* **133**, e56624 (2018)

Chapter 6

Fluorophore–Nitroxide (Profluorescent Nitroxide) Probes



6.1 Introduction

Over the last decades, scientists have faced growing requirements in novel methods of fast and sensitive analysis of antioxidant status of biological systems, redox probing and radical trapping, biological molecules' analysis, investigation of molecular dynamics, and convenient models for studies of photophysical and photochemical processes. This chapter presents a review on the use of tethered nitroxide–fluorophore molecules as probes of redox status, antioxidant activity, oxidative stress, and free radical reaction. In addition, these supermolecules have been proved to serve as tools for the study of molecular dynamics, intermolecular fluorescence quenching and electron transfer mechanism, photoswitching material and analytic reagents. Keeping all properties of spin and fluorescent probes, the dual fluorophore–nitroxide compounds (FNO•) possess important new advantages.

An idea to combine chromophore and nitroxide in one molecule for the study of the probe mobility was designed in 1965 by Jost and Griffith [1]. A supermolecule dansyl 2,2,5,5-Tetramethyl-3-amino-pyrrolidine-1-oxyl) was prepared. Then in liquids, the rotational relaxation time of the probe fluorophore fragment was measured with polarization technique, while an apparent correlation time of the nitroxide segment was estimated by EPR. This approach was developed in works of group of Likhtenstein in which the dual probes were used for the study of molecular dynamics of liquids and albumin in a wide range of temperature [2–10].

In pioneering work of Likhtenshtein with colleagues [3], three fundamental effects were first demonstrated in the dual supermolecules; namely, (1) the nitroxide fragment is a strong quencher of the fluorescence, (2) the radical photoreduction can lead to the decay of the EPR signal and the drastic increase of the fluorescence intensity, and (3) the photoreduction kinetics strongly depends on molecular dynamics of environment. Therefore, any chemical or photo-reduction event of the fragment to a corresponding hydroxylamine derivative, oxidation of the nitroxide fragment, or addition of an active radical yield would result in a decrease of electron spin resonance (ESR) signal that would be accompanied by an increase in fluorescence. These

effects form the basis of application of double probes for the quantitative study of redox reactions, molecular dynamics of objects of interest, and the establishment of factors affected on an electronic transfer.

The next principle step was a series of excellent papers by Blough et al. [11, 12] in which the potential of these tethered, optically switching molecules as potent probes of radical was realized. Blough and Simpson were the first to show that biologically relevant reductants, such as ascorbic acid, could be detected in this way using profluorescent naphthalene–nitroxide [13]. Works of the Likhtenshtein and Blough groups have paved the way for thorough investigations of numerous radical reactions in chemistry, biology, and materials science. Oxidative stress, polymer production and degradation, environment pollution are areas of “reign” of free radicals. Another fruitful avenue of the dual fluorophore–nitroxide compounds application appeared to be the analysis of nitric oxide, superoxide, vitamins, and metal ions. Dual probes also are suitable “training areas” for quantitative study factors, such as local molecular dynamics and micropolarity, on intermolecular fluorescence quenching and electron transfer. In addition, the new magnetic materials in which magnetic properties can be controlled by optical stimuli were developed by using photochromic derivatives as photofunctional units and nitroxide radical as spin sources.

The organic synthetic chemistry allows playing with the chemical structure of the dual molecules of different absorption, fluorescence, and ESR spectra, and of redox and spin properties with variety bridges (spacers) tethered to the chromophore and nitroxide segments. Dual probes are described in the literature as dual fluorophore–nitroxide, fluorescence–nitroxide, profluorescent nitroxide, prefluorescent nitroxide, double (spin and fluorescence) sensors, and fluorophore–nitronyl probes. Fundamentals and progress in the area have been discussed in the length in numerous papers and reviews (see, e.g., [10, 14–17]) and are briefly deal within this chapter.

6.2 Structure and Synthesis of Dual Fluorophore–Nitroxide Compounds

Examples of various chemical structures of fluorescence–nitroxide compounds are shown in Fig. 6.1.

Structures of numerous profluorescent nitroxide compounds were described in papers [18–37]. Several examples of the profluorescent nitroxide synthesis are given below.

A range of varying chromophore nitroxide free radicals and their non-radical methoxyamine analogs were synthesized by the reaction of dansyl chloride with the appropriate amino nitroxide in dichloromethane in the presence of base to give the desired dansyl-linked nitroxides [18]. The methyl ether analogs were obtained using Fenton chemistry by the reaction of the nitroxides with methyl radicals generated from dimethyl sulfoxide and hydrogen peroxide.

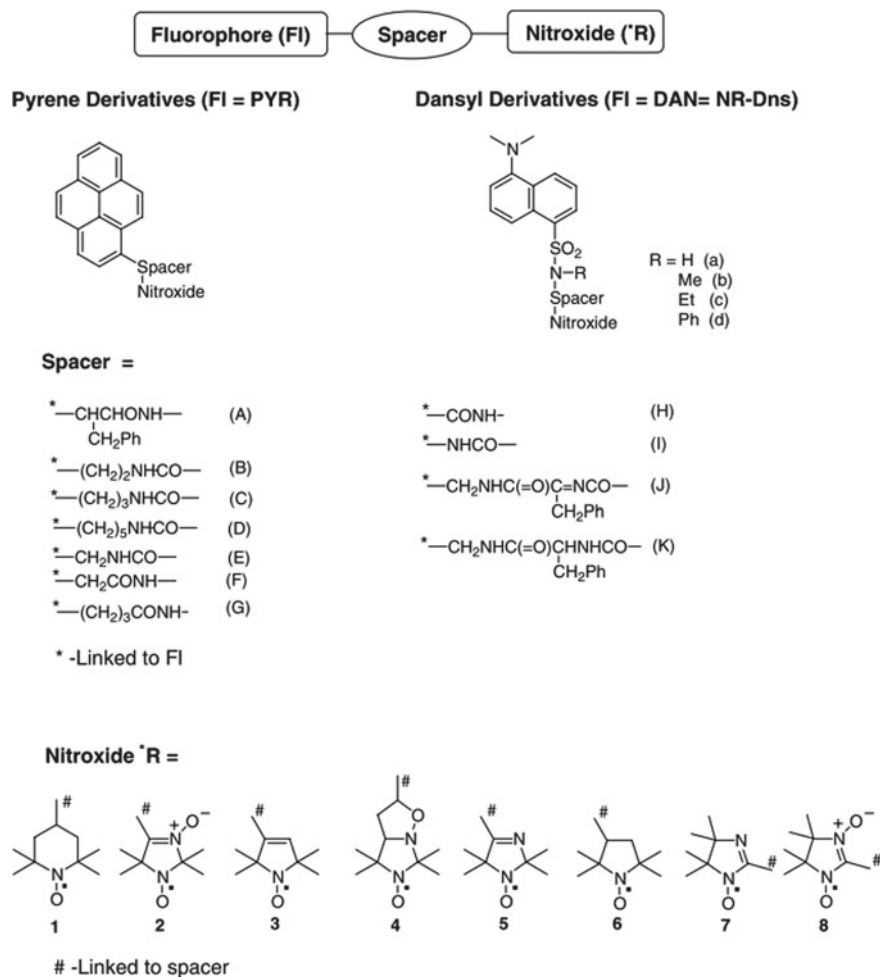
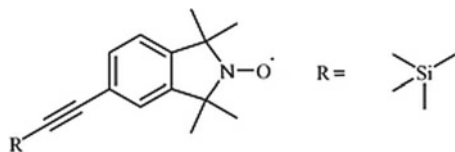
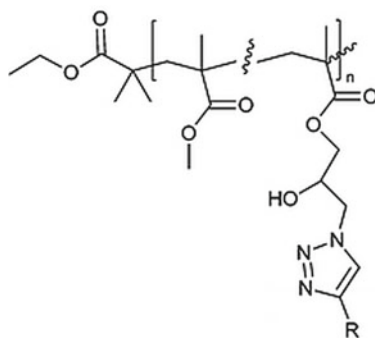


Fig. 6.1 Structure of pyrene and dansyl nitroxides (private communication from Drs. V. V. Martin and A. Weis, Lipitek International, Inc.)

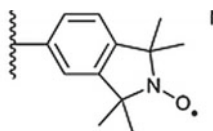
A series of novel frameworks acetylene-substituted isoindoline nitroxide analogs of



were prepared via palladium-catalyzed copper-free Sonogashira coupling [19]. The coupling gave acetylene-substituted isoindoline nitroxides via 5-iodo-1,1,3,3-tetramethylisoindolin-2-yl oxyl, **3**, as an intermediate. Subsequent reaction of the deprotected ethynyl nitroxide with iodinated polyaromatics furnished novel profluorescent aromatic nitroxides with extended conjugation. Ethyne- and butadiyne-linked nitroxide dimers were also synthesized by this cross-coupling methodology. Design and synthesis of profluorescent polymers [20].



with R



included the following stages: (1) the incorporation of an epoxide as a pendant functionality on a polymer backbone synthesized using atom transfer radical polymerization (ATRP), (2) subsequent nucleophilic ring opening with sodium azide gave hydroxyl and azide functionality within a three-bond radius, and (3) the independent attachment of fluorophore and nitroxide groups in close proximity, giving rise to a profluorescent polymer utilizing orthogonal coupling chemistry. Efficient fluorescence switch-on was observed when the materials were exposed to a model reductant or carbon-centered radical.

Dual probe (**1**) having six-membered piperidine nitroxide fragment was synthesized by treatment of the commercial amino nitroxide with dansyl chloride in pyridine (Fig. 6.2) [26]. Probe (**2**) was derived from the following reaction sequences general for nitronyl nitroxides and imino nitroxide preparation: (1) Condensation of bis-hydroxylamine (**5**) with pyrene 1-aldehyde (**6**) gave 1,3-dihydroxyimidazoline (**7**); (2) the intermediate oxidation by air in the presence of Cu catalyst to give a mixture of nitronyl nitroxide (**9**) and imino nitroxide (**2**); (3) formation of deoxygenated compound (**2**) by dehydration of the intermediate (**7**) into 1-hydroxy-2-imidazoline (**8**) and (4) oxidation into imino nitroxide (**2**).

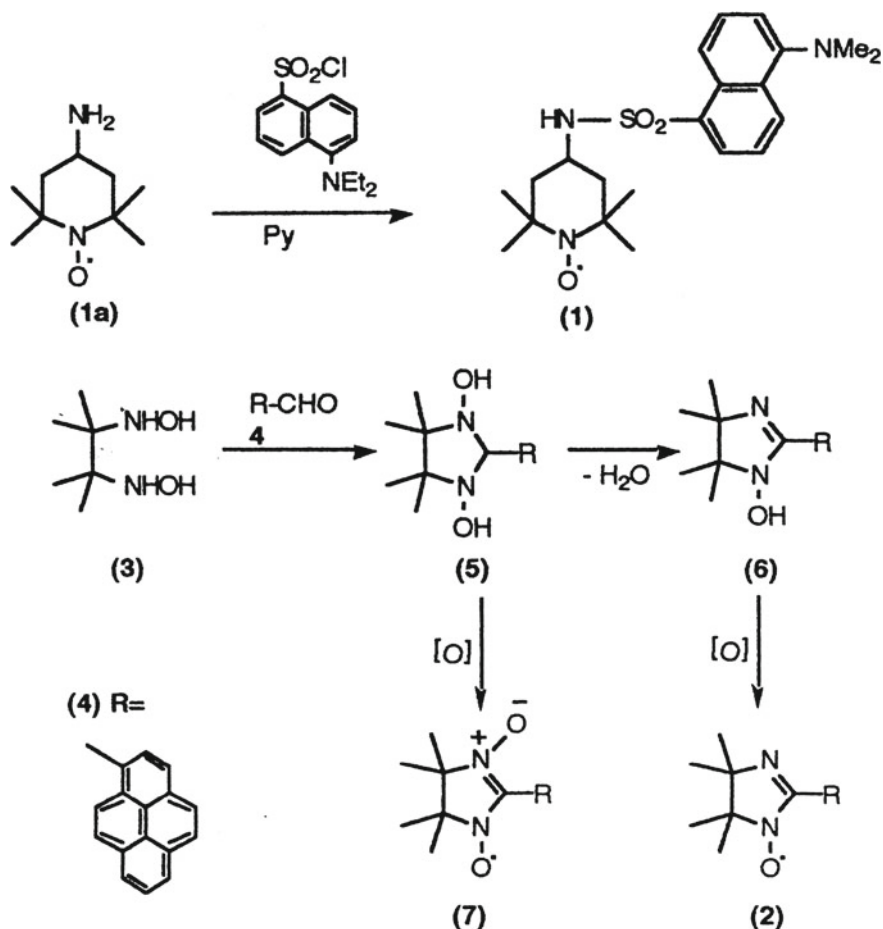
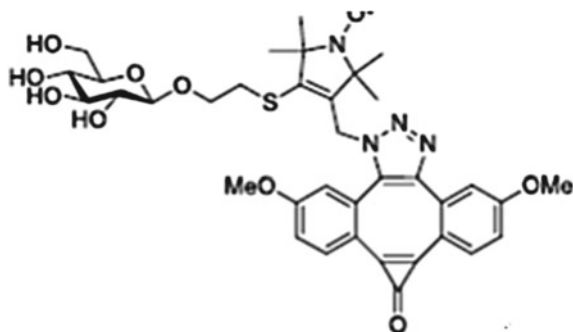


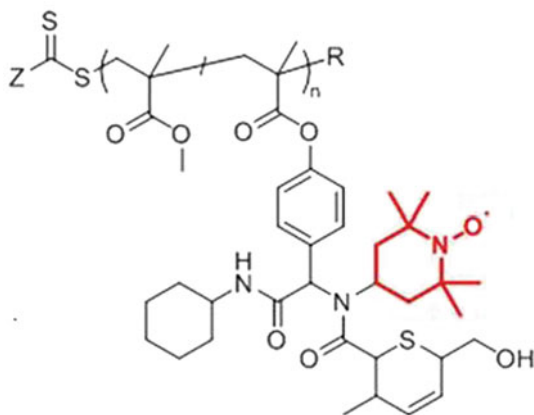
Fig. 6.2 Synthesis of profluorescent nitroxides [26]

Kieber and Blough solved the problem of labile linkages within profluorescent nitroxides by using a two-step process, whereby a simple nitroxide, a water-soluble amino nitroxide (3-(aminomethyl)-2,2,5,5-tetramethyl-1-pyrrolidinyloxy radical, 3-AMP, was prepared. This hybrid compound was firstly utilized to trap carbon-centered radicals [27].

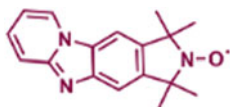
The reaction of dibenzocyclooctyne to its corresponding triazole product with azide **1** in 4:1 dichloromethane/methanol for 32 h gave the novel profluorescent nitroxide probe



Benzaldehyde-containing comonomer, 4-formylphenyl methacrylate, which was subsequently copolymerized with methyl methacrylate (MMA) utilizing the versatile reversible addition–fragmentation chain-transfer (RAFT) polymerization technique was prepared [28]. The benzaldehyde-containing copolymer was combined as with 4-amino TEMPO in the presence of a drying agent (Na_2SO_4) overnight giving a polymer

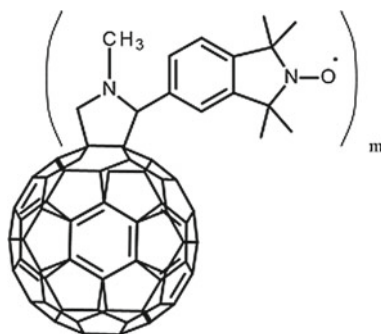


The synthesis of a new class of molecules which are hybrids of long-lived tetramethylisoinolinoxyl (TMIO) radicals and the pyrido[1,2-*a*]benzimidazole (PyrImid) scaffold was reported [29]. Non-covalent binding of nitroxide radicals to an abasic site in DNA and RNA duplexes at temperatures ranging from 0 to -30°C was evaluated. Synthesis of PyrImid-TMIO hybrids



was described in detail.

The synthesis of new profluorescent nitroxides based on 2,5-disubstituted-1,3,4-oxadiazoles as fluorescent moieties and the 2,2,6,6-tetramethylpiperidine-N-oxyl radical (TEMPO) as paramagnetic probes was performed [30]. A linear response to reducing agents, i.e., sodium ascorbate, monitored by fluorescence spectroscopy, suggests the possibility of using the synthesized compounds as potent active probes in the detection of various analytes of interest. To make novel nanomaterial spin probes, three fullerene isoindoline nitroxide N-methyl-3,4-fulleropyrrolidine-2-spiro-50- (10,10, 30, 30 tetramethylisoindolin-20-yloxy), (C60- (TMIO)m, and C70- (TMIO)n) were synthesized by the covalent bonding of 5-formyl-1,1,3,3-tetramethyl isoindolin-2-yloxy to the fullerenes C60.



Emission ability of fullerenes has been well documented. For example, at room temperature, C60 and C70 in organic solvents expose fluorescence spectra. These fullerenes modified with nitroxides can be hydrophobic dual probes for biomembranes [31]. In the work of Braslau group [32], reaction of a catechol with a B-alkyl boronic acid derivative to form a B-alkyl boronate ester in situ was carried out. In the presence of a profluorescent nitroxide, a highly fluorescent N-alkoxyamine was formed (Fig. 6.3). The experiments indicated that the generation of a fluorescent signal would be a positive indicator for the presence of the catechol functionality. The addition of two equivalents of orange-colored TEMPO to an NMR tube containing one equivalent of the preformed B-n-butylcatecholboronate ester resulted in the dissipation of the orange color and formation of the fluorescent scN-nbutoxyamine of TEMPO 5.

A series of fluorescent poly(*N*-isopropylacrylamide)s (poly(NIPAM)s) have been synthesized via reversible addition–fragmentation chain-transfer (RAFT) polymerization from a functionalized chain transfer agent (CTA) bearing either dialkoxy-naphthalene or dialkoxyphenylene moieties [33].

Exchange reactions between the isoindoline profluorescent nitroxide 1,1,3,3-tetramethyldibenzoisoindolin-2-yloxy (TMDBIO) and a fluorescent silence TEMPO capped polystyrene (PS) were used for t-synthesis of polymer:

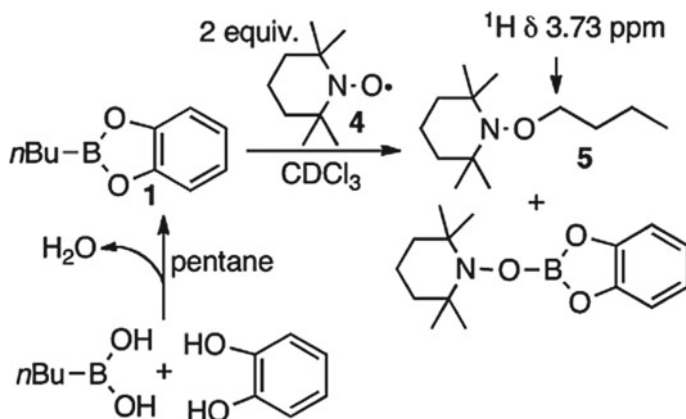
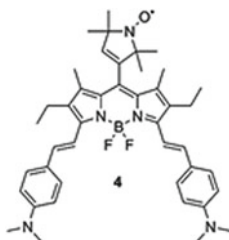


Fig. 6.3 Generation of the N-n-Butoxyamine 5 from TEMPO 4 using preformed B-n-Butylcatecholboronate ester [32]



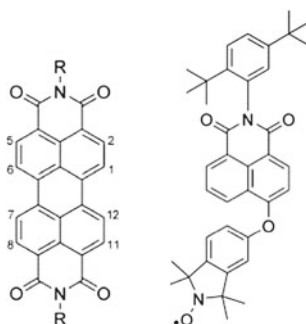
Specifically, the polymer was synthesized via NMP using α,α' -azoisobutyronitrile, as the initiator and 2,2,6,6-tetramethylpiperidine-1-oxyl (TEMPO) as the control agent, and was described as PS–TEMPO. The scope of this study was expanded by exploiting a di-nitroxide 9,10-bis(5-[1,1,3,3-tetramethylisindolin-2-yloxy])anthracene (BTMIOA) as a connector between two polymer chains forming PS–nitroxide–PS systems.

The synthesis of optically distinct BODIPY-based profluorescent probes bearing *meso*- and β -substituted isindoline nitroxides and their corresponding methoxyamine derivatives was performed [34]. The probes strongly suppressed fluorescence ($\lambda_{\text{em}} = 570\text{--}603\text{ nm}$) which was revealed upon reduction or reaction with free radicals. To extend the wavelength of fluorescence emission of the BODIPY toward the NIR region to generate profluorescent nitroxides suitable for use in biological systems, dual compounds with the nitroxide unit incorporated through an alkyne linker at the β position of the BODIPY core, for example,



were synthesized.

Polyaromatic profluorescent mono- and bis-isoxazole nitroxides linked to naphthalimide and perylene diimide structural cores



FORM 6.10

were synthesized by treating bromo-naphthalimide with 5-hydroxy-2-methoxy-1,1,3,3-tetramethylisoxazoline in a base-assisted nucleophilic phenoxide substitution reaction by heating with KOH in DMF to give substituted naphthalimide [35]. Then nitroxide was obtained by oxidation of methoxyamine with *m*CPBA in a Cope-type elimination process. (A novel synthetic avenue for the preparation of profluorescent nitroxides via nitrile imine-mediated tetrazole-ene cycloaddition (NITEC) was introduced [36]. The NITEC involves two steps: (1) under irradiated with UV light, a nitrile imine is formed via a first-order reaction with the release of nitrogen, and (2) the in situ generated nitrile imine subsequently undergoes a rapid cycloaddition with the olefin. Figure 6.4 schematically illustrates the synthesis of profluorescent nitroxides.

A bifunctional stilbene-nitroxide label (BFL1) was synthesized (Fig. 6.5) [37]. The synthesized dual stilbene–nitroxide probe was covalently immobilized onto the surface of a quartz plate as an eventual sensor for ascorbic acid and microviscosity (Fig. 6.6).

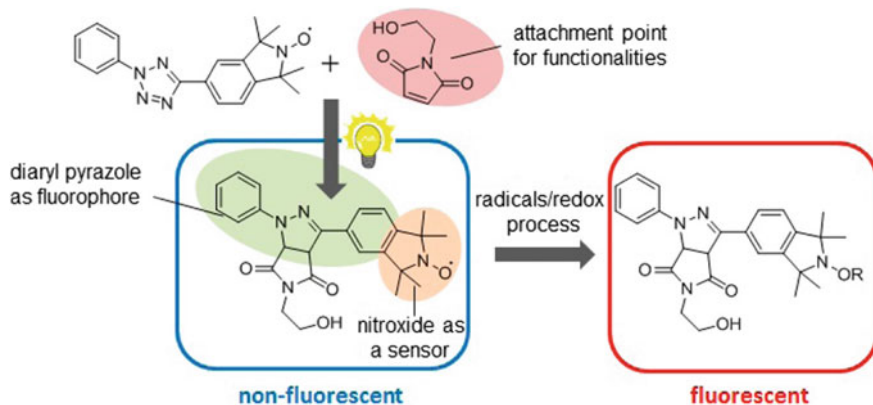
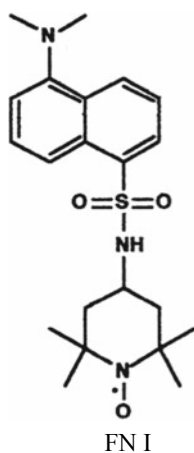


Fig. 6.4 Schematic presentation of the NITEC of diaryl tetrazole and maleimide [36]

6.2.1 Profluorescent Nitroxides as Redox Probes

As was first demonstrated in [3] in a fluorescence–nitroxide supermolecule,



the nitroxide serves as a strong intramolecular quencher of the fluorescence from the chromophore fragment and the fluorescence is restored during the nitroxide photoreduction. Later, it was shown that in such molecules, fluorescence is restored via radical scavenging to the alkoxyamine or redox processes to the hydroxylamine or oxoammonium cation [13]. Therefore, chemical reduction of the nitroxide fragment by antioxidant would result in a decrease of electron spin resonance (ESR) signal and accompanied with a rise of the fluorescence intensity and can be used in antioxidant analysis. A series of the dual FNO molecules including **FN I** and **FN II**

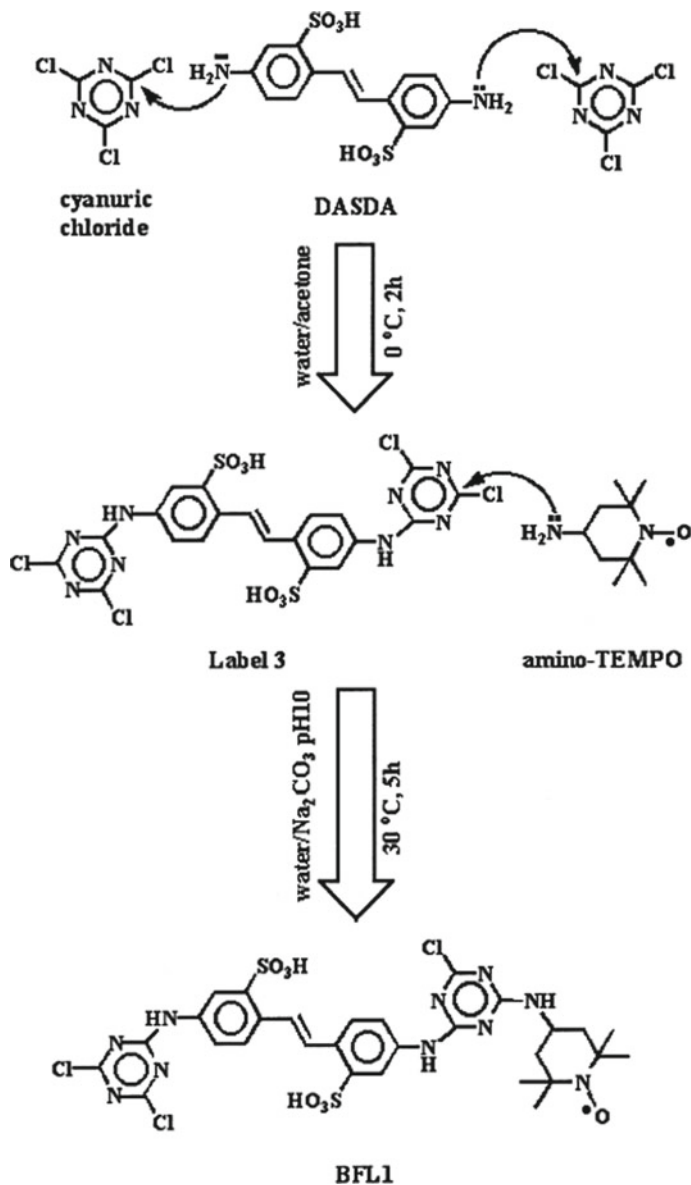
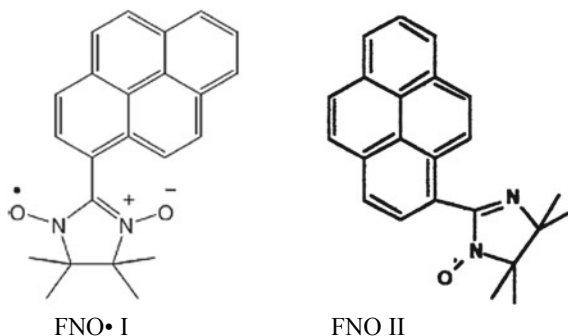


Fig. 6.5 Synthesis of the dual stilben-nitroxide probe BFL1 [37]



have been used first in the analysis of antioxidants of different reducing capacities. On the basis of the abovementioned unique properties of the dual molecules, a method for the quantitative analysis of vitamin C in biological and chemical liquids has been proposed and implemented [26, 38–41]. In the presence of ascorbic acid, an increase in the fluorescent intensity and a decay of the EPR signal of the dual probe DT occurred with the same rate constant (Figs. 6.7 and 6.8). By performing a series of pseudo-first-order reactions between the dual molecule and ascorbic acid and by consequently plotting the rate constants (k_{app}) versus the ascorbic acid concentrations, the calibration curves for the vitamin C analysis were obtained. In the fluorescence and ESR measurements (25 °C, phosphate buffer), the slope of the calibration line corresponded to the second-order constant $k = 7 \text{ M}^{-1} \text{ s}^{-1}$ for FNO I. Nitroxide FNO II displayed a faster kinetics with $k = 51 \text{ M}^{-1} \text{ s}^{-1}$. The observed order of reactivity for the probes is in agreement with oxidation potentials of their nitroxide fragments, expected from the inductive effects of the substituents. The kinetics of this series has been described in a very good approximation by the model of pseudo-first-order process with apparent rate constant k_{app} . The linear dependencies of k_{app} on ascorbic acid concentration obtained either by ESR or fluorescence measurements are shown in Fig. 6.8. The proposed method was applied to the determination of ascorbic acid in mandarin beverage.

Effect of bovine serum albumin (BSA) on the kinetics of ascorbate oxidation was evaluated [39]. The oxidation of ascorbic acid by the fluorophore–nitroxide, probe dansyl piperidine–nitroxide, was monitored by steady-state fluorescence and electron paramagnetic resonance. Experiments showed that the probe reduction by ascorbic acid was accelerated with the increase of the BSA. The influence of BSA on the rate is attributed to the adsorption of both ascorbate and the probe to BSA. Adsorption of ascorbate to BSA was confirmed by NMR relaxation experiments. In the presence of BSA, the autoxidation of ascorbate at different pH values is significantly slowed down. This effect was explained in terms of the electrostatic interaction between the ascorbate anion and the BSA molecule.

The fluorescent probe, R2c, consisted of silicon phthalocyanine and two 2,2,6,6-tetramethyl-1-piperidinyloxy radicals, and is encapsulated by the dimer of bovine serum albumin was used for detecting ascorbic acid [42]. Due to this encapsulation, the **R2c**–BSA complex was prevented from reacting with various redox species in

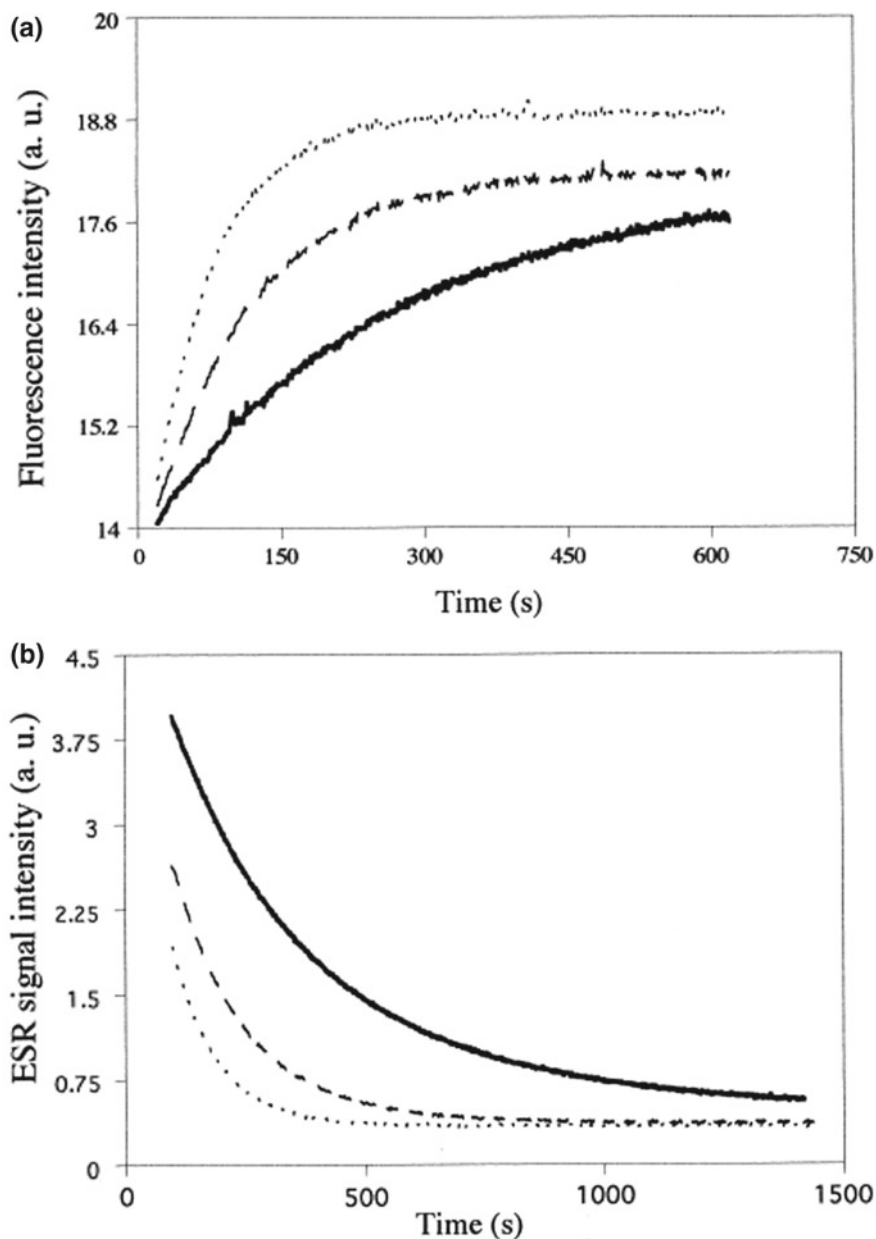


Fig. 6.7 Fluorescence enhancement (a) and ESR decay (b) of the probe (**1**) caused by excess of ascorbic acid. Solid line, 0.1 mM; dashed line, 0.4 mM; dotted line, 0.8 mM. Acquisition parameters of fluorescence: excitation slit 1 nm, emission slit 16 nm, voltage 480 V, T5258C, phosphate buffer [26]

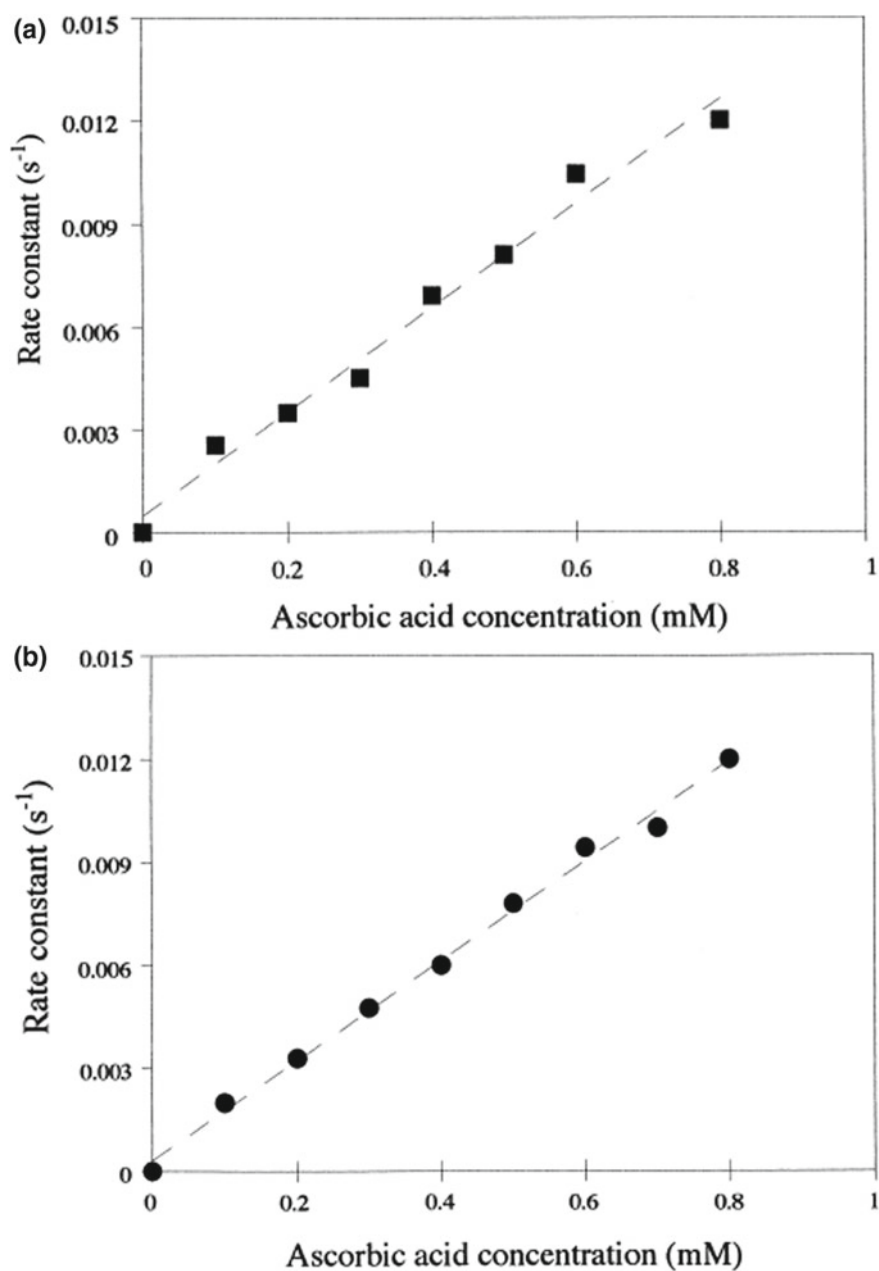


Fig. 6.8 Dependence of rate constant of reduction for the nitroxide FNO **I** on ascorbic acid concentration (25°C, phosphate buffer pH 7), **a** fluorescence, **b** ESR [26]

biological, but reacted selectively with ascorbic acid. The complex fluorescence of after ascorbic acid addition depended on the pH and fluorescence intensity increased in the order $\text{pH } 6 < \text{pH } 5 < \text{pH } 4 < \text{pH } 3$, but decreased at pH 2 compared with that at pH 3 and also decreased with increasing temperature after ascorbic acid addition. These effects were explained in terms of the relationship between the shielding effects of BSA and the folding \leftrightarrow unfolding structural changes by the change in relative proportions of α -helix and β -sheet in BSA.

A nitronyl nitroxide radical was covalently linked to an organic fluorophore, pyrene, and was used to detect superoxide radicals and to quantitatively estimate the antioxidant activity of biological compounds of different antioxidant redox potential [43]. This approach is also based on the phenomenon of intramolecular fluorescence quenching of the pyrene fragment by the nitroxide in the dual fluorophore–nitronyl ($\text{FNO}\cdot$ II). The nitroxide fragment of the dual non-fluorescence molecule can be reduced by a variety of free radicals (e.g., superoxide) and antioxidants (e.g., ascorbic acid, quercetin, galangin). The reduction of FNO is accompanied by a drastic increase in fluorescence intensity (up to 2000) (Fig. 6.9) and a corresponding decrease of the EPR signal. The fluorescence technique, which has been developed, allows the detection of antioxidants at the submicromolar concentration scale, while the EPR and light absorption techniques are limited to several micromolars (Fig. 6.10).

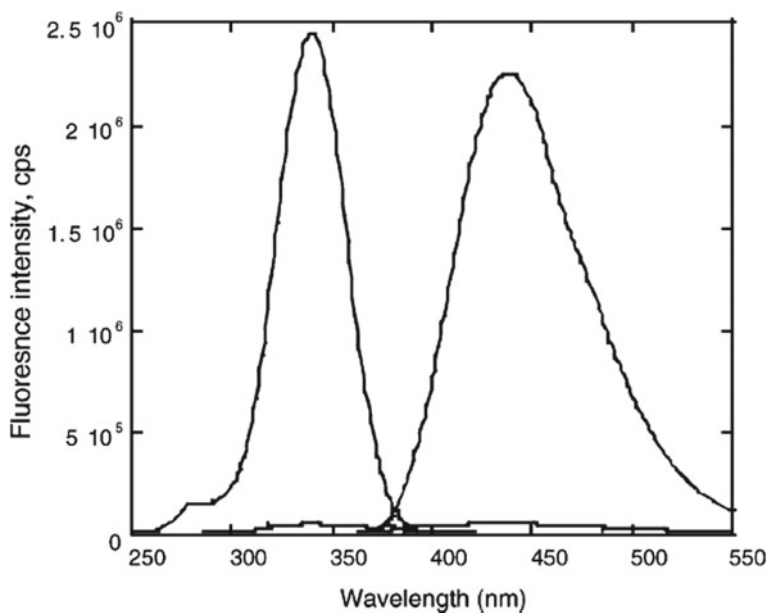
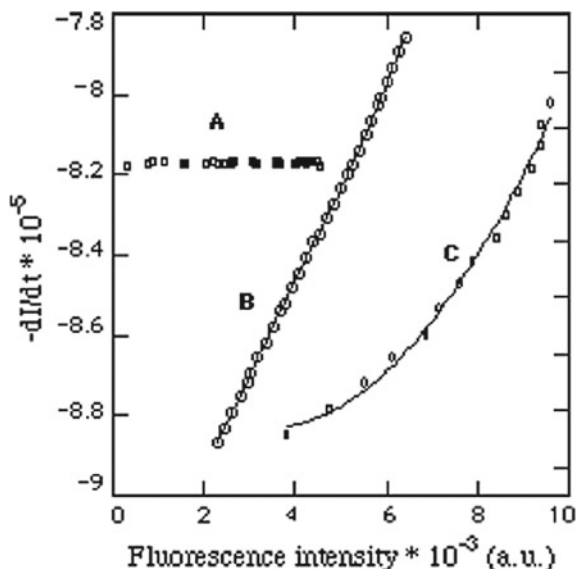


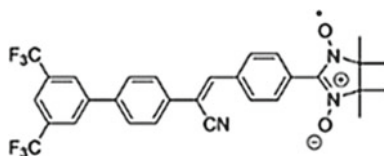
Fig. 6.9 Fluorescence emission and excitation spectra of the $\text{FNO}\cdot$ II (5×10^{-5} M) before and after reduction by quercetin (5×10^{-7} M) in PBS (pH 7.4, $T = 300$ K) [43]

Fig. 6.10 FNO fluorescence increases rate versus fluorescence intensity: **A** zero-order reduction rate of FNO (5×10^{-5} M) by superoxide ($\omega_i = 7 \times 10^{-8}$ M/min); **B** pseudo-first-order reduction rate of FNO (5×10^{-5} M) by ascorbic acid (5×10^{-6} M); and **C** second-order reduction rate of FNO (5×10^{-5} M) by ascorbic acid (5×10^{-5} M). The fluorescence kinetics was measured in the presence of catalase (280 U/ml) in PBS (pH 7.4, $T = 300$ K [43])



A scheme of the chemical reaction upon addition of reducing agent to the dual fluorescence–nitronyl probe was suggested (Fig. 6.11) This method has also been applied to the determination of hydrogen peroxide in submicromolar concentrations.

A novel nitronyl nitroxide derivative of



showed 260-fold fluorescence turn-on and diminished electron spin resonance signal upon ascorbic (AA) addition [44]. The probe could detect AA over a broad concentration range from 1 μ M to 2 mM. It was reported that the fluorescence of a polyamidoamine (PAMAM) dendrimer-entrapped gold nanocluster Au_8 cluster is quenched by the paramagnetic nitroxide radical with a combination of static and dynamic quenching processes [45]. Combined fluorescence and electron paramagnetic resonance studies formed a basis for the development of a turn-on fluorescence probe for sensing in AA in living cells. Fluorescence of negatively charged blue fluorescent carbon dots (CDs) was found to be efficiently quenched by the cationic 4-amino-2,2,6,6-tetramethylpiperidine-*N*-oxide free radical (4-AT) in solution presumably by electron transfer mechanism [46]. CDs tethered with TEMPO exhibits sensitive fluorescence and ESR bimodal response toward ascorbic acid (AA) at the μ M level.

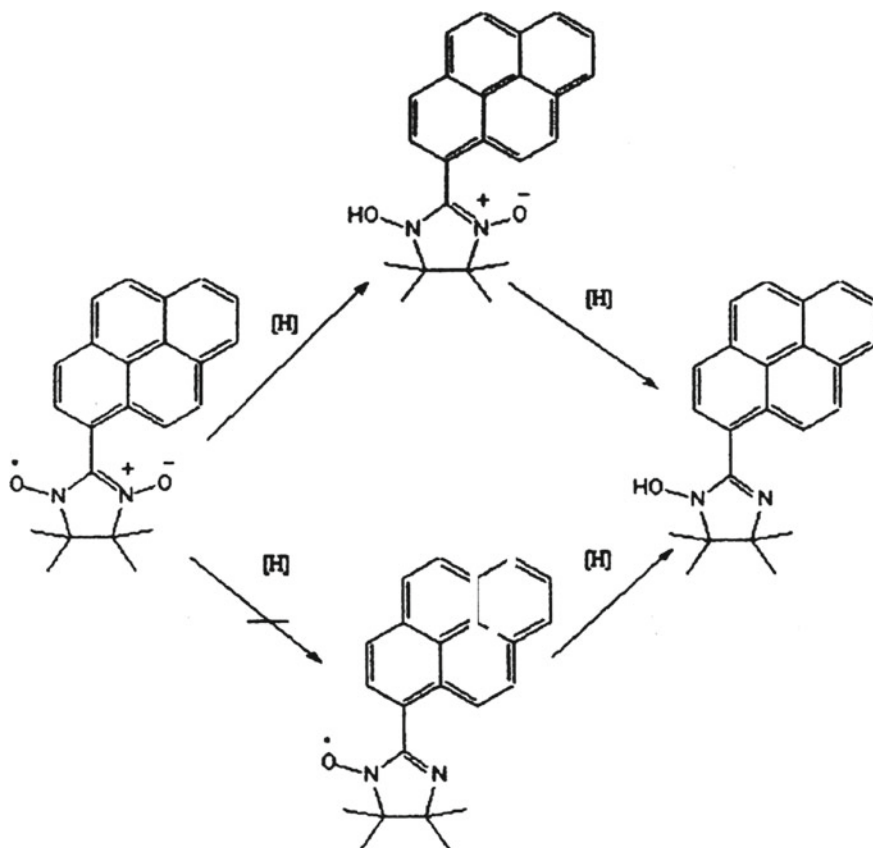
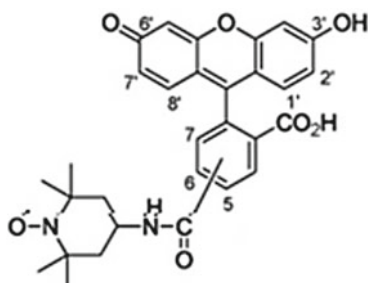


Fig. 6.11 Suggested mechanism the chemical reaction upon addition of reducing agent to the dual fluorescence–nitronyl probe [43]

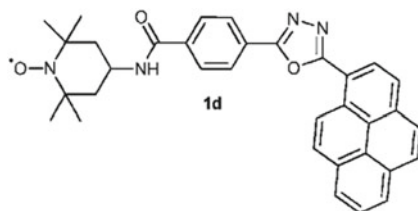
Six fluorescein-nitroxide radical hybrid compounds were synthesized, and their physical and chemical properties were characterized by fluorescence and EPR spectroscopies [25]. Fluorescence intensities (around 520 nm) of compound



after reduction by ascorbic acid of the radical increased from 1.43- to 3.21-folds.

A rhodamine nitroxide probe (R-NOc), combining rhodamine fluorophore with a 2,2,6,6-tetramethylpiperidinyl-1-oxy (TEMPO) receptor unit, was introduced to probe glutathionyl radicals (GSc) with high sensitivity and selectivity [47]. The reaction between GSc and nitroxides had low energy barriers, being radical–radical reactions, and had rate constants near the diffusion limit ($>10^8 \text{ dm}^3 \text{ mol}^{-1} \text{ s}^{-1}$) [48]. In this work, horseradish peroxidase (HRP)-catalyzed and metal-catalyzed oxidation systems were selected as the model of simulating the generation of GSc. It was found that the metal-catalyzed system had the same experimental results with the HRP-catalyzed system, demonstrating the strong oxidant ability of the hydroxyl radical ($\bullet\text{OH}$) to initiate toxic GSc. By using combined high-performance liquid chromatography (HPLC) detection and MS analysis, it was shown that the R-NOc was converted into fluorescent secondary amine derivative (R-NH).

Synthesis of novel profluorescent nitroxides, 2,5-disubstituted-1,3,4-oxadiazole–TEMPO hybrid analogs of



as dual luminescent-paramagnetic active probes for ascorbic acid assay was performed [49]. These nitroxides in solutions ($5 \times 10^{-5} \text{ M}$ in 15% DMSO in HEPES, 0.01 M, pH = 7.51) with increasing amounts of sodium ascorbate (between 0 and 2 equivalents) and measurement of the fluorescence emission at $\lambda_{\text{em}} = 388 \text{ nm}$ ($\lambda_{\text{ex}} = 295 \text{ nm}$) after incubation for 30 min showed a linear response up to the stoichiometric amount of the reducing agent (0.5 equivalents).

A method of the measurement of ascorbic acid and microviscosity of media developed in [37] is based on the use of stilbene-photochrome-fluorescence-spin probes (**BFL1**) immobilized onto the surface of a quartz plate as an eventual sensor (Fig. 6.6). In such a hybrid compound, the nitroxide moiety quenches the fluorescence of the fluorophore (stilbene moiety). The reduction of nitroxide segment by an ascorbic acid causes a rise of fluorescence of the fluorophore. The rate constant of the stilbene fragment photoisomerization in such systems is dependent upon the viscosity of the media. Therefore, this probe was applied for the parallel determination of the antioxidant status and measurement of micro- and macroviscosity of the media. Such an approach made it possible to measure the concentration of ascorbic acid in solution in a range of $(1-9) \times 10^{-4} \text{ M}$ and the viscosity of a medium in the range 1–500 cP (Figs. 6.12 and 6.13).

The hybrid compounds comprised of five nitroxides with Ibuprofen were synthesized [50]. The rate constants in reduction reaction with 200-fold excess of ascorbic acid were determined in order of $1.0-6 \text{ M}^{-1} \text{ s}^{-1}$). Two sterically shielded nitroxides

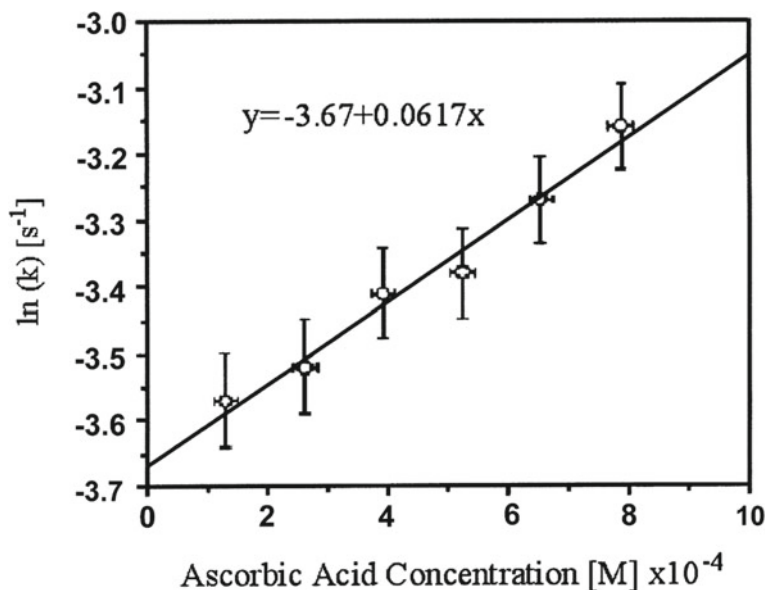


Fig. 6.12 Logarithmic dependence of the nitroxide moiety reduction rate for the immobilized stilbene-photochrome-fluorescence-spin probe (BFL1) molecule versus the ascorbic acid concentration in aqueous solution. $T = 298$ K, PBS pH 7.4 [37]

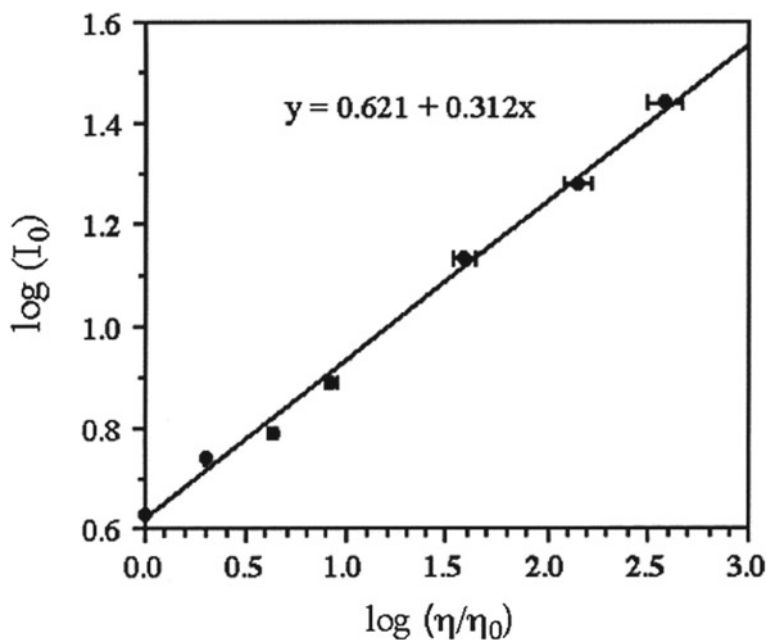
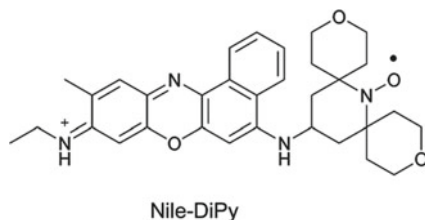


Fig. 6.13 Logarithm of initial intensity of the immobilized stilbene-photochrome-fluorescence-spin probe versus logarithm of viscosity of aqueous–glycerol solutions [37]

reacted with AA markedly slower. In the reaction with the more reactive methyl radicals, produced by 200-fold excess of Fenton's reagent, the reduction rates were in the following increasing order from 2.0 to 5.0 $\text{M}^{-1}\text{s}^{-1}$.

To increase the reactivity and selectivity toward the detection of ascorbic, the dual nitroxide probe 15-((9-(Ethylimino)-10-methyl-9*H*benzo[*a*]phenoxazin-5-yl)amino)-3,11-dioxo-7-azadispiro hexadecan-7-ylxoyl (Nile-DiPy)



was synthesized [51–53]. This fluorophore–nitroxide probe rapidly reacted with ascorbic acid and showed in parallel fluorescence enhancement in PBS at pH 7.4, containing 5% (v/v) DMSO. In the presence of ascorbic acid, the fluorescence intensity of Nile-DiPy increased in a dose-dependent manner concentration of ascorbic acid (0.13–8.0 mM). The second-order rate constant for the reaction of Nile-DiPy and of Nile-TEMPO with ascorbic acid was calculated as 246 $\text{M}^{-1}\text{s}^{-1}$ and 17.4 $\text{M}^{-1}\text{s}^{-1}$, respectively. The kinetic isotope effect (KIE) for the detection of ascorbic acid was determined to be 9.8, indicating that Nile-DiPy reacts with ascorbic acid to produce the fluorescent Nile-DiPy-H via hydrogen atom transfer. The limit of detection (LOD) of this fluorometric method was estimated to be 9.7 nM. The application of Naph-DiPy nitroxide for the measurement only ascorbic acid in the plasma of osteogenic disorder Shionogi rats when fed an ascorbic acid-deficient diet was reported. [51–53]. In this condition, other biological reductants, including uric acid, glutathione, NADH, catechin, 2,2,5,7,8-pentamethyl-6-chroman-ol (HPMC) as a vitamin E model compound, and uric acid, did not react with the nitroxide. The usefulness of Naph-DiPy nitroxide for the measurement of ascorbic acid in the plasma of streptozotocin-induced diabetic animals was confirmed.

A sensitive and selective sensor for ascorbic acid detection based on the recovered fluorescence of NAPS-NO (*N*-propyl-triethoxysilane-4-(4-ylamino-1-oxy-2,2,6,6-tetramethylpiperidine)- naphthalimide) probe was designed [54]. Over a wide range from 80 nM to 50 μM , a good linear relationship between the fluorescence intensity and the concentration of ascorbic acid was found and the detection limit was estimated to be as low as 20 nM. The use of NAPS-NO for the measurement of ASA in human blood serum and determination of the concentration of AA in HEK 293 cell lysate was demonstrated. In addition, confocal laser scanning microscopy experiments showed that this chemosensor is cell permeable and can be used as a fluorescent probe for monitoring ascorbic acid in living cells.

The kinetics of reduction of the dual fluorescence–nitroxide probe R*, 5-dimethylaminonaphthalene-1-sulfonyl-4-amino-2,2,6,6-tetramethyl-1-piperidine-oxyl by human blood and its components were studied using the EPR technique [40].

The results indicated that (1) R^* is adsorbed to the outer surface of the membrane and does not penetrate into the erythrocytes, (2) the observed first-order rate of disappearance of the nitroxide radical k is $k(\text{blood}) > k(\text{eryth}) > k(\text{plasma})$ and $k(\text{blood}) \approx k(\text{eryth}) + k(\text{plasma})$, (3) the erythrocytes catalyze the reduction of R^* by ascorbate, (4) the rate of reduction of the radical is high though it does not penetrate the cells, (5) there is an efficient electron transfer route through the cell membrane, and (6) ascorbate is the only natural reducing agent in blood that reacts with R^* . The study points out that R^* is a suitable spin label for measuring the reduction kinetics and antioxidant capacity in blood and other biological liquids as expressed by reduction by ascorbate.

There are controversial reports in the literature regarding the total antioxidant capacity of neonate blood [41]. In order to investigate directly the antioxidant properties in the newborn's and adults blood, a method of dual fluorescence–nitroxide probes was applied to investigate antioxidant status of on vein blood samples taken from 38 newborn's and 40 healthy adults using the probe R^* and EPR spectroscopy. It was found that the reduction rates of R^* by ascorbate in neonate's whole blood are significantly higher ($P < 0.001$) than the reduction rates of R^* in adult's whole blood. The authors concluded that newborn's blood has significantly higher ability to deal with oxidative stress, caused by R , in comparison with adult blood and the system that responds to the recycling of ascorbate is more efficient in neonate blood than in adult's blood.

Perylenebisimide-linked nitroxide (PBILN) was employed as a profluorescent reagent, which permits for the selective determination of ascorbic acid in a stream [55]. Under optimized conditions, a good linear relationship between the concentration of ascorbic acid, fluorescence peak height in the concentration range from 0.5 to $10 \mu\text{mol L}^{-1}$ was found, and the detection limit ($S/N = 3$) was $0.28 \mu\text{mol L}^{-1}$. The proposed method was applied to the determination of ascorbic acid in several soft drink beverages.

A novel, highly sensitive, and appropriately selective fluorescent probe consisting of silicon phthalocyanine (SiPc) and two 2,2,6,6-tetramethyl-1-piperidinyloxy (TEMPO) radicals, R2c, encapsulated in dimeric bovine serum albumin was employed for imaged ascorbic acid intravenously injected into a mice [56]. Ascorbic acid intravenously injected into mice was efficiently transported to the liver, heart, lung, and cholecyst. The proposed dual probes obeyed to principle requirements: (1) The excitation and fluorescence wavelengths should be $>650 \text{ nm}$ to penetrate deeply into living tissues and to avoid overlap with natural fluorescent species, and (2) nitroxide radicals should be shielded from biological redox-active species before injection of ascorbic acid, but should then efficiently react with ascorbic acid after injection. The changes in fluorescence before and after injection of ascorbic acid were dependent on the organs, as shown in Fig. 6.14. Eight minutes after ascorbic acid injection, the ratios of fluorescence intensity significantly increased at several organs, such as the liver, heart, and lung.

A range of novel, biostable, isoindoline nitroxide-based antioxidants, profluorescent nitroxide ME-TRN, and nitroxide DCTEIO and CTMIO

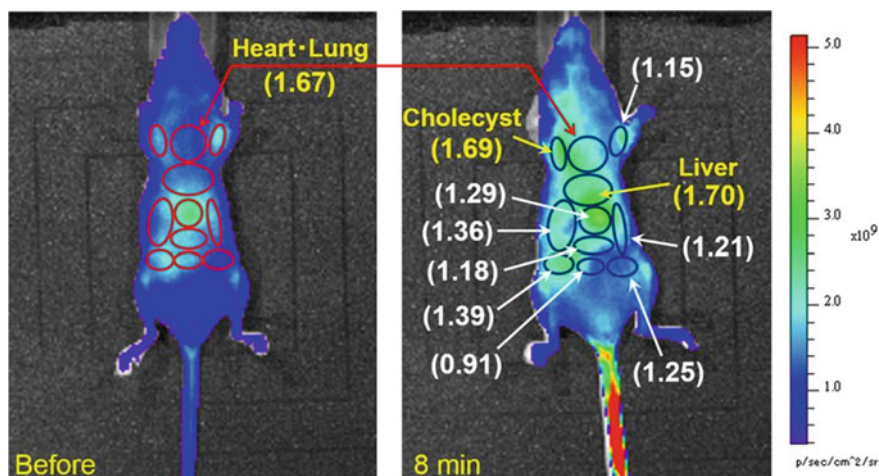
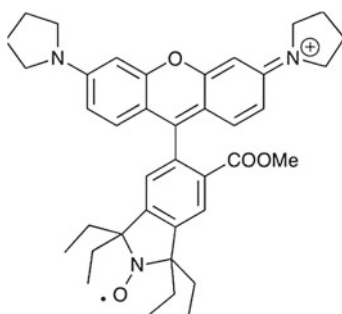


Fig. 6.14 Ratio of fluorescence intensity of imaging. Ratios were calculated using fluorescence intensities before and after ascorbic acid injection (8 min) [56]



has been prepared and used for real-time quantification of oxidative stress and the protective effect of nitroxide antioxidants [57]. The efficiency of these compounds as antioxidant therapies in reducing ROS both in vivo (the rat eye model) and in vitro (661 W photoreceptor cells) was compared with the established antioxidant resveratrol. By assessing changes in fluorescence intensity of profluorescent nitroxide ME-TRN, in the rat retina in vivo, the ability of antioxidant therapy to ameliorate ROS production and reverse of the accumulation of ROS after complete acute ischemia followed by reperfusion (*I/R*) were evaluated. The novel agents' capacity to prevent ROS-mediated metabolic dysfunction in the 661 W photoreceptor cell induced by the oxidant, tert-butyl hydroperoxide, was investigated. As an example, changes in fluorescence of reduced ME-TRN probe in induced by tert-butyl hydroperoxide ischemia/reperfusion injury (*I/R*) treated rat eyes upon antioxidant administration were quantificated in a vivo fundus imaging. The nitroxide compounds DCTEIO and CTMIO successfully reversed the effects of ROS upon ME-TRN probe fluorescence. Thus, the reversible properties of the ME-TRN probe, which can detect and

quantify dynamic alterations in the cellular redox status in vivo and in real time, in response to sequential pro- and antioxidant stimuli were demonstrated.

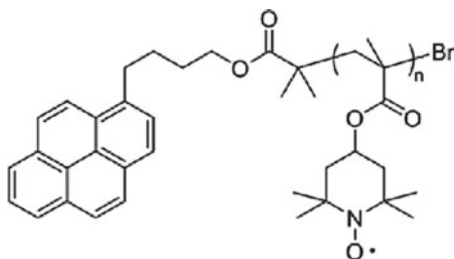
6.3 Fluorescence Detection of Free Radicals

Pioneering experiments of Blough group opened the way to the fluorescence detection of radical scavenging reactions in which the paramagnetic nitroxide-substituted naphthalene, 4-(1-naphthoxy)-2,2,6,6-tetramethylpiperidine-1-oxyl (I), is converted to a diamagnetic N-alkoxy derivative [58]. The latter showed the fluorescence quantum yield in acetonitrile and hexane 55 and 30-fold is higher, respectively, than those of paramagnetic analog. In the experiments, 2-Cyanopropyl free radicals were generated by the thermal decomposition of azobisisobutyronitrile (AIBN) in cyclohexane or in acetonitrile containing I and the fluorescence intensity of the sample increased proportionally to the decrease in its ESR signal intensity.

The profluorescent nitroxide, 1,1,3,3-tetramethyldibenzo[*e,g*]isoindolin-2-yloxy (TMDBIO), was investigated as a probe for the formation of polymer alkyl radicals during the thermo-oxidative degradation of unstabilised polypropylene [59]. A very low fluorescence quantum yield of the dual probe was drastically enhanced after reaction with alkyl radicals during the polymer oxidation. Importantly, the trapping of polymer alkyl radicals during the “induction period” at 120 C was observed, when it is not possible to detect changes in the polymer using either chemiluminescence or infrared spectroscopy.

A sensitive method for the detection of glutathionyl radical (GS[•]) based on their specific interaction with Ac-TEMPO, a non-fluorescent conjugate of fluorogenic acridine with paramagnetic nitroxide TEMPO was developed [60]. The method was employed for detection radicals generated through phenoxyl radical recycling by peroxidase. During reaction of Ac-TEMPO with GS[•], TEMPO EPR signals decayed and acridine fluorescence concurrently increased. Using combined HPLC and mass spectrometry, it was determined that 90% of the Ac-TEMPO was converted into fluorescent acridine (Ac)-piperidine.

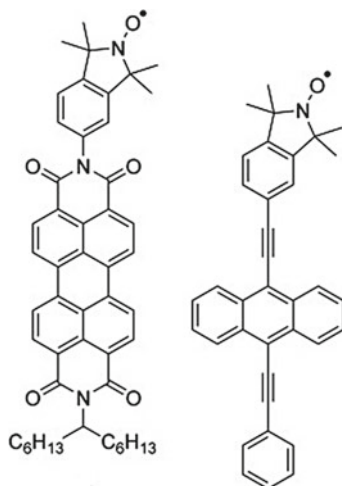
The preparation of nitroxide-containing polymer coupled to a fluorophore



was reported, and its reduction with pentafluorophenylhydrazine was examined [17]. The fluorescence switch-on kinetics and radical concentrations were monitored by

fluorescence and ESR spectroscopy. The polymeric compound displayed significant delays in reduction and fluorescence switch-on and higher turn-on ratios than their single-nitroxide counterparts.

A range of profluorescent nitroxides analogs of



were tested as probes to monitor photo-induced radical-mediated damage in film polymer materials [21]. The most stable and sensitive probe of the perylenediimide (PFNs) tested was an alkyne-linked PFN, with naphthalimide and 9,10-bis(phenylethynyl)anthranene-based versions giving lower stability and sensitivity.. It was also determined that the nitroxide-containing compounds have higher stability in the photo-oxidative environment over their non-radical analogs and the alkyne-linked perylenediimide PFN has a switch on ability when exposed to photo-induced radicals. It is important that the dual probes provided information about the early stages of the film's degree of degradation, justifying the value of the PFN technique as a tool to give deeper insight into the oxidation induction period than that IR and EPR spectroscopies.

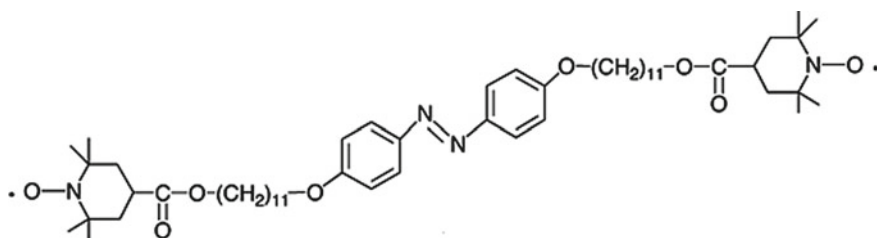
6.4 Photophysical and Photochemical Properties of Fluorescence–Nitroxide

6.4.1 Dual Compounds for Photoswitching Magnetic Materials

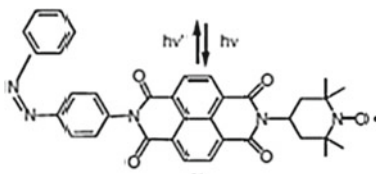
Considerable studies have recently been made by using photochromic derivatives as photofunctional units and nitroxide radical I as spin source. On this base, the new magnetic materials in which magnetic properties can be controlled by optical stimuli

were developed [61–72]. The introduction of one or more radical spins to a photochromic fluorophore would give a photofunctional magnetic material [61]. A series of anthracene derivatives with nitroxide radicals were prepared as a photochrome-nitroxide system and as a spin coupler unit [61] and references cited. A photochromic reaction based on photodimerization of anthracene chromophore and heat-mediated dissociation of the photo-dimer was investigated in details. For example, an azobenzene derivative carrying two nitronyl nitroxide (NN) radicals was prepared, and in a frozen toluene at 10 K, its ESR spectra at cryogenic temperature were found to differ before and after irradiation.

Several *trans*-azobenzene derivatives carrying a nitroxide (aminoxyl) radical analogs



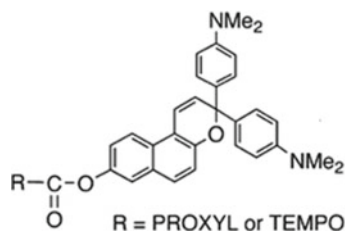
were synthesized, and their photoisomerization reactions to the corresponding *cis*-isomers were investigated [65]. These compounds, isolated as relatively stable solid substances, were isomerized by irradiation in solution to the corresponding *cis*-isomers. For example, an antiferromagnetic interaction model in the *trans*-isomer carrying TEMPO substituent with a large antiferromagnetic exchange interaction of $J = 47.6$ K was observed, while a weak ferromagnetic one of Curie–Weiss (CW) model with Weiss temperature $\theta = +0.11$ K was found in the corresponding *cis*-isomer.



The unsubstituted derivatives at the *para* position were found to show photoisomerizations by irradiation to give the corresponding *cis*-isomers. The change of intermolecular magnetic interactions was observed by the structural change for each photochromic couple. A naphthalenediimide derivative carrying TEMPO radical and azobenzene substituent was found to show photo-responsive magnetic as well as FET properties upon illumination applying magnetic field [66]. Specifically, azobenzene derivatives had shown reversible photochromism in solution as well as in thin film. The change of FET behavior has been revealed by the photoisomerization together with the change of magnetic properties. The magnetic properties of both photoisomers were found to show antiferromagnetic interactions of CW behavior. Namely,

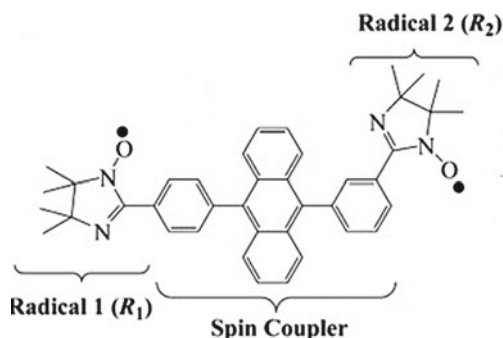
the magnitude of Weiss temperature of the compounds turns out from 1.13 K to 2.41, indicating the existence of weaker spin–spin interactions in the former isomer.

Several spiropyrans with TEMPO-substituents and naphthopyrans with TEMPO- or PROXYL-substituents



were prepared, and they showed photochromic behaviors in solution giving the respective stable open-formed merocyanines [67]. For example, naphthopyran derivatives with nitroxide substituents gave by irradiation the corresponding open-formed isomers. The product treatment with SiO_2 as a catalyst changed its back to the starting closed-formed naphthopyrans. The low-temperature region of spiropyran derivatives was found to be ferromagnetic with CW behavior ($h = 0.38$ K), whereas the interaction in the corresponding merocyanine was antiferromagnetic with CW behavior (0.82 K).

A couple of naphthalenediimide derivatives carrying a nitroxide radical and an azobenzene group were prepared, and photochromic property of compound with p-dimethylamino-substituent in solution were observed [68]. Syntheses, electronic structures in the ground state, unique photoexcited states, and spin alignment were reported for biradical **1** [69].



In the biradical electronic ground state, two radical moieties connected by an aromatic bridge in the diamagnetic state interact very weakly. On photo-irradiation, a novel lowest photoexcited state with the intermediate spin ($S = 1$), arising from four unpaired electrons with low-lying quintet ($S = 2$) photoexcited state, was detected using time-resolved ESR (TRESR). The triplet state has a unique electronic structure, the D value of which is reduced by antiferromagnetic spin alignment between

two radical spins through the excited triplet spin coupler. The general theoretical predictions of the spin alignment and the reduction of the fine-structure splitting of the triplet bis(radical) systems were also formulated.

The synthesis of two nitroxide-based diradicals connected to a 2,3,4,5-tetraphenylsilole (TPS) unit, especially designed to present high-spin photo-excited states, was reported [70]. In ground state, the diradical displays weak intramolecular antiferromagnetic interactions ($J/kB \approx -1$ K). In photo-excited high-spin states, the nature of the magnetic exchange coupling between two dangling radical spins through the spin coupler changes from antiferromagnetic to ferromagnetic after photoexcitation. Photo-physical properties of 4-(phenylazo)-benzoyl-2,2,6,6-tetramethylpiperidine-1-oxyl radical (AzO-TEMPO) and of the 4-(2-thienylazo)-benzoyl-2,2,6,6-tetramethylpiperidine-1-oxyl radical (ThiO-TEMPO) before and after their grafting to two polyethylene matrices (a copolymer ethylene/ α -olefin (co-EO) and a high-density polyethylene (HDPE) were characterized by UV–Vis, FT-IR, and EPR spectroscopy [72]. The structural (FT-IR analysis), the thermal (thermal gravimetric analysis and EPR), and the photo-physical (UV–vis) properties of the RO-TEMPO derivatives before and after their grafting were evaluated.

Two approaches to surface modification based on the use TEMPO and its derivatives are discussed [73]. The first relies on the immobilization of TEMPO moieties on the surface of various materials including silicon wafers, silica particles, organic polymers as well as diverse nanomaterials. The second approach utilizes TEMPO and its derivatives for the grafting of polymer chains and polymer brushes' formation on flat and nanostructure surfaces via nitroxide-mediated radical polymerization (NMRP).

6.4.2 Photophysical Effects in Paramagnetic Complexes Bearing Nitroxides

Dual fluorophore–nitroxide compounds have been proved to be convenient “training area” for investigation of mechanism of photophysical and photochemical processes and factor affected on these processes that are guided with the electron exchange interactions with paramagnetic species [16, 73]. Quenching mechanism of the excited chromophore by a nitroxide originates from changes in the spin multiplicity of the electronic states and is guided with the electron exchange interactions with paramagnetic species.

In a chromophore–nitroxide supermolecules (Fig. 6.15), because of the unpaired electron spin of the doublet nitroxide radical (NR), the singlet ground (S_0) state and the lowest excited singlet (S_1) state of the chromophore become the doublet (D_0 and D_n , respectively) (Fig. 6.16) [16]. On the other hand, for a dual compound consisting a chromophore in the excited triplet state (T_1) and nitroxide, the lowest excited doublet (D_1) and quartet (QA_1) states are generated by an interaction between the NR and the T_1 chromophore. In such a case, the spin-forbidden transitions of

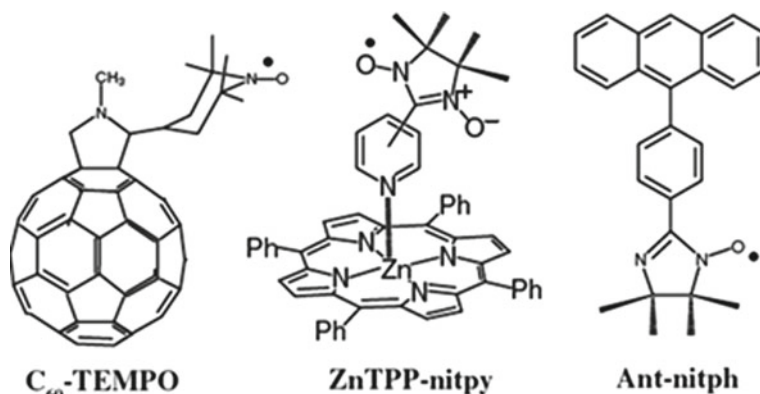


Fig. 6.15 Typical examples of the formation of excited multiplet states [16]

the chromophore, i.e., $S_1 \rightarrow T_1$ and $T_1 \rightarrow S_0$, partially transform into the $D_n \rightarrow D_1$ and $D_1 \rightarrow D_0$ transitions, respectively. These doublet states (D_n , D_1 , and D_0) have the same spin multiplicity, and the lifetimes of the excited state can be very short as comparable to those of the $S_1 \rightarrow S_0$ transition. Thus, fluorescence quenching was interpreted by the intersystem crossing (ISC) enhancement resulting from transitions between states having the same spin multiplicity.

The photophysical properties of silicon phthalocyanine (SiPc) covalently linked to one or two NR have been studied in detail by fluorescence, transient absorption, and TRESR spectroscopies [16, 73]. The electronic states of R0, R1, and R2 are depicted in Fig. 6.16. Experiments indicated that (1) quantum yield (Φ_F) decreases in the order R0 (0.57) > R1c (0.21) > R1a (0.16) > R2c (0.012) > R2a (0.0036); (2) the quantum yield of 3SiPc* (FTSiPc) increases in the order R0 (0.34) < R1a (0.54) < R1c (0.59) < R2c (0.67); (3) the fluorescence decays of R1c and R2c (R1c = 42 ps and 4.7 ns, R2c < 30 ps and 4.7 ns) are faster than that (6.8 ns) of R0; and (4) the S_1 and T_1 energies of R0 were found to be 1.47×10^4 and $8.90 \times 10^3 \text{ cm}^{-1}$, respectively; and (5) rate constants of the $D_1 \rightarrow D_0$ transitions are 3.5×10^6 , 2.1×10^6 , 3.9×10^5 and $2.0 \times 10^5 \text{ s}^{-1}$ for R1a, R1b, R1c and R1d, respectively.

As shown in Fig. 6.17, in the case of the $D_n \rightarrow D_1$ and $D_1 \rightarrow D_0$ transitions, the electron exchange process is dominant. These transitions occur along with the electron exchange process between the SiPc and NR moieties, and the decay rate of the $D_1 \rightarrow D_0$ transition is well correlated with the magnitude of the electron exchange interaction between the T_1 chromophore and the doublet NR.

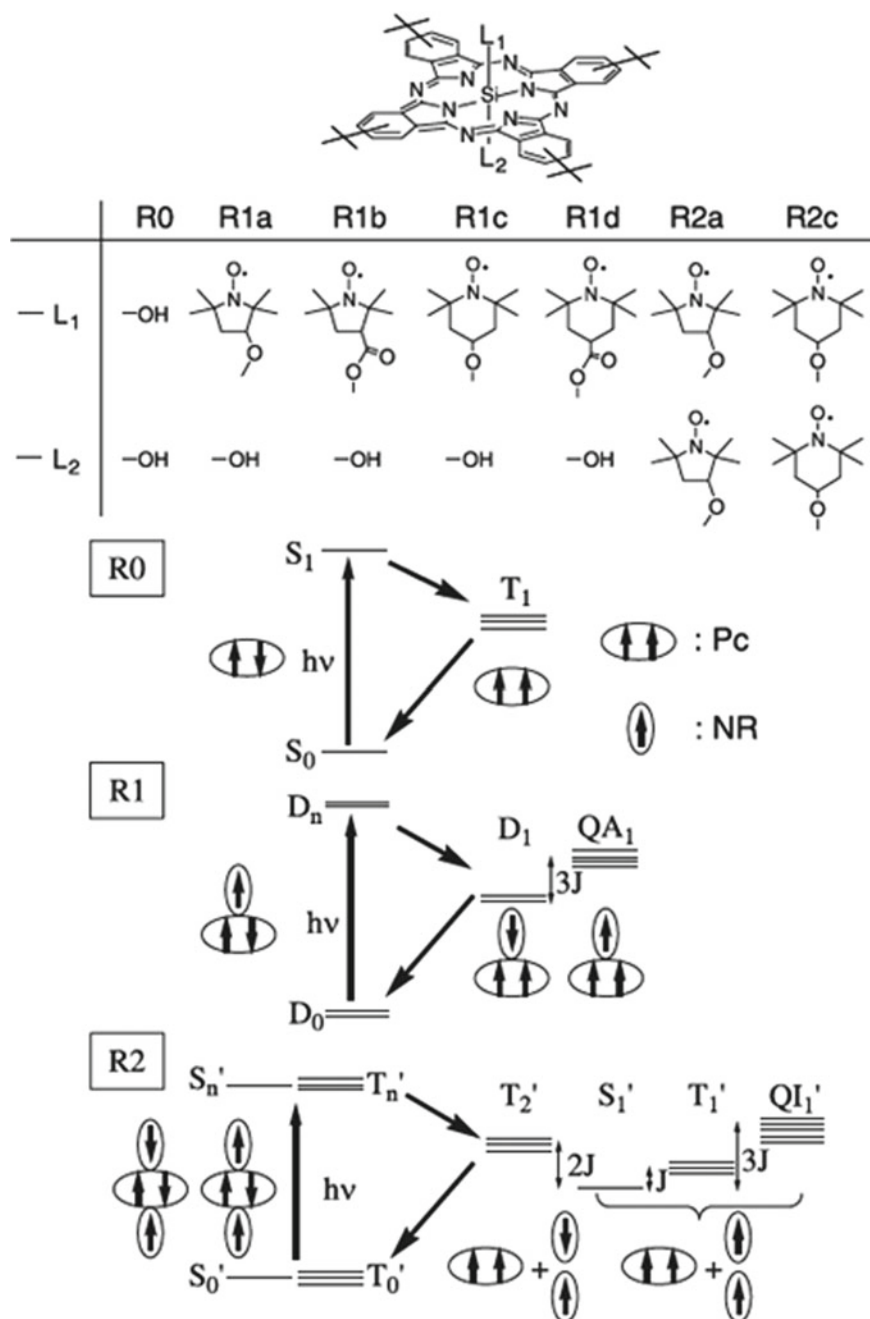


Fig. 6.16 Molecular structures and electronic states of SiPc covalently linked to NRs [16]

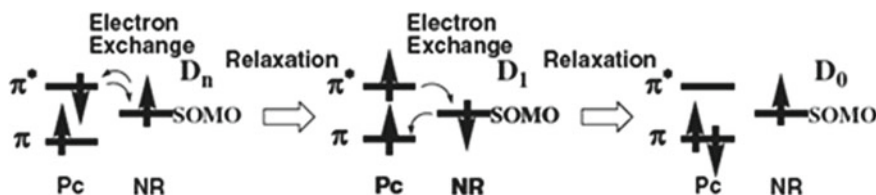


Fig. 6.17 D_n to D_1 and D_1 to D_0 transitions via electron exchange processes [7]

6.4.3 Factors Affected on Intramolecular Fluorescence Quenching, Electron Transfer, and Photoreduction in Dual Compounds

One of the principal advances of the dual probes is an ability to monitor molecular dynamics of a media of interest in wide range temperatures and correlation times, which can be affected on chemical and physical reactions including electron transfer [1–10]. To establish the effect of molecular dynamics of media on electron transfer in a donor–acceptor pair, super-slow molecular dynamic of o liquids (ethanol, water–glycerol), and albumen were investigated at temperature region 30–100 K [2]. The following parameters related to dynamical properties of the probes, two nitroxides and a dual fluorophore–nitroxide, were measured: (1) the intensity of phosphorescence, (2) the relaxation shift of phosphorescence spectra, (3) the amplitude of EPR spectra, and (4) the width of EPR spectra central lines. Experiments with the use of the probes revealed various dynamic processes from the correlation time $\tau_c = 10^2 \text{ s}^{-1}$ (30 K) to $\tau_c = 10^{-4} \text{ s}^{-1}$ (95 K). Obtained temperature dependences are in tune with correspondent data on the heat capacity and the proton NMR spectra width.

In pioneering work [3], it was first demonstrated that the nitroxide fragment is a strong quencher of the fluorescence and acts as an acceptor in the radical photoreduction, which strongly depends on molecular dynamics of environment. Specifically, irradiation of the chromophore segment of dansyl-TEMPO in a glassy liquid (glycerol 75%, water 20%, ethanol 5%) invoked producing the hydroxylamine derivative accompanying a decay of the nitroxide ESR signal and parallel eightfold increase in fluorescence. Both processes run with the same rate constant k_{red} under identical conditions with the quantum yield 8×10^{-2} (Fig. 6.18). The k_{red} values drastically increased when the temperature increased starting from 210 K (Fig. 6.19). The k_{red} increase correlated with an animation of the nanosecond relaxation dynamics in media monitored by the fluorescence (relaxation shift) and ESR techniques (change superfine splitting A_{ZZ}), while the rate constant of the intramolecular fluorescence quenching k_q was found to be temperature independent.

In order to establish a mechanism of intramolecular fluorescence quenching (IFQ) and photo-reduction of the nitroxide segment in the dual molecules, a series of c dansyl-nitroxides of different structures and flexibility of the spacer group, and different redox potentials of nitroxide (private communication from Drs. V.V. Martin

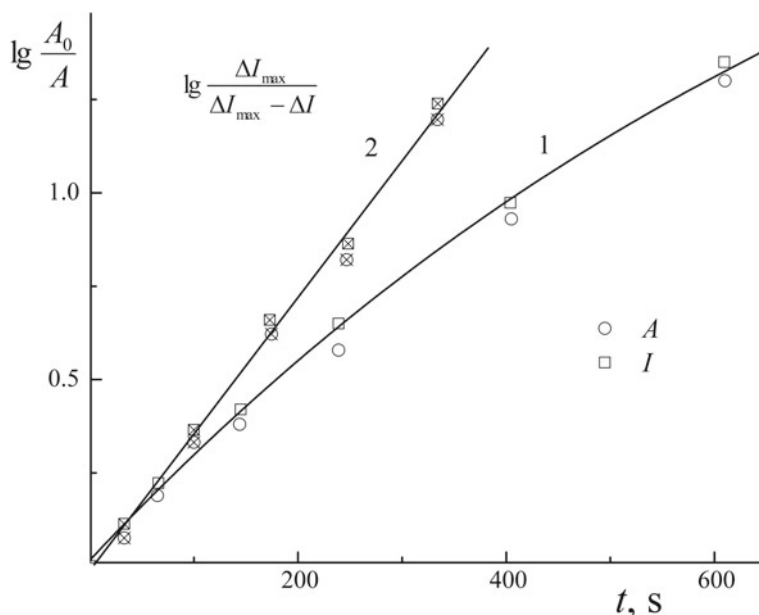


Fig. 6.18 Kinetics of change of the amplitude of nitroxide fragment EPR spectra (A) and intensity of fluorescence of the fluorophore segment (I) during photochemical reaction in the present (1) and absent (2) of oxygen in solvent (glycerol 75%, water 20%, ethanol 5%) [3]

and A. Weis, Lipitek International, Inc. (Fig. 6.1)) were synthesized and investigated [4–10, 74]. The following quantitative characteristics of the processes were obtained: (1) the rate constants of reversible electron transfer monitored by the time-resolved picosecond fluorescence technique (k_q), (2) fluorescence quantum yields of the probe fluorophore segment before and after the nitroxide moiety reduction (ϕ_{fl}) paramagnetic, and (3) the rate constant of photoreduction (k_{red}). As seen in Fig. 6.20, the positive correlation between the rate constant of the nitroxide fragment photoreduction k_{red} and the equilibrium constant K_{eq} for the chemical exchange reaction between different nitroxides depending on the nitroxide redox potential takes place [16]. On the basis of these data, two mechanisms of intermolecular quenching were proposed: the major mechanism, intersystem crossing (ISC) and the minor mechanism, irreversible intramolecular electron transfer (ET) from the excited singlet of the fluorophore (donor D) to nitroxide (acceptor A) followed by fluorophore segment regeneration and hydroxylamine formation. The latter mechanism is responsible for photoreduction. Nevertheless, the k_q values are not dependent on K_{eq} . In such a case, the fluorescence quenching occurs by the ISC mechanism or/and by reversible ET guided by the vibration modes [75, 76].

Blough et al. [12] suggested that the fluorescence quenching in a series of dual compounds arises through electron exchange, which causes relaxation of the singlet state to the triplet.

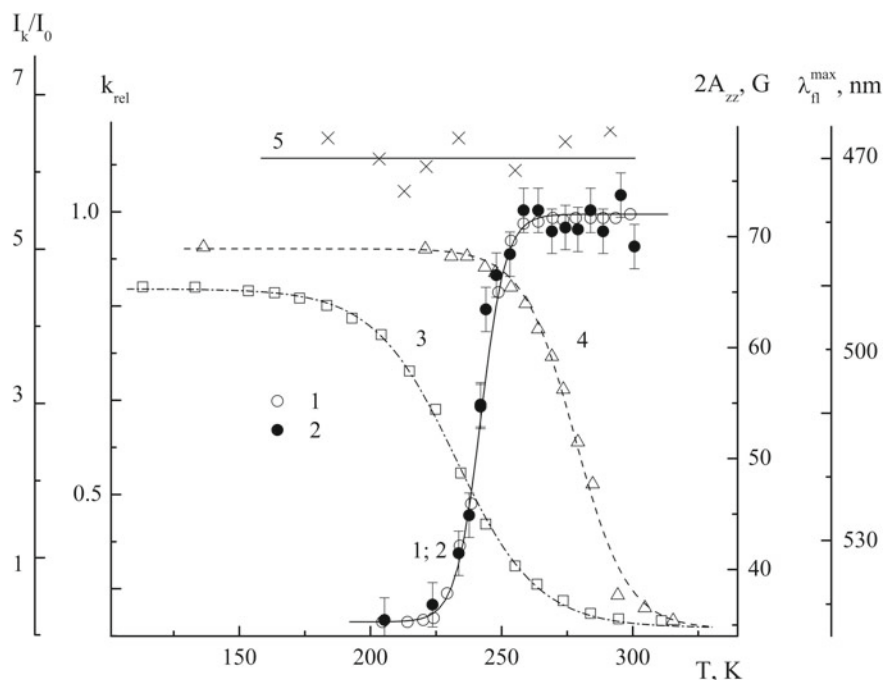


Fig. 6.19 Temperature dependences of relative rate constant of the photochemical reduction of the probe nitroxide fragment (k_{rel}) and the spectral parameters characterized dynamical state of the probe and the solvent: 1 and 2—the k_{rel} values obtained by the fluorescence and EPR techniques, respectively, 3— λ_{fl} is related to the fluorophore emission; 4— $2A_{zz}$ that is the nitroxide EPR superfine splitting of the nitroxide EPR spectra [3]

With a aim to established detail mechanism of quenching in fluorophore–nitroxide in a protein, a donor–acceptor hybrid molecule (DA) consisting of a 1-dimethylaminonaphthalene-5-sulfonate group in an excited singlet state (donor) and a nitroxide radical (acceptor) was incorporated into a hydrophobic cavity of bovine serum albumin (BSA) (Fig. 6.21) [4–10]. The kinetics of reversible intramolecular electron transfer (ET) from the donor to the acceptor and the nitroxide segment photoreduction, the micropolarity, and the intramolecular dynamics in the vicinity of the donor and the acceptor groups were monitored by fluorescence and ESR techniques in the temperature range from 77 to 300 K. The Arrhenius dependence of the reversible ET constant (k_{ET}) was found to be nonlinear and the apparent activation energy (E_{app}) changes from $E_{app} = 0$ eV (at $T = 77$ –100 K) to 0.25 eV (near $T = 298$ K). The temperature region of the E_{app} increase (100–240 K) was close to the temperature of the increase of relaxation shift of the donor fluorescent spectra. Using the Marcus-Levich [78, 79] model of electron transfer in polar media, on the basis of the obtained kinetic data and of the data of the micropolarity in the vicinity of the donor and the acceptor groups, values of standard Gibbs energy, the reorganization energy, the resonance integral and the Franck–Condon factor for reversible electron transfer were

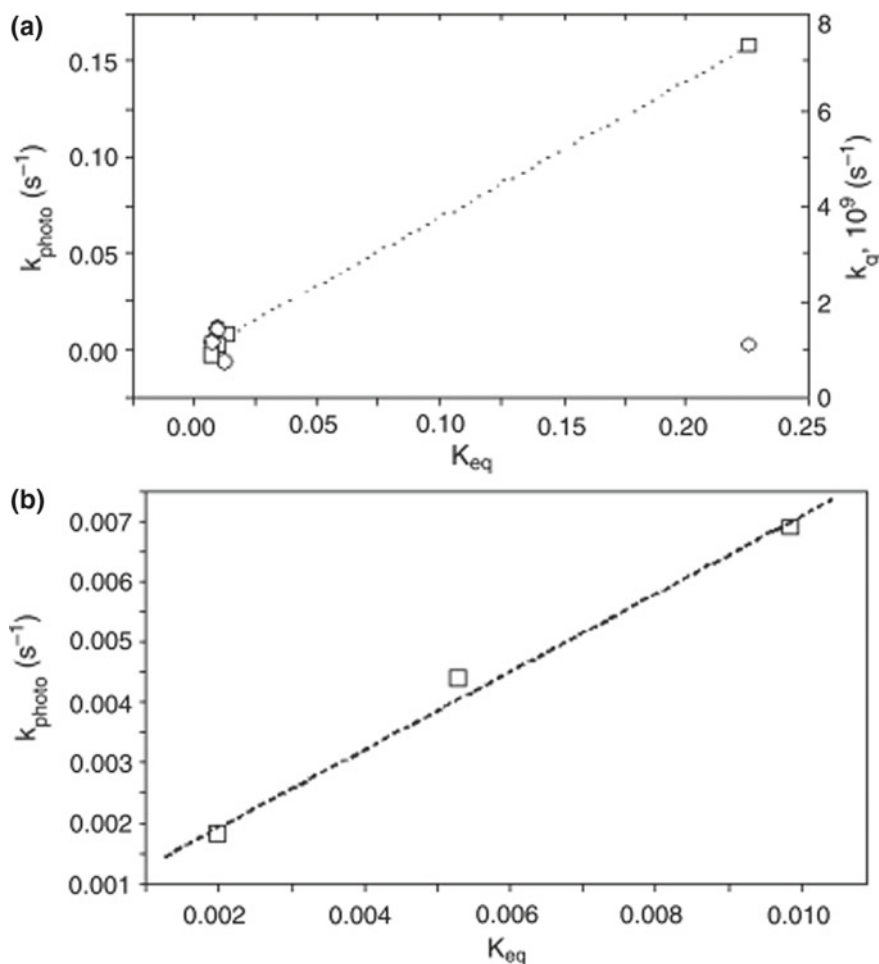


Fig. 6.20 Dependence of rate constant of photoreduction, k_{photo} , on redox power of the nitroxide fragment, K_{eq} (squares), contrary to independence of rate constant of IFQ, k_q (circles) [16]

estimated. The key role of molecular dynamics in the vicinity of the donor and the acceptor groups in the nitroxide photoreduction was stressed.

In order to model the effects of protein on the ET in **FNO•**, two doxyl-nitroxide probes FN1 and FN2 were incorporated in bovine (BSA) and human serum albumin (HSA) (Fig. 6.21) [8, 9]. The photoreduction of the nitroxide fragment was monitored by ESR, and fluorescence quenching was measured by steady-state and picosecond time-resolved techniques. The same groups allow to investigate the factors affecting the ET, namely the molecular dynamics and micropolarity of the medium in the vicinity of the donor (by fluorescence technique) and acceptor (by ESR) moieties.

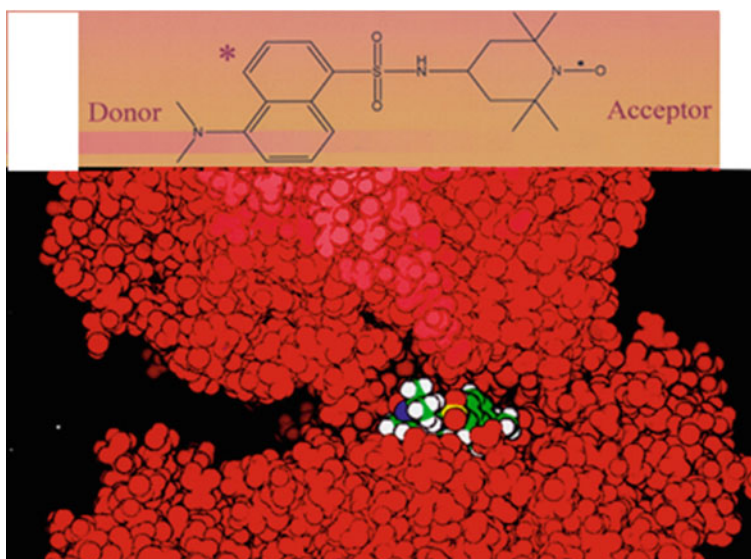


Fig. 6.21 Dual probe incorporated in hydrophobic packet of bovin serum albumin

The measurements of fluorescence polarization and ESR at ambient temperature, and by direct monitoring of relaxation dynamics of the protein-binding site around the dansyl moiety of the dual fluorophore–nitroxide probe FN2, using picosecond fluorescence time-resolved technique (Fig. 6.22), led to conclusion that the nanosecond dynamics of the protein medium is one of the decisive factors affecting the photoreduction and the light energy conversion in the given system. Such an intramolecular flexibility of the protein makes it possible to stabilize products of the reactions of the oxidized donor D^+ and acceptor A^- due to interactions with surrounding dipoles of protein, thus providing favorable thermodynamics for these reactions.

Comparison of results of modeling of the torsion angle rotation in the probe FN1 with the experimental data on the nitroxide segment dynamics in protein provided additional information about the mechanism of the protein molecular “breathing” [8, 9]. According to computer simulation in vacuum, a single C–N bond twisting around the piperidine ring undergoes minimal steric hindrances as compared to that of the dansyl fragment. The following values of the twisting correlation time τ_c were theoretically estimated (the twisting angles is shown in brackets): 3×10^{-10} s (170° – 220°), 10^{-10} s (220° – 275°), and 10^{-8} s (50° – 150°). Two first values are significantly lower than $\tau_c = 4 \times 10^{-9}$ s for the probe attached to BSA (EPR data) and especially for the rotation correlation time of the BSA molecule as a whole (8×10^{-8} s). From these findings, an important conclusion can be formulated; that is, the experimental correlation time of the probe nitroxide fragment can be attributed to its motion relative the protein globule, reflecting molecular “breathing” of the protein in the vicinity of the fragment (Fig. 6.23).

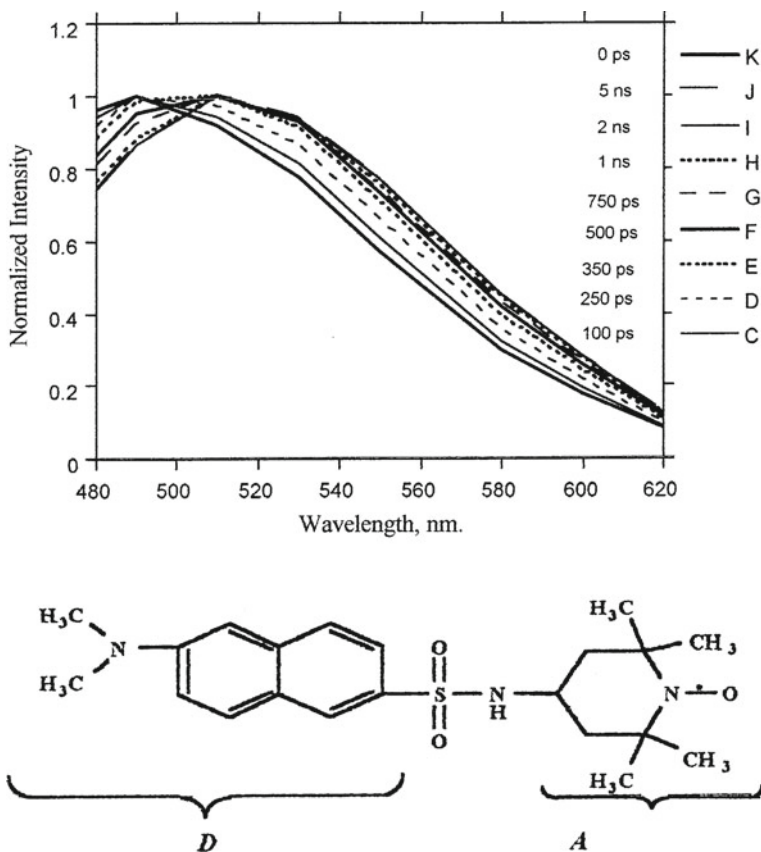


Fig. 6.22 Time-resolved fluorescence spectra of dansyl-TEMPO dual probe in HSA [77]

For analysis of experimental data obtained in the investigation of system, a Marcus–Levich formula for non-adiabatic electron transfer in a polar media was utilized (6.1) [78, 79]:

$$k_{\text{ET}} = \frac{2\pi V^2}{h\sqrt{4\pi\lambda k_{\text{B}}T}} \exp\left[-\frac{(\lambda + \Delta G_0)^2}{4\lambda k_{\text{B}}T}\right] \quad (6.1)$$

where ΔG_0 is the driving force of the value of the process, standard Gibbs free energy, λ is the reorganization energy defined as energy for ET without replacement of the nuclear frame, and V is the electronic coupling or the resonance integral. Based on experimental data on the local apparent dielectric constant ϵ_0 in the vicinity of the donor dansyl groups (fluorescence technique) and around the acceptor nitroxide segments (ESR), the following parameters of the Marcus–Levich theory were estimated for the ET at $T = 300$ K [4, 5, 9]: Gibbs energy $\Delta G_0 = -1.7$ eV, reorganization energy $[\lambda = 0.9$ eV, and free activation energy $\Delta G^\# \approx 0.25$ eV. Such a set of parameters is

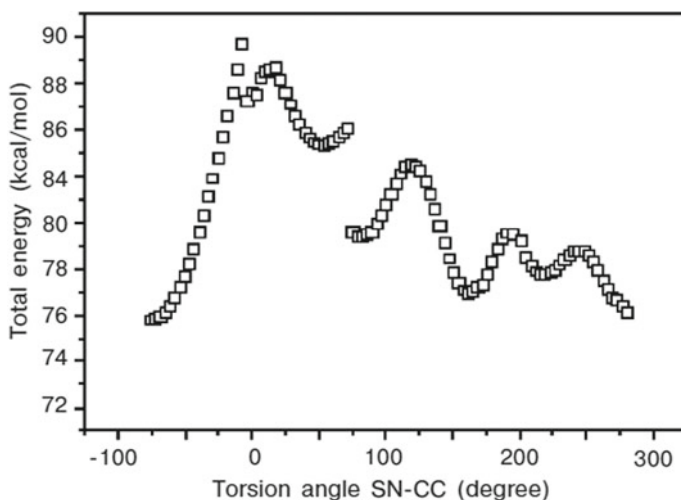
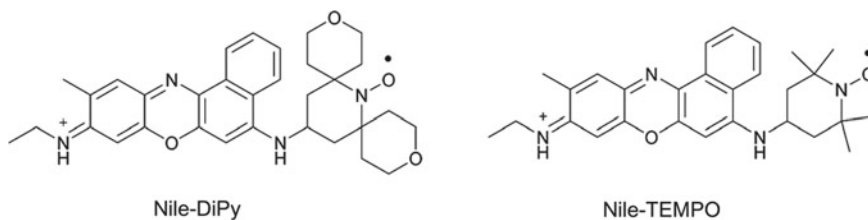


Fig. 6.23 Intramolecular rotation energy versus the torsion angle SN-CC for X in vacuum [9]

related to the inverted Marcus region. In this condition, the ET under thermodynamically equilibrium conditions can occur with the rate substantially lower ($k_{ET} \approx 10^5 \text{ s}^{-1}$) than the experimental value $k_q \approx 1 \times 10^9 \text{ s}^{-1}$. Therefore, the fast primary ET in the system under investigation occurs at the expense of vibrational stabilization of the photoseparated ionic pair (D^+A^-) and/or at the expense of partial stabilization due to the fast polar relaxation modes [75, 76].

The discussed photochemical reactions in the dual molecules may be considered as the light energy transfer processes, which meet the main requirements for any efficient light energy conversion system, that is, favorable thermodynamics, optimum orbital overlap of the donor and acceptor groups, and nanosecond dynamics in vicinity of the donor–acceptor pair [3–10].

The photochemical reaction between the fluorophore and the nitroxide radical in dual compounds



was investigated by optical, electrochemical, and femtosecond laser-induced transient absorption spectroscopy experiments [50]. Redox potentials of Nile-DiPy in MeOH containing 0.10 M TBAPF₆ were measured by cyclic voltammetry and the second harmonic alternating current voltammetry SHACV at 298 K (vs. Fc/Fc⁺). The

following values of redox potentials were found: E_{red} (Nile-Dipy) = 0.521 eV, E_{ox} (Nitroxide) = 0.786 eV, E_{red} (Nile-TEMPO) = 0.519, E_{ox} (Nitroxide) = 0.797 eV. These values were allowed to compose energy diagram for photo-induced reversible electron transfer in Nile-DiPy. The femtosecond transient spectra of Nile-DiPy in an N₂-saturated aqueous solution containing 5% DMSO displayed the very fast rise in broad transient absorption and emission around 530 and 645 nm after the selective excitation of Nile blue at 627 nm. The decay rate constants of the singlet excited state of Nile-DiPy and Nile-TEMPO were found to be as $(4.9 \times 10^9 \text{ s}^{-1})$ and $(4.5 \times 10^9 \text{ s}^{-1})$, respectively.

All in all, the dual compounds, keeping all properties of chromophore, fluorescence, and nitroxide spin probe, at the same time have gained new principal advantages. The most important new properties of chromophore–nitroxide (CN) compounds are its ability to: (1) obtain spatial and temporal information about both fluorescence and ESR behavior of the probe from the same specific part of the system under interest; (2) investigate micropolarity and molecular dynamics of media in the vicinity of fluorophore segment by the fluorescence technique and nitroxide segment by ESR; (3) monitor redox and spin trapping processes in systems of any optical density by ESR technique and of low optical density by fluorescence which is two to three orders more sensitive than ESR and optical absorption spectroscopy; (4) construct a variety of organic dual magnetic systems with photofunctionality; (5) analyze metal ions using both fluorescence and ESR techniques; (6) investigate mechanisms of intramolecular photochemical and photophysical processes in multispin systems in particular, (7) form the basis for the development of novel methods for the analysis of antioxidants and for real-time monitoring of important biochemical processes such as NO, superoxide, and reactive radical generation; (8) compose novel multispin and photoswitching systems; and (9) give a clue to the access of bland new organic photomagnetic materials such as novel multispin and photoswitching systems.

Thus, there are strong evidences to believe that the use of dual molecules will continue to be one of the most effective tools for solving excited and complicated problems in photochemistry, biochemistry, and chemistry of materials.

References

1. P.C. Jost, O.H. Griffith, The spin-labeling technique. *Methods Enzym.* **49**, 369–418 (1978)
2. I.G. Likhtenstein, V.R. Bogatyrenko, A.V. Kulikov, K. Hideg, H.O. Hankovsky, N.V. Lukoianov, A.I. Kotelnikov, B.S. Tanaschelchuk, Study of superflow motion in solid solutions by the method of physical probes. *Dokl. Akad. Nauk. SSSR* **253**, 481–484 (1980)
3. I.M. Bystryak, G.I. Likhtenshtein, A.I. Kotelnikov, O.H. Hankovsky, K. Hideg, The influence of the molecular dynamics of the solvent on the photoreduction of nitroxy-radicals. *Russ. J. Phys. Chem.* **60**, 1679–1983 (1986)
4. V.R. Vogel, E.T. Rubtsova, G.I. Likhtenshtein, K. Hideg, Factors affecting photoinduced electron transfer in a donor- acceptor pair (D-A) incorporated into bovine serum albumin. *J. Photochem. Photobiol. A, Chem.* **83**, 229–236 (1994)

5. E.T. Rubtsova, V.R. Vogel, G.I. Likhtenstein, D.V. Khudjakov and A.I. Kotelnikov Influence of molecular dynamics of protein matrix on the photoinduced electron transfer kinetics. *Biofizika* **38**, 222–227 (1993)
6. G.I. Likhtenstein, Novel fluorescent methods for biotechnological and biomedical sensing: assessing antioxidants, reactive radicals, NO dynamics, immunoassay, and biomembranes fluidity. *Appl. Biochem. Biotechnol.* **152**, 135–155 (2009)
7. G.I. Likhtenstein, *Solar Energy Conversion. Chemical Aspects* (Wiley-VCH, Weinheim, 2012)
8. G.I. Likhtenstein, Factors affecting light energy conversion in dual fluorophore-nitroxide molecules in solution and a protein. *Pure Appl. Chem.* **80**(10), 2125–2139 (2008)
9. G.I. Likhtenstein, D. Pines, E. Pines, V. Khutorsky, Effect of a protein on the light energy conversion in dual fluorophore-nitroxide probes studied by ESR and fluorescence spectroscopy. *Appl. Magn. Reson.* **35**(3), 459–472 (2009)
10. G.I. Likhtenstein, *Electron Spin in Chemistry and Biology: Fundamentals, Methods, Reactions Mechanisms, Magnetic Phenomena, Structure Investigation* (Springer, Berlin, 2016)
11. N.V. Blough, D.J. Simpson, Chemically mediated fluorescence yield switching in nitroxide-fluorophore adducts, optical sensors of radical/redox reactions. *J. Am. Chem. Soc.* **110**, 1915–1917 (1988)
12. J.A. Green, D.J. Simpson, G. Zhou, P.S. Ho, N.V. Blough, *J. Am. Chem. Soc.* **112**, 7337 (1990)
13. N.V. Blough, D.J. Simpson, Chemically mediated fluorescence yield switching in nitroxide-fluorophore adducts: optical sensors of radical/redox reactions. *J. Am. Chem. Soc.* **110**, 1915–1917 (1988)
14. A.G. Coman, C.C. Paraschivescu, A. Paun, A. Diac, N.D. Hadade, L. Jouffret, A. Gautier, M. Matache, P. Ionita, Synthesis of novel profluorescent nitroxides as dual luminescent-paramagnetic active probes. *New J. Chem.* **41**, 7472 (2017)
15. J.P. Blinco, A.C.K.E. Fairfull-Smith, B.J. Morrow, S.E. Bottle, Profluorescent nitroxides as sensitive probes of oxidative change and free radical reactions. *Aust. J. Chem.* **64**, 373–389 (2011)
16. G.I. Likhtenstein, K. Ishii, S. Nakatsuji, Dual chromophore-nitroxides: novel molecular probes, photochemical and photophysical models and magnetic materials. *Photochem. Photobiol.* **83**, 871–881 (2007)
17. K.A. Hansen, K.E. Fairfull-Smith, S.E. Bottle, J.P. Blinco, Development of a redox-responsive polymeric profluorescent probe. *Macromol. Chem. Phys.* **217**(20), 2330–2340 (2016)
18. H.-Y. Ahn, K.E. Fairfull-Smith, B.J. Morrow, V. Lussini, B. Kim, M.V. Bondar, S.E. Bottle, K.D. Belfield, Two-photon fluorescence microscopy imaging of cellular oxidative stress using profluorescent nitroxides. *J. Am. Chem. Soc.* **134**, 4721–4730 (2012)
19. D.J. Keddle, K.E. Fairfull-Smith, S.E. Bottle, The palladium-catalysed copper-free Sonogashira coupling of isoindoline nitroxides: a convenient route to robust profluorescent carbon–carbon frameworks. *Org. Biomol. Chem.* **6**, 3135–3143 (2008)
20. E.M. Simpson, Z.D. Ristovski, S.E. Bottle, K.E. Fairfull-Smith, J.P. Blinco, Modular design of profluorescent polymer. *Sensors. Polym. Chem.* **6**, 2962 (2015)
21. V.C. Lussini, J.M. Colwell, K.E. Fairfull-Smith, S.E. Bottle, Profluorescent nitroxide sensors for monitoring photo-induced degradation in polymer films. *Sens. Actuat. B Chem.* **241**, 199–209 (2017)
22. B.A. Chalmers, S. Saha, T. Nguyen, J. McMurtrie, S.T. Sigurdsson, S.E. Bottle, K-S. Masters, TMO-PyrImid hybrids are profluorescent, site-directed spin labels for nucleic acids. *Org. Lett.* **16**, 5528–5531 (2014)
23. M. Barzegar, A. Oliaa, A. Zavras, C.H. Schiesser, S.A. Alexandera, Blue ‘turn-on’ fluorescent probes for the direct detection of free radicals and nitric oxide in *Pseudomonas aeruginosa* biofilms. *Org. Biomol. Chem.* **14**, 2272–2281 (2016)
24. S. Sato, S. Endo, Y. Kurokawa, M. Yamaguchi, A. Nagai, T. Ito, T. Ogata, Synthesis and fluorescence properties of six fluorescein-nitroxide radical hybrid-compounds. *Spectrochim. Acta Part A Mol. Biomol. Spectrosc.* **169**, 66–71 (2016)

25. S. Endo, Y. Kurokawa, M. Yamaguchi, A. Nagai, T. Ito, T. Ogata, Synthesis and fluorescence properties of six fluorescein-nitroxide radical hybrid-compounds. *Spectrochim. Acta Part A Mol. Biomol. Spectrosc.* **169**, 66–71 (2016)
26. E. Lozinskaya, V.V. Martin, T.A. Berezina, A.I. Shames, A.L. Weis, G.I. Likhtenshtein, Dual fluorophore–nitroxide probes for analysis of vitamin C in biological liquids. *J. Biochem. Biophys. Methods* **38**, 29–42 (1999)
27. M.M. Haugland, J.E. Lovett, E.A. Anderson, Advances in the synthesis of nitroxide radicals for use in biomolecule spin labeling. *Chem. Soc. Rev.* **47**, 668–680 (2018)
28. M. Eing, B.T. Tuten, J.P. Blinco, C. Barner-Kowollik, Visible light activation of spin-silenced fluorescence. *Chem. Eur. J.* **24**, 12246–12249 (2018)
29. B.A. Chalmers, S. Saha, T. Nguyen, J. McMurtrie, S.T. Sigurdsson, S.E. Bottle, K.S. Masters, TMO-PyrImid hybrids are profluorescent, site-directed spin labels for nucleic acids. *Org. Lett.* **16**, 5528–5553 (2014)
30. G-P. Yan, B. Zhao, S.E. Bottle, Q. Zhang, J-L. Li Synthesis and properties of fullerene C60 and C70 spin probes containing isoindoline nitroxides. *Fuller. Nanotubes Carbon Nanostructures* **23**(8), 734–741 (2015)
31. Y. Zhao, Y. Fang, Y. Jiang, Fluorescence study of fullerene in organic solvents at room temperature. *Spectrochim. Acta A Mol. Biomol. Spectrosc.* **64**(3), 564–567 (2006)
32. R. Braslau, F. Rivera III, E. Lilie, M. Cottman, Urushiol detection using a profluorescent nitroxide. *J. Org. Chem.* **78**, 238–245 (2013)
33. J.P. Blinco, K.E. Fairfull-Smith, A.S. Micallef, S.E. Bottle, Highly efficient, stoichiometric radical exchange reactions using isoindoline profluorescent nitroxides. *Polym. Chem.* **1**, 1009 (2010)
34. J.P. Allen, M.C. Pfrunder, J.C. McMurtrie, S.T. Bottle, J.P. Blinco, K.E. Fairfull-Smith, BODIPY-based profluorescent probes containing meso- and β -substituted isoindoline nitroxides. *Eur. J. Org. Chem.* **2017**(3), 476–483 (2017)
35. V.C. Lussini, K.E. Fairfull-Smith, S.E. Bottle, Polyaromatic profluorescent nitroxide probes with enhanced photostability. *Chem. A Eur. J.* **21**(50), 8258–8268 (2015)
36. P. Lederhose, N.L. Haworth, K. Thomas, S.E. Bottle, M.L. Coote, C. Barner-Kowollik, J.P. Blinco, Design of redox/radical sensing molecules via nitrile imine-mediated tetrazole-ene cycloaddition (NITEC). *J. Org. Chem.* **80**, 8009–8017 (2015)
37. P. Parkhomyuk-Ben Arye, N. Strashnikova, G.I. Likhtenshtein, Stibene-photochrome-fluorescence-spin molecules: covalent immobilization on silica plate and application as redox and viscosity probes. *J. Biochem. Biophys. Methods* **51**, 1–15 (2002)
38. G.I. Likhtenshtein, Dual phluorophore-nitroxides as a tool for analysis of antioxidants, nitric oxide and superoxide in biological liquids and tissues, in *International Conference “Recent Advantages in Sensoring, Signals and materials”*, November 3–5, 2010, Faro, Portugal, pp. 162–168 (2010)
39. E. Lozinsky, A. Novoselsky, A.I. Shames, O. Saphier, G.I. Likhtenshtein, D. Meyerstein, *Biochim. Biophys. Acta Gen. Subj.* **1526**(1), 53–60 (2001)
40. O. Saphier, T. Silberstein, A.I. Shames, G.I. Likhtenshtein, E. Maimon, D. Mankuta, M. Mazor, M. Katz, D. Meyerstein, N. Meyerstein, *Free Radic. Res.* **37**, 301–308 (2003)
41. T. Silberstein, D. Mankuta, A.I. Shames, G.I. Likhtenshtein, D. Meyerstein, N. Meyerstein, O. Saphier, Neonatal blood is more resistant to oxidative stress induced by stable nitroxide radicals than adult blood. *Arch. Gynecol. Obstet.* **277**(3), 233–237 (2008)
42. T. Yokoi, K. Ishii, Dependence of phthalocyanine-based fluorescence on albumin structure: a fluorescent probe for ascorbic acid. *J. Photochem. Photobiol. A* **364**, 1–5 (2018)
43. N. Medvedeva, V.V. Martin, A.L. Weis, G.I. Likhtenshten, Dual fluorophore-nitronyl probe for investigation of superoxide dynamics and antioxidant status of biological systems. *J. Photochem. Photobiol. A* **163**, 45–51 (2004)
44. H. Nam, J.E. Kwon, M.-W. Choi, J. Seo, S. Shin, S. Kim, S.Y. Park, Highly sensitive and selective fluorescent probe for ascorbic acid with a broad detection range through dual-quenching and bimodal action of nitronyl-nitroxide. *ACS Sens.* **1**(4), 392–398 (2016)

45. C.-P. Liu, T.-H. Wu, C.-Y. Liu, H.-J. Cheng, S.-Y. Lin, Interactions of nitroxide radicals with dendrimer-entrapped Au₈-clusters: a fluorescent nanosensor for intracellular imaging of ascorbic acid. *J. Mater. Chem. B* **3**, 191–197 (2015)
46. F. Lin, D. Pei, W. He, Z. Huang, Y. Huang, X. Guo, Electron transfer quenching by nitroxide radicals of the fluorescence of carbon dots. *J. Mater. Chem.* **22**, 11801–11807 (2012)
47. H. Yu, L. Cao, F. Li, Q. Wu, Q. Li, S. Wang, Y. Guo, The antioxidant mechanism of nitroxide TEMPO: scavenging with glutathionyl radicals. *RSC Adv.* **5**, 63655 (2015)
48. M.A. Lam, D.I. Pattison, S.E. Bottle, D.J. Keddie, M.J. Davies, Nitric oxide and nitroxides can act as efficient scavengers of protein-derived free radicals. *Chem. Res. Toxicol.* **21**, 2111–2119 (2008)
49. A.G. Coman, C.C. Paraschivescu, A. Paun, A. Diac, N.D. Hădăde, L. Jouffret, A. Gautier, M. Matache, P. Ionita, Synthesis of novel profluorescent nitroxides as dual luminescent-paramagnetic active probes. *New J. Chem.* **41**, 7472 (2017)
50. K. Sasaki, T. Ito, H.G. Fujii, S. Sato, Synthesis and reduction kinetics of five Ibuprofen-nitroxides for ascorbic acid and methyl radicals. *Chem. Pharm. Bull.* **64**(10), 1509–1513 (2016)
51. M. Yamato, T. Yamasaki, F. Mito, K. Yamada, Rapid and convenient detection of ascorbic acid using a fluorescent nitroxide switch. *Free Radic. Biol. Med.* **53**(11), 2112–2118 (2012)
52. Y. Matsuoka, K. Ohkubo, T. Yamasaki, M. Yamato, H. Ohtabu, T. Shirouzu, S. Fukuzumi, K.-i. Yamada, A profluorescent nitroxide probe for ascorbic acid detection and its application to quantitative analysis of diabetic rat plasma. *RSC Adv.* **6**, 60907–60915 (2016)
53. Y. Matsuoka, M. Yamato, K.-i. Yamada, Fluorescence probe for the convenient and sensitive detection of ascorbic acid. *J. Clin. Biochem. Nutr.* **58**(1), 16–22 (2016)
54. T. Yang, B. Zheng, H. Liang, Y. Wan, J. Du, D. Xiao, A sensitive and selective chemosensor for ascorbic acid based on a fluorescent nitroxide switch. *Talanta* **132**, 191–196 (2015)
55. T. Maki, N. Soh, K. Nakano, T. Imato, Flow injection fluorometric determination of ascorbic acid using perylenebisimide-linked nitroxide. *Talanta* **85**, 1730–1733 (2011)
56. T. Yokoi, T. Otani, K. Ishii, In vivo fluorescence bioimaging of ascorbic acid in mice: development of an efficient probe consisting of phthalocyanine, TEMPO, and albumin. *Sci. Rep.* **8**, 1560 (2018)
57. C.L. Rayner, S.E. Bottle, G.A. Gole, M.S. Ward, N.L. Barnett, Real-time quantification of oxidative stress and the protective effect of nitroxide antioxidants. *Neurochem. Int.* **92**, 1–12 (2016)
58. J.L. Gerlock, P.J. Zacmanidis, D.R. Bauer, D.J. Simpson, N.V. Blough, I.T. Salmeen, Fluorescence detection of free radicals by nitroxide scavenging. *Free Radic. Res. Commun.* **10**(1–2), 119 (1990)
59. A.S. Micallef, J.P. Blinco, G.A. George, D.A. Reid, S.E. Bottle, The application of a novel profluorescent nitroxide to monitor thermo-oxidative degradation of polypropylene. *Polym. Degrad. Stabil.* **89**(3), 427–435 (2005)
60. G.G. Borisenko, I. Martin, Q. Zhao, A.A. Amoscato, V.E. Kagan, Nitroxides scavenge myeloperoxidase-catalyzed thyl radicals in model systems and in cells. *Am. Chem. Soc.* **126**, 9221. (2004)
61. S. Nakatsuj, Preparation, reaction and properties of functional nitroxide radicals, in *Nitroxides: Application in Chemistry, Biomedicine, and Materials Science*, ed. by G.I. Likhtenshtein, J. Yamauchi, S. Nakatsuj, A. Smirnov, R. Tamura (Wiley-VCH, Weinheim, 2008)
62. photoswitching of an intramolecular magnetic interaction, K. Matsuda, K. M. Irie Photochromism of diarylethenes with two nitronyl nitroxides. *Chemistry* **7**, 3466–3473 (2001)
63. K. Matsuda, K.M. Irie, Diaryethene as a photoswitching unit. *J. Photochem. Photobiol. C, Photochem. Rev.* **5**, 169–182 (2004)
64. S. Nakatsuj, Recent progress toward the exploitation of organic radical compounds with photo-responsive magnetic properties. *Chem. Soc. Rev.* **33**, 348–353 (2004)
65. S. Nakatsuj, M. Fujino, H. Akutsu, J. Yamada, V.S. Gurman, A.K. Vorobiev, Azobenzene derivatives carrying a nitroxide radical. *J. Org. Chem.* **72**, 2021–2029 (2007)
66. M. Nakagawa, H. Akutsu, J.-i Yamada, M. Karakawa, Y. Aso, S. Fall, T. Heiser, S. Nakatsuj, A spin-carrying naphthalenediimide derivative with azobenzene unit. *Chem. Lett.* **41**(2), 175–177 (2012)

67. T. Kaneko, T. Amano, H. Akutsu, J. Yamada, S. Nakatsuji, Photochromic radical compounds based on a naphthopyran systems. *Org. Lett.* **5**, 2127–2129 (2003)
68. M. Nakagawa, H. Akutsu, J.-i. Yamada, M. Karakawa, Y. Aso, S. Nakatsuji. Photo-responsive naphthalenediimide derivative carrying a nitroxide and an azobenzene group. *Ann. Acad. Roman. Sci. Ser. Chem. Sci.* **1**(1) (2014) Online ISSN 2393–2902
69. Y. Teki, T. Toichi, S. Nakajima, π -Topology and spin alignment in unique photoexcited triplet and quintet states arising from four unpaired electrons of an organic spin system. *Chem. Eur. J.* **12**, 2329–2336 (2006)
70. N. Roques, Ph. Gerbier, Y. Teki, S. Choua, P. Lesniakova, J.-P. Sutter, P. Guionneau, C. Guerin, Towards a better understanding of photo-excited spin alignment processes using silole diradicals. *New J. Chem.* **65**, 1319–1326 (2006)
71. S. Nakatsuji, Organic multifunctional spin systems based on aminoxyl radicals. *Adv. Mater.* **13**, 1719–1724 (2001)
72. F. Cicogna, I. Domenichelli, S. Coiai, F. Bellina, M. Lessi, R. Spiniello, E. Passaglia, Structural, thermal and photo-physical data of azo-aromatic TEMPO derivatives before and after their grafting to polyolefins. *Data Brief.* **6**, 562–570 (2016)
73. S. Takeuchi, K. Ishii, N. Kobayashi, Time-resolved EPR transient absorption studies on phthalocyaninatosilicon covalently linked to two PROXYL radicals. *J. Phys. Chem. A* **108**, 3276–3280 (2004)
74. E. Lozinsky, A. Shames, G.I. Likhtenshtein, Dual fluorophore-nitroxides: MODELS for investigation of intramolecular quenching and novel redox probes, in *Recent Research Development in Photochemistry and Photobiology*, vol. 2, ed. by S.G. Pandalai (Transworld Research Network, Trivandrum, India, 2000), pp. 41–45
75. S. Efrima, M. Bixon, Vibrational effects in outer-sphere electron-transfer reactions in polar media. *Chem. Phys.* **13**, 447 (1976)
76. M. Bixon, J. Jortner, in *Advances in Chemical Physics*, vol. 107, Part 1, ed. by J. Jortner, N. Bixon (Wiley, New York, 1999), pp. 35–202
77. G.I. Likhtenshtein, F. Febrario F, Nucci R. Intramolecular dynamics and conformational transitions in proteins studied by biophysical labeling methods. Common and specific features of proteins from thermophilic microorganisms. *Spectrochem. Acta Part A. Biomolec. Spectrosc.* **56**, 2011–2031 (2000)
78. V.G. Levich, R. Dogonadze, *Dokl. Akad. Nauk* **78**, 2148 (1959)
79. R.A. Marcus, N. Sutin, Electron transfers in chemistry and biology. *Biochim. Biophys. Acta* **811**, 265 (1985)